ELECTRONIC RESPONSE OF PHOSPHORUS AND NITROGEN BASED LIGANDS ON METAL COORDINATION

Dissertation zur Erlangung des
naturwissenschaftlichen Doktorgrades
der Bayerischen Julius-Maximilians-Universität Würzburg

vorgelegt von
Alexander Murso
aus Heilbronn

Würzburg 2004

Eingereicht am: _____

bei der Fakultät für Chemie und Pharmazie

1. Gutachter: _____

2. Gutachter: _____

der Dissertation

1. Prüfer: _____

2. Prüfer: _____

3. Prüfer: _____

des Öffentlichen Promotionskolloquiums

Tag des öffentlichen Promotionskolloquiums: _____

Doktorurkunde ausgehändigt am: _____

Die Neugier steht immer an erster Stelle eines Problems, das gelöst werden will.

Galileo Galilei

Danksagung

Die vorliegende Arbeit wurde in der Zeit von April 2001 bis März 2004 im Arbeitskreis von Prof. Dr. D. Stalke am Institut für Anorganische Chemie der Universität Würzburg angefertigt.

An erster Stelle möchte ich mich besonders bei Herrn Prof. Dr. D. Stalke für die interessante Themenstellung, seine stetige Diskussionsbereitschaft in ausgesprochen freundlicher Atmosphäre, die mir gegebene große Freiheit bei der Durchführung dieser Arbeit und die Ermöglichung der Teilnahme an Konferenzen bedanken. Zusätzlich gebührt ihm mein Dank für die Gewährung eines Promotionsstipendiums der DFG im Rahmen des Graduiertenkollegs 690. Durch dieses Programm konnte ich Einblicke in die verschiedensten Teilbereiche der Chemie erlangen.

Allen gegenwärtigen und früheren Mitgliedern des Arbeitskreises gilt mein Dank für die Unterstützung während dieser Arbeit, sowie das hervorragende Arbeitsklima, das gewährleistet hat, dass nie Laboralltag vorherrschte.

Besonderer Dank gebührt Herrn T. Stey für das sorgfältige Korrekturlesen dieser Arbeit und seine stetige Diskussionsbereitschaft im Bereich unseres gemeinsamen Arbeitsgebietes der Phosphan-Metallkoordination.

Herrn Dr. D. Leusser danke ich für die Einführung in die hohe Kunst der Kristall–applikation und der Einkristallstrukturbestimmung.

Bei meiner Laborkollegin Frau Dr. C. Selinka bedanke ich mich für eine sehr angenehme Arbeitsatmosphäre im gemeinsamen Labor.

Ebenso sei Herrn Dr. N. Kocher für die hervorragende Zusammenarbeit, nicht nur im Bereich der P–N-Bindungsanalyse, gedankt.

Herrn Dipl.-Chem. S. Deuerlein danke ich für die Unterstützung bei und der Übernahme der Soft- und Hardwareadministration.

Allen früheren und derzeitigen Mitgliedern des Graduiertenkollegs 690 sei herzlich für ihre stete Diskussionsbereitschaft, das hervorragende Arbeitsklima und ihrer Unterstützung bei Veranstaltungen gedankt. Insbesondere danke ich Herrn Prof. Dr. B. Engels für die Organisation des Graduiertenkollegs.

Bei unserem Glasbläser Herrn B. Fertig bedanke ich mich für die Anfertigung von speziellen Glasgeräten.

Für die Ausführung analytischer Untersuchungen gilt mein Dank den Mitarbeitern der Serviceabteilungen der Universität, hierbei besonders Herrn Dr. R. Bertermann für die Durchführung zahlreicher NMR-Experimente und die interessante Gestaltung des NMR-Praktikums im Rahmen des Graduiertenkollegs.

Last but not least danke ich herzlich meinen Eltern für die Unterstützung während meines Studiums, meinem Bruder für zahlreiche schöne Abende in Stuttgart, Würzburg und Bremen und meiner Freundin Evelyn Selig für ihre nicht enden wollende Geduld.

Contents

Abbreviations

ADP	anisotropic displacement parameter
AIM	atoms in molecules
Ar	aryl
av.	average
BCP	bond critical point
bpy	2,2'-bipyridine
Bu	butyl
calcd.	calculated
CCD	charge coupled device
COSY	correlated spectroscopy
Cp	cyclopentadienyl
Cp*	pentamethylcyclopentadienyl
CSD	Cambridge Structural Database
cy	*cyclo*
dme	dimethoxyethane
dmpe	1,2-bis(dimethyl)phosphinoethane
dppe	1,2-bis(diphenyl)phosphinoethane
DTA	differential thermo analysis
e	electron
e.g.	for example
esd	estimated standard deviation
ext.	external
Et	ethyl
h	hour
HMBC	hetero multiple bond correlation
i	*iso*
L	ligand
M	metal (fragment)
m	*meta*
Me	methyl
Ment	mentyl
Mes	mesityl

min	minute
n	*neo*
NLO	non-linear optic
NMR	nuclear magnetic resonance
o	*ortho*
p	*para*
Ph	phenyl
pmdta	pentamethyldiethylentriamine
Pr	propyl
Py	2-pyridyl
R	substituent
r.t.	room temperature
rac.	*racemic*
sat.	saturated
sec.	*secondary*
t	*tertiary*
thf	tetrahydrofuran
tmeda	tetramethylethylendiamine
VE	valence electron
vs.	*versus*
VSCC	valence shell charge concentration
X	halide

List of new Compounds

no.	compound	Lewis-diagram
1	$Ph_2P(CH_2Py)$	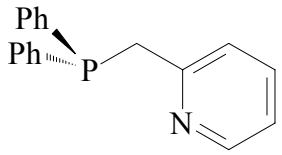
2	$[(thf)_2Li\{Ph_2P(CHPy)\}]$	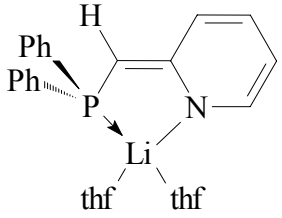
3	$[(thf)Li\{Ph_2P(CHPy)\}(Ph_2P)\}]_2$	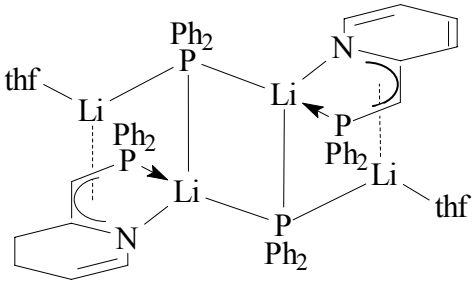
4	$[(thf)_3Sr\{Ph_2P(CHPy)\}_2]$	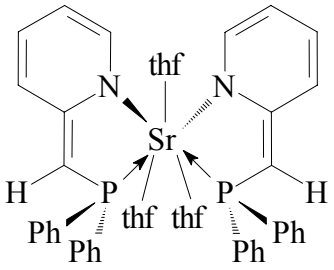
5	$[Pb\{Ph_2P(CHPy)\}\{N(SiMe_3)_2\}]$	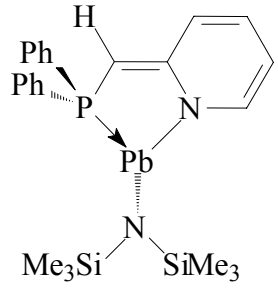

no.	compound	Lewis-diagram
6	$[Zn_3O\{Ph_2P(CHPy)\}_4]$	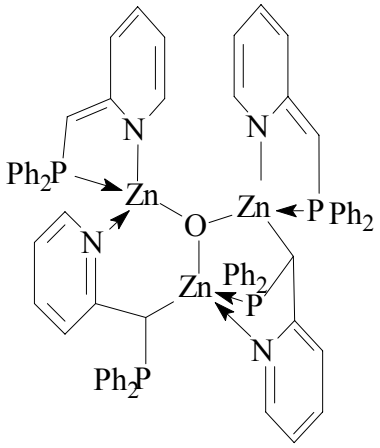
7	$[\{Ph_2P(CH_2Py)\}Fe\{Ph_2P(CHPy)\}_2]$	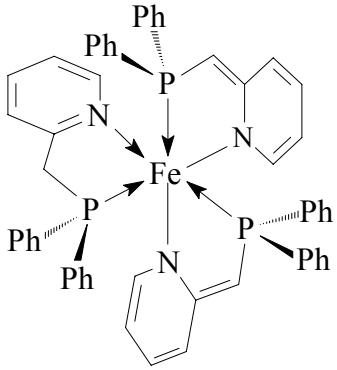
8	$[Fe\{Ph_2P(CHPy)\}\{N(SiMe_3)_2\}]_2$	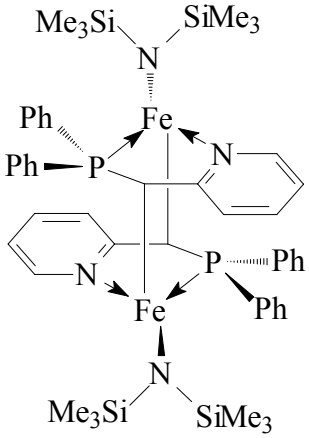

no.	compound	Lewis-diagram
9	$Ph_2P(CH_2Py)NSiMe_3$	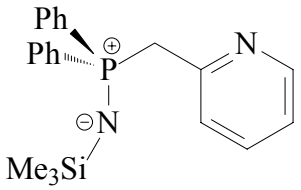
10	$[Ph_2P(CH_2Py)NH_2][N_3]$	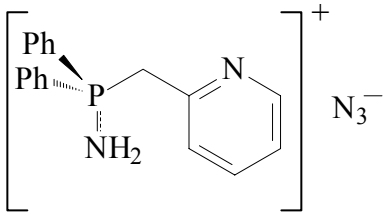
11	$[(Et_2O)Li\{Ph_2P(CHPy)NSiMe_3\}]$	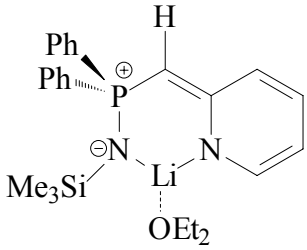
12	$[\{Ph_2P(CH_2Py)NSiMe_3\}Li–\{Ph_2P(CHPy)NSiMe_3\}]$	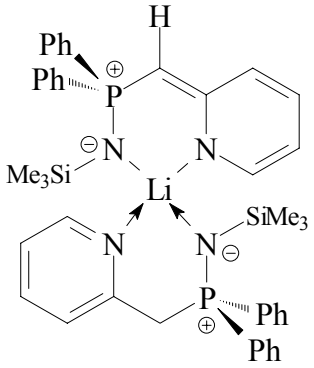
13	$[\{Ph_2P(CH_2Py)NSiMe_3\}Na–\{Ph_2P(CHPy)NSiMe_3\}]$	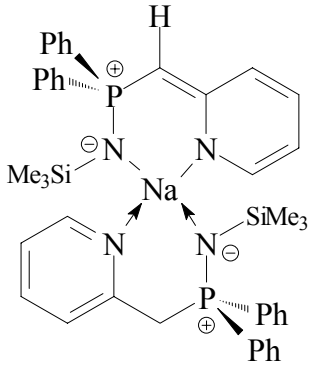

no.	compound	Lewis-diagram
14	$[Zn\{Ph_2P(CHPy)NSiMe_3\}_2]$	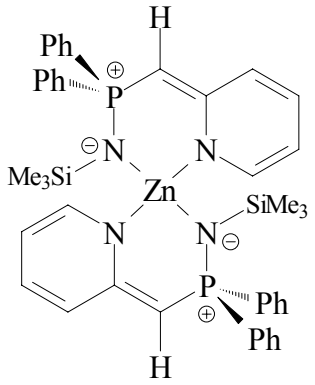
15	$[Fe\{Ph_2P(CHPy)NSiMe_3\}_2]$	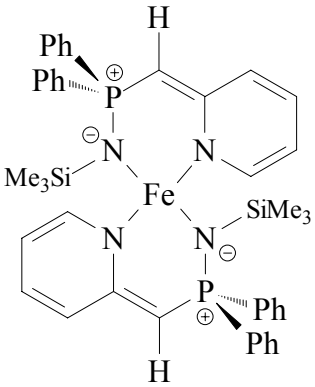

1 Introduction

Ligand design is one of the most challenging research fields in modern chemistry. The complexes formed in reactions of ligands with specific properties with metal fragments are employed in various fields and their applications are closely related to the nature of the ligands.[1] For example, the properties of materials are based on co-operative interactions between the components of the bulk assembly and are not exhibited by the individual molecule. The superconductive behaviour of molecules and the one-, two- or three-dimensional magnetism of materials is due to a precise ordering of discrete molecules with respect to one other in condensed phase.[2] Many other examples of coordination complexes as materials are based on infinte polymeric rather than molecular structures. Mesoporous solids build network polymers, which can form zeolite-like structures with cavities reversibly binding various molecules as guests.[3] Many complexes integrate a particular combination of structure and electronic properties, furnish them abbilities in the application as molecular devices by specific redox behaviour or optical properties such as absorption, luminescence or non linear optic (NLO) behaviour.[4]

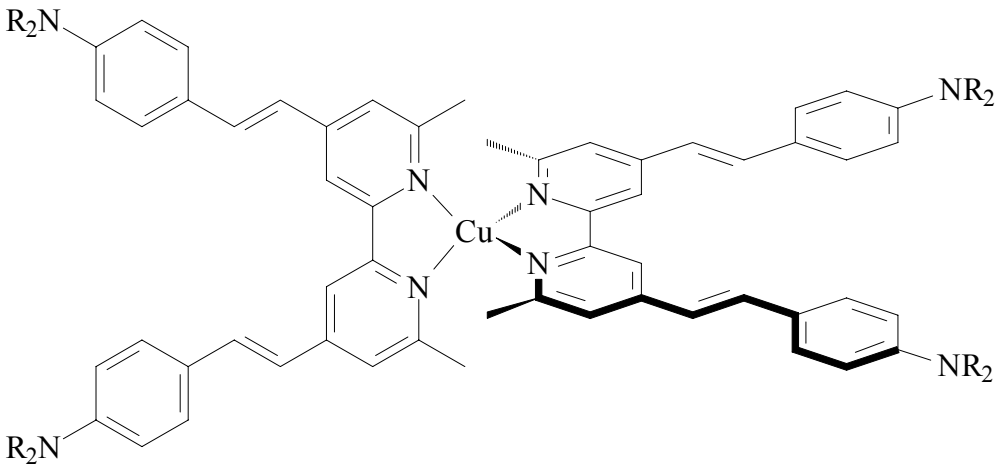

Scheme 1.1: *Octopolar complex for second-order NLO studies based on assemblies of donor substituted bipyridyl ligands.*[4c]

The fine control of the number and types of coordinating atoms is one of the most challenging tasks in the synthesis of biomimetical metal complexes with coordination geometry and reactivity as close as possible to metalloenzymes and –proteins. The

complexes should not only model the direct metal coordination sphere, but also the remote functionalities, which play an important role in substrate recognition and in preventing product inhibition.[5]

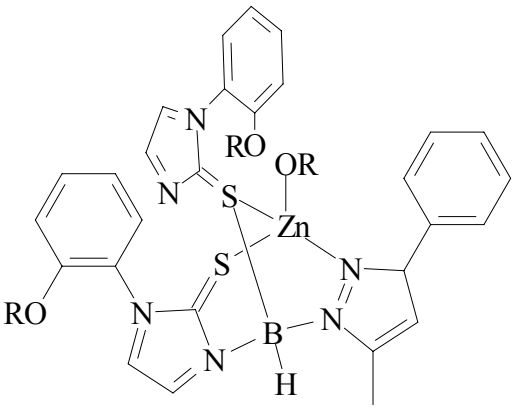

Scheme 1.2: *Model complex of liver alcohol dehydrogenase.*[5e]

In the last decades great effort was made in the field of homogeneous catalysis. The catalytically properties of metal complexes are highly dependent on the ligand environment. A principal strategy is the employment of tailor made ligand systems to create metal complexes of specific nuclearity, coordination number, geometry and reactivity. Typical functions of such ligands are to inhibit oligomerization reactions, to stabilize the low valent form and/or the low oxidation state of the metal centre and to model the shape of the complex periphery. Thus, the interplay between metal, ligands and reagents controls the reactivity, selectivity, stability and lability in catalytical reactions.[6]

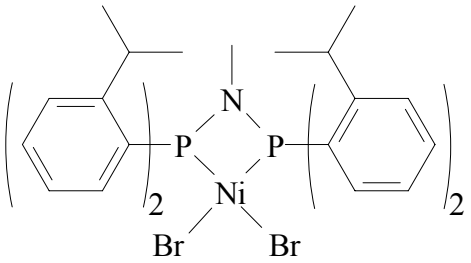

Scheme 1.3: *Late transition metal complex with bidentate ligands for polymerization.*[6i]

These examples illustrate that the syntheses of new ligands and the understanding of their specific properties is vital in the design of new materials, biochemistry and catalysis. Generally, the properties of coordination complexes are dependant on the nature of the

metal, but mutually on the steric, electronic and stereogenic effects of the fragments ligated to the metal *via* one sort of donor atoms (homotop ligands) or *via* different types of donor centres (heterotop ligands). Tuning these effects and understanding the resulting coordination patterns and reactivities is the challenge in ligand design.

The following scheme illustrates the different manipulation sites present in a chelating ligand. Solubility can be adjusted by the introduction of various organic substituents in the periphery of the donating atoms. Additionally, these residues provide steric bulk and can mimic hydrophilic or lipophilic sites. Different substituents at the donor centres might provide stereo information. The length of the spacer determines the bite angle of the ligand, the geometry and the conformations of the metallacycles, when acting as a chelat. Asymmetric centres in the spacer control stereoselectivity as auxiliaries. The choice of either hard or soft donor atoms determines the interactions with the metal fragments in terms of complex stabilities. These are the basic features to tailor a classical chelating ligand like diphosphanes, diamines or bipyridines (Scheme 1.4).

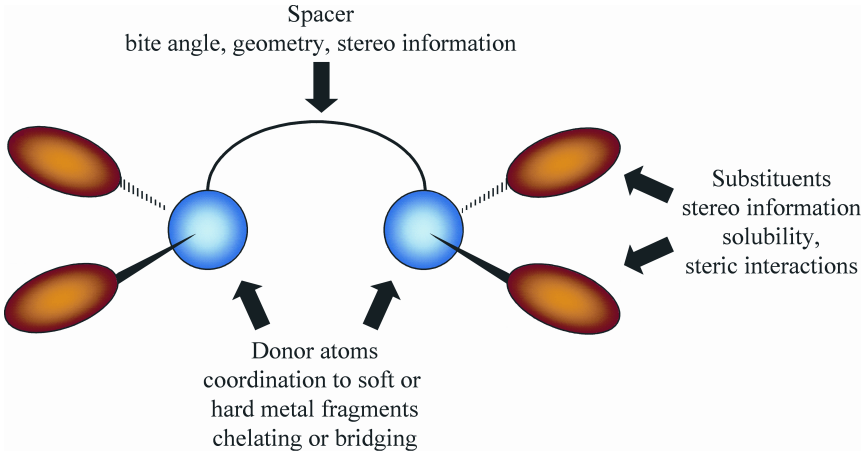

classical chelating ligand

Scheme 1.4: *Classical chelating ligands.*

The combination of donor atoms with different hardness or softness in one molecule leads to the design of polyfunctional, ambidentate ligand systems with unique properties, because the different features associated with each donor atom confer unique reactivity to their metal complexes. The donor centres can either bridge different metals or chelat them *via* different metal–ligand interactions. Also monodentate behaviour is possible. The introduction of reactive sites in the ligand periphery gives rise to the formation of charged,

localized or delocalized species, which enable electronic differentiation and switching of the coordination behaviour, dependent on the requirements of the metal (Scheme 1.5).

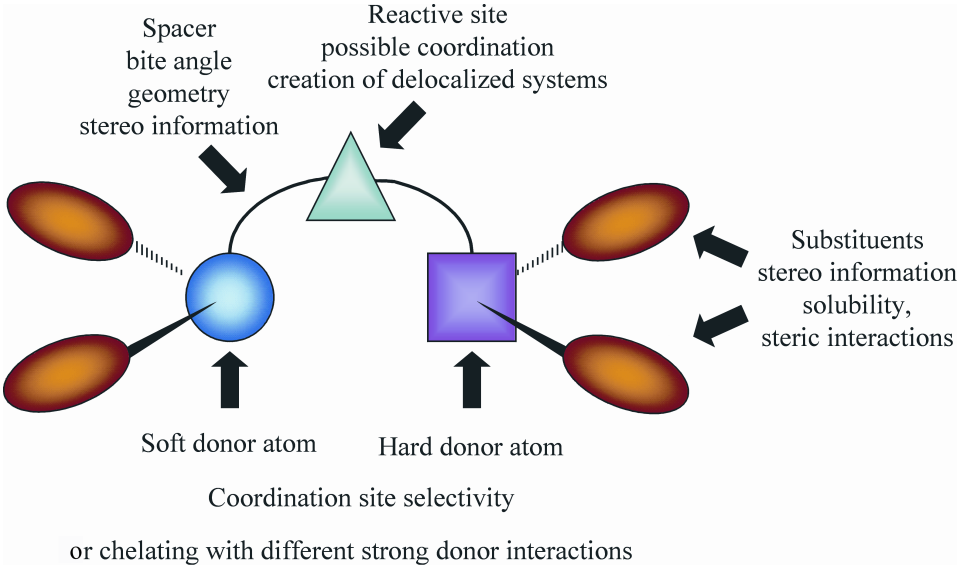

Scheme 1.5: *Polyfunctional, hemilabile systems.*

In this work, the reactivity and coordination behaviour of multifunctional phosphorus-nitrogen based ligand systems is examined (Scheme 1.6).

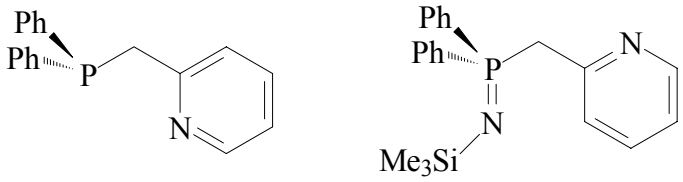

A **B**

Scheme 1.6: *Multifunctional, ambivalent phosphorus-nitrogen based ligands.*

The core structure of both ligands is comprised of a central phosphorus atom, substituted with two phenyl groups, providing steric bulk and solubility and a heterocycle bound to a methylene bridge. In the phosphane **A**, the soft phosphorus atom and the hard ring nitrogen atom are potential competive donating sites in metal complexes, whilst the methylene bridge supplies coordination flexibility. Monodentate and (*P,N*)-chelating behaviour of the neutral phosphane **A** is already described.[7] However, the acidic hydrogen atoms at the

methylene bridge provide the opportunity to generate monoanionic ligands with quite different coordination patterns and properties to those found for the neutral species. In this work, this reactive site will be explored, and some unusual coordination patterns for the potentially tridentate (*P,N,C*)-coordinating ligand will be described. Recently, some derivatives of the phosphane **A** found an application in catalytic reactions.[8]

The iminophosphorane **B** is the oxidized derivative of the phosphane **A**. Here, the former phosphorus(III) donor centre is blocked by an $NSiMe_3$-moiety. This substituent not only ensures good solubility, but has also other functions as will be described in chapter three. The reactive sites in the iminophosphorane **B** are the two different nitrogen donor centres and the acidic hydrogen atoms at the methylene C_α-atom. Here, the coordination flexibility and the bonding of the neutral ligand as well as its anion will be elucidated.

2 Diphenyl(-2-)picolylphosphane

2.1 Scope

An essential concept in ligand design is that of hemilabile ligands, introduced by *Rauchfuss* in 1979.[9] Hemilabile ligands combine the properties of soft and hard donor atoms in one molecule. The term *"hemilabile"* was originally used for (*P,N*)- and (*P,O*)-ligands, that "would bind well enough to permit isolation, but would readily dissociate the hard end component, thus generating a vacant site for substrate binding". There has been an increasing interest in synthesis, characterization and use of hemilabile ligands, as the different features associated with each donor atom confer unique reactivity to their metal complexes.[10]

An important property of these potentially multidentate ligands is to stabilize metal cations in different oxidation states and geometries.[11] Additionally, one donor atom is weakly coordinated to the metal centre and can easily dissociate in solution, creating a vacant site for substrate binding, whereas their chelat effect gives stability to the potential catalyst precursor in the absence of substrate. This versatility is of current interest in basic research and for applications.[12] It is interesting to note that also in some metalloenzymes a similar behaviour is observed: The opening of a zinc–cystein bond, allowing coordination of a water molecule occurs when going from an inactive to an active form of a metalloenzyme.[13] Furthermore, double functionalized porphyrins with imidazole containing "arms" reversibly bind O_2 or CO, involving displacement of one imidazole arm.[14]

The combination of phosphorus and nitrogen atoms makes a distinguished family of hemilabile ligands. These ligands can display quite different coordination modes compared to the classical (*P,P*)- or (*N,N*)-chelats.[15] The π-acceptor character of the phosphorus atom can stabilize metal centres in low oxidation states, while nitrogen σ-donor ability makes the metals more susceptible to oxidative addition reactions. This can help to stabilize intermediate oxidation states or geometries during a catalytic cycle.

Recently, attention has been focused on chiral (*P,N*)-ligands: they have been employed very successfully in asymmetric catalytic reactions such as allylic substitution,[16] hydrosilylation,[17] hydroboration[18] and hydrogen transfer reactions.[19]

Polydentate ligands combining hard and soft donor atoms are excellent candidates for the preparation of heterobimetallic compounds containing a hard and a soft mixed-metal centre. Compounds, comprised of more than one metal in close proximity might exhibit different properties, compared to the monometallic fragments that constitute them: cooperative reactivity patterns, stabilization of unusual ligand coordination modes, higher catalytic activity or different selectivity than the corresponding mononuclear moieties.[20]

In our group we are interested in the synthesis and coordination behaviour of 2-pyridyl substituted *sec*.-phosphanes and *sec*.-phosphanides.[21,22] Pyridine is an electron deficient aromatic system, because the electronegative ring nitrogen atom attracts π-electron density. In metal complexes the localized electron pair at the hard ring nitrogen atom acts as σ-donor. Additionally, this ligand has π* orbitals with low energies, which enhances π-backbonding from a metal to the ligand. These properties explain the stability of pyridine complexes also with metals in low oxidation states.[23] The incorporation of pyridyl substituents at a soft phosphorus centre in the place of commonly applied alkyl or phenyl groups alters and augments the coordination flexibility of the ligand and leads to mulitdentate hemilabile ligands. Free rotation about the P–C_{ipso} bond can easily bring the pyridyl nitrogen atoms into the right position to coordinate metals of different radii. Pyridyl substituted *sec*-phosphanes are easily deprotonated giving delocalized anionic systems. Thus, apart from the geometrical flexibility, the *sec*-phosphanides provide electronic adaptility as well. Towards hard metal fragments the $[Py_2P]^-$-anion acts as (*N,N*)-bidentate chelat (Scheme 2.1, **A**, **B**). The phosphanide $[(thf)_2Li(Py_2P)]$ forms an almost planar metallacycle with the thf molecules above and below the plane of the ring system (**A**).[24] However, in the aluminium species $[AlMe_2(Py_2P)]$, the ligand shows a butterfly arrangement (**B**).[25] With soft metals, like cesium, the ligand behaves like a (*P,N*)-chelat, but additionally binds the metal *via* π-interactions, forming a dimer, in which one pyridyl nitorgen atom is not involved in coordination (**C**).[26] The coordination mode of the $[Py_2P]^-$-anion in the iron phosphanide $[(CO)_4Fe_2(Cp)_2(Py_2P)][BMe_4]$ shows, that the central phosphorus atom is *Lewis*-basic enough to bridge two iron centres. In this complex none of the ring nitrogen atoms coordinates the metal (**D**).[26]

These results show, that the dipyridylphosphanide ligand shows a metal-dependent coordination response, although theoretical calculation for [$AlMe_2(Py_2P)$] suggest, that there is not much electron density left at the divalent phosphorus centre (Scheme 2.1).[21,22,24–27]

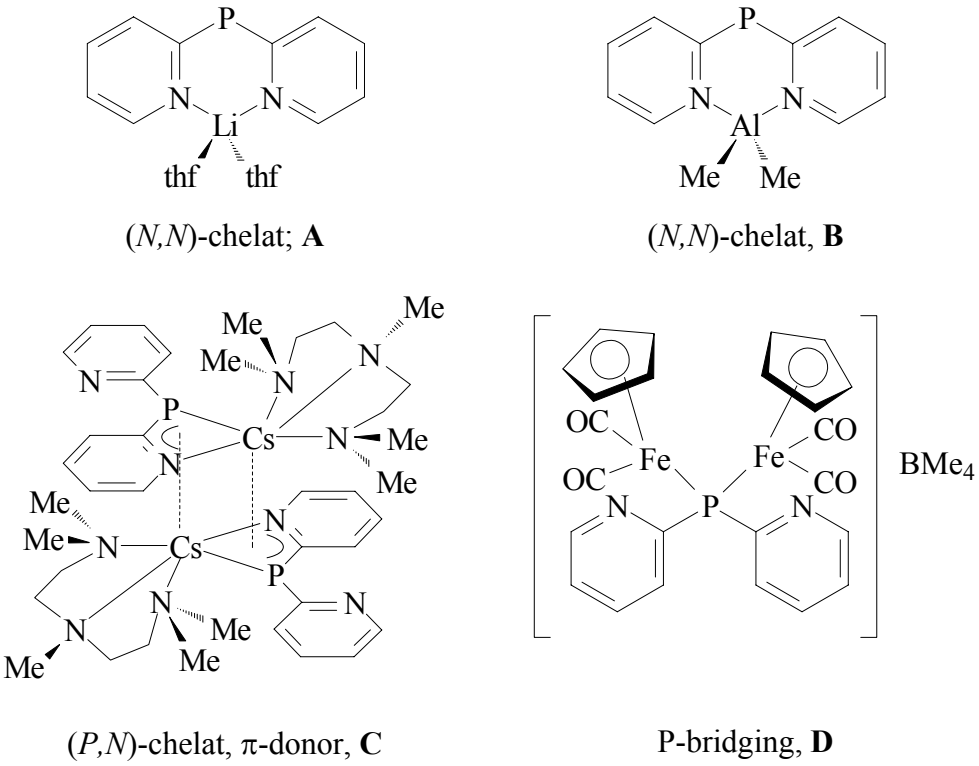

Scheme 2.1: *Coordination flexibility of the [Py_2P]$^-$-anion.*

To get a higher geometrical adaptability it is of interest to introduce alkyl bridges between the phosphorus atom and the heterocycle. Depending on the length of the alkyl bridge it is possible to tune the bite angle of the chelats and therefore tune them to various organometallic fragments. Although known for a long time, pyridylphosphanes with the phosphorus centre separated from the pyridyl ring by methylene links have not been studied extensively in contrast to the pyridylphosphanes $Ph_{3-n}Py_nP$ (n = 1–3), which have been widely used as homo- and heterometallic binucleating ligands.[15]

The methylene bridged phosphane Ph_2PCH_2Py, (**1**), and the metal complexes $[(Ph_2PCH_2Py)_2NiX_2]$ (X = NCS, Cl), $[(Ph_2PCH_2Py)_2NiX][X]$ (X = Br, I) and $[(Ph_2PCH_2Py)_2Ni][ClO_4]_2$ were reported by *Uhlig* in 1968.[7a] Also some molybdenum and iron complexes of **1** are already known (Scheme 2.2).[7]

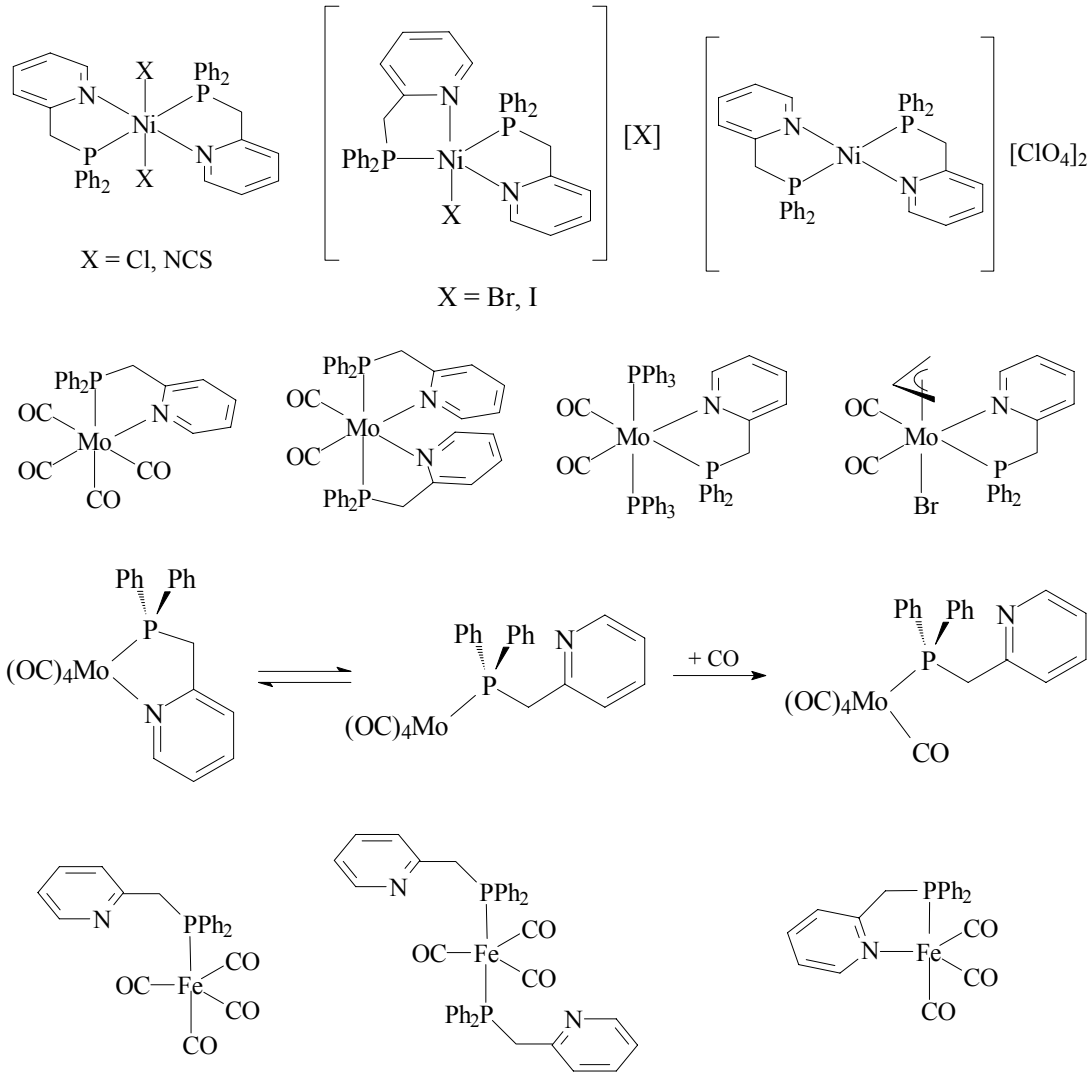

Scheme 2.2: *Metal complexes of Ph_2PCH_2Py, (1).*

Recently, pyridylphosphanes of the type $Ph_2PC(H)(R)Py$ (R = H, H_2COEt, $C_3H_6Si(OMe)_3$, $H_2COMent$) gained increasing importance in catalysis as neutral hemilabile ligands and several coordination complexes have been isolated and studied (Scheme 2.3).[28]

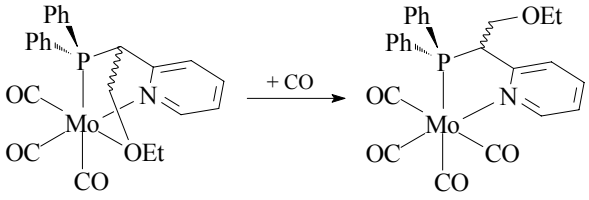

A

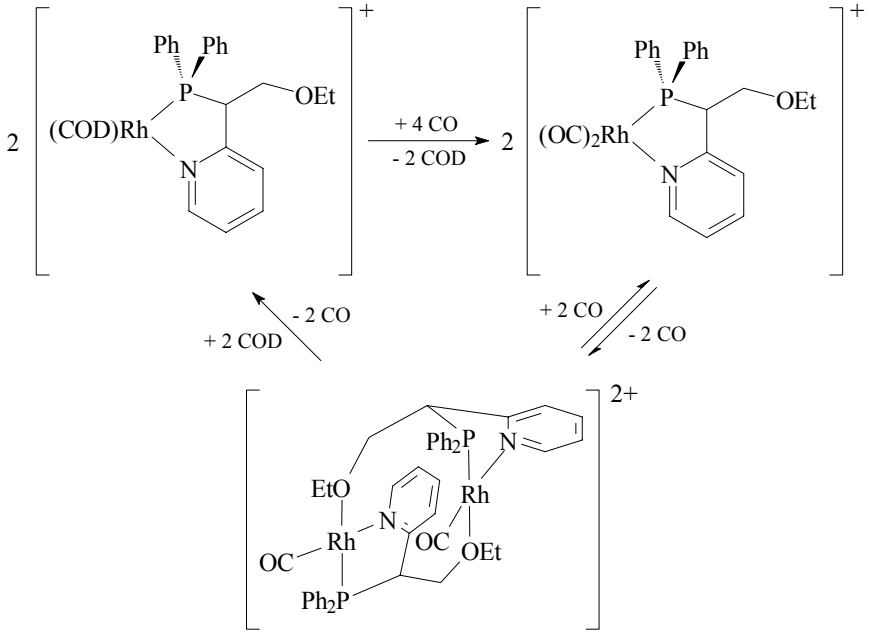

B

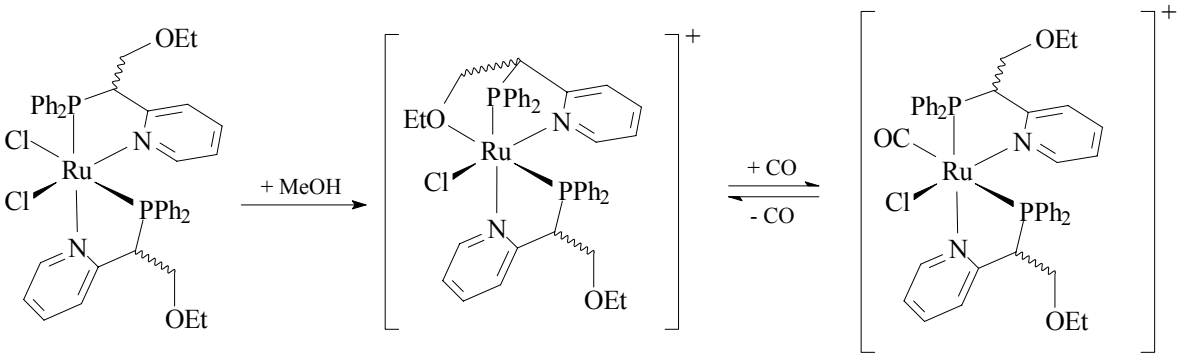

C

Scheme 2.3: *Hemilabile behaviuor of pyridylphosphanes of the type $Ph_2PC(H)(R)Py$.*

The C_α-substituted derivative of Ph_2PCH_2Py, (**1**), $Ph_2PCH(CH_2OEt)Py$ acts as a tridentate ligand, but if a substrate like CO is present, the CH_2OEt side-arm dissociates from the molybdenum centre and CO binds to the metal (Scheme 2.3, **A**). Scheme 2.3, **B** depicts the

(*P,N*)-chelating behaviour of the ligand. Like in the last example in the rhodium complex a CO-substituent can reversibly dissociate. If the ether function is employed in the coordination it acts as bridge between two rhodium centres, yielding a dinuclear complex. The dichlororuthenium complex in **C** of scheme 2.3 also reflects the hemilabile behaviour of the neutral $Ph_2PCH(CH_2OEt)Py$ ligand. In polar protic solvents a chlorid ion dissociates from the metal centre and the vacant coordination site is reoccupied by intramolecular O side-arm donation. In the presence of CO this labile Ru–O bond is cleaved and the CO molecule binds to the ruthenium atom.[28]

The dichlororuthenium complex **A** of scheme 2.4 is one of the most efficient ruthenium based catalysts for the transfer hydrogenation of ketones to propan-2-ol.[8a] In **B**, the ethyl group of the ether side-arm of **A** is replaced by the chiral menthyl substituent. Complex **B** can be prepared enantiomerically pure and is tested in asymmetric transfer hydrogenations.[8b] The rhodium complex **C** shows high activities and selectivities in the transformation of arenes, when tethered to a silica-supported palladium catalyst (Scheme 2.4).[8c]

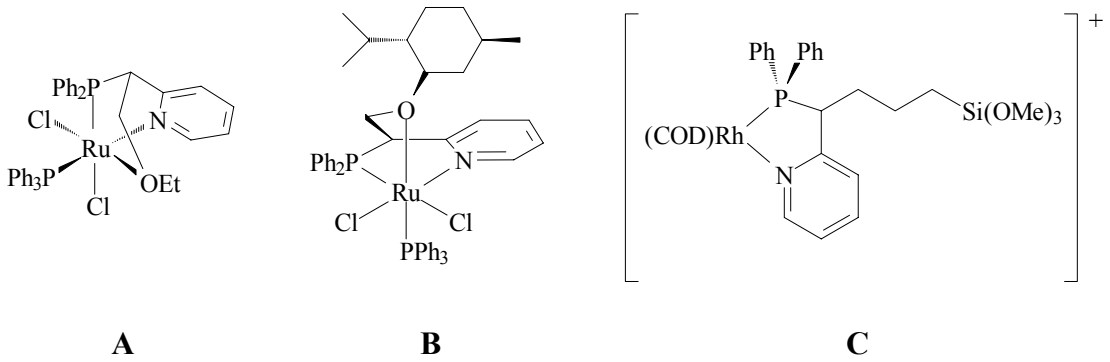

A **B** **C**

Scheme 2.4: *Catalytical active pyridylphosphanes of the type $Ph_2PC(H)(R)Py$.*

In all the abovementioned complexes the C_α-substituted derivatives of the phosphane Ph_2PCH_2Py, (**1**) were employed as neutral ligands. However, the acidic hydrogen atoms at the methylene bridge also open the way to new mono- or dianionic phosphanide compounds. This reactive site of the phosphane **1** and its derivatives was not examined so far. The electropositive phosphorus centre should be able to stabilize the negative charge at the C_α-position, but the electron deficient nature of the pyridyl susbstituent may lead to delocalization. Thus, apart from the geometrical flexibility, given by the methylene bridge and free rotation about the $P–CH_2$ bond, these charged species should have an enhanced electronical adabtility as well. They may act as (*P,N*)-chelats with a delocalized negative

charge and with quite different bonding properties compared to the neutral phosphane Ph_2PCH_2Py, (**1**) (Scheme 2.5, **A**). Dependent on the electronic requirements of the metal, also C-coordination seems feasible. Together with the potential P- and N-donor centres this may even lead to dinuclear homo- or heterometallic complexes (Scheme 2.5, **B** and **C**).

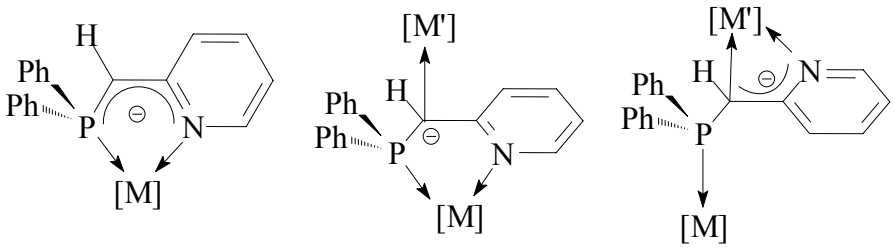

A **B** **C**

Scheme 2.5: *Potential coordination modes of the $[Ph_2PC(H)Py]^-$-anion.*

In this work, the coordination behaviour of the C_α-deprotonated diphenyl-2-picolylphosphane $Ph_2P(CH_2Py)$, (**1**), is elaborated.

2.2 Synthesis of the diphenyl(-2-)picolylphosphane (1)

The phosphane Ph_2PCH_2Py, (**1**), was synthesized in a modified procedure to that described by *Alvarez et al*.[28] To a solution of Ph_2PCl in Et_2O a solution of $[(Et_2O)Li(H_2CPy)]_2$[29] in Et_2O was added very slowly at -78°C. After evaporation of the solvent, the residue was distilled in vacuum, leading to a yellow oil. The addition of hexane to the oil, cooling to -10°C and stirring resulted in the formation of **1** as a white solid, hardly soluble in non-polar solvents. It turned out that the yield of **1** can be increased up to 85% using a large amount of solvent for the reaction and slow addition of the lithiumalkyl to the diphenylchlorophosphane over a period of five hours (Equation 2.1).

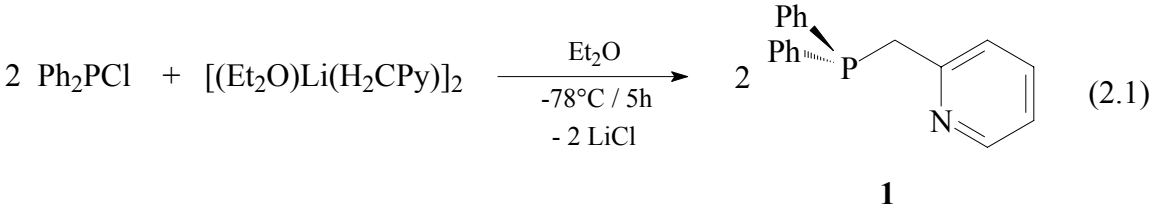

(2.1)

1

The phosphane Ph_2PCH_2Py, (**1**), melts at 54°C. The NMR-data of **1** are in agreement with those published. A $^{1}H,^{15}N$-HMBC-NMR experiment resulted in a signal at -62 ppm for the pyridyl nitrogen atom.

The solid state structure of Ph_2PCH_2Py, (**1**), depicted in Figure 2.1, was determined by a X-ray diffraction experiment form crystals grown from a solution of **1** in Et_2O. Selected bond lengths and angles of **1** are given in table 2.1.

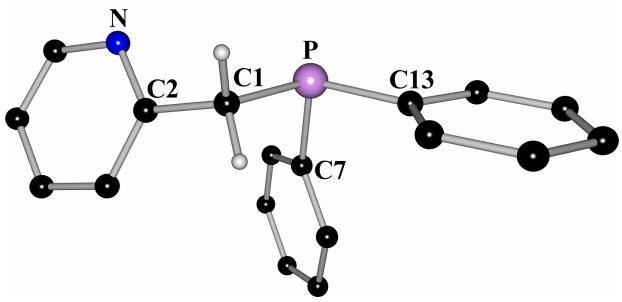

Figure 2.1: *Solid state structure of Ph_2PCH_2Py, (**1**).*

Table 2.1: *Selected bond lengths [pm] and angles [°] of Ph_2PCH_2Py, (**1**).*

P–C1	185.59(14)	P–C1–C2	112.14(9)
C1–C2	149.95(18)	C1–P–C7	99.32(6)
C2–N	133.97(18)	C1–P–C13	99.87(6)
av. P–C_{Ph}	183.95	C7–P–C13	101.44(6)

As expected, the central phosphorus atom shows a pyramidal coordination sphere with a stereochemically active lone pair. The C–P–C angles with an average value of 100.21° are smaller than the ideal tetrahedral angle of 109.4°. The P–C1 and P–C_{Ph} bond lengths are in the range quoted for P–C single bonds (P–C: 185 pm),[30] with the P–C_{Ph} distances ca. 1.6 pm shorter than the P–C1 bond, due to the smaller radius of the sp^2-hybridized carbon atoms C7 and C13 *versus* the sp^3-hybridization of C1.

2.3 Reactions of the diphenyl(-2-)picolylphosphane (1) with lithiumorganics

2.3.1 Synthesis of $[(thf)_2Li\{Ph_2PC(H)Py\}]$, (2)

The deprotonation at the C_α-position in the phosphane Ph_2PCH_2Py, (**1**), with lithiumorganics was previously described. However, the lithiated derivative was used *in situ* for the preparation of C_α-substituted phosphanes $Ph_2PC(H)(R)Py$ (R= H, H_2COEt, $C_3H_6Si(OMe)_3$, $H_2COMent$), without any characterization of the intermediate species.[8,28] To examine the coordination behaviour of the C_α-deprotonated $[Ph_2PC(H)Py]^-$-anion, the phosphane **1** was reacted with *n*-BuLi at -78°C in diethyl ether. Evaporation of the solvent resulted in an orange powder, which was recrystallized from a hexane/thf solution (Equation 2.2).

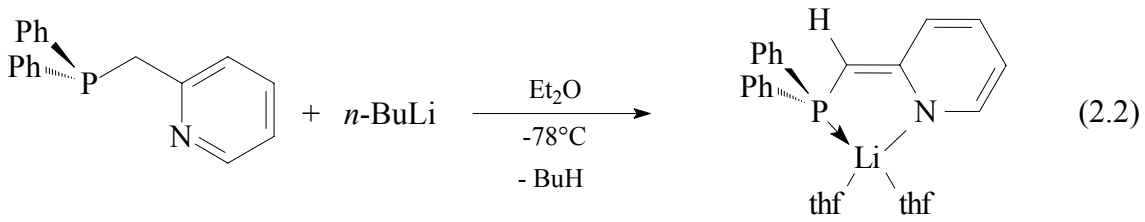

1 **2** (2.2)

Storage of the solution at 4°C for two days gives orange needles, decomposing at 82°C. Figure 2.2 shows the solid state structure of the lithium complex $[(thf)_2Li\{Ph_2PC(H)Py\}]$, (**2**), selected bond lengths and angles are summerized in table 2.2.

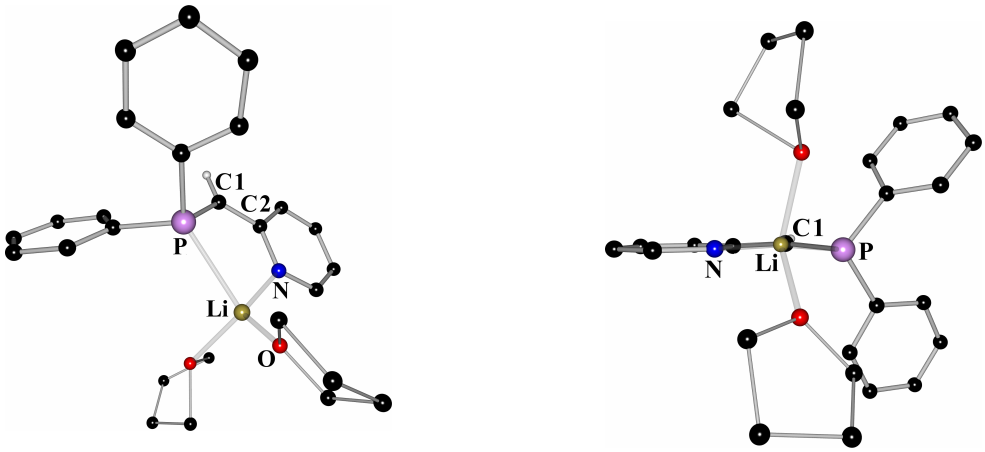

Figure 2.2: *left: Solid state structure of $[(thf)_2Li\{Ph_2PC(H)Py\}]$, (**2**), and right: view along the Li1–C1 bond of **2**, to illustrate the planarity of the five membered metallacycle.*

Table 2.2: *Selected bond lengths [pm] and angles [°] of [(thf)$_2$Li{Ph$_2$PC(H)Py}], (**2**).*

P–C1	175.9(2)	P–C1–C2	122.69(16)
C1–C2	139.0(3)	P–Li–N1	83.34(14)
C2–N	138.0(3)	O–Li–N	124.7(2)
Li–N	202.2(5)	C1–P–Li	91.76(12)
Li–P	257.4(4)	C7–P–Li	129.51(11)
	av. P–C_{Ph} 184.65		

In **2**, the central lithium cation is integrated in a five membered metallacycle by simultaneous coordination to the phosphorus atom and the pyridyl nitrogen atom of the anionic ligand. The four fold coordination sphere is completed by two oxygen atoms of two thf donor molecules. The coordination polyhedron around Li is best described as a severely distorted tetrahedron with angles varying from 83.34° for the endocyclic angle N–Li–P to 124.7° for O–Li–N. The five membered metallacycle in **2** is almost planar as the C1–C2–N1-plane intersects the C2–C1–P1- and P–Li–N-planes at angles of 6.1° and 6.2°, respectively (Figure 2.2. right). The two thf molecules, coordinated to the lithium cation, are positioned above and below the plane defined by the metallacycle. The phosphorus atom also shows distorted tetrahedral coordination with the endocyclic C1–P–Li angle the narrowest (91.76(12)°) and the exocyclic angles varying from 101.87(10)° to 129.51(11)°. The angle P–C1–C2 is 122.69(16)°, indicating sp^2-hybridization for the C1 atom. The sum of the angles at C1 of 360° illustrates the planar coordination sphere of this atom. The Li···C1 distance of 316.2 pm indicates, that the cation does not interact with the deprotonated 'carbanionic' C1 atom. The monomeric nature of [(thf)$_2$Li{Ph$_2$PC(H)Py}], (**2**), and the fact, that the lithium cation in **2** prefers coordination to the soft phosphorus atom rather than to the hard carbanionic centre is quite surprising as alkali metal complexes tend to form oligomeric structures.[31]

The P–C_{Ph} distances of on average 184.65 pm are identical within their esds and show no significant difference in comparison to the phosphane Ph$_2$PCH$_2$Py, (**1**) (av. 183.95 pm). The P–C1 bond length of 175.9(2) pm is substantially shorter than expected for a P–C single bond (185 pm),[30] suggesting significant P–C multiple bond character and charge delocalization. This distance is similar to those observed in lithiated phosphanemethanide complexes, like [(tmeda)Li(H$_2$CPPh$_2$)]$_2$ (175.2 pm)[32] and [(tmeda)Li(H$_2$CPMe$_2$)]$_2$ (av. 175.3 pm).[33] Furthermore, the C1–C2 distance of 139.0(3) pm is shorter than a formal C–C single bond. In comparison to the phosphane **1**, the P–C1 bond is 9.7 pm and the

C1–C2 bond is 10.95 pm shorter. As a consequence the C2–N distance in the pyridyl substituent of 138.0(3) pm in [(thf)$_2$Li{Ph$_2$PC(H)Py}], (**2**), is ca. 4 pm longer than in **1**. These structural parameters illustrate, that the negative charge generated by the deprotonation at the bridging C1 is delocalized over the [P–C(H)–Py]-fragment in the anionic ligand, leading to short P–C1 and C1–C2 distances, due to high electrostatic interactions and/or polarization effects.

The canonical formulas, which can be derived form the structural parameters are depicted in scheme 2.6.

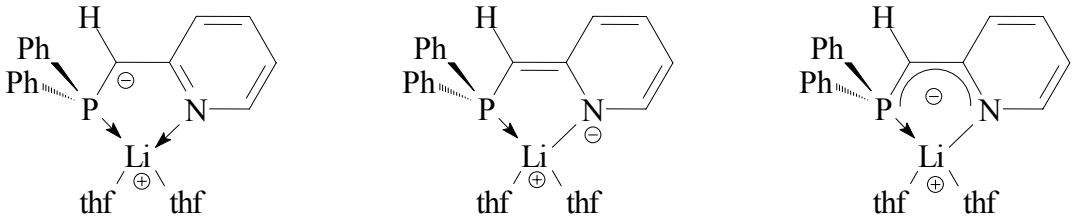

Scheme 2.6: *Canonical structures of [(thf)$_2$Li{Ph$_2$PC(H)Py}], (**2**): a) shows the carbanionic character of the ligand; b) depicts the amidic resonance form and c) illustrates charge delocalization over the [P–C(H)–Py]$^-$-fragment.*

The Li–P distance in [(thf)$_2$Li{Ph$_2$PC(H)Py}], (**2**), of 257.4(4) pm is in the range quoted for Li–P contacts (246 – 291 pm).[34] It is comparable to those found in lithium phosphane–methanide complexes, like [(tmeda)Li{C(PPh$_2$)$_2$(SiMe$_3$)}] (253.0 pm),[35] [(tmeda)Li-{HC(PPh$_2$)$_2$}] (258.2 pm)[36] or [(tmeda)Li(H$_2$CPMe$_2$)]$_2$ (av. 260.4 pm).[33]

In **2**, the Li–N bond is 202.2(5) pm long. Comparable Li–N contacts in pyridyl substituted anions vary from 197 to 208 pm.[37] In [(Et$_2$O)Li(H$_2$CPy)]$_2$ the Li–N distances range from 212.1 pm for the η^3-aza-allyl-coordinated lithium atom to 201.8 pm for the σ-type Li–N interaction.[29] In **2**, the Li–N bond length is similar to the amidic Li–N interaction found in the N-deprotonated amide [(thf)$_2$Li$_2$\{PhP(CH$_2$SiMe$_2$NPh)$_2$\}] (205.8 to 213.4 pm).[38]

To get insight in the charge distribution of the anion, several NMR spectra of [(thf)$_2$Li{Ph$_2$PC(H)Py}], (**2**), were recorded in solution. In comparison to the phosphane Ph$_2$P(CH$_2$Py), (**1**) , the signal in the ^{31}P-NMR spectra (δ = -11.4), is shifted upfield to δ = -23.5. In the ^{1}H-NMR spectra, the single hydrogen atom at the carbon atom of the methylene bridge gives rise to a doublet at 3.83 ppm with a coupling constant of

$^{2}J_{P-H}$ = 7.1 Hz. In the ^{7}Li-NMR spectrum, the lithium atom resonates as a singulet at δ = 1.65. As expected, for the electron deficient nature of the pyridyl substituent at the deprotonated carbon atom, the signal for the pyridyl nitrogen atom in the ^{1}H, ^{15}N-HMBC-NMR spectra is remarkably shifted upfield to -160 ppm. The difference to the ^{15}N shift observed in the phosphane **1** (δ = -62.2) is Δδ = -98 ppm. This might be taken as a hint that the negative charge in [(thf)$_2$Li{Ph$_2$PC(H)Py}], (**2**), is predominantly accumulated at the pyridyl nitrogen atom.

The structural parameters together with the NMR data obtained for **2**, suggest a descriptipon of **2** more as a phosphanamide rather than a carbanionic phosphanemethanide (Scheme 2.7).

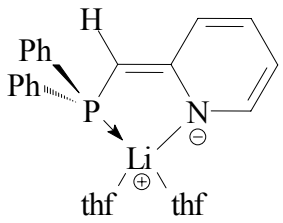

Scheme 2.7: *Lewis structure of [(thf)$_2$Li{Ph$_2$PC(H)Py}], (**2**), according to the structural parameters and NMR-data.*

2.3.2 Alkyllithium mediated P–C bond cleavage in Ph_2PCH_2Py, (1)

The reaction of Ph_2PCH_2Py, (**1**), with *n*-BuLi in Et_2O described in the previous chapter yields the phosphanamide $[(thf)_2Li\{Ph_2PC(H)Py\}]$, (**2**), in which the deprotonated C_α-centre shows no contact to the lithium cation. It is known that the degree of aggregation in lithium complexes is highly dependent on the presence of donating solvents, like thf in **2**.[31] Thus, the use of non-polar solvents in the reaction of **1** with lithium organics should force the lithium cation to coordinate to the carbanionic centre by formation of an oligomeric structure. Hence, Ph_2PCH_2Py, (**1**), was reacted with methyl lithium in toluene (Equation 2.3). The reaction product $[(thf)_2Li_4(PPh_2)_2\{Ph_2PC(H)Py\}_2]$, (**3**), was crystallized by dropwise addition of thf to the orange suspension obtained after seven days reaction time and cooling the orange solution to -16°C.

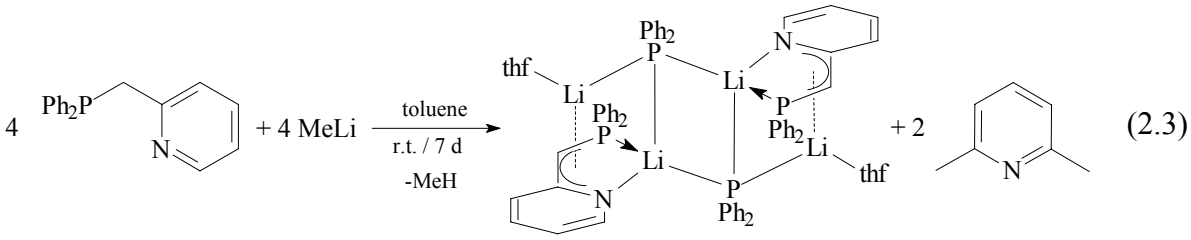

(2.3)

1 **3**

The lithium complex $[(thf)_2Li_4(PPh_2)_2\{Ph_2PC(H)Py\}_2]$, (**3**), contains two different anions. Firstly, the phosphane $Ph_2P(CH_2Py)$, (**1**), is deprotonated at the C_α-position, yielding an anionic $[P–C(H)–Py]^-$-fragment similar to that found in $[(thf)_2Li\{Ph_2PC(H)Py\}]$, (**2**). Secondley, a $P–CH_2$ bond is cleaved, resulting in the formation of the diphenyl–phosphanide $[Ph_2P]^-$-anion.

It is known, that tertiary phosphanes can undergo ligand exchange and coupling reactions in the presence of lithium organics.[39] Several theoretical studies elucidate the reaction mechanisms involved in the formation of the different products.[40,41] *Budzelaar* examined ligand coupling reactions of pyridyl substituted phosphanes with lithium organics. For monopyridyl substituted phosphanes PyR_2P he showed, that the attack of the carbanion of the lithiumorganic reactant at the pyridyl carbon atom neighbouring the ring nitrogen atom is the energetically most favourable reaction pathway.[41,42] Considering these results, the

mechanism, depicted in scheme 2.8 seems reasonable for the formation of the diphenylphosphanide anion.

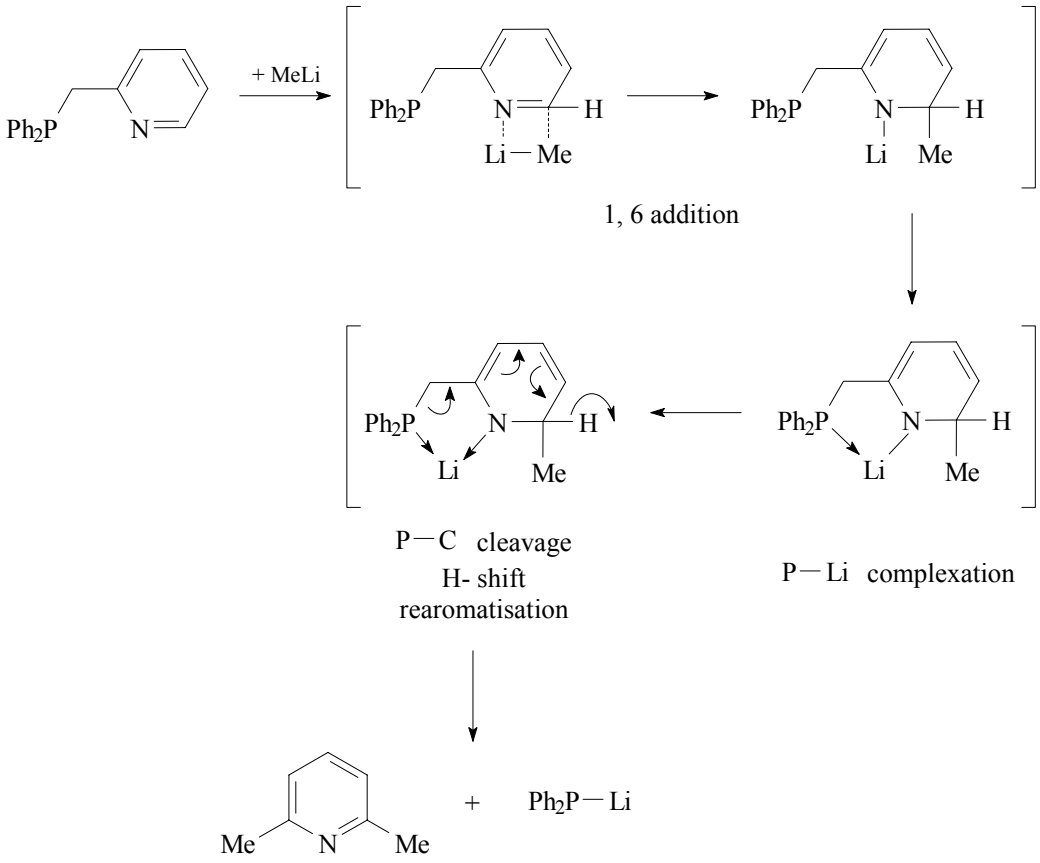

Scheme 2.8: *Proposed mechanism for the formation of the [Ph_2PLi].*

A 1,6-addition of methyl lithium to the pyridyl ring leads to the formation of a dihydropyridyl derivative. The cation gets coordinated by the lone pair of the phosphorus centre. The cleavage of the P–CH_2 bond gives an exocyclic dihydropyridyl olefin, which can reorganize by $[H]^+$-shift or elimination of the proton at the methyl substituted carbon atom of the pyridyl ring and addition of this proton to the terminal carbon atom of the olefin, yielding the stable aromatic 2,6-dimethylpyridine. However, the dimethylpyridine could not be isolated or characterized unambiguously up to now.

The solid sate structure of $[(thf)_2Li_4(PPh_2)_2\{Ph_2PC(H)Py\}_2]$, (**3**), is shown in figure 2.3; selected bond lengths and angles are given in table 2.3.

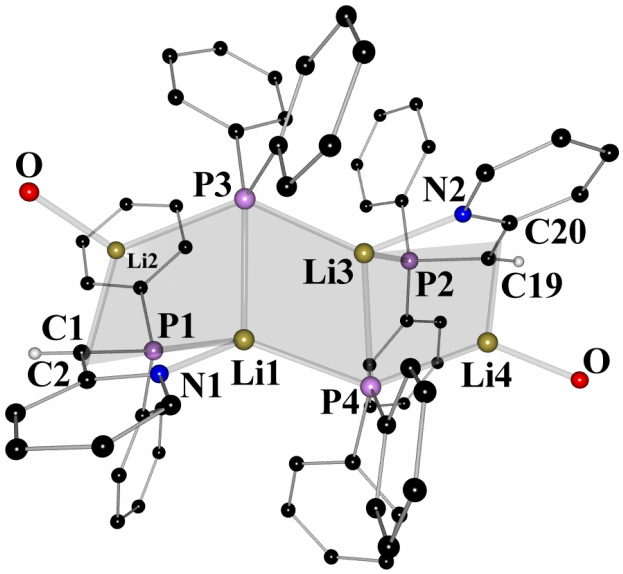

Figure 2.3: *Solid state structure of $[(thf)_2Li_4(PPh_2)_2\{Ph_2PC(H)Py\}_2]$, (**3**). The carbon atoms of the thf molecules at Li2 and Li4 omitted for clarity.*

Table 2.3: *Selected bond lengths [pm] and angles [°] of $[(thf)_2Li_4(PPh_2)_2\{Ph_2PC(H)Py\}_2]$,(**3**).*

P1–C1	177.0(2)	P2–C19	177.3(2)	Li2–P3	256.1(4)
C1–C2	142.0(3)	C19–C20	141.3(3)	Li2–N1	245.2(5)
C2–N1	137.4(3)	C20–N2	137.6(3)	Li2–C1	228.1(4)
Li1–N1	202.6(4)	Li3–N2	204.7(4)	Li2–C2	236.8(4)
Li1–P1	254.9(4)	Li3–P2	253.9(4)	Li4–P4	255.3(4)
Li1–P3	264.7(4)	Li3–P3	260.5(4)	Li4–N2	261.4(5)
Li1–P4	255.9(4)	Li3–P4	263.0(4)	Li4–C19	226.8(5)
P1–C1–C2	119.64(17)	P2–C19–C20	118.74(17)	Li4–C20	242.1(5)
Li2–P3–Li3	134.91(13)	Li4–P4–Li1	139.24(13)		

At first sight the solid state structure seems to be symmetrical with a centre of inversion in the middle of the Li1–P3–Li3–P4 four membered ring, however, the two thf molecules coordinated at the terminal Li2 and Li4 atoms, respectively, point to the same side.

The two products of the reaction [$Li(Ph_2PC(H)Py$] and [$LiPPh_2$] co-crystallize in a ladder-type framework, built by association of a single four membered Li_2P_2 and two $Li_2PN\eta^2$-(CC)-rings. The oxygen atoms at Li2 and Li4, respectively, terminate this ladder-type structure. Steric interactions in the assembly lead to changes in the structural parameters of the similar subunits, each consisting of two lithium cations (Li1/2 *vs.* Li3/4), a $[Ph_2P]^-$-

anion (P3 *vs.* P4), a [P–C(H)–Py]$^-$-unit (P1–C1–C2–N1 *vs.* P2–C19–C20–N2) and one thf molecule each.

The phosphorus atoms P3 and P4 of the diphenylphosphanide anions each bridge three lithium cations. The Li–P distances show remarkable differences (253.9(4)–264.7(4) pm). In [(pmdta)LiPPh$_2$] the Li–P distance is 256.7 pm,[43] whereas in the tmeda analogue [(tmeda)LiPPh$_2$]$_2$,containing a Li_2P_2 four membered ring, the Li–P contacts range from 257.3 to 262.9 pm. The mean Li–P distance in this molecule is 261 pm.[43] Comparable differences in Li–P bond lengths are also found in [(thf)Li$_2$(μ_3-^{t}Bu$_2$P)(μ_2-^{t}Bu$_2$P)]$_2$.[44]
Both phosphorus atoms P3 and P4 show a considerably distorted trigonal bipyramidal coordination sphere. The axial angles are 134.91(13)° for Li2–P3–Li3 and 139.24(13)° for Li4–P4–Li1 (Figure 2.4).

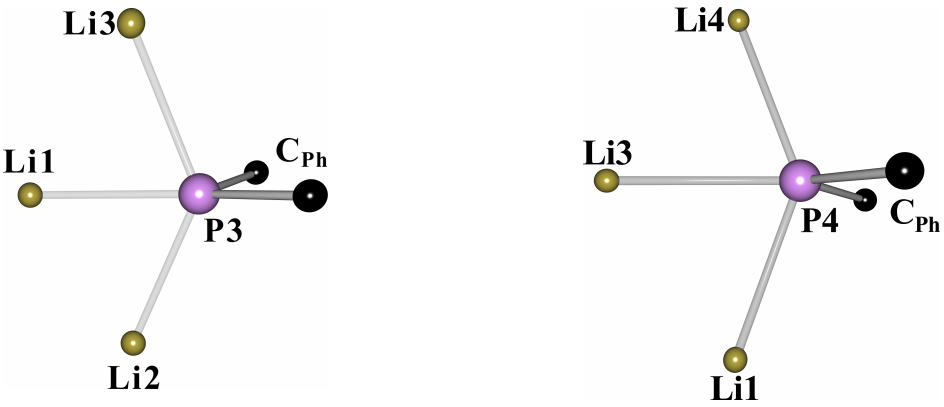

Figure 2.4: *Trigonal bipyramidal coordination sphere of the phosphorus atoms of the [Ph$_2$P]$^-$ ligands.*

Each lithium cation Li1 and Li3 is chelated *via* the phosphorus and ring nitrogen atom of a bidentate [Ph$_2$PC(H)Py]$^-$-anion. The tetrahedral coordination spheres of those lithium atoms are completed by interaction with both the P3 and P4 atoms of the [Ph$_2$P]$^-$-anions. The Li1–P1 (254.9(4) pm) and Li3–P2 distances (253.9(4) pm) are almost equal and comparable to those found in lithium phosphanemethanide complexes.[33,35,36] In comparison to [(thf)$_2$Li{Ph$_2$PC(H)Py}], (**2**), (257.4(4) pm) they are on average 3 pm shorter as a result of the different coordination behaviour of the [Ph$_2$PC(H)Py]$^-$-anion. The Li1–N1 contact is 202.6(4) pm, the Li3–N2 distance with 204.7(4) pm is ca. 2 pm longer. Both are in the range quoted for amidic lithium nitrogen interactions[37,38] and comparable to the Li–N contact found in **2** (202.2(5) pm).

The terminal thf complexed lithium cations Li2 and Li3 bind to the phosphorus atoms P3 and P4, respectively. Additionally, they are η^2-coordinated to the related [C1–C2]- and [C19–C20]-bonds. The nitrogen atoms N1 and N2 seem not to be involved in coordination to the cations, as the distances Li2···N1 of 245.2(5) pm and Li4···N2 of 261.4(5) pm are too long. In N-donor-base complexed lithiumorganics the average Li←N donor bond length is 215 pm.[31] The Li2–C1 distance in **3** of 228.1(4) pm is 8.7 pm shorter than the Li2–C2 contact (236.8(4) pm). This difference is remarkably larger in the Li4–C19/20 bond lengths, which differ by 15.3 pm. The Li–C contacts in $[(thf)_2Li_4(PPh_2)_2\{Ph_2P(CHPy)\}_2]$, (**3**), are in the range generally quoted for lithium carbon bonds (230 pm).[31] In **3**, they are comparable to those found in $[(tmeda)Li\{\eta^3\text{-}CH(CHSiMe_2{}^tBu)_2]$ (211–223 pm)[45] and in aza-allyl lithium compounds such as $[Li\{CH(SiMe_3)C(^tBu)N(SiMe_3)\}]_2$ (243–244 pm).[46,47]

As a result of the η^2-interaction together with the (*P,N*)-coordination to two different lithium cations, the structural parameters in the anions of **3** differ from those found in the (*P,N*)-coordinating anion in $[(thf)_2Li\{Ph_2PC(H)Py\}]$, (**2**). However, the comparable bond lengths and angles of both $[Ph_2PC(H)Py]^-$-anions in **3** are very similar. Thus, in the following discussion the averages are quoted; the exact values are given in table 2.3. The P1/2–C1/19 bond distances measure 177.2 pm and are 1.3 pm longer than in **2**. The C1/19–C2/20 distances (141.65 pm) are elongated as well by 2.65 pm in comparison to **2**. Like in $[(thf)_2Li\{Ph_2PC(H)Py\}]$, (**2**), these bond lengths are substantially shorter than formal P–C and C–C single bonds. The C2/20–N1/2 bonds of 137.5 pm match the distance found in **2** (138.0(3) pm). Whereas in **2**, the sum of the angles around the C_α-atom is 360°, in **3** this sum of angles around C1 and C19 is on average 355°, consistent with a slight pyramidalization due to the η^2-coordination of the lithium metal. Also the observed planarity of the [N–C–C–P–Li] five membered ring in **2** is not maintained in the solid state structure of **3** (Figure 2.5).

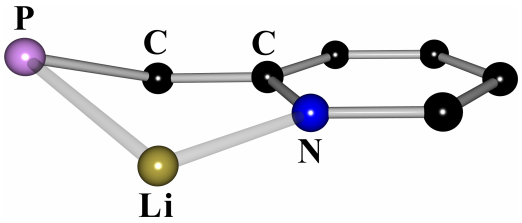

Figure 2.5: *Conformation of the five membered rings in $[(thf)_2Li_4(PPh_2)_2\{Ph_2PC(H)Py\}_2]$, (**3**).*

These parameters show, that the delocalization of the negative charge over the [P–C(H)–Py]⁻-fragments is not as pronounced as in **2**. The η^2-coordinations of the lithium cations result in longer P–C and C–C_{ipso} bonds and a more pyramidal environment of the C_α-atoms than in [(thf)$_2$Li{Ph$_2$PC(H)Py}], (**2**). It is obvious, that the electronic situation in the [Ph$_2$PC(H)Py)]⁻-anion is flexible, switching from more pronounced amidic, observed in [(thf)$_2$Li{Ph$_2$PC(H)Py}], (**2**), to more "carbanionic" found in [(thf)$_2$Li$_4$(PPh$_2$)$_2${Ph$_2$PC–(H)Py}$_2$], (**3**).

The ^{31}P-NMR spectra of **3** shows only two resonances at δ = -24.5 for the phosphorus atoms in the phosphanide [PPh$_2$]⁻-anion and at δ = -18.3 for the P-atoms in the [Ph$_2$P–C(H)Py]⁻-anion, indicating a centrosymmetric dimer on the NMR timescale. The single hydrogen atoms at the C_α-atoms resonate at δ = 3.60, shifted upfield by Δδ = 0.23 in comparison to the corresponding hydrogen atom in [(thf)$_2$Li{Ph$_2$PC(H)Py}], (**2**). In addition the signal for the C_α-atom in the ^{13}C-NMR spectrum is shifted to higher field in [(thf)$_2$Li$_4$(PPh$_2$)$_2${Ph$_2$PC(H)Py}$_2$], (**3**).

2.4 Syntheses of main group metal phosphanamides

2.4.1 Synthesis of [(thf)$_3$Sr{Ph$_2$PC(H)Py}$_2$], (4)

To get insight in the coordination behaviour of the [Ph$_2$PC(H)Py]⁻-anion to soft main group metal cations two equivalents of the phosphane Ph$_2$PCH$_2$Py, (**1**), were reacted with the strontium amide [(thf)$_2$Sr{N(SiMe$_3$)$_2$}$_2$].[48] The reaction yields the phosphanamide [(thf)$_3$Sr{Ph$_2$PC(H)Py}$_2$], (**4**). Each amide anion of [(thf)$_2$Sr{N(SiMe$_3$)$_2$}$_2$] deprotonates one equivalent of the phosphane **1** at C_α-positions. (Equation 2.4).

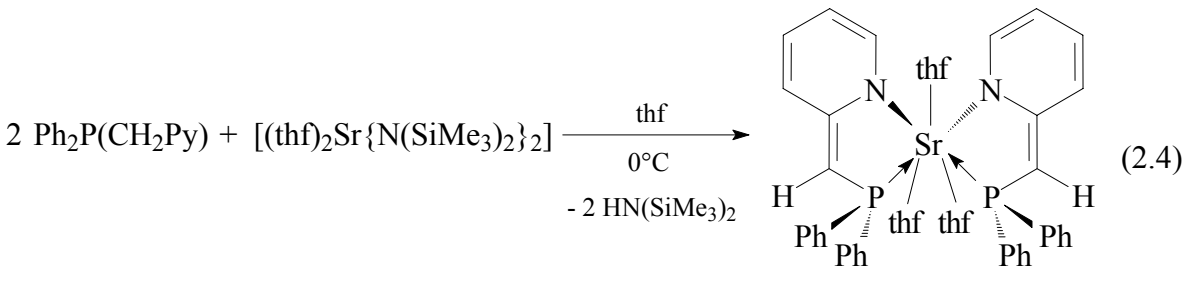

(2.4)

1 **4**

The amide **4** crystallizes at 4°C in orange blocks from a saturated thf solution. They melt at 108°C. The molecular structure of **4** is depicted in figure 2.6; selected bond lengths and angles are given in table 2.4. Structure solution and refinement was performed in the centrosymmetrical space group C2/c.

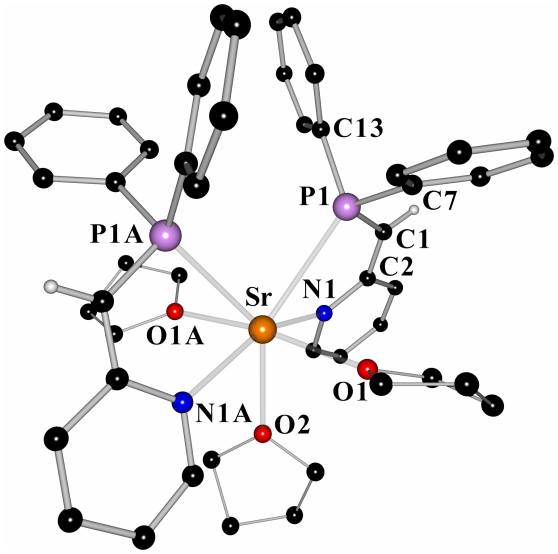

Figure 2.6: *Solid state structure of [(thf)$_3$Sr{Ph$_2$PC(H)Py}$_2$], (**4**).*

Table 2.4: *Selected bond lengths [pm] and angles [°] of [(thf)$_3$Sr{Ph$_2$PC(H)Py}$_2$], (**4**).*

P1–C1	174.55(15)	P1–C1–C2	123.92(11)
C1–C2	138.8(2)	P1–Sr–N1	63.40(3)
C2–N1	137.8(2)	P1–Sr–P1A	83.192(15)
Sr–P1	318.39(4)	N1–Sr–N1A	157.66(6)
Sr–N1	268.30(12)	N1–Sr–O2	78.83(3)
av. Sr–O	255.1		
	av. P–C$_{Ph}$ 184.15		

In [(thf)$_3$Sr{Ph$_2$PC(H)Py}$_2$], (**4**), the central strontium cation is coordinated to the phosphorus atoms P1 and P1A and the pyridyl nitrogen atoms N1 and N1A of the two deprotonated ligands. The two [Ph$_2$PC(H)Py]$^-$-anions coordinate to the strontium cation in a *cisoid* arrangement. The seven fold coordination sphere of the strontium atom is completed by the oxygen atoms of three thf donor molecules. The strontium cation is placed 35.5 pm above the N1–N1A–O1–O1A least square plane. Thus, the oxygen atom O2 and the phosphorus atoms P1 and P1A occupy apical positions. The P1–Sr–P1A angle of 83.192(15)° is acute, while the N1–Sr–N1A angle of 157.66(6)° is wide. This coordination situation enables the apical thf molecule to approach the metal ion to

complete the hepta coordination envelope around the strontium atom by fitting in perfectly between the two pyridyl nitrogen atoms (N1–Sr–O2 78.83(3)°).

The [P1–C1–C2–N2]-units are almost planar, as the P1–C1–C2-plane intersects the C1–C2–N1-plane at an angle of only 1.8°. Figure 2.7 illustrates the envelope conformation of the five membered rings and the displacement of the cation from the metallacycle ring plane (65 pm).

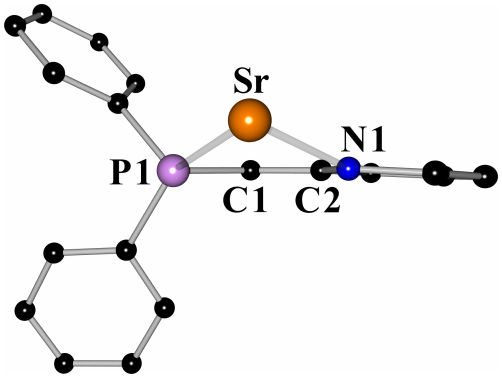

Figure 2.7: *View along the Sr····C1 vector, illustrating the conformation of the five membered ring in [(thf)$_3$Sr{Ph$_2$PC(H)Py}$_2$], (**4**).*

The main structural features of the two anionic ligands are very similar to those discussed for the lithium complex [(thf)$_2$Li{Ph$_2$PC(H)Py}], (**2**). The P1–C1 (175.9(2) pm) and C1–C2 distances (139.0(3) pm) are contracted by ca. 9.7 and 11.0 pm, respectively, with regard to the neutral phosphane Ph$_2$PCH$_2$Py, (**1**). Thus, both bond lengths suggest multiple bond character and illustrate the charge delocalization over the [P–C(H)–Py]$^-$-fragment. Like in **2**, the C2–N1 bond is approximately 3.8 pm longer than in the phosphane **1**, consistent with charge transfer to the electron deficient pyridyl ring system.

The Sr–N1 bond length in [(thf)$_3$Sr{Ph$_2$PC(H)Py}$_2$], (**4**), is 268.30(12) pm. This distance is comparable to those in [(thf)$_3$Sr{Me$_3$SiNC(Ph)PSiMe$_3$}$_2$] (263.1–266.3 pm)[49] and [(thf)$_2$Sr{(NSiMe$_3$)$_2$PPh$_2$}$_2$] (av. 263.8 pm),[50] but much longer than those found in [(dme)$_2$Sr{N(SiMe$_3$)$_2$}$_2$] (244 pm).[51] In comparison to [(C$_5$H$_5$N)$_5$SrBr$_2$] (271.9–275.5 pm), with the pyridine molecules as neutral donor bases,[52] the Sr–N distances in **4** are slightly shorter.

Hitherto, very little is known about phosphorus strontium complexes. The Cambridge Structural Database contains only 13 structures, with a P–Sr contact.[53] The Sr–P distances in these complexes vary from 322.00 pm in $[Sr(\eta^5\text{-}P_3C_2{}^tBu_2)_2]_\infty$[54] to 297.3 pm in $[(thf)Sr_3\{(PSi{}^tBu_3)_2(P(H)Si{}^tBu_3)_2\}]_2$.[55] The Sr–P1 distance of 318.39 pm in **4**, is located at the longer end of the range of Sr–P interactions described so far[54,55,56] and it exceeds the sum of the covalent radii (302 pm)[57] by 16.4 pm. The angles at the phosphorus atoms vary from 99.65(7)° for C7–P1–C13 to 128.60(5)° for C13–P1–Sr. However, the angle at P1 defined by the centre of the plane of the three P-bound carbon atoms and the cation of 169° illustrate that the lone pair at the phosphorus atom points to the metal ion.

In the ^{31}P-NMR spectrum of **4**, the phosphorus atom resonates at δ = -21.1. In the ^{1}H NMR spectrum, the single proton at the carbon atom of the CH-bridge gives rise to a doublet at 3.40 ppm.

2.4.2 Three coordinated lead(II) in the phosphanamide $[Pb\{Ph_2PC(H)Py\}\{N(SiMe_3)_2\}]$, (5)

In an analogue reaction to that described above, the lead(II) amide $[Pb\{N(SiMe_3)_2\}_2]$[58] was reacted with two equivalents of Ph_2PCH_2Py, (**1**). In contrast to the formation of the homoleptic complex $[(thf)_3Sr\{Ph_2PC(H)Py\}_2]$, (**4**), instantaneous decomposition is ob–served. However, the reaction of undissolved **1** with solid $[Pb\{N(SiMe_3)_2\}_2]$ in a 1:1 ratio gives the phosphanamide $[Pb\{Ph_2PC(H)Py\}\{N(SiMe_3)_2\}]$, (**5**), in high yields. One amid anion of $[Pb\{N(SiMe_3)_2\}_2]$ deprotonates the phosphane **1** at the C_α-position. The other $[N(SiMe_3)_2]^-$-anion remains coordinated to the lead(II) cation as a heteroleptic lead(II) complex is formed (Equation 2.5).

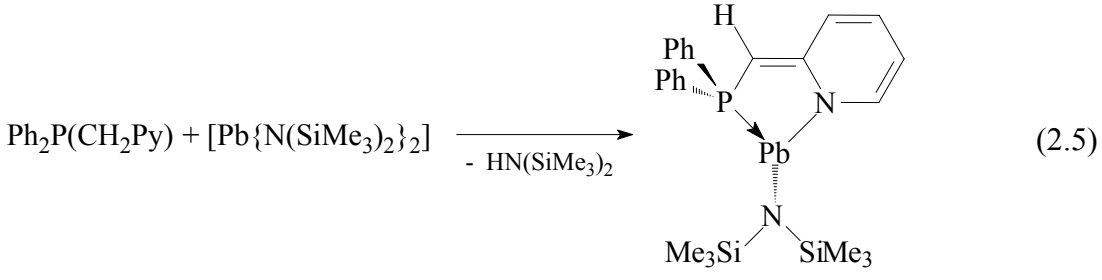

(2.5)

1 **5**

It turned out that **5** is only stable in the solid state. Dissolving **5** in various solvents results in slow decomposition. However, dark red blocks of crystalline [Pb{$Ph_2PC(H)Py$}–{$N(SiMe_3)_2$}], (**5**), suitable for the X-ray diffraction experiment were grown from a solution of [Pb{$Ph_2PC(H)Py$}{$N(SiMe_3)_2$}], (**5**), in hexane at -24°C. The blocks decomposes at 43°C.

The asymmetric unit contains two independent molecules of **5**. As the structural parameters of the two molecules are almost identical within their esds, the bond lengths and angles given in table 2.5 are averages; the standard deviations are maximum values. The molecular structure of **5** is depicted in figure 2.8.

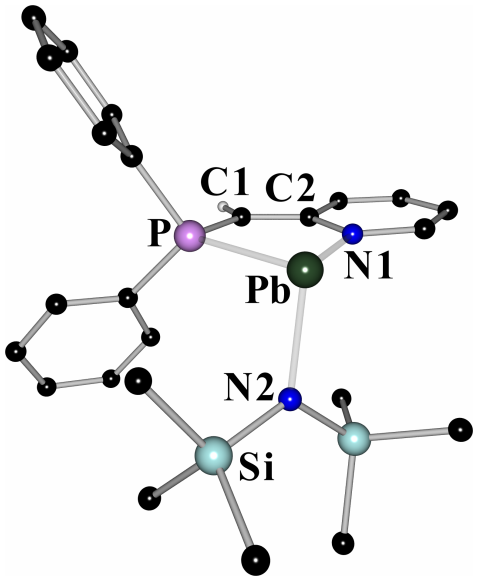

Figure 2.8: *Solid state structure of [Pb{$Ph_2PC(H)Py$}{$N(SiMe_3)_2$}], (**5**). Only one out of two molecules in the asymmetric unit is shown.*

Table 2.5: *Selected bond lengths [pm] and angles [°] of [Pb{$Ph_2PC(H)Py$}{$N(SiMe_3)_2$}], (**5**). Values are averages of the corresponding distances of the two molecules in the asymmetric unit; standard deviations are maxima.*

P–C1	173.9(2)	P–C1–C2	122.46(17)
C1–C2	139.4(3)	P–Pb–N1	73.78(5)
C2–N1	138.4(3)	N1–Pb–N2	100.37(7)
Pb–P	275.01(7)	P–Pb–N2	93.30(5)
Pb–N1	236.32(19)	N2–Si	172.00(19)
Pb–N2	223.31(18)	P–C_{Ph}	182.3(2)

In [Pb{$Ph_2PC(H)Py$}{$N(SiMe_3)_2$}], (**5**), the central lead(II) cation is three fold coordinated. The $[Ph_2P(CHPy)]^-$-anion acts as a (*P*,*N*)-bidentate ligand, giving rise to a five membered

planar metallacycle. The P–C1–C2-plane intersects the C1–C2–N1- and P–Pb–N1-plane at angles of only 1.8° and 0.4°, respectively. The $[N(SiMe_3)_2]^-$-anion, completing the coordination sphere of the central metal ion, is arranged almost perpendicular to the five membered metallacycle. The respective angles are 93.30(5)° for P–Pb–N2 and 100.37(7)° for N1–Pb–N2. The sum of the bond angles at the cation of 267.45° illustrates the pyramidal coordination sphere and the prescence of a lone pair at the lead(II) atom (Figure 2.9).

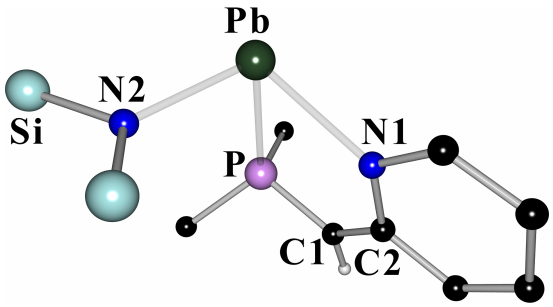

Figure 2.9: *Pyramidal coordination sphere of the cation in [Pb{$Ph_2PC(H)Py$}{$N(SiMe_3)_2$}], (**5**).*

The main structural parameters in the $[Ph_2PC(H)Py]^-$-residue in **5** are very similar to those already discussed for the lithium complex **2** and the strontium complex **4**. Both, the P–C1 (173.9(2) pm) and C1–C2 (139.4(3) pm) bond distances are shorter with regard to the starting material Ph_2PCH_2Py, (**1**) and therefore fall in the range between P–C single and P=C double and C–C single and C=C double bonds.

The lead amide [Pb{$Ph_2PC(H)Py$}{$N(SiMe_3)_2$}], (**5**), is a good bench-mark system to judge on the nature of lead nitrogen interactions, because it contains the $[N(SiMe_3)_2]^-$-amide and the delocalized amidic $[Ph_2PC(H)Py]^-$-fragment. In **5**, the Pb–N(Py) distance of 236.32(19) pm is ca. 13 pm longer than the Pb–$N(SiMe_3)_2$ bond (223.31(18) pm), which indicates that the Pb–N1 interaction has to be regarded weaker due to charge delocalization in the $[P–C(H)–Py)]^-$-moiety. In the starting material [Pb{$N(SiMe_3)_2$}$_2$] the Pb–N distances are 226.0 pm.[59] A good example for Pb←N_{Py} donor interactions is [(C_5H_5N)Pb{2,6-(2,4,6-^{i}Pr-C_6H_2)C_6H_3}Br], with the pyridine solvent molecule acting as N-donor.[60] In this complex, the Pb←N bond length is 250.2 pm. In the solvent separated ion pairs of $[HNC_2H_4N(H)C_2H_4NH)Pb][X]_2$ (X = NO_3; ClO_4) the Pb–N distances range from 240.8 to 244.6 pm.[61] For the organometallic complex [Pb{$C(SiMe_3)_2Si(Me_2)Py$}Cl] a Pb–N bond length of 246.7 pm is observed,[62] which is much longer than the observed distance in **5**. Thus, in **5** the Pb–N1 interaction has a considerable amidic character, which is in

accordance with a tranfer of the negative charge in the $[Ph_2PC(H)Py]^-$-anion towards the pyridyl nitrogen atom N1.

The Pb–P bond length in **5** is 275.01(7) pm. Interestingly, this value is in the range found for Pb–P interactions in lead phosphanides with the coordination number of three at the lead(II) atom akin **5**. For example the Pb–P bonds in $[Pb(P^tBu_2)_2]_2$ range from 278.1 to 281.2 pm[63] and in $[Pb_2\{P(SiMe_3)_2\}_4]$ from 269.4 to 279.7 pm.[64] In **5**, the Pb–P distance is comparable to those found in the (*P*,*P*)-chelated lead complex $[Pb_2\{N(PPh_2)_2\}_2]$ (270.9–278.0 pm)[65] and the organolead complex $[Pb\{HC(PPh_2)_2\}_2]$ (271.5–297.1 pm).[66]

In the ^{31}P-NMR spectrum the resonance for the phosphorus nucleus is remarkably shifted downfield to $\delta = 61.17$ and is found as a singulet with satellites giving a coupling constant of $^1J_{Pb-P} = 2679.5$ Hz. Apparently, the phosphorus atom in **5** is more positive than in the other isolated main group metal complexes **2**–**4**. The single hydrogen atom at the C_α-atom shows a doublet at $\delta = 4.58$, the coupling constant $^2J_{P-H}$ is 6.4 Hz. The ^{15}N spectroscopical shifts were obtained from a ^{1}H,^{15}N-HMBC experiment. Remarkably, they reflect the different electron densities at the nitrogen nuclei. Whereas the nitrogen atom of the $[N(SiMe_3)_2]^-$-moiety resonates upfield at $\delta = -268.0$, the resonance for the pyridyl nitrogen atom is shifted downfield at $\delta = -145.3$. A comparison of the shift for the ring nitrogen atom in the starting phosphane $Ph_2P(CH_2Py)$, (**1**) (δ= -62), with that found for **5**, clearly proves that the negative charge in **5** is transferred in direction to the ring nitrogen atom, resulting in an amidic character for this atom, in accordance with the observed structural parameters.

2.5 Organometallic transition metal complexes containing the [PC(H)Py]-residue

2.5.1 Synthesis of $[Zn_3\{Ph_2PC(H)Py\}_4O]$, (6)

The coordination behaviour of the $[Ph_2PC(H)Py]^-$-anion accomplished so far showed, that the anion acts as a (*P*,*N*)-bidentate chelat to soft metal cations, with the negative charge delocalized over the $[PC(H)Py]^-$-residue. Even the hard lithium cation in $[(thf)_2Li\{Ph_2PC(H)Py\}]$, (**2**), shows no contact to the deprotonated C_α-atom. However, in

$[(thf)_2Li_4(PPh_2)_2\{Ph_2PC(H)Py\}_2]$, (**3**), a lithium cation is η^2-coordinated to a $[(H)C–C_{Py}]$-moiety, illustrating that it would be feasible to employ cations of the appropriate size and charge in carbon coordination. The zinc cation Zn^{2+} is higher charged than the lithium cation and has only a by 5 pm increased ion radius.[57] Therefore, the lithium complex **2** was reacted with $ZnCl_2$ to give an organometallic zinc complex. However, a ^{31}P-NMR experiment from the reaction mixture after 48 hours showed various signals. The clear solution obtained after filtration was stored for 12 hours at room temperature, yielding yellow blocks suitable for a structure determination. It turned out that the $ZnCl_2$ used in the reaction was contaminated with ZnO, because in the isolated product $[Zn_3\{Ph_2P–C(H)Py\}_4O]$, (**6**), a central oxygen dianion is coordinated to three zinc atoms. Diffusion of oxygen into the reaction mixture can be excluded, because this process rather leads to oxidation of the phosphorus(III) atoms than to formation of ZnO. Hydrolysis with water would have caused protonation of the ligand and formation of the phosphaneoxide $Ph_2P(O)CH_2Py$.

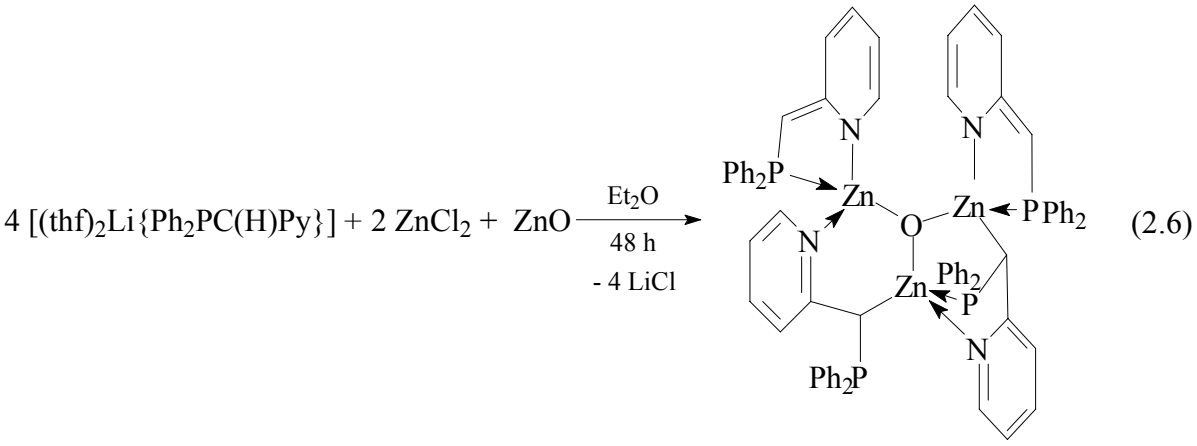

2 **6**

The structure refinement of the zinc complex $[Zn_3\{Ph_2PC(H)Py\}_4O]$, (**6**), was difficult due to various disordered residues in the solid state. They were resolved and modeled using distance and similarity restraints, giving reasonable standard deviations and *R* values. For the disordered residues the averaged bond lengths and angles are given in table 2.6, the standard deviations are maximum values. Figure 2.10 depicts the moleculare structure of the zinc complex **6**. The non-coordinating ether molecule on a special position is omitted for clarity.

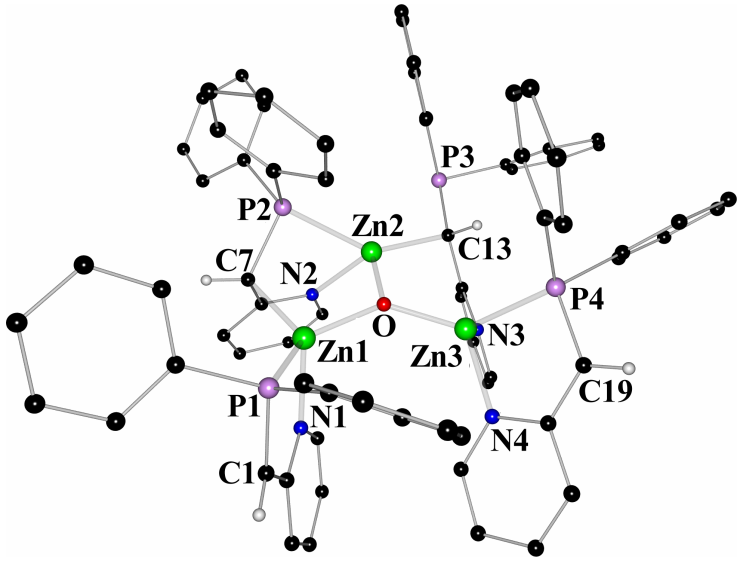

Figure 2.10: *Solid state structure of [Zn_3{$Ph_2PC(H)Py$}$_4$O], (**6**). The non-coordinating ether molecule is omitted for clarity.*

Table 2.6: *Selected bond lengths [pm] and angles [°] of [Zn_3{$Ph_2PC(H)Py$}$_4$O), (**6**).*

P1–C1	174.4(2)	P2–C7	180.33(18)	Zn1–N1	206.66(15)
C1–C2	138.8(3)	C7–C8	147.6(3)	Zn1–C7	214.67(18)
C2–N1	138.1(2)	C8–N2	136.0(2)	Zn1–O	190.66(12)
av. P1–C_{Ph}	183.42	av. P2–C_{Ph}	182.83	Zn2–P2	239.28(5)
P4–C19	173.9(2)	P3–C13	180.7(7)	Zn2–N2	212.57(16)
C19–C20	139.1(3)	C13–C14	147.4(7)	Zn2–C13	204.7(6)
C20–N4	138.5(2)	C14–N3	135.3(2)	Zn2–O	192.80(12)
av. P4–C_{Ph}	182.96	av. P3–C_{Ph}	186.2	Zn3–N3	210.33(15)
P1–C1–C2	120.97(15)	P2–C7–C8	109.64(13)	Zn3–P4	239.41(5)
P4–C19–C20	121.67(16)	P3–C13–C14	109.5(6)	Zn3–N4	202.72(16)
P1–Zn1–N1	84.73(4)	P2–Zn2–N2	79.85(4)	Zn2–C13	204.7(6)
P4–Zn3–N4	86.10(5)	Zn1–P1	240.09(5)	Zn3–O	186.97(12)

In [Zn_3{$Ph_2PC(H)Py$}$_4$O], (**6**), the zinc cation Zn1 is coordinated to the P1 and N1 atoms of one anionic [$Ph_2PC(H)Py$]$^-$-moiety and to the bridging C_α-atom C7 of another [$Ph_2PC(H)Py$]$^-$-anion. The latter anion further chelats the Zn2 cation *via* the heteroatoms P2 and N2. The cation Zn2 shows a contact to the C_α-atom C13 of a third [$Ph_2PC(H)Py$]$^-$-residue, which additionally coordinates the Zn3 atom *via* the nitrogen atom N3. The Zn3 ion is capped by coordination to P4 and N4 of a fourth [$Ph_2PC(H)Py$]$^-$-anion. The fourth coordination site of each zinc cation is occupied by the oxygen dianion, μ_3-bridging all three metal centres. The three zinc cations show severely distorted tetrahedral coordination geometry. The phosphorus atoms P1, P2 and P4 are tetrahedrally coordinated as well. The

core structure of **6**, built up by one six membered and four five membered metallacycles, is depicted in figure 2.11.

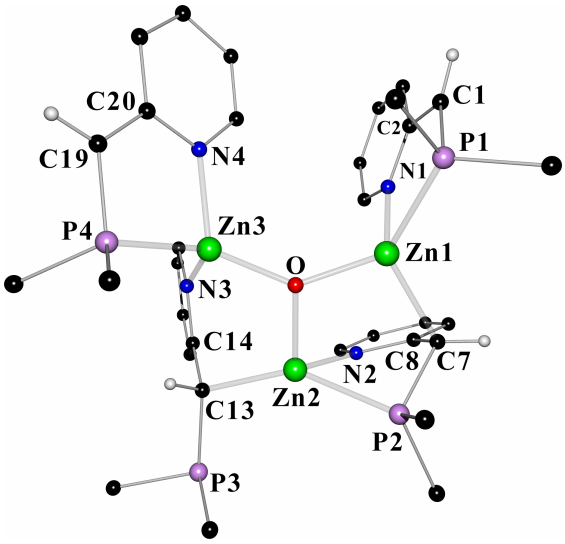

Figure 2.11: *Core structure of [Zn_3{$Ph_2PC(H)Py$}$_4$O], (**6**).*

The solid state structure of **6** is comprised of three zinc cations, a single oxygen O^{2-}-di–anion and four monoanionic $[Ph_2PC(H)Py]^-$-fragments. Two of them are solemnly (*P*,*N*)-bidentate chelats (**A, B** in figure 2.12), coordinating the zinc atoms Zn1 and Zn3. Another ligand features an additional Zn–C contact besides the Zn–P and Zn–N contacts (**C**) and the last $[Ph_2PC(H)Py]^-$-anion coordinates exclusively *via* the nitrogen atom N3 and the carbon atom C13 (**D**) while the phosphorus atom P3 is a pendent spectator ligand (Zn2···P3 314.5 pm). Interestingly, the lone pair at this phosphorus atom points away from the zinc cation Zn2 (Figure 2.12).

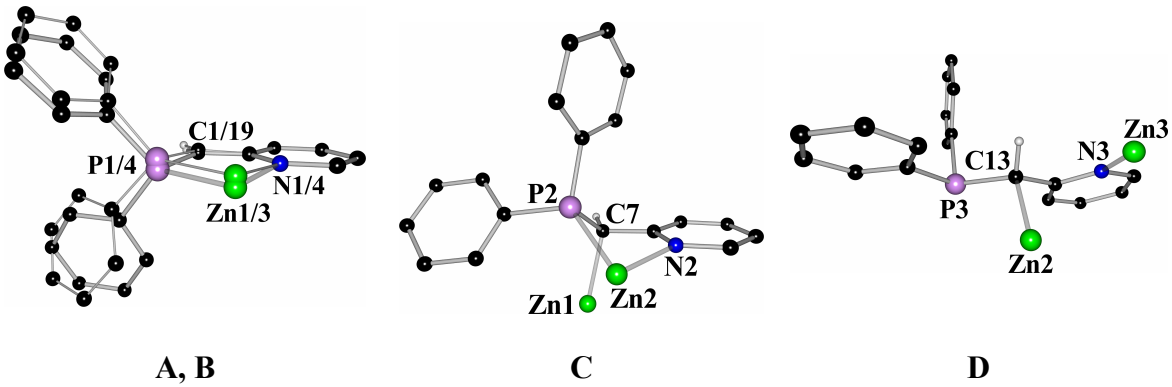

Figure 2.12: *Superpostion plot of the two (P,N)-chelating anions (**A** bold lines , **B** narrow lines), coordination mode of the (P,N,C)-tridentate ligand (**C**) and the (N,C)-coordinating anion (**D**).*

As expected for the different coordination behaviour of the (*P,N*)-ligands in **6**, the structural parameters in the $[Ph_2PC(H)Py]^-$-fragments differ significantly. The two (*P,N*)-chelating ligands (**A**, **B**) adopt almost planar five membered metallacycles. The cations Zn1 and Zn3 are displaced by 11.2 pm and 0.2 pm, respectively, from the best plane of the corresponding anion. The bonding parameters of these two ligands are almost equal and closely related to those found for the main group metal complexes **2**, **4** and **5**. The P1/4–C1/19 bond lengths with on average 174.2 pm and the C1/19–C2/20 distances (av. 139.0 pm) are shorter than the corresponding contacts observed in the other anions (**C**, **D**) in **6**. Therefore, the C2/20–N1/4 bond lengths of on average 138.3 pm are longer. The angles P1/4–C1/19–C2/20 at the deprotonated C_α-atoms (av. 121.32°) and the sum of the angles around these atoms of approximately 360° illustrate the sp^2-hybridization. Thus, the negative charge in these anions is delocalized over the [P–C(H)–Py]-unit, and shifted towards the ring nitrogen atoms N1 and N4, leading to an amidic character of these atoms. The bite angles of the ligands **A** and **B** are 84.73(4)° for P1–Zn1–N1 and 86.10(5)° for P4–Zn3–N4.

The remaining two anions of **C** and **D** each coordinate a zinc cation *via* the C_α-atoms C7 and C13, respectively. They represent the metallorganic component in the zinc complex $[Zn_3\{Ph_2PC(H)Py\}_4O]$ (**6**). The P2/3–C7/13 bond lengths are on average 180.5 pm. They are ca. 6.3 pm longer than those in the above mentioned purely (*P,N*)-chelating anions in **A** and **B** (174.2 pm) and only 4.5 pm shorter than a formal P–C single bond (185 pm).[30] Also the C7/13–C8/14 distances, which are equal within their esds, are with 147.5 pm substantially longer in comparison to the corresponding contacts in the other two anions (av. 139.0 pm for **A**, **B**). They are only 2.5 pm shorter than in the phosphane Ph_2PCH_2Py, (**1**), and therefore in the range of formal C–C single bond distances. The C8–N2 and C14–N3 distances in the pyridyl substituents of **C** and **D**, averaging at 135.7 pm, are significantly shorter than in the exclusively (*P,N*)-chelating anions (**A**, **B**: C_{Py}–N_{Py}: av. 138.3 pm) and only 1.7 pm longer than in **1** (133.97(18) pm). The average angles P2–C7–C8 and P3–C13–C14 of 109.5°, respectively, illustrate the tetrahedral environment of the metal coordinated C_α-atoms in the two anions **C** and **D** in contrast to the planar coordination sphere observed for the corresponding atoms C1 and C19 not interacting with any zinc cation. In both anions **C** and **D**, the sp^2-hybridized C_α-atom of the starting lithiated complex **2** rehybridizes to sp^3. This kind of rehybridization from sp^2 in the starting compound to sp^3 in the product was observed earlier in the reaction of $[(thf)_2Li\{HC(Py_2)\}]$ with $ZnMe_2$, to give $[MeZn\{HC(Py_2)\}]_2$.[67] Thus, in the anions of **C** and **D** in figure 2.12

the negative charge is accumulated and they exhibit carbanionic rather than amidic character.

In contrast to the five membered metallacycles of **A** and **B**, which are planar as described above, the ring system comprised of the [Zn2–P2–C7–C8–N2]-unit in **C** shows envelope conformation, due to the C7–Zn1 interaction. The Zn2 cation is displaced by 77.6 pm from the best plane of the anion.

In $[Zn_3\{Ph_2PC(H)Py\}_4O]$, (**6**), the three Zn–P distances are almost equal and range from 239.28(5) for Zn2–P2 to 240.09(5) pm for Zn1–P1. They are comparable to Zn←P donor bonds, like in $[Zn\{Ph_2PNSiMe_3\}\{N(SiMe_3)_2\}]_2$ (240.54 pm),[68] $[(Ph_2MeP)_2ZnI_2]$ (241.6 pm)[69] and $[Zn\{2\text{-}(Ph_2P)\text{-}6\text{-}(Me_3Si)C_6H_3S\}_2]$ (238.7 pm).[70] The Zn–P bond lengths are invariant towards the different coordination behaviour of the $[Ph_2PC(H)Py]^-$-anions.
The average value quoted for Zn–N_{Py} contacts is 208.3 pm.[71] In the zinc complex **6**, the Zn–N_{Py} distances are comparable to those found in $[Zn(PSi^iPr_3)_2Zn_2\{HC(Py)(NSiMe_2{}^tBu)\text{-}C(H)(Py)(NSiMe_2{}^tBu)\}]$ (207.1–209.1 pm).[72] In the organo zinc complex $[Zn\{C(SiMe_3)_2(Py)]$ the Zn–N distances vary from 225.6 to 233.5 pm and are much longer than in **6**.[73] To estimate the covalent or dative character of the Zn–N_{Py} bonds, complex **6** is best compared with the bis(1,4-dihydropyridin-1-yle)-bis(pyridine)zinc system (Scheme 2.9):[74]

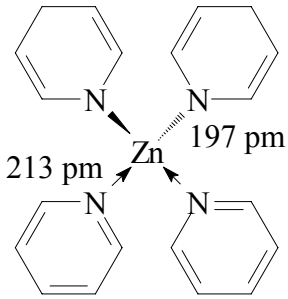

Scheme 2.9: *Covalent and dative Zn–N interactions in bis(1,4-dihydropyridin-1-yle)-bis(pyridine)zinc.*[74]

Whereas the Zn–P bond lengths in **6** do not change significantly, this is different to the Zn←N_{Py} distances in **6**, as they vary by ca. 10 pm from 202.72(16) to 212.57(16) pm. The shortest Zn–N_{Py} contact is found for Zn3–N4 (202.72(16) pm), which is consistent with an amidic character for N4. The Zn1–N1 distance of 206.66(15) pm is ca. 4 pm longer than the – in terms of amidic character of the nitrogen atom – comparable Zn3–N4 contact. The

difference arise from the coordination of Zn1 to the carbanionic C7 centre of another anion, in contrast to the Zn3 atom, which features a more dative Zn3–N3 bond (210.33(15) pm) and has no additional carbanionic contact. The Zn2–N2 bond length is 212.57(16) pm, hence ca. 2.25 pm longer than the Zn3–N3 bond. This slight bond elongation can be assigned to the interaction of Zn2 with the carbanionic C13 centre, whereas the Zn3 cation is bound to the delocalized fragment containing the amidic pyridyl nitrogen atom N4.

The Zn–C distances show remarkable differences although the coordination number is four in any case. The Zn2–C13 bond length is 204.7(6) pm and much shorter than the Zn1–C7 contact of 214.67(18) pm. This elongation is due to the different electronic environments of the two zinc cations. While Zn1 is additionally coordinated to the more pronounced amidic nitrogen atom N1, Zn2 is only coordinated to the less-charged nitrogen atom N2. However, both Zn–C bond lengths are in the range normally observed in organozinc complexes.[75] In [Zn{C(SiMe$_3$)$_2$(Py)] they vary from 204.3 to 210.0 pm,[73] in [MeZn{HC(Py)$_2$}] from 197.4 (Me–Zn) to 226.9 pm (HC–Zn)[67] and in the donor base stabilized [(tmeda)ZnEt$_2$] they are on average 217.4 pm long.[76]

The differences in Zn–N and Zn–C bond lengths are also reflected in the Zn–O distances. The shortest contact is found for Zn3–O with 186.97(12) pm, in accordance with the observed additional amidic N4 and the more dative N3 coordination of the cation, followed by the Zn1–O distance (190.66(12) pm). The Zn1 atom is further bound to the amidic atom N1 and the carbanionic C7 centre. The longest Zn–O bond is observed for Zn2–O (192.80(12) pm). The Zn2 atom is coordinated to the less negatively charged ring nitrogen atom N2, but additionally shows the shortest Zn–C contact (C13). The Zn–O distances are comparable to those observed in other zinc complexes containing a trigonal planar μ_3-O^{2-}-anion bridging three zinc centres.[77] All three distances are considerably shorter than the two different distances in the Wurtzite structure of zincoxide (197.3 and 199.2 pm),[78] because in the latter the coordination number of the monoxide is four rather than three in **6** and four metals compete for the charge rather than only three.

In conclusion, the solid state structure of [Zn$_3${Ph$_2$PC(H)Py}$_4$O], (**6**), exhibits three different coordination modes of the [Ph$_2$PC(H)Py]$^-$-anion. The anion either acts exclusive as a (*P*,*N*)-chelat, in which the negative charge is delocalized or in addition behaves as a

carbanion. If the carbanionic nature is employed an additional metal centres can be bound by (*P*,*N*)-chelating or only coordinating to the ring nitrogen atom.

The ^{31}P NMR spectrum of **6** in solution shows the from the solid-state structure anticipated four signals at δ = -27.5, -29.8, -32.4 and -35.6 ppm with intensities of 1:1:1:1. Due to the missing metal contact of the phosphorus atom P3, the signal at δ = -27.5 is assigned to this atom. The phosphorus atom P2 resonates at δ = -29.8. The almost equal coupling constants $^{2}J_{P\text{-}H}$ of the methylene protons, together with a ^{31}P, ^{1}H-HMBC-NMR spectra show, that the two signals at -32.4 ppm and -35.6 ppm originate from the phosphorus atoms P1 and P4. However these signals cannot be assigned unambiguously. The signals for the hydrogen atoms at the C_α-atoms and the pyridyl hydrogen atoms could be assigned using 1D and 2D spectroscopical techniques. Their assignments and chemical shifts are given in the experimental section. The NMR-spectroscopical investigations from solution prove that the solid-state structure is retained employing non-donating solvent like C_6D_6.

2.5.2 The donor base complexed iron(II) phoshaneamide *rac*-[*OC*-6-43]-[(Ph_2PCH_2Py)Fe{$Ph_2PC(H)Py$}$_2$], (7)

Considering, the broad application of hemilabile coordinated iron complexes in catalysis, it seems worthwhile to react the phosphane Ph_2PCH_2Py, (**1**), with the iron(II) amide [Fe{$N(SiMe_3)_2$}$_2$].[79] The 2:1 reaction instantaneously causes a redox processes yielding multiple products, which could not be characterized unequivocally. However, it turned out, that the use of an excess of the phosphane **1** in the reaction stabilizes the iron centre to give the iron(II) amide *rac*-[(Ph_2PCH_2Py)Fe{$Ph_2PC(H)Py$}$_2$], (**7**) (Equation 2.7).

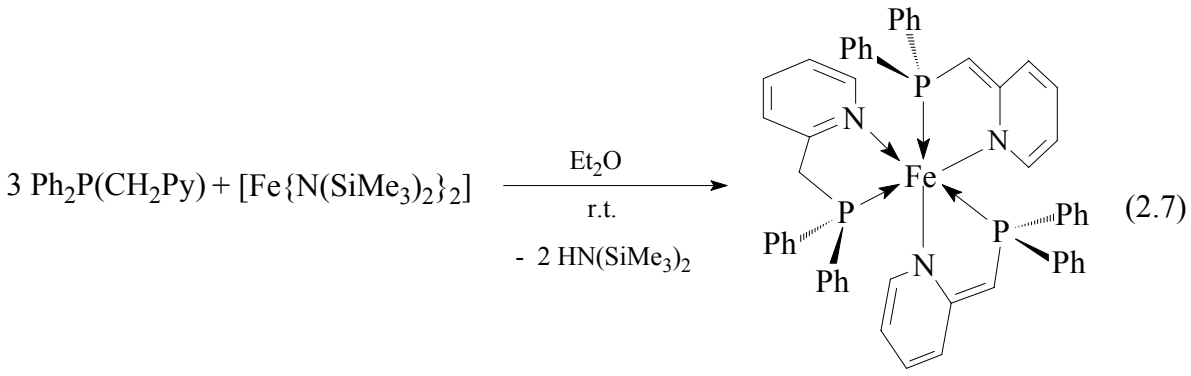

(2.7)

1 **7**

Both of the two $[N(SiMe_3)_2]^-$-anions of the iron amide starting material remove a single proton at C_α-position in the phosphane **1**. A third equivalent of $Ph_2P(CH_2Py)$, (**1**), is employed as a neutral chelating donor ligand and stabilizes the intermediate 14 VE iron complex, to give the 18 VE complex *rac*-$[(Ph_2PCH_2Py)Fe\{Ph_2PC(H)Py\}_2]$, (**7**).

The dark red iron complex **7** decomposes at 212°C. It crystallizes from the reaction solution at r.t. as a racemic mixture with the two diastereomers arranged along the two fold axis in helical strands. The solid state structure of **7** is shown in figure 2.13; selected bond lengths and angles are summerized in table 2.7. The asymmetric unit of **7** contains a non coordinating ether molecule, which is omitted for clarity.

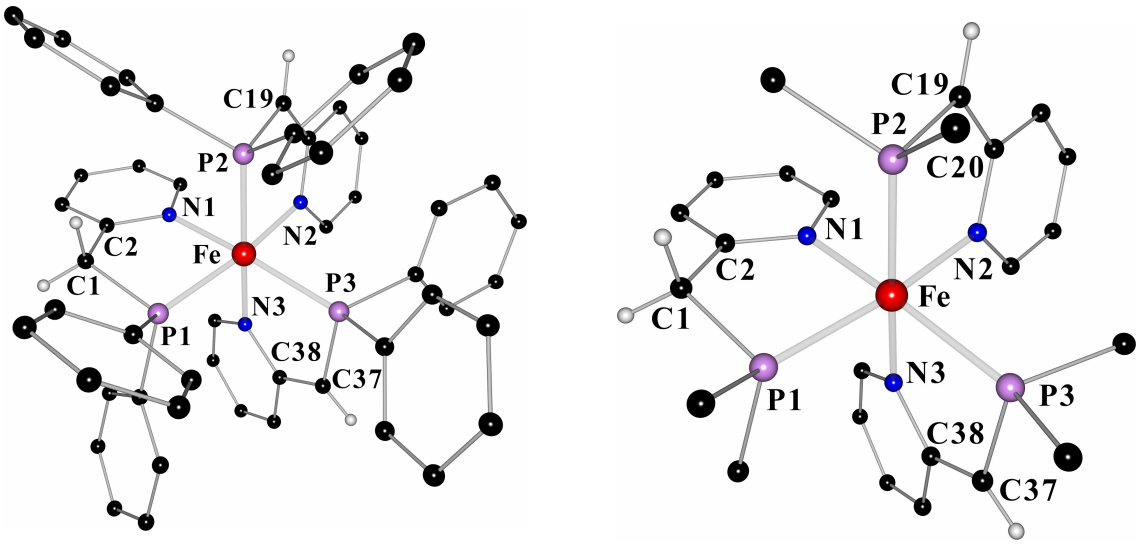

Figure 2.13: *Solid state structure of rac-[(Ph₂PCH₂Py)Fe{Ph₂PC(H)Py}₂], (7). The non coordinating solvent molecule omitted for clarity.*

Table 2.7: *Selected bond lengths [pm] and angles [°] of rac-[(Ph₂PCH₂Py)Fe{Ph₂PC(H)Py}₂], (7).*

P1–C1	181.3(2)	P2–C19	174.7(2)	P3–C37	175.7(2)
C1–C2	146.9(3)	C19–C20	138.6(3)	C37–C38	139.7(3)
C2–N1	135.9(2)	C20–N2	138.6(2)	C38–N3	138.3(2)
av. P1–C_{Ph}	183.81	av. P2–C_{Ph}	185.05	av. P3–C_{Ph}	185.19
Fe–P1	224.58(5)	Fe–P2	227.42(5)	Fe–P3	228.66(5)
Fe–N1	208.74(16)	Fe–N2	203.69(15)	Fe–N3	207.44(16)
P1–C1–C2	112.06(14)	P2–C19–C20	116.90(15)	P3–C37–C38	116.17(15)
P1–Fe–N1	83.07(5)	P2–Fe–N2	83.83(5)	P3–Fe–N3	82.84(5)
P1–Fe–N2	171.16(5)	P2–Fe–N3	174.07(5)	P3–Fe–N1	171.04(5)

The two anionic $[Ph_2PC(H)Py]^-$ ligands, and the neutral phosphane $[Ph_2PCH_2Py]$ act as (*P*,*N*)-bidentate chelats to the central iron(II) cation. The coordination polyhedron at the metal is a nearly perfect octahedron. The angles P1–Fe–N2 (171.16(5)°), P2–Fe–N3

(174.07(5)°) and P3–Fe–N1 (171.04(5)°) are close to the ideal value of 180°. The bite angles of the three ligands (P–Fe–N) are very similar and on average 83.25°. Thus, there is no significant difference in the bite of the anionic and the neutral ligands in **7**.

The iron amide **7** is an ideal sample to elucidate the bonding in the phosphane Ph_2PCH_2Py, (**1**), the metal coordinated neutral phosphane and the related anion. In comparison to the parent phosphane **1**, the (*P*,*N*)-coordination of the neutral ligand in **7** results in shorter P1–C1 and C1–C2 bonds. The C1–C2 bond in **7** (146.9(3) pm) is ca. 3.0 pm shorter than in **1** (149.95(18)pm). This bond contraction is a result of the Fe–N1 contact, which influences the bonding parameters in the electron deficient pyridyl substituent. In **1**, the C2–N1 bond is 133.97(18) pm long, whereas in **7** it is 135.9(2) pm, indicating the electronic perturbation at the pyridyl nitrogen atom in the neutral ligand caused by metal coordination. The electron density is shifted towards the ring and accumulated at the nitrogen atom. As a consequence the C1–C2 bond gets contracted and the C2–N2 bond gets elongated.

The P–C1 distance in **1** is 185.59(14) pm long, in **7** the corresponding P1–C1 bond is only 181.3(2) pm long. The Fe–P1 interaction, observed in **7**, results in a more pronounced electropositive character of the phosphorus atom in comparison to the isolated phosphane **1**, because electron density is transferred to the metal ion. Therefore, the P1–C1 bond of the more electropositive phosphorus atom with the electronegative carbon atom gets contracted by stronger electrostatic interaction. The $P–C_{ipso}$ distances in **7** (av. 183.81 pm) are very similar to those found in the phosphane **1** (av. 183.95 pm).

In the anionic ligands, the respective P2–C19 (174.7(2) pm) and P3–C37 bond lengths (175.7(2) pm), and the C19–C20 (138.6(3) pm) and C37–C38 distances (139.7 pm) are very similar and differ by only 1 pm. The contraction of the P–C and C–C bonds is due to charge delocalization and multiple bond character as already discussed previously. The $P2/3–C_{Ph}$ distances with on average 185.12 pm are identical within their standard deviations and slightly longer than the $P1–C_{Ph}$ contacts.

The Fe–P distances in **7** show remarkable differences. Whereas, the distances of the iron cation to the phosphorus atoms in the anionic ligands are almost identical (Fe–P2 227.42(5) pm, Fe–P3 (228.66(5) pm), the Fe–P1 contact of 224.58(5) pm is on average 3.5 pm shorter. Thus, the neutral ligand is a stronger P donor than the anionic ones. In the C_α-deprotonated ligands the electron density at the phosphorus centres is considerably influenced by the negative charge in the $[P–C(H)–Py]^-$-moiety, resulting in weaker P–Fe

interactions. The Fe–P distances in **7** are in the range found for diphosphane chelated octahedral iron(II) complexes, like $[(dmpe)_2FeCl_2]$ (224.0 pm)[80] and $[(dppe)(MeCN)_2Fe][BF_4]_2+(CH_2Cl_2)$ (234.2 pm).[81] They are comparable to the Fe–P contacts found in the iron(0) complexes $[Fe(CO)_2\{cy\text{-}H_2C_2C(O)OC(O)\}\{Ph_2PC(H)\text{-}(PPh_2)Py\}]$ (223.1 pm) and $[Fe(CO)_3\{Ph_2PC(H)(PPh_2)Py\}$ (220.77–222.12 pm).[82]

The Fe–N distances in the iron complex **7** are all different. The contact of the iron cation to the nitrogen atom in the neutral ligand, Fe–N1, of 208.74(16) pm is the longest, followed by the distances of the Fe^{2+}-cation to the nitrogen atoms of the negatively charged ligands Fe–N3 (207.44(16) pm) and Fe–N2 (203.69(15) pm). Interestingly, the latter two contacts differ by ca. 3.7 pm, although they are expected to be similar, because of the same electronic situations in the two ligands. In addition, the Fe–P3, P3–C27 and C37–C38 distances are slightly longer than the comparable bonds lengths in the other anionic ligand. These differences seem to originate from steric crowding in the iron amide **7**. This is further illustrated in the different conformations of the PC_2NFe five membered metallacycles. The iron centre is displaced by 31 pm from the best plane defined by the P2–C19–C20–N2 atoms and by 53 pm from the corresponding plane of the other anionic ligand. The displacement of the iron atom from the P1–C1–C2–N1 least square plane of the neutral ligand is with 43 pm half between.

In **7**, the Fe–N_{Py} distances are at the lower end of the range generally observed for iron(II) complexes.[83] For example, in $[(HCPy_3)_2Fe][NO_3]_2$ the Fe–N distance is 194.7 pm,[83g] in $[(H_2NCH_2Py)Fe][Br]_2$ the Fe–N_{Py} contact is 222.3 pm long.[83b]

The ^{31}P-NMR spectrum of **7** in solution shows three doublets of doublets at δ = 36.01, δ = 39.77 and δ = 54.03 with identical intensities. The two first are caused by the phosphorus nuclei of the anionic ligands. The coupling constant is $^2J_{P2-P3}$ = 44.2 Hz. The phosphorus atom of the neutral ligand resonates at 54.03 ppm with coupling constants of $^2J_{P1-P2}$ = 41.7 Hz and $^2J_{P1-P3}$ = 32.2 Hz.

2.5.3 The $[Ph_2PC(H)Py]^-$-anion as a *Janus* head ligand in $[Fe\{Ph_2PC(H)Py\}_2N(SiMe_3)_2\}]_2$, (8)

The reaction of the phosphane Ph_2PCH_2Py, (**1**), with $[Fe\{N(SiMe_3)_2\}_2]$ in a 1:1 ratio gives the dinuclear, heteroleptic 14 VE organoiron(II) complex $[Fe\{Ph_2PC(H)Py\}\{N(SiMe_3)_2\}]_2$, (**8**) (Equation 2.8).

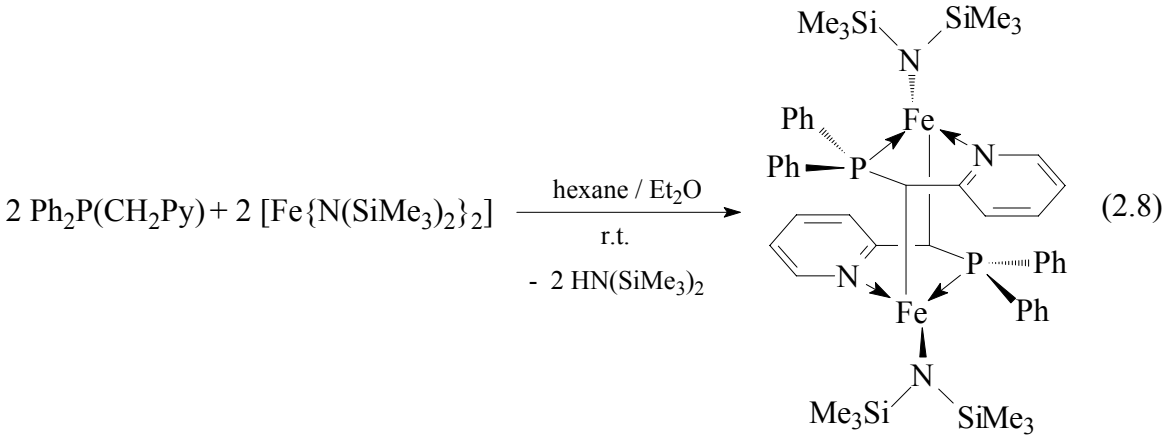

(2.8)

1 **8**

Recrystallization from hexane/Et_2O (2:1) yields the organoiron complex **8** as red needles, which decompose at 123°C. The $FeN(SiMe_3)_2$-fragment containing Fe2 in the solid state structure of **8**, shows heavy disordering. The three positions found for this residue were refined using distance and simularity restraints, giving reasonable *R* values and standard deviations. The bond lengths and angles for this residue, given in table 2.8 are averages, the standard deviations are maximum values. The solid state structure of **8** is shown in figure 2.14.

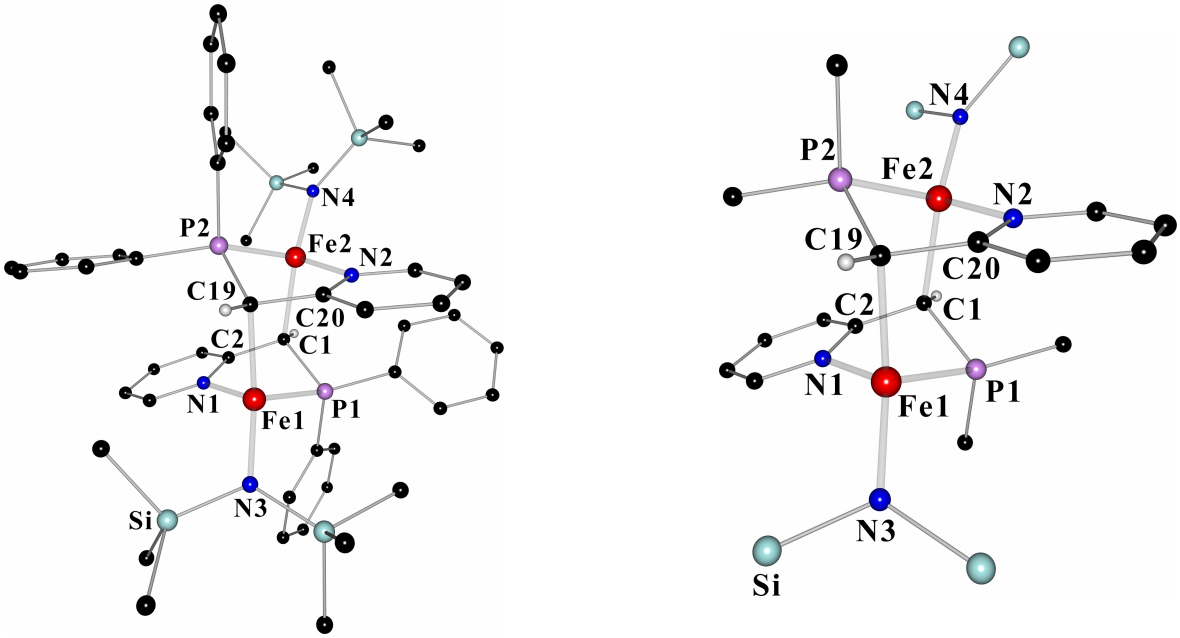

Figure 2.14: *Solid state structure of [Fe{Ph$_2$PC(H)Py}{N(SiMe$_3$)$_2$}]$_2$,* ***(8)****.*

Table 2.8: *Selected bond lengths [pm] and angles [°] of [Fe{Ph$_2$PC(H)Py}{N(SiMe$_3$)$_2$}]$_2$,* ***(8)****.*

P1–C1	180.9(3)	P2–C19	179.1(2)
C1–C2	146.9(3)	C19–C20	147.4(3)
C2–N1	135.6(3)	C20–N2	135.8(3)
Fe1–P1	253.51(11)	Fe2–P2	242.2(8)
Fe1–N1	215.2(2)	Fe2–N2	223.1(8)
Fe1–N3	195.8(2)	Fe2–N4	196.4(7)
Fe1–C19	217.5(2)	Fe2–C1	220.7(8)
P1–C1–C2	107.81(17)	P2–C19–C20	110.43(17)
P1–Fe1–N1	76.05(7)	P2–Fe2–N2	77.88(20)
	av. P–C$_{Ph}$ 183.13		

One amide anion of [Fe{N(SiMe$_3$)$_2$}$_2$] deprotonates one molecule of the phosphane **1**. The second [N(SiMe$_3$)$_2$]$^-$-anion remains coordinated to the iron(II) centre. The [Ph$_2$PC(H)Py]$^-$-anion acts as (*P*,*N*)-chelat to one iron cation, forming a five membered metallacycle. Two of these building blocks dimerize in a head-to-tail fashion with both iron atoms Fe1 and Fe2 coordinated to the deprotonated carbon atoms C19 and C1, respectively, giving a dinuclear, heteroleptic complex. Thus, the main structural feature is a [2.2.1.1] metallacycle. Each of the two iron atoms shows a distorted tetrahedral coordination sphere. The bite angles of on average 76.97° in the two [Ph$_2$PC(H)Py]$^-$-anions (P–Fe–N) are more acute than in the iron complex **7**. The exocyclic angles at the iron atoms Fe1 and Fe2 vary from 124.8(7)° for N1–Fe1–C19 to 101.5(3)° for N2–Fe2–C1. The two phosphorus atoms P1 and P2 show distorted tetrahedral coordination.

The P1–C1 and P2–C19 bond lengths in [Fe{$Ph_2PC(H)Py$}{$N(SiMe_3)_2$}]$_2$, (**8**), are similar and on average 180.0 pm long. They are remarkably shorter than a formal P–C single bond (185 pm)[30] and ca. 5.6 pm shorter than in the phosphane **1**. However, in comparison to the structural parameters of the delocalized anionic ligands in the complexes **2**, **4**, **5** and **7** they are approximately 5 pm longer. A comparable P–C bond elongation is found in the lithium complex [$(thf)_2Li_4(PPh_2)_2${$Ph_2PC(H)Py$}$_2$], (**3**), where a lithium cation is η^2-coordinated to the HC–C_{Py} system. In addition, the C1–C2 and C19–C20 bonds in **8**, which are equal within esds and measure on average 147.15 pm are much longer than in the anionic fragments of the previously mentioned complexes **2**–**7**. Theses distances in **8** are similar to those found in the neutral donor base of complex **7** (146.9(3) pm) and are only 2.8 pm shorter than in the phosphane **1**. Thus, in the organoiron complex **8**, the negative charge created by deprotonation at C_α-position seems not delocalized like in the previously discussed complexes, but is predominantly accumulated at the C_α-atom. This is further illustrated in the C2–N1 and C20–N2 distances (av. 135.7 pm) which are only 1.73 pm longer than in the posphane **1** and identical to the C2–N1 distance found in the neutral donor ligand [Ph_2PCH_2Py] of the iron complex **7**. As expected from these bonding parameters the angles at the carbon atom C1 and C19 are very close to 109.5°, indicating sp^3-hybridization for these atoms in contrast to the more sp^2-hybridisized C_α-atoms in the complexes **2**–**5** and **7**.

Due to the displacement of the iron atoms from the best plane of the corresponding anionic ligand (56 pm for Fe1 and 45 pm for Fe2) and the additional coordination to the carbon atoms C1 and C19, the Fe1–N1, Fe2–N2 and the Fe1–P1 and Fe2–P2 distances are much longer than in the iron amide **7**. However, the corresponding Fe–P and Fe–N distances in [Fe{$Ph_2PC(H)Py$}{$N(SiMe_3)_2$}]$_2$, (**8**), show significant differences. The Fe1–P1 distance of 253.51(11) pm is ca. 10.9 pm longer than the corresponding Fe2–P2 contact (242.2(8) pm). Therefore, the Fe1–N1 (215.2(2) pm) contact is ca. 8.0 pm shorter than the Fe2–N2 distance of 242.2(8) pm. This asymmetric bonding situation is certainly due to steric interaction of the [$Ph_2PC(H)Py$]$^-$- and [$N(SiMe_3)_2$]$^-$-anions and to minimize transannular repulsion in the [2.2.1.1] metallacycle. Similar differences in Fe–N bond lengths are found in the organoiron(II) complex [Fe{$C(H)(Si^tBuMe_2)Py$}$_2$]$_2$, in which they vary from 209.7 to 218.9 pm.[84] The Fe–N contacts in **8** are significantly longer than in the diethyl complex [$(bpy)_2FeEt_2$] (193.7 to 194.3 pm)[85] but comparable to those found in the dimesityl derivative [$(C_5H_4N)_2FeMes_2$] (216.9 to 217.9 pm)[86] and to the organoiron compounds

[Fe{C(H)(SiMe$_3$)Py}$_2$ (211.1 – 213.5 pm)[84] and [(tmeda)Fe{C(Ph)(SiMe$_3$)Py}Cl] (220.6 to 228.4 pm)[84] both containing C-deprotonated [C(R)(R')Py]$^-$-anions, related to the [Ph$_2$PC(H)Py]$^-$-anions in **8**.

The contacts of the iron centres to the [N(SiMe$_3$)$_2$]$^-$ -nitrogen atoms, Fe1–N3 and Fe2–N4 are on average 196.1 pm long and similar to those observed in the monomeric [(thf)Fe{N(SiMe$_3$)$_2$}$_2$] (191.5 pm).[79b]

The Fe1–P1 (253.51(11) pm) and Fe2–P2 distances (242.2(8) pm) in [Fe{Ph$_2$PC(H)Py}–{N(SiMe$_3$)$_2$}]$_2$, (**8**), are quite long. They exceed the sum of the covalent radii of the iron and phosphorus atoms (226.5 pm)[57] by 27.0 and 15.7 pm, respectively. However, the angles around the two phosphorus atoms P1 and P2 which vary from 91.71(9)° to 139.90(9)° and the angles between the centre of the planes defined by the coordinated carbon atoms and the iron cations of 155.4° for P1 and 163.0° for P2 illustrate, that the lone pairs at the phosphorus atoms point towards the metal ions. Similarly long Fe–P interactions are found in ironphosphane complexes as e.g. in [(Et$_3$P)$_2$FeBr$_2$] (240.6–245.1 pm),[87] [{^{i}Pr$_2$P(C$_2$H$_4$)P^{i}Pr$_2$}Fe{H$_2$C(*p*-tol)$_2$}$_2$] (246.2 pm)[88] and [{Ph$_2$P(C$_2$H$_2$)–PPh$_2$}FeCl$_2$] (257.6 and 259.2 pm).[89]

For the Fe1–C19 and Fe2–C1 bond lengths, 217.5(2) pm and 220.7(8) pm were determined, respectively. Thus, they match the range generally observed in organo iron complexes (202.1–231.0 pm).[85,86,88,90] In **8**, they are comparable to those described for [(tmeda)Fe{C(Ph)(SiMe$_3$)Py}Cl] (221.2 and 231.0 pm)[84] and [Fe{C(H)(Si^{t}BuMe$_2$)Py}$_2$]$_2$ (213.3–216.3 pm).[84]

Unfortunately, no reasonable NMR data were obtained for the organoiron complex [Fe{Ph$_2$PC(H)Py}{N(SiMe$_3$)$_2$}]$_2$, (**8**), due to paramagnetic contributions in the NMR samples.

2.6 Comparison of selected parameters of compounds 1–8

2.6.1 Comparison of selected structural parameters of 1–8

In the following table selected structural parameters of the $[Ph_2P(CHPy)]^-$-anion in the metal derivatives **2**–**8** are compared, taking the different coodination modes into account. Additionally, the corresponding distances in the phosphane **1** are given. The distances for similar coordinated anions in one complex are average values (**3**, **5**, **6** and **7**).

Table 2.9: *Selected structural parameters [pm], [°] of the $[Ph_2P(CHPy)]^-$-anions in **2**–**8**, in comparison to the parent phosphane **1**.*

	P–CH	HC–C_{Py}	P–C(H)–C	P–CH	HC–C_{Py}	P–C(H)–C
1	185.6	150.0	112.1	-	-	-
	(*P,N*)-coordination			(*P,N,C*)-coordination		
2	175.9	139.0	122.4	-	-	-
3	-	-	-	177.2	141.7	119.2
4	174.6	138.8	123.9	-	-	-
5	173.9	139.4	122.5	-	-	-
6	174.2	139.0	121.3	180.3	147.6	109.6
7	175.2	139.2	116.5	-	-	-
8	-	-	-	180.0	147.2	109.1

Standard bond lengths: P–N: 170 pm, P=N: 155 pm, P–C: 185 pm , P=C: 167 pm , Si–N: 174 pm, C–C: 154 pm, C=C: 134 pm.[30]

Deprotonation at the methylene bridge of the phosphane **1** and coordination of the metal cation only *via* the P- and N-centres results in 9.7–11.7 pm shorter P–C(H) and ca. 11.0 pm shorter HC–C_{Py} distances, relative to the phosphane **1**, due to delocalization of the negative charge over the whole $[P–C(H)–Py]^-$-unit. These bonds have significant multiple bond character. The P–C(H)–C angles are close to 120°. The anion is best described as a phosphanamide.

If a metal cation is coordinated to the C_α-atom, the P–C(H) and HC–C_{Py} distances are only 5.4 and 2.6 pm shorter than in the phosphane **1**, respectively. The multiple bond character for these bonds is less pronounced. The P–C–C angles are near 109.5°. The anion is rather a carbanion than an amide. The distances in the $[Ph_2P(CHPy)]^-$-anions in the lithium

complex **3** are half-way between these two bonding situations. In this complex a lithium cation is η^2-coordinated to the [HC–C_{Py}]-moiety.

The degree of delocalization of the negative charge, hence the amidic character of the pyridyl nitrogen atom is reflected in the bonding parameters of the pyridyl rings. Table 2.10 lists these distances according to the following scheme:

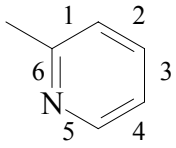

Table 2.10: *Bond lengths [pm] in the pyridyl substituents of **1**–**8**:*

		1	2	3	4	5	6
1		139.2	138.0	137.9	138.4	134.0	134.0
2		143.8	136.8	138.7	137.2	134.9	138.0
3		142.5	136.6	139.4	136.5	135.2	137.5
4		144.2	135.2	139.8	137.2	134.8	137.8
5		144.2	135.9	141.2	136.4	135.9	138.4
6	**a***	143.6	134.8	140.4	136.4	135.3	138.3
	b*	140.2	137.1	138.9	136.8	134.5	136.0
	c*	140.4	137.2	138.4	137.4	134.5	135.3
7	**a****	143.2	135.7	140.6	137.2	135.5	138.5
	b**	140.3	137.5	139.3	139.7	136.0	135.9
8		139.7	137.4	137.0	136.3	134.8	135.7

bond lengths cited for similar coordinating ligands are averages
a* = (*P,N*)-coordinating, b* = (*P,N,C*)-coordinating, c* = (*N,C*)-coordinating
a** = anionic ligands, b** = neutral ligand

In the exclusively (*P*,*N*)-chelating ligands, the distances in the pyridyl residues differ remarkably from those in the isolated phosphane **1** and in the neutral coordinating phosphane (**7b**). The most prominent differences are observed in the bond lengths 1 and 6, which are elongated by 4.4–5.0 pm and 4.0–4.4 pm, respectively. The bonds 2 and 4 are contracted and suggest located double bond character.

For the (*P,N,C*)- and (*N,C*)-coordinating ligands, (**6a**, **b** and **8** in table 2.10) the corresponding distances are similar to those of the parent phosphane **1** or the neutral donor

ligand in (**7b**). The bond distances 1 to 6 vary by 2 pm, relative to the isolated phosphane **1**. The aromatic character of the pyridyl ring system is maintained.

2.6.2 Comparison of spectroscopical data of 1–7

Apparently the charge density at a nucleus is correlated to the NMR chemical shift. Resonances at low fields correspond to less electron density at the observed nucleus, although this relation is not straight forward and complicated by paramagnetic contributions to nuclear shielding.[91] Of course, chemical shifts are also sensitive to the solvents used in the NMR experiment. In the following table the ^{31}P-NMR chemical shifts of the metalated derivatives **2**–**7** are given in dependence of the coordination mode of the anionic $[Ph_2PC(H)Py]^-$ ligands. The phosphorus nucleus in the isolated phosphane **1** resonates at δ = -11.4.

Table 2.11: *^{31}P-NMR chemical shifts [ppm] in **2**–7.*

	2 (M=Li)	**3** (M=Li)	**4** (M=Sr)	**5** (M=Pb)	**6** (M=Zn)	**7** (M=Fe)
NMR-solvent	C_7D_8	C_6D_6	C_4D_8O	C_7D_8	C_6D_6	C_4D_8O
(*P,N*)-coordination delocalized charge	-23.5	-18.3	-21.1	61.17	-35.6 / -32.4	36.1 / 39.8
(*P,N,C*) / (*C,N*)-coordination charge more localized at C_α					-29.8 / -27.5	
(*P,N*)-coordination neutral ligand						54.03

*^{31}P-NMR: δ = -11.4 for $Ph_2P(CH_2Py)$, (**1**).*

The ^{31}P-NMR resonances of the phosphorus atoms of the exclusively (*P,N*)-chelating anions in **2** (Li), **4** (Sr) and **6** (Zn) are located upfield in comparison to the parent phosphane **1**. Deprotonation at the C_α-position of the phosphane **1** increases the electron density at the electropositive phosphorus atom. Remarkably, these shifts reflect the different hard/soft *Lewis*-acidic character of these s- and p-block metals bound to the phosphorus atom. The coordination to the hard Zn^{2+}-cation in **6** results in the highest upfield resonances for the soft phosphorus atoms. The only marginally smaller mono–cationic lithium atom entails a shift located more downfield (**2**). For the soft phosphorus

atoms coordinated to the much more polarizable, hence softed, twofold charged Sr^{2+}-cation the resonance shifted most downfield is observed (**4**). Hence, the coordination of the soft phosphorus atom to a hard cation results in a high electron density at the P-nucleus, whilst coordination to a soft atom, gives a decreased electron density.

Interestingly, the resonances of both the neutral and anionic (*P,N*)-coordinating ligands in the iron complex **7** indicate a weaker shielding for phosphorus nuclei. They are located downfield in comparison to the parent phosphane **1** and the derivatives **2**, **4** and **6**. Whereas for the s- and p-block complexes the [M] ←P-bonding reflects closed-shell interactions, the d-orbitals in the [M]–P bond synergism of the iron centre must be taken into account for **7**. The interaction of the lone pairs at the phosphorus atoms with the empty d-orbitals of the d^6-Fe^{2+}-cation decreases the electron density at the phosphorus nuclei. As expected by the influence of deprotonation on the shielding of the phosphorus nuclei in **2**, **4** and **6**, the ^{31}P-NMR resonances found for the anionic ligands in **7** are shifted upfield with regard to that of the neutral ligand. The ^{31}P-NMR shift found for the lead complex **5** is at first sight most striking. As expected, by the softer *Lewis*-acidic character of the Pb^{2+}-cation *vs.* the Sr^{2+}-cation in **4**, it is located more downfield. However, the difference of $\Delta\delta = 82.3$ between the resonances of **4** and **5** is quite large. Additionally, in **5**, the signal shifted most downfield in comparison to all derivatives of **1** is observed. First results, of a theoretical investigation of this ^{31}P-NMR resonance indicate, that the weak shielding originates from spin-orbit effects between the phosphorus and lead atom. Calculations of the ^{31}P-NMR-parameter, neglecting spin-orbit effects overestimate the electron density at the phosphorus centre.[92]

The influence of additional [M]–C-coordination on the electron density at the phosphorus nuclei can be deduced from the ^{31}P-NMR shifts of **2** and **3** and the differently coordinated anions in **6**. The Li–η^2-(C–C)-coordination in **3** decreases the electron density at the phosphorus nucleus in comparison to the exclusively (*P,N*)-coordinating anion in **2**, because two electropositive atoms combite for the charge of the bound carbon atom. The same argument holds for the the zinc complex **6**. The resonances of the phosphorus atoms of the exclusively (*P,N*)-chelating anions are found at higher field than those of the anions with additional [M]–C contact. In quintescence this illustrates, that the negative charge in the [M]–C-coordinating anions is more located at the C_α-atom and the electropositive phosphorus atom is more electronically depleted while in the (*P,N*)-chelating ligands it benefits from marginal charge tranfer of the formally carbanionic center in the $[PC(H)Py]^-$-moiety.

3 Diphenyl(-2-)picolyliminophosphorane

3.1 Introduction

An important class of phosphorus ligands are iminophosphoranes of the general type $R_3P{=}NR'$, with the phosphorus atom in the oxidation state +V. They were first reported by *Staudinger* and *Meyer* in 1919,[93] but virtually no additional chemistry was reported until the late 1950s. In the last 50 years iminophosphoranes gained increasing importance in organic and organometallic chemistry[94] and they proved their value for example in the Aza-Wittig reaction,[95] in the formation of carbodiimides,[96] sterically hindered *sec*. amines[97] and heterocycles.[98] Very recently, it was shown, that iminophosphoranes can effectively catalyzse C=N metathesis *via* an addition/elimination mechanism.[99] The P–N bond is the most versatile bond in main group chemistry and still fuels an innumerable amount of various new compounds, frequently of great stability. Particularly the strength of the bond and the short P=N distance are still interpreted in terms of partial double bond character. The inherent stability and robustness even under harsh chemical conditions of e. g. polyphosphazenes make them advantageous materials for membranes in separation or in fuel cells.[100] Despite this stability polyaminoacid esters of polyphosphazenes turned out to be bio-degradable.[101] This will definitely open a wide avenue to biomedical applications.

The two synthetically most important approaches for the preparation of the P=N motif in iminophosphoranes are the *Staudinger reaction*[93,94,102] of tertiary phosphanes with organic azides under elimination of dinitrogen and the *Kirsanov reaction*[103] of dihalophosphoranes with primary amines, carried out in the presence of an auxiliary base (Scheme 3.1).

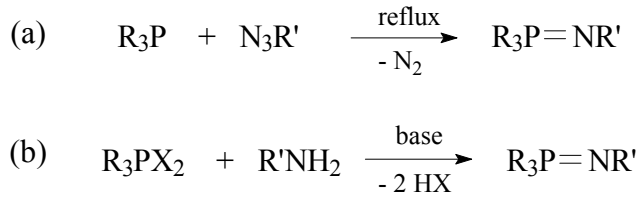

Scheme 3.1: *The Staudinger reaction (a) and the Kirsanov reaction (b) for the preparation of iminophosphoranes.*

Iminophosphoranes can be regarded as the isoelectronical analogues of phosphane oxides ($R_3P=O$) and phosphonium ylides ($R_3P=CR_2$').[104] In comparison to the latter, they are more stable and show lower basicity.[105] The nature of the P=E (E = C, N, O) bonding situation is an issue of current debate as the more subtle aspects still elude a detailed and satisfactory description. A P=N double bond in iminophosphoranes would require valence expansion and d-orbital population at the tetrasubstituted phosphorus(V) centre, not obeying the eight electron rule. As a consequence, iminophosphoranes were vigorously discussed as "hypervalent" species. However, recent findings in the chemical reactivity do not support a P=N double bond, because this bond is cleaved in various reactions.[94,99,106,107] Since the theoretical investigations of *Trinquier* and *Ashby*[108] P=E bonds are mostly discribed as a resonance hybride between the dipolar ylidic form (**A**) and the double bonded ylene form (**B**), already emphasising **A**, as presented in the following scheme.[94,104]

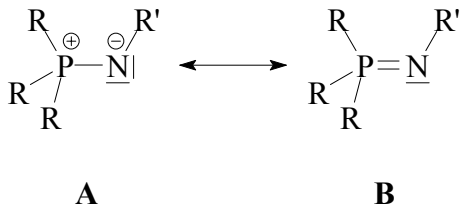

A **B**

Scheme 3.2: *Canonical formulas of iminophosphoranes.*

Calculations on main group "hypervalent" compounds suggest, that although the implementation of d-orbitals in a satisfactory theoretical model is necessary to describe the heavier main group elements, they do not play a significant role in p_π-d_π-bonding and are mainly employed as polarization functions. It was proposed that negative hyperconjunction may be responsible for any π-character in the P–O, P–C or P–N bonds.[109,110] These results were substantiated recently by calculations of the Wittig type reactivity of phosphorus ylides[111] and iminophosphoranes[112] as well as by the results of experimental charge density studies of a phosphane ylide.[113]

Basic iminophosphoranes are described as neutral monodentate ligands donating *via* the lone pair at the imino nitrogen atom.[104,114] They are considered to be predominantly two-electron σ-donors with only minor π-acceptor properties and are easily exchanged by other ligands.[115] The reactivity of tertiary iminophosphoranes is mainly due to the inherent

polarity of the phosphorus–nitrogen bond, which makes them reactive towards both electrophilic and nucleophilic reagents.[94]

Silylated iminophosphoranes $R_3P{=}NSiMe_3$ react with main group-[116] or transition metal-halides[117] under cleavage of the Si–N bond, leading to iminato complexes, containing the $[R_3PN]^-$ building block.[118] These iminato ligands show steric and electronic characteristics similar to the cyclopentadienyl ligand,[119] widely applied in catalysis. Recently, *Stephan et al.* proved the high catalytic activity of iminato complexes towards ethylene polymerization.[120]

Similar to ketones, sulfones and hydrazones,[121] P–alkyl substituated iminophosphoranes are moderatly CH-acidic and can be deprotonated at the C_α-positions by strong bases. Several alkali metal complexes of α-deprotonated iminophosphoranes have been obtained and structurally characterised. The cations are (*C*,*N*)-chelated by the deprotonated carbon and the imino nitrogen atom. The steric demand of the substituents and the nature of the donor solvents determine the aggregation ranging from monomers to tetramers.[104,122,123]

To provide sufficient shielding and solubility even in non-polar solvents it is advantageous to introduce chelating anions of the type $[R–N–E–N–R]^-$ (E = CR,[124] SiR_2,[125] and SR[126]) to metal centres. Isoelectronic replacement of an alkyl substituent in iminophosphoranes by amine groups gives the aminoiminophosphorane $R_2P(NR')N(H)R''$ precursors. These systems and their anions are widely used in transition metal as well as in main group chemistry, as they act as both electron-rich and shielding bidentate (*N*,*N*)-chelats.[50,127] The aminoiminophosphorane $Ph_2P(NSiMe_3)N(H)SiMe_3$ is prepared by the reaction of the Ph_2PH with two equivalents of N_3SiMe_3 in a dual *Staudinger reaction* (Equation 3.1).[128]

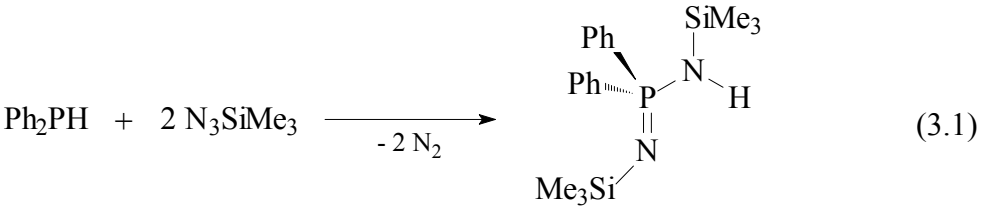

(3.1)

In our group we were interested in the reactivity of heteroaromatic substitued iminophosphoranes and aminoiminophosphoranes.[21] Phosphorus based ligand systems with one or more donating atoms in the periphery gain increasing importance in catalysis and in the design of self assembling ligands.[15,129] Substitution of the organic alkyl or aryl groups in the classical $[NP(R_2)N]^-$-chelating anionic ligand by two pyridyl groups converts it into a *Janus head* $[NP(Py_2)N]^-$ tripodal ligand. At least one pyridyl ring nitrogen in addition to only one imido nitrogen atom is used in metal coordination. The active ligand periphery opens up several avenues: (a) coordination site selectivity $[NPN]^-$ *versus* PyPPy, (b) adaptability in ligation composition depending on the geometric constraints and coordination capability of the metals and (c) the possibility of forming heterobimetallic complexes where the dipyridyl aminoiminophophoranes are employed as flexible metal linkers and not only as bulky protectants. Surprisingly, in pyridyl substituted aminoiminophophoranes it is easy to cleave either one or both P–N bonds. This reduction of P(V) species to P(III) compounds is very uncommon and supplies easy access to phosphanylamines and secondary phosphanes, not easy to make by different routes.

Interestingly, substitution of the phenyl groups in the aryl substituted $Ph_3PNSiMe_3$ by 2-pyridyl substituents and reaction with organolithiums results in the reduction of the parent iminophosphorane(V) to phosphane(III) amides, whereas the triphenyliminophosphorane $Ph_3PNSiMe_3$ reacts by *ortho*-deprotonation of one phenyl ring. In this reaction pathway the $Ph_2PNSiMe_3$-group acts as a *ortho*-directing metallation group, a concept pioneered by *van Koten*,[130] *Brandsma*[131]and *Reich*.[132]

The reduction process of the pyridyliminophosphorane $Py_3PNSiMe_3$ involves dual P–C bond cleavage and substituent coupling reactions together with an exchange of a pyridyl substituent by the carbanionic part of the lithiumorganyl (Scheme 3.3).[21,133,134]

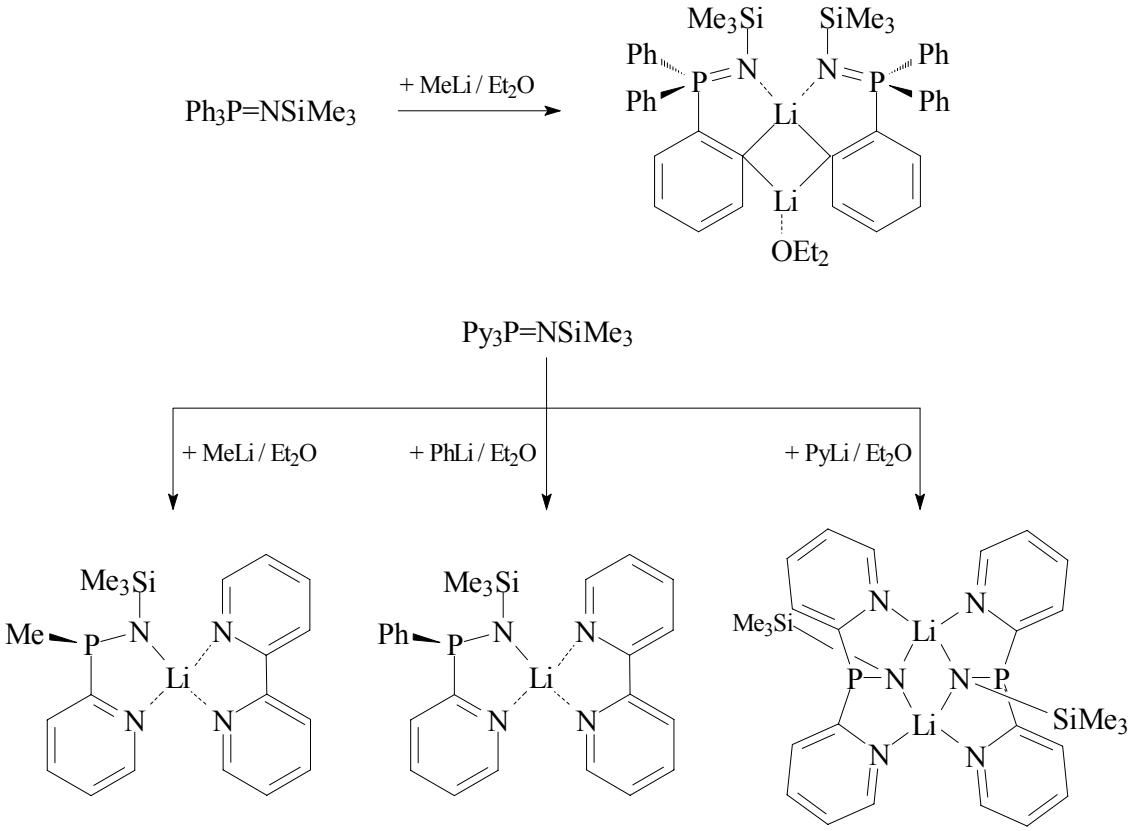

Scheme 3.3: *Reactivity of $Ph_3PNSiMe_3$ and pyridyl substituated iminophosphorane $Py_3PNSiMe_3$ towards lithiumorganics.*

Although the mechanism of the above mentioned reductions is not yet fully understood, these reactions provide facile access to chiral phosphanamides, not easy to make by any other reaction sequences.

The reduction of $Ph_3PNSiMe_3$ is also possible, but requires harsher conditions than the addition of lithiumorganics. The reaction of $Ph_3PNSiMe_3$ with elemental sodium, followed by hydrolysis gives the phosphaneamine $Ph_2PN(H)SiMe_3$ (equation 3.2).[21,68,134,135]

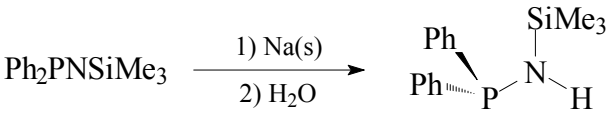

(3.2)

Either as a neutral molecule or as an anionic phosphanamide with the phosphorus next to the nitrogen atom this *Janus head* ligand, provides two adjectent coordination sites. According to steric demand, size and *Lewis*-acidity of the metal centre, the ligand can

coordinate *via* the harder nitrogen or the softer phosphorus(III) atom. The canonical formulas in scheme 3.4 illustrate, that the anion can be described as a phosphanamide (**A**), as well as an iminophosphanide (**B**) (Scheme 3.4).[21,68,134,135]

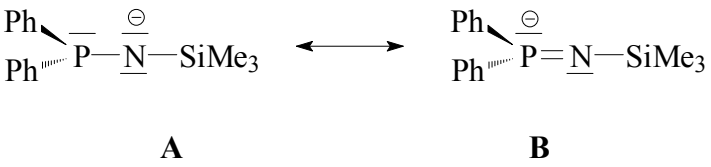

A **B**

Scheme 3.4: *Mesomeric structures of the [$Ph_2PNSiMe_3$]$^-$-anion.*

$Ph_2PN(H)SiMe_3$ reacts with $[Zn\{N(SiMe_3)_2\}_2]$ to give the dimer $[\{(Me_3Si)_2N\}Zn–\{P(Ph_2)(NSiMe_3)\}]_2$. The anionic ligands coordinate in a *s-cis* conformation *via* the phosphorus and the nitrogen atoms to the zinc centres. Similar to this reaction, $Ph_2PN(H)SiMe_3$ was reacted with $[Sn\{N(SiMe_3)_2\}_2]$. Although the recovered product $[Sn_2\{P(Ph_2)(NSiMe_3)\}_2\{NPPh_2\}]$ shows a six membered ring as well, the structure is considerably different to the zinc derivate. In the ring, the two $[Ph_2PNSiMe_3]^-$-anions are organized in a head-to-head arrangement. One tin atom is coordinated by both phosphorus atoms, while the other by both nitrogen atoms of the ligands. Electroneutrality is maintained by a single imidophosphandiide dianion $[Ph_2PN]^{2-}$, bridging both tin centres across the ring. With elemental cesium, the phosphane(III)amine is reduced to a phosphorus(II) species, $[(thf)Cs_2\{Ph(NSiMe_3)P\}_2]_n$. A P–P bond is formed, and metal coordination is provided only by the nitrogen atoms. Oxidative substituent coupling to the P(IV) species $[Ph_2PNSiMe_3]_2$, occurs when $Ph_2PN(H)SiMe_3$ is deprotonated with *n*-BuLi first and subsequently reacted with bismuth trichloride (Scheme 3.5).[21,68,135]

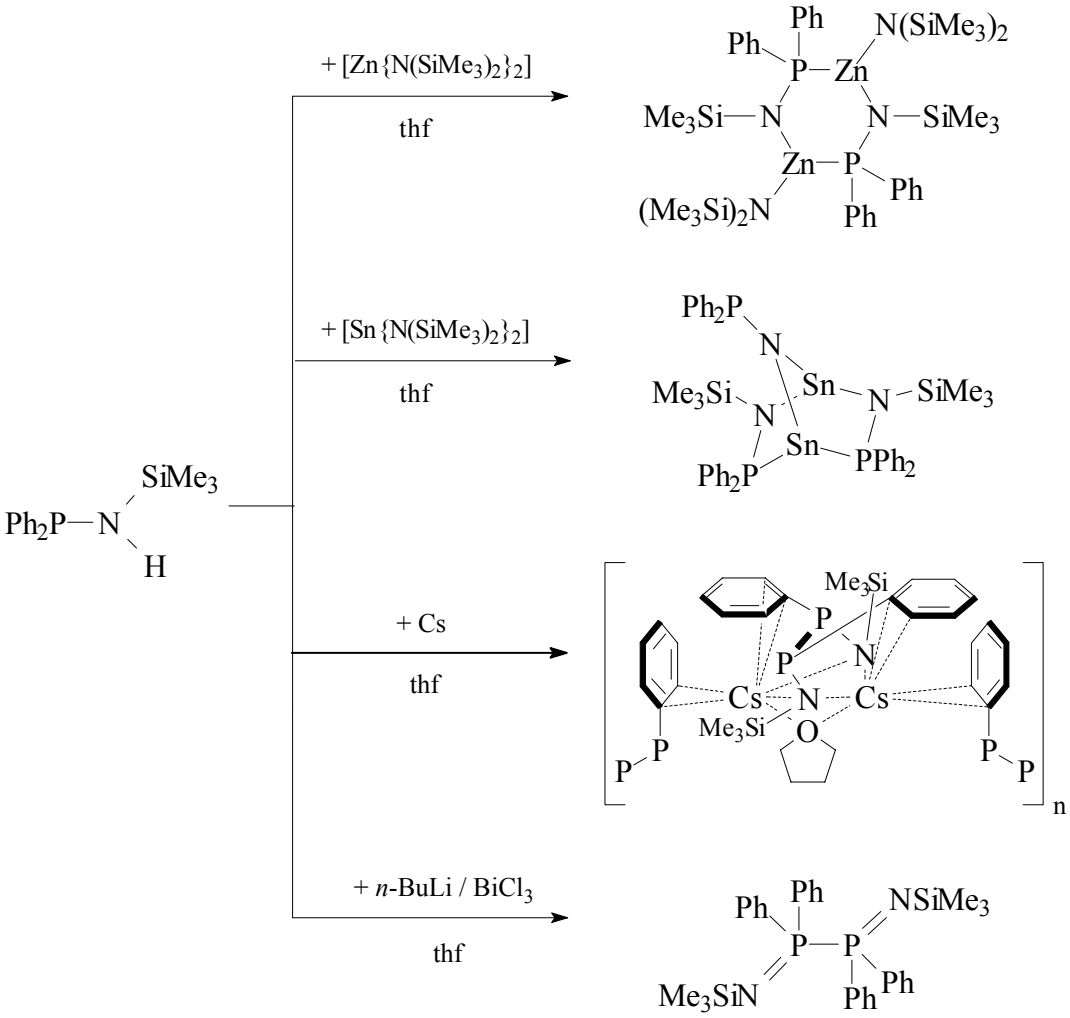

Scheme 3.5: *Reactivity of $Ph_2PN(H)SiMe_3$.*

For the aminoiminophosphorane $Ph_2P(NSiMe_3)N(H)SiMe_3$, the substitution of the phenyl groups by 2-pyridyl units leads to more active reaction sites, as not only the amino function can be deprotonated and not only the $[N–P–N]^-$-skeleton, but also the pyridyl ring nitrogen atoms acting as side arm donors can be involved in complexation.[21,107] The pyridyl substituted aminoiminophosphorane $Py_2P(NSiMe_3)N(H)SiMe_3$ can be prepared in analogy to the formation of $Ph_2P(NSiMe_3)N(H)SiMe_3$. Deprotonation of the amine group is possible with strong metal bases like $[M\{N(SiMe_3)_2\}_2]$ (M = Sr, Ba) or with $ZnMe_2$ (Scheme 3.6).[21,107]

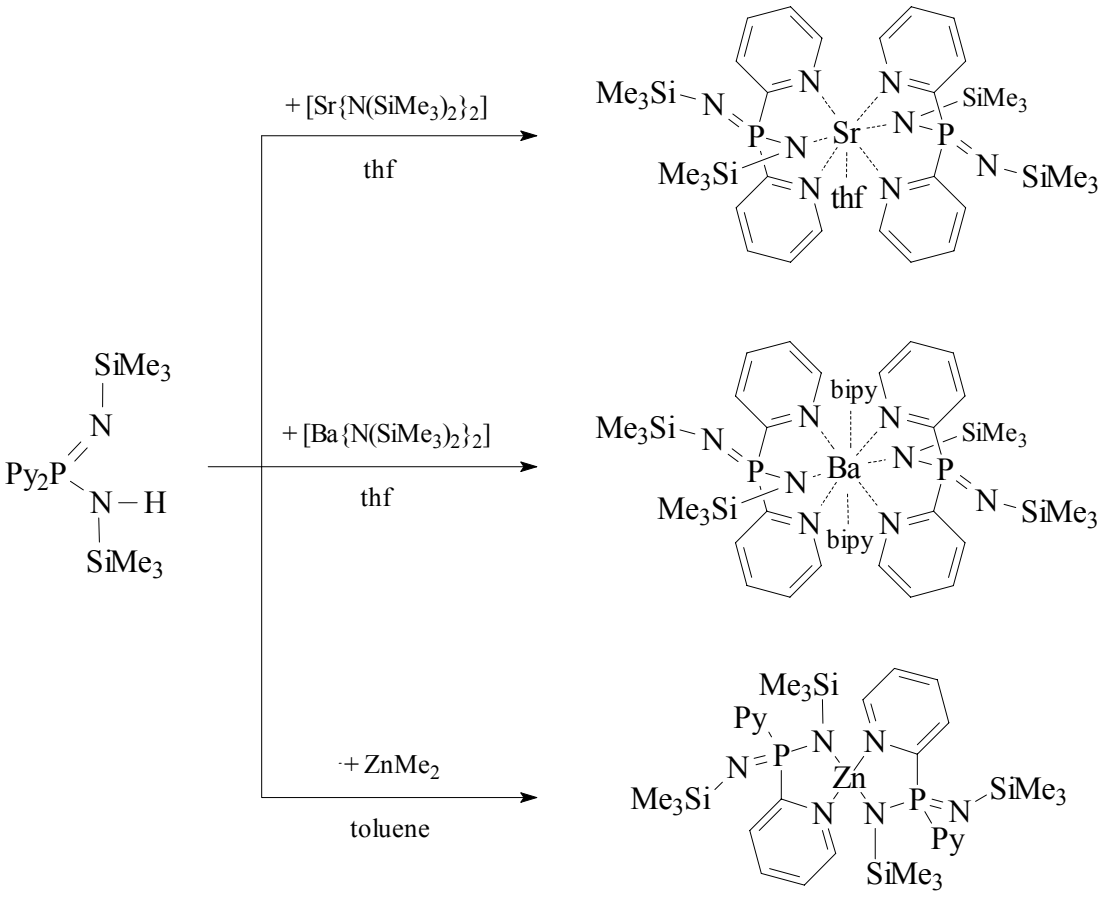

Scheme 3.6: *Reactions of $Py_2P(NSiMe_3)N(H)SiMe_3$ with $[M\{N(SiMe_3)_2\}_2]$ (M = Sr, Ba) and $ZnMe_2$.*

It is interesting to note, that in all the metal derivatives of $Py_2P(NSiMe_3)N(H)SiMe_3$ shown in scheme 3.6 the dipyridylaminoiminophosphoranate anion $[Py_2P(NSiMe_3)]^-$ utilizes at least one pyridyl ligand in conjunction with an amido nitrogen for coordination, illustrating the great geometrical adabtility and the various possibilities of side arm donation to stabilize metal cations of different size. This additional ability prompts the new ligand superior to the phenyl substituted $[Ph_2P(NSiMe_3)]^-$ anion.

With lithiumorganics or lithium amides like $[(thf)Li\{N(SiMe_3)_2\}]$, reduction of $Py_2P(NSiMe_3)N(H)SiMe_3$ to the phosphanide $[(thf)_2Li(Py_2P)]$ and phosphanamide $[Li(Py_2PNSiMe_3)]_2$ is observed, respectively (Scheme 3.7).[21,107]

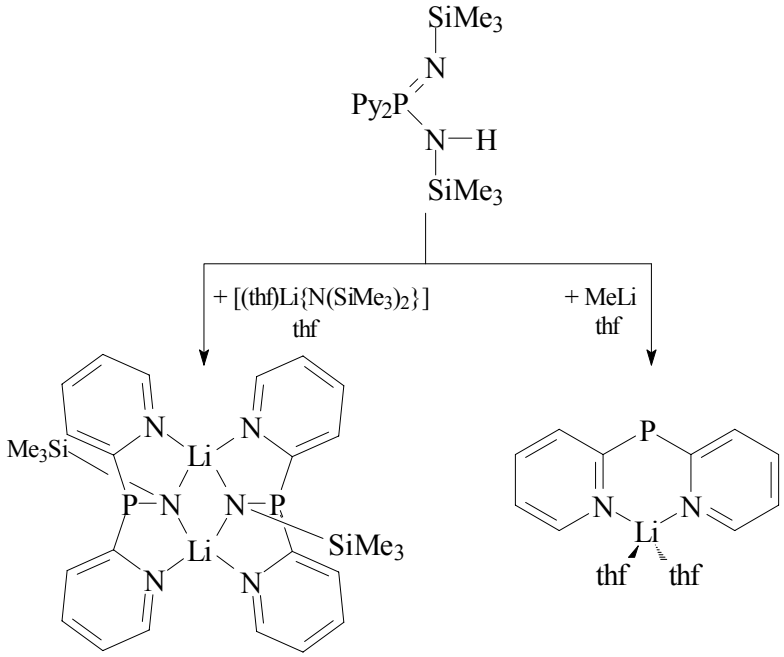

Scheme 3.7: *Reduction of $Py_2P(NSiMe_3)N(H)SiMe_3$ to the phosphanamide $[Li(Py_2PNSiMe_3)]_2$ and the phosphanide $[(thf)_2Li(Py_2P)]$.*

These unprecedented reactions, involving single and dual P–N bond cleavages are remarkable, because reduction of P(V) species is not easy to achieve. They prove that heteroaromatic substituted aminoiminophosphoranes can be useful synthons in transimination reactions. Analogous reactions with the phenyl substituted $Ph_2P(NSiMe_3)N(H)SiMe_3$ proceed on deprotonation and the cations are coordinated by the N–P–N skeleton.[50,127e]

Alkyl substituted iminophosphoranes and the isoelectronical aminoiminophosphoranes show potential applications in catalytical processes and tranformation reactions in organic synthesis. Moreover the implementation of donating atoms in the ligand periphery furnish flexible multidentate *Janus head* ligands.

This work, synergetically combines the side arm donation concept and the acidic properties of alkyl substituted iminophosphoranes to generate a highly flexible ligand system. A improved geometrical adaptability and a higher degree of delocalization is achieved by introducing an alkyl bridge between the phosphorus atom and the donating heterocycle. The so far unknown N-trimethylsilyldiphenyl(-2-)picolyliminophosphorane $Ph_2P(CH_2Py)$–$(NSiMe_3)$, (**9**), was chosen as a target molecule for further investigations (Scheme 3.8).

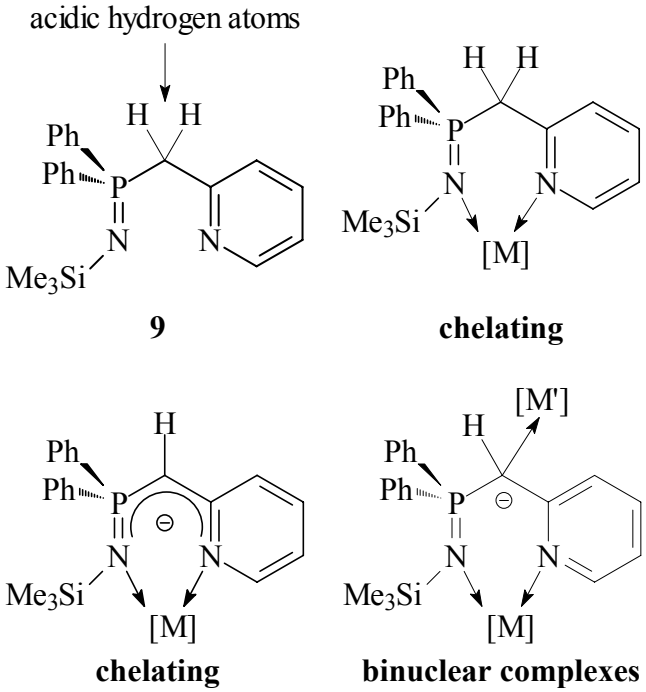

Scheme 3.8: *$Ph_2P(CH_2Py)(NSiMe_3)$, (**9**), and its reactive sites.*

The neutral molecule is a potential (*N*,*N*')-bidentate chelating ligand. Deprotonation at the C_α-carbon atom furnishes new mono- or dianionic phosphorus-centred ligands. To elucidate the properties and coordination modes of these anions, $Ph_2P(CH_2Py)(NSiMe_3)$, (**9**), was reacted with several main group metal and transition metal bases. The main questions to be answered in this context are:

1. Would the deprotonated starting material give a carbanion, coordinating hard metal cations *via* the carbanionic, ylidic centre or is just (*N*,*N'*)-chelation feasible?
2. Is the hypervalency-concept valid to describe the bonding in the anion as [–N=P–C^-<] or [–$^-$N–P=C<] or would the more ionic interpretation along [–$^-$N–P^+–C^-<] be more appropriate ?
3. How does the electron deficient pyridyl substituent influence the stability and coordination modes of the anion by means of delocalization?
4. Which impact has the negative charge of the ligand and the nature of the coordinated metal on the bonding ?
5. Can the anion stabilize low valent transition metals in low oxidation states, important for catalytical approaches, by side arm donation?

During the course of this work, *Leung et al.* achieved to synthesize the methylene bridged iminophosphorane $^{i}Pr_2P(CH_2Py)NSiMe_3$. They focused on the preparation of stable, low valent 1,3-dimetallacyclobutanes $[M\{C(^{i}Pr_2PNSiMe_3)(2\text{-}Py)\}]_2$ (M = Ge(II), Sn(II), Pb(II)) (Scheme 3.9).[136]

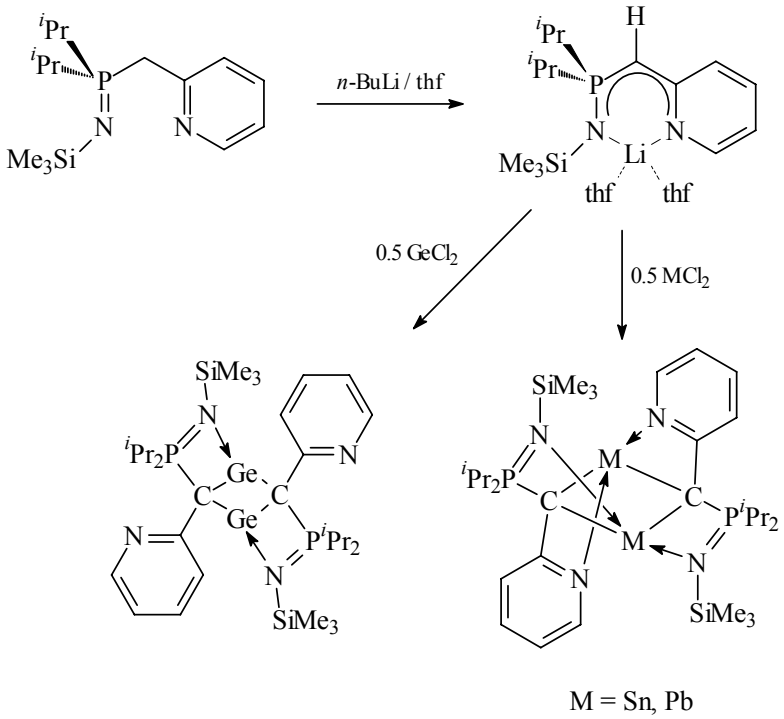

Scheme 3.9: *Preparation of 1,3-dimetallacyclobutanes $[M\{C(^{i}Pr_2PNSiMe_3)(2\text{-}Py)\}]_2$ (M = Ge(II), Sn(II), Pb(II)).*

The above mentioned metallacycles were synthesized *in situ* by deprotonation of $^{i}Pr_2P(CH_2Py)NSiMe_3$ at the C_α-carbon atom with one equivalent of *n*-BuLi, followed by transmetallation with the corresponding group 14 chlorides.[136] The nature and bonding situation of the monoanionic $[^{i}Pr_2P(CHPy)(NSiMe_3)]^-$-intermediate was not studied.

3.2 Preparation of diphenyl-2-picolyliminophosphorane

3.2.1 Synthesis and crystal structures of $Ph_2P(CH_2Py)(NSiMe_3)$, (9a) and $[Ph_2P(CH_2Py)(NSiMe_3)]_2$, (9b)

The starting material for this study, N-(trimethylsilyl)diphenyl-2-picolyliminophosphorane (**9**), is readily available *via* the *Staudinger* reaction[94] of diphenyl-2-picolyl–phosphane(**1**)[28] with trimethylsilylazide (Equation 3.3).[137]

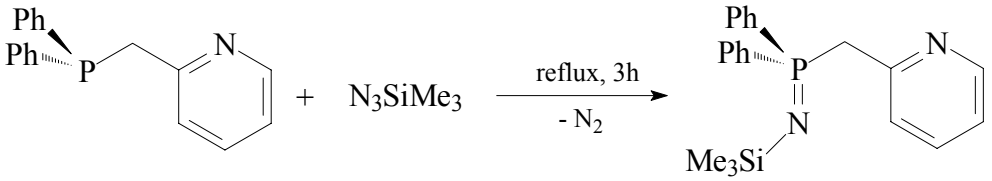

1 **9** (3.3)

For the preparation of $Ph_2P(CH_2Py)(NSiMe_3)$, (**9**), one equivalent of freshly distilled trimethylsilylazide was added to solid Ph_2PCH_2Py, (**1**). Refluxing the reaction mixture and distilling the crude product in vacuum leads to a colourless viscous oil. The iminophosphorane **9** crystallizes form a hexane solution at -16°C as colourless plates, melting at 44°C to give the polymorph **9a**. Figure 3.1 depicts the solid state structure of $Ph_2P(CH_2Py)(NSiMe_3)$, (**9a**).[137] Selected bond lengths and angles are summerized in table 3.1.

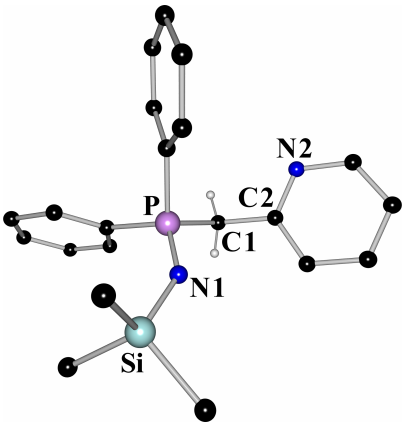

9a

Figure 3.1: *Solid state structure of the first polymorph $Ph_2P(CH_2Py)(NSiMe_3)$, (**9a**).*

Table 3.1: *Selected bond lengths [pm] and angles [°] of $Ph_2P(CH_2Py)(NSiMe_3)$, (**9a**).*

P–N1	154.13(12)	N1–Si	168.08(12)
$P–C_{Ph}$	av. 181.67	P–N1–Si	143.91(8)
P–C1	182.57(14)	P–C1–C2	111.98(9)

As anticipated, the central phosphorus atom in $Ph_2P(CH_2Py)(NSiMe_3)$, (**9a**), is tetrahedrally coordinated by three carbon atoms and one nitrogen atom. The $P–C_{Ph}$ distances (av. 181.67 pm) are slightly shorter than the P–C1 bond (182.57(14) pm) because of the smaller radius of a sp^2- compared to a sp^3-hybridized carbon atom. The P–N1 bond length of 154.13(12) pm is in the range normally quoted for a formal P=N double bond in iminophosphoranes (147–162 pm).[50,94,127e,138]

Like in all N-silyl substituted iminophosphoranes, the Si–N1 contact (168.08(12) pm) is shorter than a formal Si–N single bond (174 pm).[30,94] In the solid-state **9a** adopts a *transoid* conformation with the two nitrogen atoms N1 of the imino group and N2 of the pyridyl ring pointing in opposite directions, due to the repulsion of the N-lone pairs. N···H–C-hydrogen bonding is not observed.[137]

Interestingly, crystallization of $Ph_2P(CH_2Py)(NSiMe_3)$, (**9**), from the crude oily product, after distillation, yields the iminophosphorane as a second polymorph **9b** (Figure 3.2).[139]

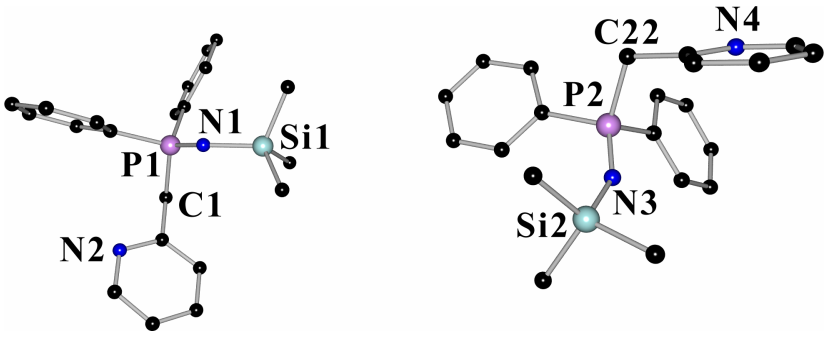

9b

Figure 3.2: *Solid state structure of the second polymorph $[Ph_2P(CH_2Py)(NSiMe_3)]_2$, (**9b**). Crystals obtained by crystallization of the oil.*

Table 3.2: *Selected bond lengths [pm] and angles [°] of $[Ph_2P(CH_2Py)(NSiMe_3)]_2$, (**9b**).*

N1–Si1	169.72(14)	N3–Si2	168.37(14)
P1–N1–Si1	135.52(9)	P2–N3–Si2	149.55(10)
av. P–N	154.12	$av. P–C_{Ph}$	181.80
	av. P1/2–C1/22(sp^3) 183.50		

Polymorphism is a challenging phenomenon in crystal engineering, drug design and theory.[140] Different to $Ph_2P(CH_2Py)(NSiMe_3)$, (**9a**), the asymmetric unit of **9b** consists of two molecules of $Ph_2P(CH_2Py)(NSiMe_3)$ (**9**). With regard to bond lengths there is no significant difference between the polymorphous iminophosphoranes **9a** and **9b**. However, it is remarkable, that in **9b** the angles at the imino nitrogen atoms (135.52(9)° for P1–N1–Si1 and 149.55(10)° for P2–N3–Si2) differ by ca. 14°, while the corresponding angle in **9a** (P–N–Si: 143.91(8)°) is half-way between these two values. The angles $P–CH_2–C_{Py}$ in **9b** are slightly different and splayed up to an average of 112.83° in comparison to the related angle in **9a** (111.98(9)°). These variations at the imino nitrogen atoms might cause the different crystal packings of **9a** and **9b** (Figure 3.3).[139]

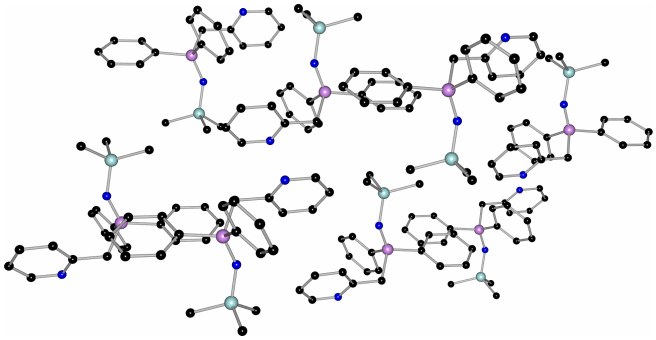

9a

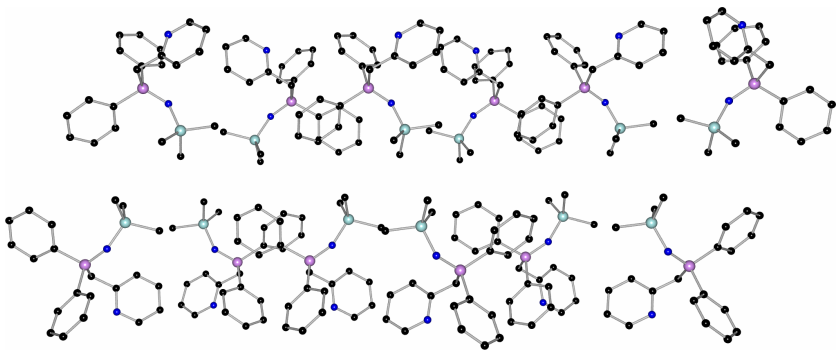

9b

Figure 3.3: *Crystal packing of $Ph_2P(CH_2Py)(NSiMe_3)$ (**9a**) and $[Ph_2P(CH_2Py)(NSiMe_3)]_2$ (**9b**).*

In both packings, the molecules are arranged in layers. N···H–C-hydrogen bonding is not observed. Whereas the orientation of the $N–SiMe_3$ groups in a layer in **9a** alternates between up and down, the corresponding groups in **9b** all point in the same direction. This

results in steric interactions of the neighbouring Me_3SiN-substituents in **9b** and leads to different angles at the imino nitrogen atoms.[139]

The ^{31}P-NMR spectrum of **9**, in solution shows a singulet at -0.32 ppm. For the Si-atom a resonance at δ = -10.61 is observed. The two protons of the methylene group resonate at δ = 3.56 as a doublet with a coupling constant of $^2J_{P-H}$ = 14.1 Hz. A ^{1}H, ^{15}N-HMBC-NMR experiment reveals an upfield shifted signal at -343 ppm for the imino nitrogen atom and a signal at δ = -61 for the pyridyl nitrogen atom.[137]

3.2.2 Synthesis of $[Ph_2P(CH_2Py)NH_2][N_3]$, (10)

If the phosphane $Ph_2P(CH_2Py)$, (**1**), is reacted with crude trimethylsilylazide, i. e. if N_3SiMe_3 is not dried and distilled prior to use, the formation of a minor product is indicated by ^{31}P-NMR studies, later identified as $[Ph_2P(CH_2Py)(NH_2)][N_3]$, (**10**). It can be isolated from $Ph_2P(CH_2Py)(NSiMe_3)$ by solvation in thf/hexane and crystallisation at -16°C (Figure 3.4).[139]

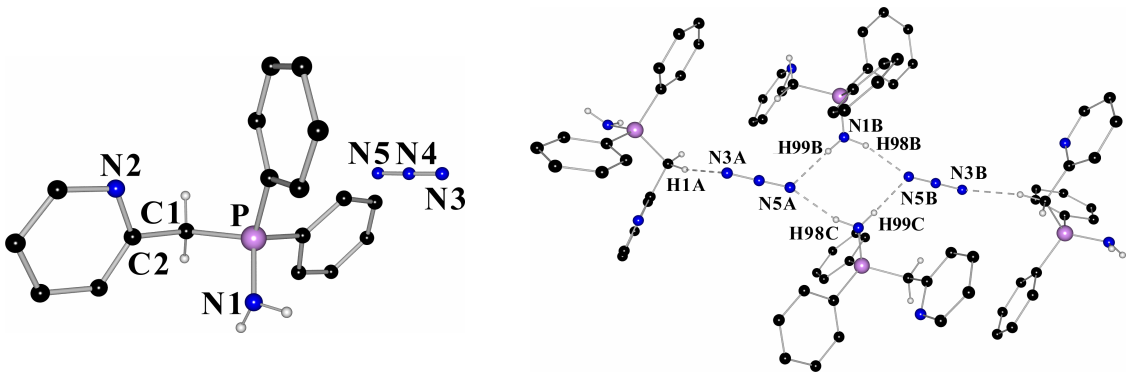

Figure 3.4: *Solid state structure of $[Ph_2P(CH_2Py)(NH_2)][N_3]$, (**10**, left) and the intermolecular hydrogen bonded chain (right). For clarity, only the hydrogen atoms of the methylene bridge and those of the NH_2-group are depicted.*

Table 3.3: *Selected bond lengths [pm] and angles [°] of $[Ph_2P(CH_2Py)(NH_2)][N_3]$, (**10**).*

P–N1	161.3(3)	av. P–C_{Ph}	179.9
P–C1	180.1(3)	P–C1–C2	113.1(2)
N5A····H98C	206.8	N5A····H99B	205.0
N3A····H1A	248.7	C1A–H1A····N3A	167.9
N1B–H99B····N5A	167.9	N1B–H98C····N5A	177.9

The structure of the salt $[Ph_2P(CH_2Py)(NH_2)][N_3]$, (**10**), consists of a cationic $[Ph_2P(CH_2Py)(NH_2)]^+$-fragment and as counterion an azide anion. These two units are linked by hydrogen bonding in the solid state, leading to an infinite chain structure. The N3A atom of the azid anion binds to the hydrogen atom H1A of the methylene bridge. The other end of the N_3^--anion, the N5A atom, serves as an acceptor in a bifurcated hydrogen bond to the hydrogen atoms H98C and H99B of two different amine units (Figure 3.4, right).[139] In related salts like $[Me_3PNH_2][Cl]$[141] and $[Ph_3PNH_2][Cl]$[142] this arrangement was also observed.The N3A····H1A distance in **2** of 248.7 pm is 42.8 pm longer than the N5A····H98C/H99B contacts (av. 205.9 pm). The angles X–H····N vary from 167.9° for C1A–H1A····N3A and N1B–H99B····N5A, respectively, to 177.9° for N1C–H98C····N5A. Both types of hydrogen bonds show high directional preferences. Thus, according to *Jeffrey*,[143] the N3A····H1A interaction can be described as a weak hydrogen bond, while the N5A····H98C/H99B interactions are mainly electrostatic and correspond to moderately strong hydrogen bonds.[144]

The $P–C_{Ph}$ bond lengths in **10** are on average 179.9 pm and slightly shorter than those in **9a** (av. 181.67 pm) and **9b** (av. 181.80 pm). The P–C1 distances are shortened from 182.57(14) pm in **9a** to 180.1(3) pm in **10**. Both are in the range quoted for P–C single bond lengths (185 pm).[30] In $[Ph_2P(CH_2Py)(NH_2)][N_3]$ (**10**) the P–N1 distance of 161.3(3) pm is much longer than in the iminophosphorane **9a** (154.13(12) pm), but shorter than a normal P–N single bond (170 pm).[30] In related salts $[R_3PNH_2][X]$ (R = Me, Et, Ph; X = Cl, I, ICl_2, SCN) P–N distances from 160 to 165 pm are observed.[141,142,145] The sum of the bond angles at N1 in **10** of only 345.5°, indicates a pyramidal geometry and a stereochemically active lone-pair.[139]

The ^{31}P-NMR spectrum of $[Ph_2P(CH_2Py)(NH_2)][N_3]$, (**10**), shows a singulet at 22.03 ppm, which is a remarkable downfield shift in comparison to the iminophosphorane $Ph_2P(CH_2Py)(NSiMe_3)$, (**9**), (δ = -0.32). The hydrogen atoms at the nitrogen atom can be detected as a broad signal at 2.85 ppm. A ^{1}H, ^{15}N-HMBC-NMR experiment resulted in resonances at δ = -335 for the phosphorus bounded nitrogen atom and at -60 ppm for the pyridyl nitrogen atom. Interestingly, these ^{15}N shifts differ not much from those of the iminophosphorane **9**. This means, that the electronic situation of the nitrogen atoms in **9** and **10** are very similar.

The formation of phosphonium salts is not unprecidented. In general it is observed as a side product in reactions of silylated iminophosphoranes with halogenides, due to small amounts of water solved in the crude halides.[146] *Vogt* et al. reported, that the reaction of Ph_3P with N_3SiMe_3 in crude dichloromethane or on addition of water results in the formation of $[Ph_3PNH_2][Cl]$.[147] Employing this strategy we tried to synthesize $[Ph_2P(CH_2Py)(NH_2)][N_3]$, (**10**), selectively. Therefore $Ph_2P(CH_2Py)$ was solved in thf and H_2O was added. After addition of an excess of N_3SiMe_3, the solution was stirred for one hour at r.t. In the ^{31}P-NMR spectrum the formation of small amounts of **10** is observed exclusively. No signal for the iminophosphorane $Ph_2P(CH_2Py)(NSiMe_3)$, (**9**), was detected. After refluxing the solution for 2 h and work up we were able to isolate **10** in 46% yield (Equation 3.4).[139]

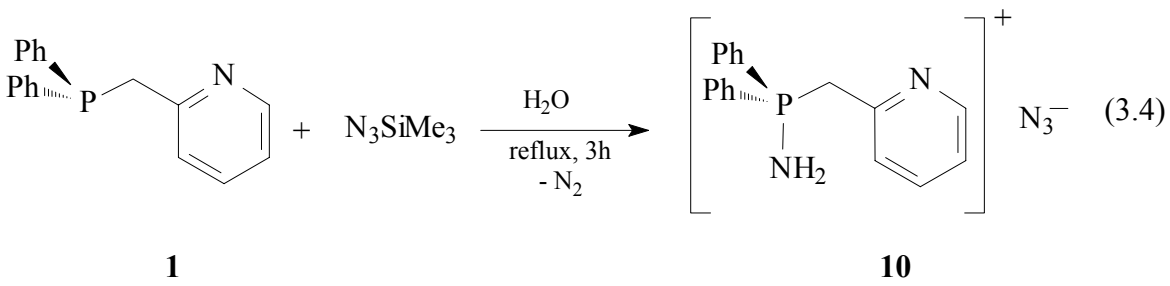

1 **10** (3.4)

The observations from ^{31}P-NMR studies reveal that for the formation of **10** N_3H is involved, which is built *in situ* by the reaction of N_3SiMe_3 with water. This is responsible for the tendency of not properly dried trimethylsilylazide to explode upon heating and suggests the following mechanism (Scheme 3.10).[139]

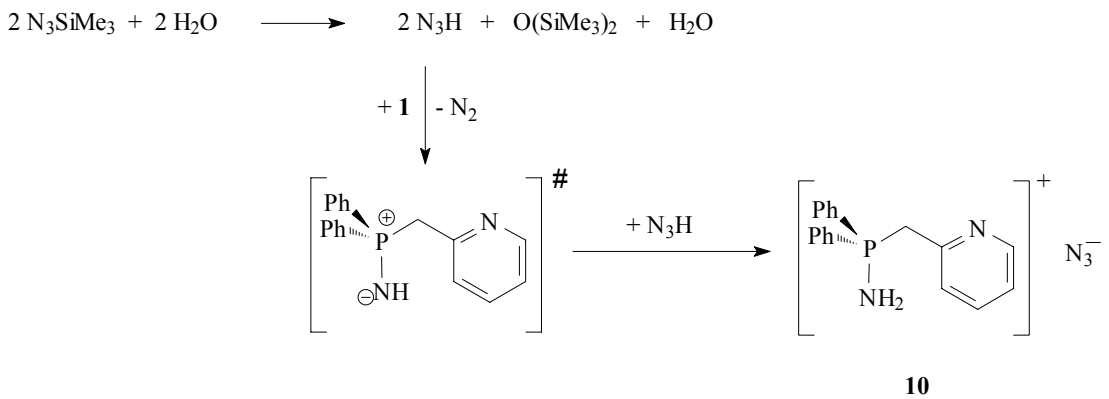

10

Scheme 3.10: *Proposed mechanism for the formation of $[Ph_2P(CH_2Py)(NH_2)][N_3]$, (**10**).*

The trimethylsilylazide reacts with water to give N_3H. A *Staudinger* reaction of hydrogenazide with the phosphane gives the intermediate [$Ph_2P(CH_2Py)NH$]. Reaction of the basic NH function with further N_3H yields the product [$Ph_2P(CH_2Py)(NH_2)$][N_3], (**10**).

3.3 Reactions with group one organyls and amides

3.3.1 Deprotonation of $Ph_2P(CH_2Py)(NSiMe_3)$, (9), with lithiumalkyls and -amides

To elucidate the coordination behaviour and bonding modes of the [$Ph_2P(CHPy)(NSiMe_3)$]$^-$-anion, $Ph_2P(CH_2Py)(NSiMe_3)$, (**9**), was deprotonated at the methylene bridge with one equivalent of MeLi, *n*-BuLi and the lithium amide [$(Et_2O)Li\{N(SiMe_3)_2\}$][148] in diethyl ether at -78°C. All reactions lead to the formation of the lithium complex [$(Et_2O)Li\{Ph_2P(CHPy)(NSiMe_3)\}$], (**11**) (Equation 3.5).[137]

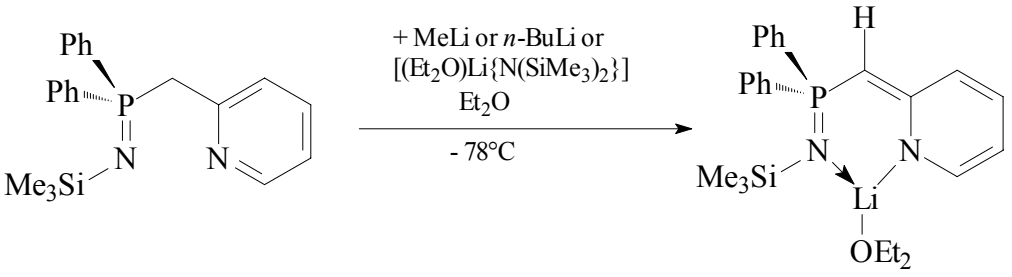

9 **11** (3.5)

The lithium complex [$(Et_2O)Li\{Ph_2P(CHPy)(NSiMe_3)\}$], (**11**), crystallizes as yellow blocks from diethyl ether after several days at r.t. The crystals melt at 104°C. The solid state structure of **11** is shown in figure 3.5; selected bond lengths and angles are summerized in table 3.4.

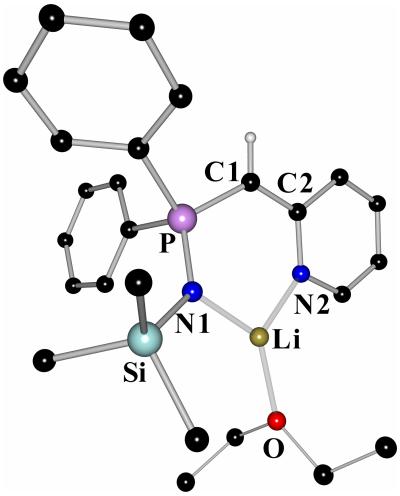

Figure 3.5: *Solid state structure of [(Et$_2$O)Li{Ph$_2$P(CHPy)(NSiMe$_3$)}], (**11**).*

Table 3.4: *Selected bond lengths [pm] and angles [°] of [(Et$_2$O)Li{Ph$_2$P(CHPy)(NSiMe$_3$)}], (**11**).*

P–N1	159.19(10)	Si–N1	170.77(10)
P–C1	172.76(12)	Li–N1	194.6(2)
av. P–C$_{Ph}$	182.66	Li–N2	196.1(2)
C1–C2	139.86(17)	P–C1–C2	127.37(9)
C2–N2	137.10(16)	P–N1–Si	130.51(6)

In [(Et$_2$O)Li{Ph$_2$P(CHPy)(NSiMe$_3$)}], (**11**), the trigonal planar coordination sphere of the lithium cation is made up of the imino nitrogen atom N1, the pyridyl nitrogen atom N2 and the oxygen atom of the donating diethyl ether molecule. The metal cation is displaced only 22.6 pm from the plane determined by these three atoms. As anticipated from the coordination behaviour,[24,25,31,149] a six membered metallacycle is formed. The conformation of this ring shows a distorted boat arrangement with the deprotonated carbon atom and the metal in the bow and stern positions. They are located 29 and 14 pm, respectively, out of the best plane defined by N1-P-C2-N2. The sum of the bond angles at N1 is close to 360°, indicating a planar environment around this atom. The same is valid for the pyridyl ring nitrogen atom N2. In contrast to the chemically related monomeric bis(iminophosphorane)methanides [(Et$_2$O)Li{HC(Cy$_2$PNSiMe$_3$)$_2$}],[150] [(thf)Li{HC(Ph$_2$P-NSiMe$_3$)$_2$}][151] and the dimeric [Li{HC(Ph$_2$PNSiMe$_3$)$_2$}]$_2$,[152] the lithium cation in **11** shows no contact to the deprotonated carbon atom C1 (Li···C1 322.5 pm). The bond angles at C1 are close to 120°, indicating sp^2-hybridization. Different to the parent iminophosphorane **9a**, (*N,N'*)-chelation to the metal causes a N1/N2 *cisoid* conformation. It seems remarkable that the Li–N1 distance in **11** ((194.6(2) pm) is only slightly shorter than the Li–N2 contact of 196.1(2) pm. Both contacts are at the short end of the range

reported for Li–N bond distances in lithium amides[153] (e.g. [(Et_2O)Li{$N(SiMe_3)_2$}]: 206 pm),[154] lithium iminophosphoranats[106,155] (e.g. [(Et_2O)$_2$Li{$Ph_2P(C(H)SiMe_3)(NSiMe_3)$}]: av. 201.8 pm)[122d] and lithium aminidinates[156] (e.g. [Li{(^{n}Bu)C(N^tBu)$_2$}]$_2$·LiX+(thf)$_2$: X = Cl, Br: 194 – 208 pm).[157]

In contrast to the P–C_{Ph} bond lengths (av. 182.66 pm), which do not differ significantly from those found in the starting material $Ph_2P(CH_2Py)(NSiMe_3)$ (**9**) and which are in the range found for P–C single bonds (av. 185 pm),[30] the P–C1 bond (172.76(12) pm) length is shortened by 9 pm. In phosphaalkenes, the formal P=C double bond distances vary from 161 to 171 pm and the average value is 167 pm.[158] Ylidic P–C bond lengths are found between 163 and 173 pm[159] and *Gilheany* quotes an average value of 169 pm.[109] Thus, the P–C1 bond in **11** would be consistent with a partial double bond character as depicted by the resonance structure **b** in scheme 3.11 The P–C1 bond length is comparable to those found in bis(iminophosphorane)methanide chelate complexes.[122d,150,151,152]
The C1–C2 distance of 150.39(19) pm in **9** also decreases by approximately 10 pm to 139.86(17) pm in [(Et_2O)Li{$Ph_2P(CHPy)(NSiMe_3)$}], (**11**), reflecting a partial C=C double bond character as depicted in **c** of scheme 3.11. The value, generally quoted for C=C double bonds is 134 pm.[30] Furthermore, the C_{ipso}–N_{Py} bonds of the anionic ligand (137.10(16) pm) is ca. 4 pm longer than the corresponding bond in the neutal iminophosphorane **9**, indicating a perturbation of the aromatic ring system. This might be interpreted as a result of the transfer of the negative charge from the deprotonated carbon atom to the pyridyl ring nitrogen atom.
Although the P1–N1 bond length in **11** (159.19(10) pm) is widened by about 5 pm with respect to **9a** it is still in the range generally quoted for formal P=N double bonds in iminophosphoranes.[94,138] Likewise, the N1–Si bond (170.77(10) pm) is elongated by 2.7 pm in comparison to the N–Si bond in the iminophosphorane **9a**. Similar elongations are observed in [(Et_2O)Li{(o-C_6H_4)$Ph_2PNSiMe_3$}]$_2$[106] and lithiated bis(iminophosphoran)-methanides[151,152] with regard on the respective starting materials.[133,160]

These geometrical features suggest canonical formulas as depicted in scheme 3.11. However, all of them require valence expansion at the phosphorus atom, not obeying the eight electron rule, but chemical reactivity neither supports P=N nor P=C double bonds because both are easily cleaved in various reactions.[94,99,106,107]

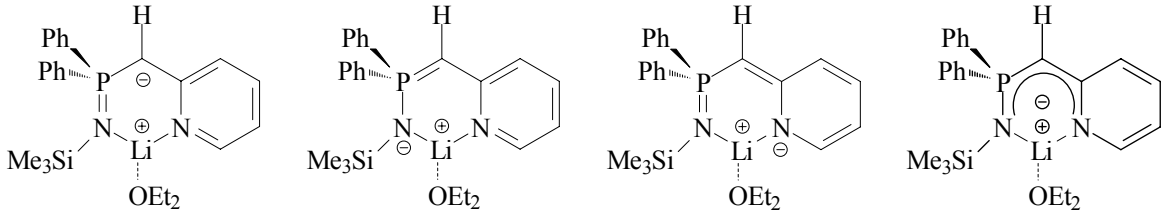

Scheme 3.11: *Resonance forms of [(Et₂O)Li{Ph₂P(CHPy)(NSiMe₃)}], (**11**): **a)** indicates a carbanionic ylidic contribution; **b)** shows the amidic ylenic resonance structure; **c)** emphasizes the amidic olefinic resonance form and **d)** visualizes the delocalization of the negative charge.*

To gain more information on the charge density distribution at the phosphorus atom and to elucidate the bonding situation several NMR spectra of [(Et$_2$O)Li{Ph$_2$P-(CHPy)(NSiMe$_3$)}], (**11**), in solution were recorded. The ^{31}P-NMR spectrum shows a singulet at δ = 18.03. In the ^{29}Si-NMR, the silicon atom resonates at δ = -8.63. The proton at the methylene bridge gives a doublet at 3.58 ppm, with a coupling constant of $^{2}J_{P-H}$ = 18.2 Hz. An interesting result gave a ^{1}H,^{15}N-HMBC-NMR experiment. Whereas the signal for the imino nitrogen atom in **11**, resonates at δ = -331, which is almost unchanged (Δδ = 12) compared to the iminophosphorane Ph$_2$P(CH$_2$Py)(NSiMe$_3$), (**9**), the pyridyl nitrogen atom in **11** shows a remarkable upfield shift to δ = -145 (Δδ = -84 relative to **9**). These NMR-shifts can be explained by a considerable charge transfer from the carbanionic atom C1 to the heteroaromatic ring and accumulation at the pyridyl nitrogen atom. Additionally, the almost constant ^{15}N-NMR spectroscopical shifts of the imino nitrogen atom in **9** and **11** indicate, that the charge density at these nitrogen atoms is less affected by the deprotonation. In quintessence neither the geometrical parameters from the structure nor the NMR spectroscopical data of **11** provide a conclusive criterion to decide which resonance form in scheme 3.11, if any, contributes most to the bonding in the lithium complex.[137]

To elucidate the charge density distribution in [(Et$_2$O)Li{Ph$_2$P(CHPy)(NSiMe$_3$)}], (**11**), *Kocher*[137,161] in our group performed a multipole refinement based on the formalism of Hansen and Coppens[162] with 100K high resolution data up to $(\sin\theta/\lambda)_{max}$ = 1.145Å^{-1}. The results of the topological analysis are presented in terms of the charge density ρ(**r**), the Laplacian $\nabla^2\rho(\mathbf{r})$ and the charges obtained from the integration over the atomic basins along Baders theory of „Atoms in Molecules“ (AIM).[163] All bond critical points (BCPs) at the P–E bonds are displaced closer to the electropositive phosphorus atom. A comparison

of the densities $\rho(\mathbf{r}_{BCP})$, the algebraic sum of the eigenvalues (λ_i) of the Hessian matrix, $\nabla^2\rho(\mathbf{r}_{BCP})$, of these bonds and the integrated charges are presented in table 3.5.[137,161]

***Table 3.5**: Topology of the P–N and P–C bonds in [(Et$_2$O)Li{Ph$_2$P(CHPy)(NSiMe$_3$)}], (**11**).*

A–B	d(A–B)	d(A–BCP)	d(BCP–B)	$\rho(\mathbf{r}_{BCP})$	$\nabla^2\rho(\mathbf{r}_{BCP})$	Charge at B
P–N1	1.5903	0.6566	0.9337	1.508(10)	5.874(28)	–1.98
P–C1	1.7252	0.7753	0.9499	1.336(8)	-8.325(22)	–0.54
P–C7	1.8294	0.8047	1.0248	1.134(6)	-6.402(15)	–0.31
P–C13	1.8147	0.7784	1.0364	1.151(8)	-6.145(16)	–0.34

d(A-B): distance between atoms A and B along the bondpath in Å; d(A-BCP), d(BCP-B): distance between the BCP and atom A and B, respectively; $\rho(\mathbf{r}_{BCP})$: charge density at the BCP in eÅ^{-3}; $\nabla^2\rho(\mathbf{r}_{BCP})$: Laplacian of $\rho(\mathbf{r})$ at the BCP in eÅ^{-5}; Charges of B from integration over atomic basins in electrons, charge of the phosphorus atom A = +2.20.

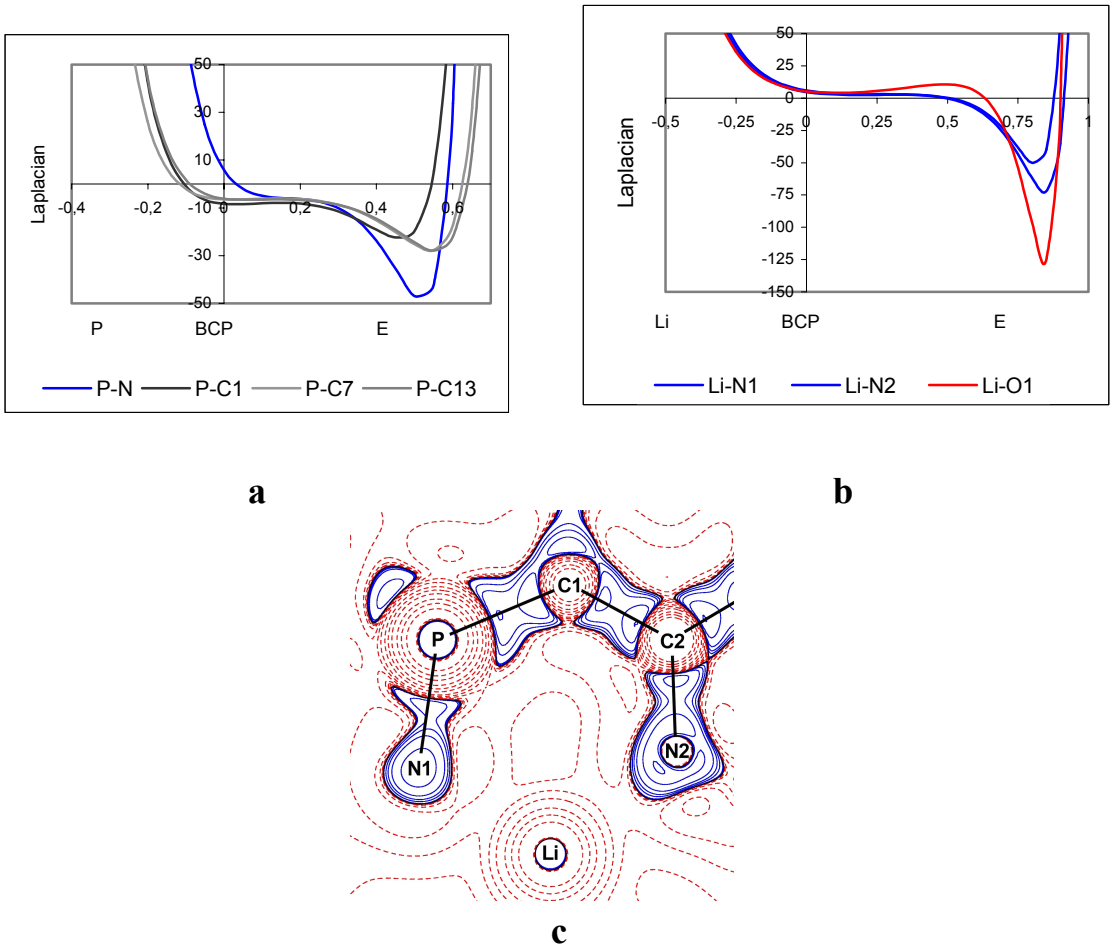

***Figure 3.6:** a) Laplacian along the bond paths of the P–C and P–N bonds; b) Laplacian in the P1–C2–Li plane (blue lines indicating charge concentrations, red lines indicating charge depletions);(c) Laplacian along the bond paths of the Li–N and Li–O bonds, respectively. The zero-value of the x-axis indicates the position of the BCP.[137,161]*

The properties at the BCPs of the aromatic carbon bonds in the phenyl rings as well as those in the $SiMe_3$ group are in the expected range. The two topologically analysed P–C_{Ph} bonds in **11** are comparable to those in the triphenylphosphane donor molecule of a transition metal complex.[164] Different to the P–C_{Ph} bonds in triphenylphosphonium benzylide $Ph_3P{=}C(H)Ph$ no variance in the topology between the two P–C_{Ph} bonds in **11** could be observed.[113] Compared to the latter, the P–C1 bond displays higher charge density and a more negative Laplacian at the BCP. An inspection of the Laplacian along the P–C bond paths (Figure 3.6) in **11** reveals an almost equal charge distribution in the phosphorus basin, while the main difference of the Laplacian in the basin of the carbon atoms is related to the shorter distance between C1 and $BCP_{P–C1}$. This rather short P–C bond results from distinct electrostatic interactions between the negatively polarised deprotonated C1 and the electropositive phosphorus atom reflected by the charges of -0.52 e for C1 and +2.20 e for P from the integration over the atomic basins.[165]

The properties of the exocyclic C1–C2 bond, which are almost the same as an aromatic C–C bond as well as the aromatic character of the C2–N2 bond of the pyridine ring fuels the idea of a delocalisation of the negative charge in the C1–C2–N2 residue. This exocyclic delocalisation slightly perturbs the aromaticity of the heteroaromatic ring. The bond lengths and electron densities in the pyridyl substituent differ from those in undisturbed rings.[166]

The Laplacian distribution $\nabla^2\rho(\mathbf{r})$ along the P–N1 bond is completely different to the P–C_{ipso} bonds. The Laplacian at the BCP is positive and charge density is exclusively concentrated in the nitrogen basin (Figure 3.6a). This indicates a severe contribution of electrostatic interaction to the bonding energy, further substantiated by the integration of the atomic basins.[165] The two basins related to the nitrogen atoms give distinct negative values. The imino nitrogen atom N1 is bonded to three electropositive neighbours and therefore the charge of -1.91 e is higher than -1.11 e for the ring nitrogen atom N2. The charge of the deprotonated carbon atom C1 is about 0.2 e higher than those of the two phosphorus bonded *ipso* carbon atoms (C7: -0.30 e, C13: -0.34 e). All these findings support a ylidic $P^+–C^-$ simultaneously to a $P^+–N^-$ bond not yet present in the resonance forms of scheme 3.11. The determination of the (3;-3) critical points in the spatial distribution of $-\nabla^2\rho(\mathbf{r})$ and quantification of the VSCCs (VSCC = Valence Shell Charge Concentration) around the electronegative atoms (N1, N2, O1, C1) confirm this view. Isosurface presentations around N1 and a contour plot in the plane containing the (3;-3) critical points are presented in Figure 3.7a. They indicate sp^3 hybridisation at N1 with two

lone-pairs, both oriented towards the Li cation. The same is valid for O1 (Figure 3.7b). The angle between the lone-pairs LP1–N1–LP2 of approximately 71° is much more acute than the expected 109°, but can be rationalised by the closer approach of the critical points by the simultaneous interaction of both VSCCs with the lithium cation. Obviously, the lone-pairs at N1 and O1 act as a bifurcated donor to the electropositive metal acceptor.[137,161] We found the same arrangement at S-bonded sp^3 hybridised nitrogen atoms in an intramolecular hydrogen bond.[167]

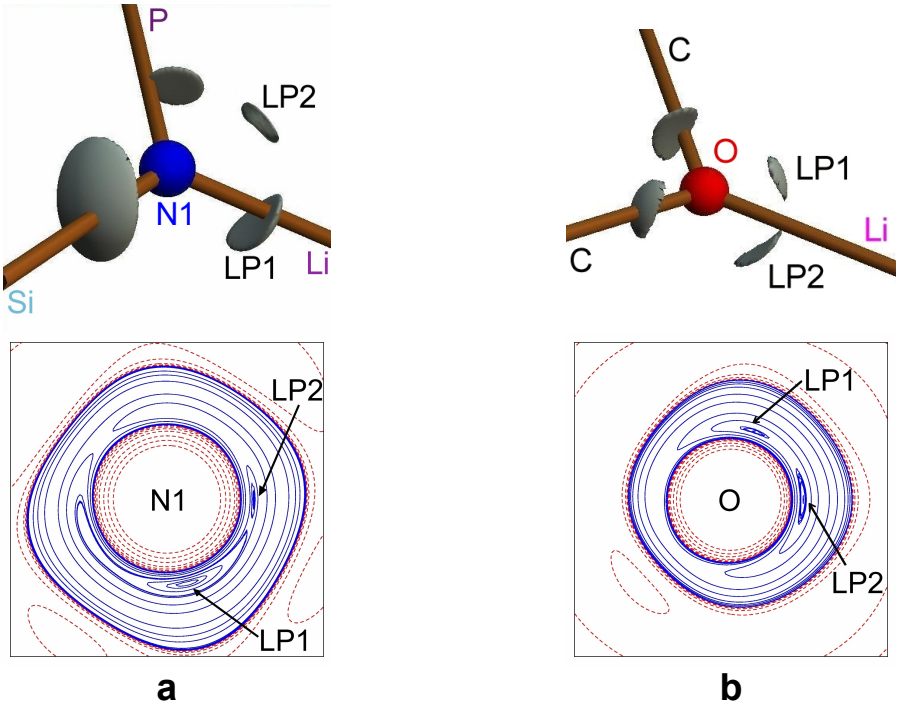

Figure 3.7: *Isosurface maps at constant $\nabla^2\rho(\mathbf{r})$ values indicating bonding and non-bonding charge concentrations around the displayed atoms and contour plots in a plane with the two lone-pairs oriented towards Li1 for N1 (a) and O1 (b) in* ***11****; (a) N1, $\nabla^2\rho(\mathbf{r})$ = -48eÅ^{-5} (bonding-) and -41eÅ^{-5} (non-bonding VSCCs); (b) O1, $\nabla^2\rho(r)$ = -125eÅ^{-5} (bonding-) and -105eÅ^{-5} (non-bonding VSCCs). Blue contours indicate charge concentration, red contours charge depletion, respectively.*

The experimental charge density distribution in [(Et_2O)Li{$Ph_2P(CHPy)(NSiMe_3)$}], (**11**), clearly proves, that the formal P=N imino double bond and the potential ylenic P=C double bond have to be written as polar P^+–N^- and P^+–C^- single bonds augmented by electrostatic contributions. As predicted from calculations, a hypervalent central phosphorus atom is not required to describe the bonding. It is much more appropriate to assign charges in the resonance formula even of the starting material $Ph_2P(CH_2Py)(NSiMe_3)$, (**9**). The almost invariant imino nitrogen signals in the ^{15}N NMR spectra of **9** and **11** further supplies

credibility to these canonical forms. The iminophosphorane $Ph_2P(CH_2Py)(NSiMe_3)$, (**9**), is better been written as a zwitterionic phosphoniumamide $Ph_2(PyCH_2)P^+–^-NSiMe_3$.[137]

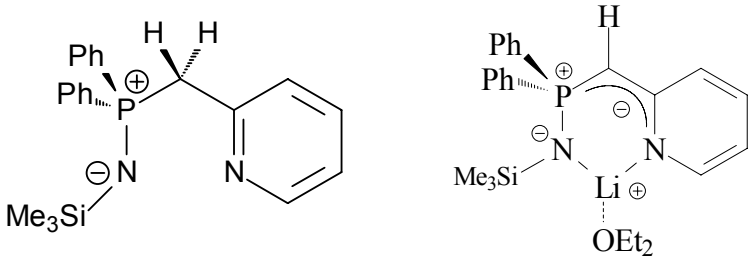

9 **11**

Scheme 3.12: *Canonical formulae of $Ph_2P(CH_2Py)(NSiMe_3)$, (**9**), and [$(Et_2O)Li\{Ph_2P(CHPy)(NSiMe_3)\}$], (**11**), according to a topological analysis of the bonding perfomed by Kocher[161] and a correlation of the NMR-data of **9** and **11**[137]*

This polar single bond corresponds best with the reactivity: metalorganics in polar solvents can easily cleave this bonding rather than the wrongly assigned P=N double bond. Therefore, deimination or the *retro*-Staudinger reaction of iminophosphoranes seems an unorthodox but suitable synthetic access to phosphanes.

3.3.2 The donor base adduct [{$Ph_2P(CH_2Py)(NSiMe_3)$}Li{$Ph_2P(CHPy)(NSiMe_3)$}], (12)

Treating $Ph_2P(CH_2Py)(NSiMe_3)$ (**9**) with only 0.5 equivalents of MeLi in ether at -78 °C gives the complex [{$Ph_2P(CH_2Py)(NSiMe_3)$}Li{$Ph_2P(CHPy)(NSiMe_3)$}], (**12**), in which the neutral starting material **9** and the related anion both chelate the same lithium atom. Formally, the diethyl ether donor molecule in **11** is replaced by the iminophosphorane **9** (Equation 3.6).[137]

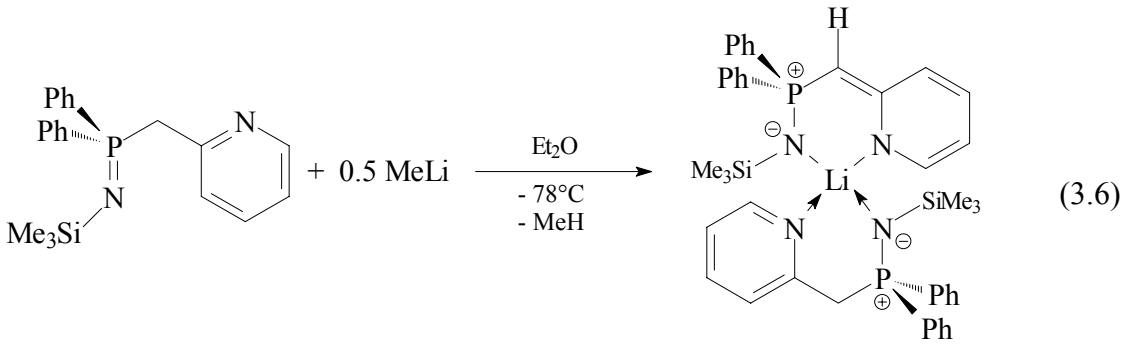

(3.6)

9 **12**

Crystals of **12** were obtained from the reaction solution at r.t. after three days. The yellow blocks decompose at 77°C. Figure 3.8 shows the solid state structure of **12**.[137]

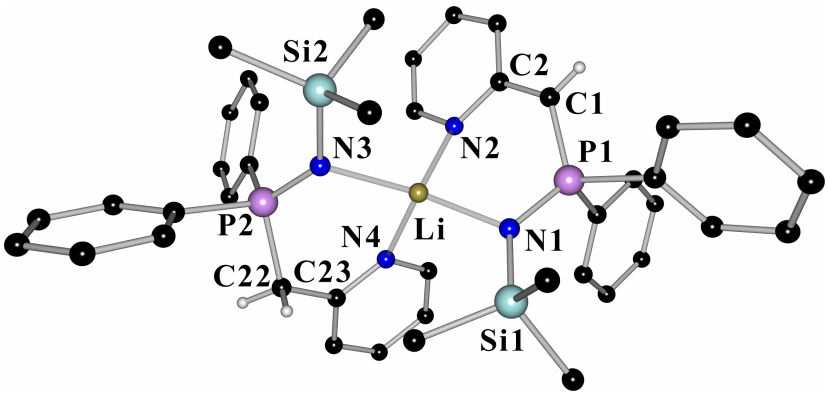

Figure 3.8: *Solid state structure of [{$Ph_2P(CH_2Py)(NSiMe_3)$}Li{$Ph_2P(CHPy)(NSiMe_3)$}], (**12**).*

Table 3.6: *Selected bond lengths [pm] and angles [°] of [{$Ph_2P(CH_2Py)(NSiMe_3)$}Li{$Ph_2P(CHPy)(NSiMe_3)$}], (**12**).*

P1–N1	158.96(15)	P2–N3	156.55(15)
N1–Si1	170.69(16)	N3–Si2	172.17(15)
P1–C1	172.95(19)	P2–C22	181.46(19)
C1–C2	140.5(3)	C22–C23	149.8(3)
C2–N2	137.5(2)	C23–N4	134.3(2)
Li–N1	206.9(3)	Li–N3	216.5(3)
Li–N2	209.1(4)	Li–N4	210.2(3)
P1–C1–C2	123.33(15)	P2–C22–C23	119.06(14)
P1–N1–Si1	130.67(9)	P2–N3–Si2	132.91(9)
av. P1–C_{Ph} 182.53			

One deprotonated equivalent of the starting material **9** contributes the monoanionic [N–P–C(H)–Py]$^-$ chelating ligand already present in **11**, while the second equivalent acts as neutral bidentate (*N,N'*)-donor base to the lithium cation. The complex [{$Ph_2P(CH_2Py)$-$(NSiMe_3)$}Li{$Ph_2P(CHPy)(NSiMe_3)$}], (**12**), is ideal for a structural comparison of both, the neutral donor base **9** and the anionic ligand in [(Et_2O)Li{$Ph_2P(CHPy)(NSiMe_3)$}], (**11**), as the two fragments can be studied in the same molecule.[137]

In **12** the lithium cation is tetrahedrally distorted coordinated by the four nitrogen atoms (the N–Li–N angles vary from 98.23(14)° to 128.49(17)°). In the metallaspirocycle both six membered LiN_2C_2P rings adopt a distorted boat conformation each. It seems remarkably that the lithium cation is displaced by 46 pm from the best plane of the anionic ligand and only 12 pm from the plane of the neutral ligand. As expected, the deprotonated

sp^2-carbon atom C1 is closer to the plane than the methylene carbon atom C22 (displacements are 45 and 61 pm, respectively). The Li···C1 distance in **12** is 324.3 pm, hence 2 pm longer than in **11**. However, due to the more pronounced boat conformation the lithium cation is 16 pm closer to the deprotonated carbon atom C1 than to C22 of the neutral ligand (Li···C22: 340.4 pm). The P1–C1–C2 angle of 123.33(15)° indicates sp^2-hybridization. In the neutral donor ligand the related angle at C22 of 119.06(14)° is only marginally more acute. The sum of the bond angles at both imino nitrogen atoms N1 and N3 is close to 360° indicating planar environment. For the pyridyl ring nitrogen atoms N2 and N4 the sum of the angles shows slight displacement of the metal from the heteroaromatic ring plane (352.2° and 357.7°, respectively). This illustrates the transfer of the negative charge of the anionic ligand towards the pyridyl nitrogen atom N2, pertubing the sp^2-hybridization and leading to a pyramidalization at N2. This is substantiated by a 3.2 pm longer C2–N2 bond with regard to the corresponding bonds in $Ph_2P(CH_2Py)(NSiMe_3)$ (**9**) and the C23–N4 bond length in the neutral $[Ph_2P(CH_2Py)(NSiMe_3)]$-fragment in **12**.[137]

The P–C_{Ph} bond lengths in **12** are all equal (av. 182.53 pm) and do not change in comparison to the parent iminophosphorane **9** or the lithiated complex **11**. Akin $[(Et_2O)Li\{Ph_2P(CHPy)(NSiMe_3)\}]$, (**11**), the P1–C1 (172.95(19) pm) and C1–C2 distances (140.5(3) pm) in **12** are approximately 9 pm shorter than the corresponding values in the iminophosphorane **9** and the P2–C22 (181.46(19) pm) and C22–C23 distance (149.8(3) pm) in the neutral donor fragment of **12**, respectively. Like in **11**, they are in the range found for ylidic P–C interactions[109,159] and aromatic C=C bonds.[30]
The P1–N1 distances in the anionic ligand of **11** (159.19(10) pm) and **12** (158.96(15) pm) are identical within esds and ca. 5 pm longer compared to the iminophosphorane **9** (154.13(12) pm). The P2–N3 bond distance of 156.55(13) pm in the neutral donor ligand in **12** is half-way between them.[137]

As anticipated from the higher coordination number of the lithium cation and the greater steric bulk of the two ligands, the Li–N bonds in $[\{Ph_2P(CH_2Py)(NSiMe_3)\}Li\{Ph_2P(CHPy)(NSiMe_3)\}]$, (**12**), are longer than in $[(Et_2O)Li\{Ph_2P(CHPy)(NSiMe_3)\}]$, (**11**). It seems important to note that the Li–N_{imino} bond distances in **12** vary remarkably. Whereas the Li–N1 distance to the anion is only 206.9(3) pm the Li–N3 distance to the donor ligand is 9.6 pm longer. The imino N-atom of the anion seems much more attractive to the lithium cation.[137]

Metal coordination at the imino nitrogen atom N3 of the neutral ligand shifts electron density from the electrostatically contracted P^+–N^- single bond in direction to the metal, weakening and lengthening the P2–N3 interaction. Metal coordination at N1 together with deprotonation at the methylene bridge next to the phosphorus atom P1 leads to a further elongation of the P^+–N^- bond as the bond is additionally perturbed by the interaction of the negatively polarized carbon atom C1 with the positive phosphorus centre P1, last having now two negative neighbours. This leads to a more pronounced charge accumulation at the N1 atom in the anion and a strong Li–N1 interaction, and a polarization of the P2–N3 bond in the neutral ligand, giving a weaker Li–N3 bond.

This interpretation is further substantiated by a comparison of the N–Si bond lengths in the iminophosphorane **9**, and the lithiated derivatives **11** and **12**. In **9**, the negative charged imino N-atom interacts with the positive phosphorus atom and the electropositive silicon atom. This bonding situation results in short N–Si bonds (168.08(12) pm). Metal coordination at the imino nitrogen atom N3 of the neutral ligand in **12** leads to 4.1 pm longer N3–Si2 bonds (172.17(15) pm), now the imino N-atom stonger interacting with the positive phosphorus atom P2 and the Li^+ cation. The electrostatic contribution to the N–Si bonding is reduced and the Si–N bond length is only ca. 2 pm shorter than a standard Si–N single bond (174 pm).[30] Metal coordination at N1 in the anionic ligands of **11** and **12**, results in N1–Si1 contacts (av. 170.73 pm) half way between the bond lengths of the iminophosphorane **9** and the neutral ligand of **12**. Charge stabilization at N1 is achieved by coordination to the Li^+ cation and interaction with the electropositive silicon atom, as now the interaction with the positive phosphorus atom is weaker, because P1 is additionally interacting with the negatively polarized carbon atom C1.[137]

The Li–N_{Py} contacts in **12** with 209.1(4) pm for Li–N2 and 210.2(3) pm for Li–N4 differ only by ca. 1 pm, These distances are not unusual for Li–N_{Py} interactions and similar bond lengths are found in [(bipy)Li{$PhPyPNSiMe_3$}] (Li–N_{Py}: 203.9 pm; Li–N_{bipy}: 207.8 pm),[134] [(bipy)Li{$MePyPNSiMe_3$}] (Li–N_{Py}: 203.3 pm; Li–N_{bipy}: 208.3 pm),[106,133] [(Et_2O)Li–{$N(SiMe_3)_2$}] (av. 206 pm)[148] or [$(Py)_3$Li($CHCl_2$)] (Li–N: 201.7–207.7 pm)[168]. Comparable small differences are observed in [{$HC(SiMe_3)_2(Py)$}Li{$C(SiMe_3)_2(Py)$}] (Li–N_{Py}, 199.8 / 201.2 pm).[169]

In conclusion, **12** mirrors the bonding situation and structural properties of both the lithium complex [(Et_2O)Li{$Ph_2P(CHPy)(NSiMe_3)$}], (**11**), and the iminophosphorane **9** by very good and close accordance of the structural features of each of them.

The ^{31}P-NMR spectrum of [{$Ph_2P(CH_2Py)(NSiMe_3)$}Li{$Ph_2P(CHPy)(NSiMe_3)$}], (**12**), shows two signals, one at 8.46 ppm, originating from the phosphorus atom in the neutral ligand, the second at 15.36 ppm for the phosphorus nucleus in the anion. A ^{1}H, ^{29}Si-HMBC correlation spectra results in two signal at δ = -9.5 and δ = -1.82. The upfield resonance is assigned to the silicon nucleus in the anion, that at lower field to the silicon atom in the neutral ligand. The two protons at the methylene bridge in the neutral residue resonate at δ = 3.78, with a coupling constant of $^{2}J_{P-H}$ = 13.9 Hz. The single hydrogen atom at the methylene bridge in the anionic fragment gives a signal at 4.11 ppm ($^{2}J_{P-H}$ = 23.6 Hz).
To get a comparison of the electronic situation at the nitrogen atoms in **12**, a ^{1}H, ^{15}N-HMBC-NMR measurement was performed, which resulted in four separated signals. The two resonances at δ = -339 and δ = -68 can be assigned to the imino and pyridyl nitrogen atoms in the neutral ligand, respectively. In comparison to the isolated iminophosphorane $Ph_2P(CH_2Py)(NSiMe_3)$, (**9**), these resonances are very similar (N_{imino}: δ = -343, N_{Py}: δ = -61). The imino and pyridyl nitrogen atoms in the anionic ligand resonate at δ = -334 and δ = -139, respectively. They fall in the same range, observed for the lithium amide [(Et_2O)Li{$Ph_2P(CHPy)(NSiMe_3)$}], (**11**), (N_{imino}: δ = -331, N_{Py}: δ = -145).[137]

These ^{15}N chemical shifts found for the lithium complex **12**, in which both, neutral iminophosphorane and its anion are coordinated, further substantiate the view of the PN bonding situation in iminophsophoranes as a P^{+}–N^{-} bond, because the resonances for the imino nitrogen atoms are almost unchanged with regard to the lithiated species **11** and the parent iminophsophorane **9**. Furthermore, they show that the electronic situation at the pyridyl nitrogen atom in the neutral ligand of **12** coordinating to a metal cation is almost the same as in the iminophosphorane **9**. Charge transfer into the pyridyl substituent towards the nitrogen atom in the anionic ligand of **12** is reflected in the remarkable upfield shifted ^{15}N resonance for this atom, relative to the neutral residue (Δδ = -68).[137]

3.3.3 The donor base adduct [{$Ph_2P(CH_2Py)(NSiMe_3)$}Na{$Ph_2P(CHPy)(NSiMe_3)$}], (13)

To gain insight into the geometrical adabtility and reactivity of $Ph_2P(CH_2Py)(NSiMe_3)$, (**9**), the iminophosphorane was reacted with sodium amide in thf at r.t. As the ligand already proved to be a good bidentate donor in the lithiated complex **12**, the reaction was performed with only 0.5 equivalents of $NaNH_2$, inducing **9** to react and to donate at the same time akin [{$Ph_2P(CH_2Py)(NSiMe_3)$}Li{$Ph_2P(CHPy)(NSiMe_3)$}], (**12**) (Equation 3.7).[137]

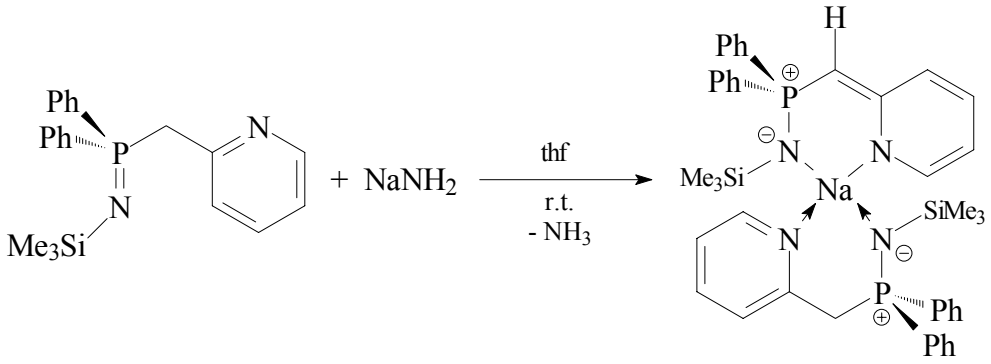

9 **13** (3.7)

The isolated product [{$Ph_2P(CH_2Py)(NSiMe_3)$}Na{$Ph_2P(CHPy)(NSiMe_3)$}], (**13**), gives yellow blocks, on crystallization from a saturated thf solution. **13** decomposes at 33°C. The solid state structure of **13** and selected bond lengths and angles are depicted in figure 3.9 and table 3.7, respectively.[137]

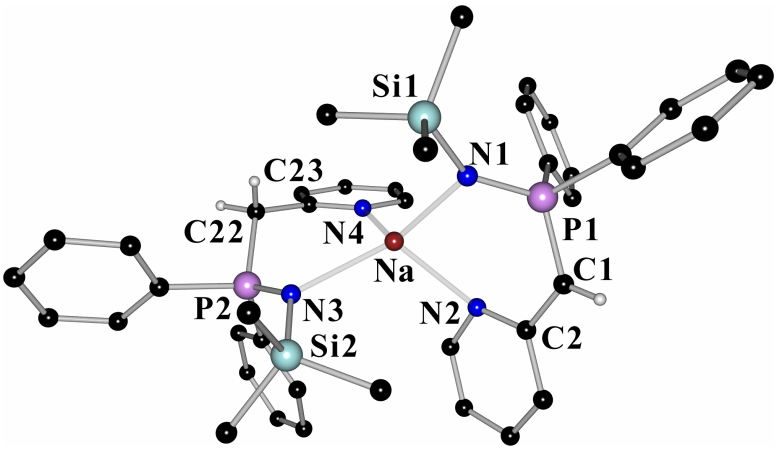

Figure 3.9: *Solid state structure of [{$Ph_2P(CH_2Py)(NSiMe_3)$}Na{$Ph_2P(CHPy)(NSiMe_3)$}], (**13**).*

Table 3.7: *Selected bond lengths [pm] and angles [°] of [{$Ph_2P(CH_2Py)(NSiMe_3)$}Na{$Ph_2P(CHPy)(NSiMe_3)$}], (**13**).*

P1–N1	157.79(14)	P2–N3	156.28(13)
N1–Si1	168.69(14)	N3–Si2	172.04(14)
P1–C1	173.43(17)	P2–C22	183.48(17)
C1–C2	141.1(2)	C22–C23	150.6(2)
C2–N2	137.6(2)	C23–N4	134.1(2)
Na–N1	233.51(15)	Na–N3	237.09(14)
Na–N2	239.16(15)	Na–N4	240.00(15)
P1–C1–C2	125.42(13)	P2–C22–C23	117.95(11)
P1–N1–Si1	140.06(9)	P2–N3–Si2	130.47(8)
	av. P1–C_{Ph} 182.25		

Like in the previously mentioned reactions of the iminophosphorane **9** with lithium amides and organyls, the reaction with sodium amide yields a monomeric product. Alkali metal complexes tend to form oligomeric aggregates depending on the steric demand of the substituents, the radius and polarisability of the metal and the nature and amount of the donating solvent.[31,170] Akin [{$Ph_2P(CH_2Py)(NSiMe_3)$}Li{$Ph_2P(CHPy)(NSiMe_3)$}], (**12**), the core structure of **13** is comprised of a metallaspirocycle, in which the central sodium atom is coordinated *via* the nitrogen atoms N1 to N4 of the two ligands. The four fold coordination of the sodium cation within the cycles forces the local geometry to be distorted tetrahedral with angles far away from the ideal value of 109.5° (N3–Na–N4: 93.16(5)°; N1–Na–N3: 129.61(5)°). Similar to **12** the metal atom is more displaced from the best plane of the anion than from that of the neutral ligand (20 *vs*. 17 pm) and the deprotonated carbon atom is closer to that plane than the methylene carbon atom (34 *vs*. 75 pm).[137]

The imino nitrogen atoms N1 and N3 in **13** show trigonal planar coordination each. The same is valid for the pyridyl ring nitrogen atom N4 of the neutral ligand. However, the sum of the angles at the pyridyl ring nitrogen atom N2 in the anionic ligand of 343.4° indicates a displacement of the sodium metal towards the π-electron density of the ring. This more pronounced haptotropic shift of the softer metal was observed earlier[37b] and is emphasised with the gradual increase of the ordering numbers of the alkali metals.[171]

The basic structural features of the two ligands match those already discussed for the lithiated complex **12** and differences result only from the slightly different conformations of the spirocycles and the larger radius of the central cation. Figure 3.10 depicts a superposition plot of the two analogue core structures.

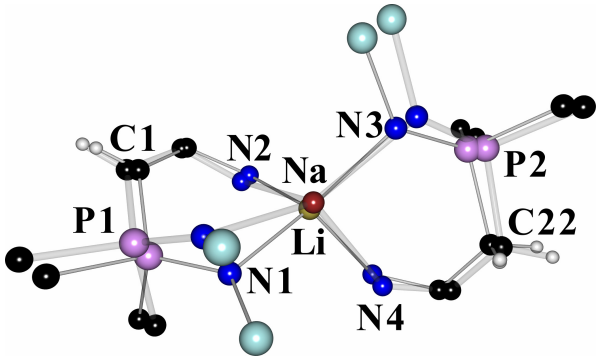

Figure 3.10: *Superposition plot of the core structures of [{$Ph_2P(CH_2Py)(NSiMe_3)$}Li{$Ph_2P(CHPy)(NSiMe_3)$}], (**12**) (narrow lines), and [{$Ph_2P(CH_2Py)(NSiMe_3)$}Na{$Ph_2P(CHPy)(NSiMe_3)$}], (**13**) (wide lines).*

As expected for the softer *Lewis*-acidity of the Na^+-cation in comparison to Li^+, the effects of metal coordination at the imino nitrogen atoms N1 and N3 have less impact on the P–N bond lengths in **13**. The P1–N1 bond (157.82(14) pm) in the anionic ligand in **13** is 3.7 pm longer than in $Ph_2P(CH_2Py)(NSiMe_3)$ (**9**) (154.13(12 pm) and 1.1 pm shorter than in [{Ph_2P{CH_2(2-Py)}$(NSiMe_3)$}Li{Ph_2P{CH(2-Py)}$(NSiMe_3)$}] (**12**) (158.96(13) pm). The P2–N3 bond length is 156.29(13) pm and is approximately 2.2 pm longer than in the starting material **9**.

In **13**, the difference in the two Si–N bond lengths (3.35 pm) is larger than in the lithium derivative **12** (1.48 pm). The N1–Si1 distance of 168.69(14) pm reflects strong electrostatic contributions in the N–Si bonding, because the imino nitrogen atom N1 is weaker interacting with the larger sodium cation.[137]

The sodium nitrogen distances in **13** span the range from 233.51(15) pm to 240.00(15) pm and are comparable to those of the structurally related monomeric [$(thf)_2$Na{$HC(Ph_2PNSiMe_3)_2$}] (241.6 pm)[150] and dimereric ([Na{$HC(Ph_2PNSiMe_3)_2$}]$_2$ (233.4–253.8 pm))[152] complexes. The values correspond rather to those found in sodium amides than in amine donor base coordinated complexes as e. g. [(pmtda)NaPh]$_2$ of 260.9 to 271.2 pm.[172] However, the Na–N_{Py} distances are similar to those in e. g. [$(C_5H_5N)_3NaCp^*$] (245.0 to 248.8 pm),[173] [(C_5H_5N)Na{$O^tBu(SiMe_2)NSiMe_3$}] (239.1 pm)[125b] and [$(thf)_3$Na$(PyCPh_2)$] (241.4 pm).[37b]

In the ^{31}P-NMR spectrum of **13** two signals at δ = -0.60 and δ = 11.3 are observed. The upfield signal originates from the phosphorus atom of the neutral donor ligand, that at lower field is due to the phosphorus nucleus of the anion. The two different silicon atoms

in **13** resonate at δ = -12.8 for the silicon nucleus in the neutral ligand and at δ = -13.9 for the Si-atom in the anionic moiety. The single proton at the methylene bridge of the anionic ligand resonates at δ = 3.39, the two of the neutral ligand at δ = 3.85. The coupling constants are $^{2}J_{P-H}$ = 22.3 Hz and $^{2}J_{P-H}$ = 14.1 Hz, respectively. The ^{1}H,^{15}N, HMBC-NMR spectrum revealed four well separated signals for the four different nitrogen atoms. The pyridyl nitrogen atom in the neutral donor ligand resonates at δ = -63, the pyridyl nitrogen atom in the anion at δ = -137. The imino nitrogen atom in the anion gives a signal at δ = -332, the imino nitrogen atom in the neutral fragment at δ = -345. These ^{15}N shifts are in good agreement with the results obtained for the iminophosphorane **9** (N_{imino}: -343, N_{Py}: -61 ppm), the lithiated complexes **11** (N_{imino}: -331, N_{Py}: -145 ppm) and **12** (neutral ligand: N_{imino}: -339, N_{Py}: -68 / anionic ligand: N_{imino}: -334, N_{Py}: -139 pm). Remarkably, they reflect the polarizing abilities of the metal, hence the upfield shift due to sodium coordination is less pronounced than the changes induced from the lithium cation.

These NMR parameters substantiate yet again, that the nature of the P–N bond in the iminophosphorane $Ph_2P(CH_2Py)(NSiMe_3)$, **9**, is almost the same as in the different metal complexes **11** to **13**, and with regard to the results of the multipole refinement of compound **11** is best described as a P^{+}–N^{-} bond.[137]

3.4 Reactions with transition metal amides

3.4.1 The zinc(II) amide [Zn{Ph$_2$P(CHPy)(NSiMe$_3$)}$_2$], (14)

In literature, the imino nitrogen atom in iminophosphoranes is commonly described as a two-electron σ-donor with only minor π-acceptor properties.[115] However, *Kocher* found both lone pairs at the sp^3-hybridized imino nitrogen atom in [(Et$_2$O)Li{Ph$_2$P–(CHPy)(NSiMe$_3$)}], (**11**), to be directed towards the cation.[137,161] Hence, the metal–imino nitrogen interactions cannot be regarded as simple 2e-donor bonds. This bifurcated 4e-coordination pattern and the sidearm donation capability of the pyridyl nitrogen atom in the [Ph$_2$P(CHPy)(NSiMe$_3$)]$^-$-anion should be investigated in reactions of the iminophosphorane Ph$_2$P(CH$_2$Py)(NSiMe$_3$), (**9**), with transition metal amides. Therefore, the iminophosphorane Ph$_2$(CH$_2$Py)NSiMe$_3$, (**9**), was reacted with the zinc amide [Zn{N(SiMe$_3$)$_2$}$_2$].[174] Each of the [N(SiMe$_3$)$_2$]$^-$-anions removes a single hydrogen atom at the methylene bridge of each molecule of **9**, yielding [Zn{Ph$_2$P(CHPy)(NSiMe$_3$)}$_2$], (**14**) (Equation 3.8).[175]

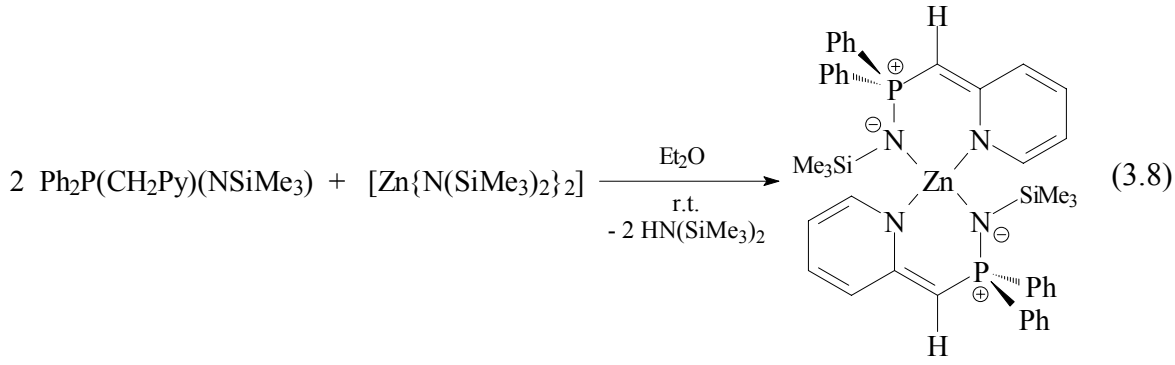

(3.8)

9 **14**

In the ^{31}P-NMR spectrum a single resonance at δ = 26.4 is observed for the two magnetically equivalent phosphorus atoms. The silicon atoms give rise to a doublet at δ = 1.32. The resonance at δ = 3.32 in the ^{1}H-NMR originates from the single protons of the methylene bridges of the two anionic ligands. The coupling constant is $^2J_{P–H}$ = 20.9 Hz. Again, a ^{1}H, ^{15}N-HMBC-NMR measurement was performed to elucidate the electronic situation at the nitrogen atoms and to facilitate comparison to the shifts obtained for the alkali metal complexes **11** to **13**. The imino nitrogen atoms resonate at -348 ppm. This signal is in the same range as in the alkali metal complexes **11**–**13** and in the

iminophosphorane **9**. The equivalent pyridyl nitrogen atoms give a single resonance at δ = -182. This signal is remarkably shifted upfield, in comparison to the pyridyl nitrogen resonances in the anionic ligands of the complexes **11**–**13** (Δδ = -37– -45). Thus, the negative charges in [Zn{$Ph_2P(CHPy)(NSiMe_3)$}$_2$], (**14**), seem to be shifted more to the pyridyl nitrogen atoms than in **11**–**13**, indicating the very hard character of the zinc dication.[175]

[Zn{$Ph_2P(CHPy)(NSiMe_3)$}$_2$], (**14**), crystallizes in the space group $P\bar{1}$ as yellow plates. The zinc amide **14** decomposes at 176°C. The results from a x-ray diffraction experiment are shown in figure 3.11, selected bond lengths and angles are summerized in table 3.8.[175]

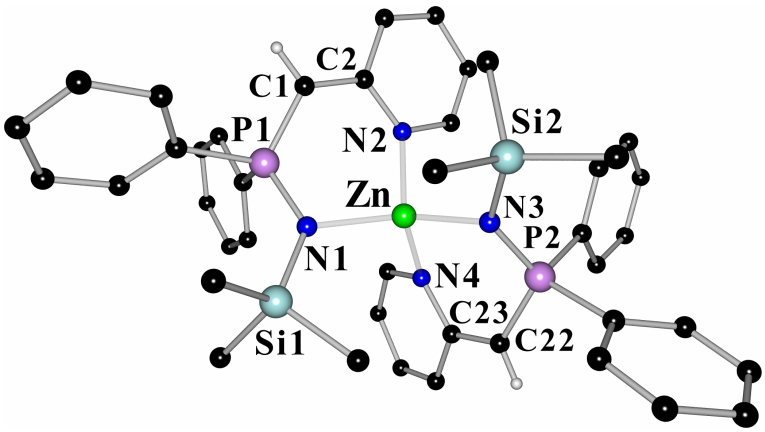

Figure 3.11: *Solid state structure of [Zn{$Ph_2P(CHPy)(NSiMe_3)$}$_2$], **(14)**.*

Table 3.8: *Selected bond lengths [pm] and angles [°] of [Zn{$Ph_2P(CHPy)(NSiMe_3)$}$_2$], **(14)**.*

Zn–N1	201.70(15)	Zn–N3	201.15(16)
Zn–N2	203.96(16)	Zn–N4	203.88(16)
P1–N1	160.92(16)	P2–N3	161.43(16)
N1–Si1	173.41(16)	N3–Si2	173.43(16)
P1–C1	172.1(2)	P2–C22	172.28(19)
C1–C2	138.9(3)	C22–C23	139.6(3)
C2–N2	137.5(2)	C23–N4	137.5(2)
P1–C1–C2	123.75(15)	P2–C22–C23	123.35(15)
P1–N1–Si1	131.10(10)	P2–N3–Si2	128.80(10)
	av. P1–C_{Ph} 181.6		

The central zinc cation is four fold coordinated by the nitrogen atoms N1 to N4 of the two anionic ligands. The coordination polyhedron around the Zn^{2+} atom is a nearly ideal tetrahedron, as the angles are between 103.70(6)° (N4–Zn–N2) and 111.31(6)° (N3–Zn–

N2). Both anionic $[Ph_2P(CHPy)(NSiMe_3)]^-$-units act as bidentate (*N*,*N'*)-chelats. The two six membered rings of the metallaspirocycle show distorted boat conformation each with the deprotonated carbon atom and the metal cation in the stern and bow position. The displacement of the deprotonated carbon atoms C1 and C22 from the best plane of the ligands is on average 45 pm and for the zinc cation 21 pm.[175]

In $[Zn\{Ph_2P(CHPy)(NSiMe_3)\}_2]$, (**14**), the distances between the zinc atom and the imino nitrogen atoms N1 and N3 are (av. 201.43 pm) equal within esds. Zn–N contacts span a wide range from 182 for covalent bonded zinc amides to 231 pm for donor base complexed dimethylzinc.[176,177] In **14** they are comparable to amidic $Zn–N_{imino}$ contacts like in the related zinc bis(iminophosphorane)methanides $[Zn\{HC(Ph_2PNR\}_2X]$ (R = Mes, $SiMe_3$; X = Me, $N(SiMe_3)_2$, $OCPh_3$),[178] or to the zinc iminatocomplex $[BuZn(NPMe_3)]_4$.[179] In the *ortho*-deprotonated $[Zn(o\text{-}C_6H_4PPh_2NSiMe_3)_2]$ 14.4 pm longer Zn–N contacts (215.8 pm) are present.[180] In the dimethyl zinc complexes $[(PyPh_2PNSiMe_3)ZnMe_2]$ and $[(Py_2PhPNSiMe_3)ZnMe_2]$, in which the iminophosphorane acts as a neutral (*N,N'*)-donor base, the $Zn–N_{imino}$-contacts are 226.6 and 223.7 pm, respectively.[134] An ideal comparison of amidic and donor interactions in the same molecule provides the structure of $[HZnN(Me)C_2H_4NMe_2]_2$ where the two amidic Zn–N bonds within the central four membered ring are 206.1 pm long, while the two Zn←N(Me)R donor bonds are 218.6 pm long.[181] Thus, the Zn–N1/3 contacts in $[Zn\{Ph_2P(CHPy)(NSiMe_3)\}_2]$, (**14**), are in the range of zinc amides.[175]

In **14**, the $Zn–N_{Py}$ distances are identical (Zn–N3/4: av. 203.92 pm) and only 2.5 pm longer than the $Zn–N_{imino}$ interactions. In $[Zn\{Py_2P(NSiMe_3)_2\}_2]$ the $Zn–N_{Py}$ bond lengths are 207.3 pm long,[107] whereas in the already mentioned donor base adducts $[(PyPh_2PNSiMe_3)ZnMe_2]$ and $[(Py_2PhPNSiMe3)ZnMe_2]$ they are 226.6 pm and 223.5 pm long, respectively.[134] The average value quoted for $Zn–N_{Py}$ contacts is 208.3 pm.[71] To judge on the covalent or dative character of the $Zn–N_{Py}$ bonds, complex **14** is best compared to the bis(1,4-dihydropyridin-1-yle)-bis(pyridine)zinc system. In $[Zn\{Ph_2P(CHPy)(NSiMe_3)\}_2]$, (**14**), the $Zn–N_{Py}$ distances are 4.4 pm longer than the covalent bonds in bis(1,4-dihydropyridin-1-yle)-bis(pyridine)zinc (197 pm), but 11.6 pm shorter than the dative ones (213 pm), clearly emphasizing the amidic character of the $Zn–N_{Py}$ interactions in **14**.[74]

The structural parameters in the anionic $[Ph_2P(CHPy)(NSiMe_3)]^-$ ligands in **14**[175] do not differ significantly from those discussed in the alkali metal complexes **11** to **13**.[137] As expected from the higher charge and the only 5 pm larger ion radius of Zn^{2+} in comparison to the Li^+ cation , the P–N bonds (av. 161.18 pm) in **14** are 2 pm longer than in $[(Et_2O)Li\{Ph_2P(CHPy)(NSiMe_3)\}]$ (**11**). As a result of the imino nitrogen coordination of N1 and N3 to a small and higher charged metal cation, the N–Si distances (av. 173.42 pm) are in the range of formal N–Si standard single bond lengths.[30] Electrostatic interaction of the negative nitrogen atom with the electropositive silicon atom is reduced in opposite to the iminophosphorane **9** and the alkali metal complexes **11** to **13**.

The sum of the bond angles around the pyridyl nitrogen atoms N2 and N4 is on average 356.3°, reflecting a marginal pyramidal environment and a shift of the cation towards the π-density of the rings. The imino nitrogen atoms N1 and N3 show planar coordination spheres.[175]

3.4.2 Formation of $[Fe\{Ph_2P(CHPy)(NSiMe_3)\}_2]$, (15)

Leung et al. reported a homoleptic 14 VE iron(II) complex containing intramolecular side arm donating nitrogen atoms.[84] The so far established properties of the anionic $[Ph_2P(CHPy)(NSiMe_3]^-$ building block prompted us to investigate the option of the C_α-deprotonated ligand system to stabilize low valent transition metal cations in low oxidation states. The reaction of the iron(II)amide $[Fe\{N(SiMe_3)_2\}_2]_2$[79] with the iminophosphorane $Ph_2P(CH_2Py)(NSiMe_3)$, (**9**), in a 1:2 ratio in polar solvents such as thf or Et_2O results, even at -78°C, in dark red to black solutions containing several products. In contrast, the addition of pure $[Fe\{N(SiMe_3)_2\}_2]_2$ to the solid iminophosphorane $Ph_2P(CH_2Py)(NSiMe_3)$ at r.t. gives immediately a red oily suspension of solid $[Fe\{Ph_2P(CHPy)(NSiMe_3)\}_2]$, (**15**), in liquid $HN(SiMe_3)_2$, formed in the C_α-deprotonation of the iminophosphorane.The yield is (93%) (Equation 3.9).[175]

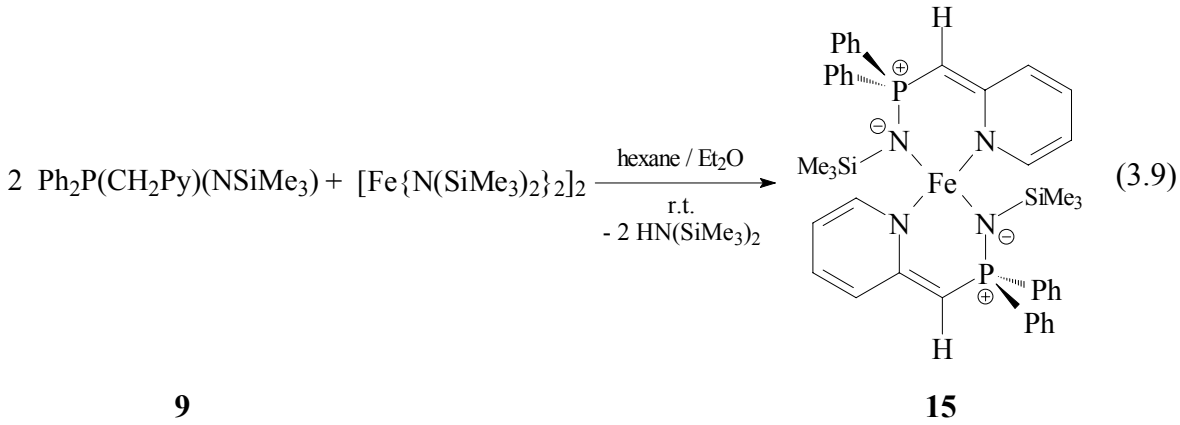

(3.9)

9 **15**

The red iron complex decomposes at 258°C. The molecular structure of **15**, depicted in figure 3.12, was determined by a X-ray diffraction experiment from crystals obtained after three days from a hexane/Et_2O (2:1) solution.[175]

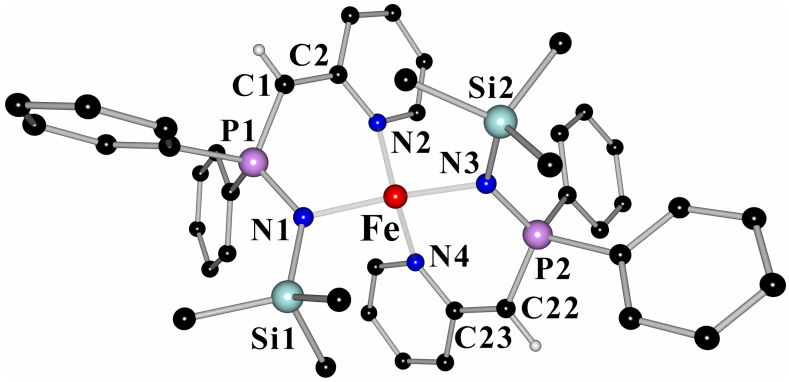

Figure 3.12: *Molecular structure of [Fe{$Ph_2P(CHPy)(NSiMe_3)$}$_2$], (**15**).*

Table 3.9: *Selected bond lengths [pm] and angles[°] for [Fe{$Ph_2P(CHPy)(NSiMe_3)$}$_2$], (**15**).*

Fe–N1	204.6(2)	Fe–N3	204.2(2)
Fe–N2	207.5(2)	Fe–N4	207.9(2)
P1–N1	161.2(2)	P2–N3	161.3(2)
N1–Si1	173.7(2)	N3–Si2	173.7(2)
P1–C1	172.5(2)	P2–C22	172.7(2)
C1–C2	139.4(3)	C22–C23	140.3(3)
C2–N2	137.9(3)	C23–N4	137.5(3)
P1–C1–C2	124.08(19)	P2–C22–C23	123.42(19)
P1–N1–Si1	132.07(12)	P2–N3–Si2	129.83(12)
av. P1–C_{Ph} 182.2			

The central iron(II) cation is coordinated *via* the nitrogen atoms N1 to N4 of the two ligands. The coordination sphere is best described as a distorted tetrahedron with the angles

varying from 100.92(8)° to 124.40(8)°. In the metallaspirocycle, the two six membered FeN_2C_2P rings adopt a distorted boat conformation each with the deprotonated carbon atoms C1 and C22 displaced by on average 45 pm from the respective N–P–C–N least square plane and the Fe^{2+}-centre by 29 pm, respectively.[175]

The Fe–N_{imino} distances (av. 204.4 pm) are equal within their esds. They are in the range found in iron(II) complexes, in which the cation is coordinated to imino functions, like in [Fe{(*o*-C_6H_4)$Ph_2PNSiMe_3$}$_2$] (211.1 pm),[182] [ClFe(Et_3PN)]$_4$ (205.7 pm),[183] or the 12 VE iron (II) complex [Fe(H_2CPh){HC($CMeNAr)_2$}] (198.2 pm).[184] In comparison to the dibromo iron(II) compound [{2, 6-($Ph_2PNSiMe_3$)Py}$FeBr_2$] (228.8 pm)[185] the Fe–N_{imino} contacts in **15** are ca. 24.4 pm shorter.
In [Fe{Ph_2P(CHPy)$NSiMe_3$}$_2$], (**15**), the Fe–N_{Py} distances (av. 207.7 pm) are only 3.3 pm longer than the Fe–N_{imino} contacts. As expected for the delocalization of the negative charges in the $[HC–Py]^-$ backbones of the two ligands, they are remarkable shorter than in the donor base coordinated iron complexes.[83]

Like in the zinc amide **14**, the sum of the bond angles at the pyridyl nitrogen atoms N2 and N4 (av. 355.55°) in **15** reflect a marginally pyramidal environment of these atoms and a shift of the cation towards the π-density of the pyridyl rings. The imino nitrogen atoms N1 and N3 show planar coordination spheres.[175]
The structural parameters in the anionic ligands match those observed for the alkali metal complexes **11** to **13**[137] and for the zinc derivative **14**.[175] Due to the similar ion radii of Zn^{2+} and Fe^{2+} the P–N (av. 161.25 pm) and Si–N bond lengths (av. 173.56 pm) in **14** and **15** are identical within their estimated standard deviations. The P–N distances are elongated by 7.1 pm in comparison to the iminophosphorane **9**, the N–Si bonds are 5.48 pm longer.[137,175]

Due to paramegnetic parts in the NMR samples no NMR data could be obtained for the iron complex [Fe{Ph_2P(CHPy)$NSiMe_3$}$_2$], (**15**).

3.5 Comparison of selected parameters of compounds 9–15

3.5.1 Comparison of selected structural parameters of 9a and 11–15

The following table gives an overview of the mean structural features of the iminophosphorane $Ph_2(CH_2Py)(NSiMe_3)$, (**9a**), and the ligands in the metal derivatives **11**–**15**.[137,175]

Table 3.10: *Mean structural parameters of **9** and the ligands in the metal complexes **11** to **15**.*

	deprotonated ligand				neutral ligand			
	P–N	N–Si	P–CH	HC–C_{Py}	P–N	N–Si	P–CH_2	H_2C–C_{Py}
9a	–	-	–	–	154.13	168.08	182.57	150.39
11	159.19	170.77	172.76	139.86	–	–	–	–
12	158.96	170.69	172.95	140.5	156.55	172.17	181.46	149.8
13	157.79	168.69	173.43	141.1	156.28	172.04	183.48	150.6
14	161.18	173.42	172.19	139.25	–	–	–	–
15	161.25	173.7	172.6	139.85	–	–	–	–

Standard bond lengths: P–N: 170 pm, P=N: 155 pm, P–C: 185 pm , P=C: 167 pm , Si–N: 174 pm, C–C: 154 pm, C=C: 134 pm.[30]

The P–N bond lengths fall in a narrow range from 154.13 to 161.25 pm (Δ = 7.12 pm). In the metal coordinated neutral ligands they are only ca. 2.3 pm longer than in the iminophosphorane **9a**, and show no strong dependence on the nature of the coordinated metal. In the anionic ligands, they differ between 157.79 and 161.25 pm, depending on the *Lewis*-acidity of the coordinated cation. For the large soft sodium atom in **13**, the shortest P–N distance is found. The dual charged zinc and iron cations in **14** and **15**, respectively, cause the greatest impact on the P–N distances. These cations are of similar size and only ca. 5 pm larger than the lithium cation. The resulting higher charge concentration affects the P–N bond lengths more than a more dilute one. Hence in the lithium complexes **11** and **13**, the P–N distances (av. 159.1 pm) are ca. 2.1 pm shorter than in the zinc and iron complexes (av. 161.2 pm). Thus, in the anionic ligands, in which the P–N bond is perturbed by the additional negative charge created by deprotonation, the P–N distances are strongly dependent on the electronic requirements of the metal cations.

These tendencies are mirrored in the N–Si distances. The soft sodium atom in **13**, leads to augmented electrostatic contributions to the N–Si bonding in the anionic ligands and

therefore the N–Si distances (168.7 pm) are similar to those observed for the neutral iminophosphorane **9a** (168.0 pm). The harder lithium cations in **11** and **12** reduce the electrostatic contributions to the N–Si bonding, reflected in longer N–Si contacts (av. 170.7 pm) in the anionic ligands. In the zinc and iron complexes **14** and **15**, the N–Si distances (av. 173.6 pm) are in the range of formal N–Si single bonds (174 pm). Like for the P–N bond lengths, the charge concentration of the cations strongly affects the negatively charged imino nitrogen atoms.

The N–Si distances in the neutral ligands in **12** and **13** are of similar length (av. 172.1 pm) and ca. 4 pm longer than in the uncomplexed free iminophosphorane **9a**. The metal cations strongly interact with these imino nitrogen atoms, reducing the electrostatic contributions in the N–Si bonding and thus weakening the N–Si bonds.

The P–CH and HC–C_{Py} bonds in the anionic ligands are all of similar length (av. 172.8 pm) and much shorter than formal P–C, and C–C single bonds. This contraction is a result of the delocalization of the negative charge over the [HC–Py]-backbone. The sum of the bond angles at the pyridyl ring nitrogen atoms in the anionic ligands is smaller than 360° and indicates a displacement of the cations towards the π-electron density of the ring.

The accumulation of the negative charge is reflected in the bonding parameters of the pyridyl ring system. In table 3.11 the respective bond lengths are summerized, together with the bond distances in pyridine. The bond distances are assigned according to the following scheme:

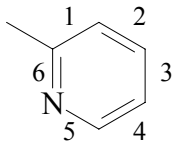

Table 3.11: *Comparison of the structural parameters in the pyridyl substituents in* ***9a****,* ***11****–****13*** *and pyridine [pm].*

		1	2	3	4	5	6
pyridine		139.4	139.2	139.2	139.4	133.8	133.8
9a		138.9	138.0	137.5	137.0	134.3	133.2
11		143.5	136.1	139.9	137.1	134.9	137.1
12	**a**	142.5	136.2	140.2	137.5	134.8	137.5
	b	138.9	138.0	137.9	137.7	134.6	134.3
13	**a**	143.4	136.6	139.9	138.0	134.7	137.6
	b	138.9	138.9	137.0	137.4	134.6	134.0
14		143.2	135.9	140.5	136.8	135.3	137.5
15		143.5	136.3	139.5	136.6	136.1	137.9

a= anionic ligand, b = neutral ligand

The bonds 1 and 6 are remarkably ellongated in the anionic ligands, compared to pyridine, the parent iminophosphorane **9a** or the neutral ligands in **12** and **13**. Furthermore, the bond 2 is significantly shorter and shows double bond character (C=C: 134 pm). The other bond lengths, 3, 4 and 5, are less affected by delocalization of the negative charge and are in the range of the distances in pyridine, **9a** and the neutral residues in **12** and **13**.

3.5.2 Comparison of spectroscopical data of compounds 9 and 11–14

In the following tables 3.12 and 3.13 the NMR spectroscopical data of the compounds **9** and **11**–**14** are summerized. Due to paramagnetic parts in the samples no NMR data are given for the iron complex **15**. The shielding of the different nuclei correlates with the chemical shifts. Resonances at high fields result from high electron density at the observed nucleus.

Table 3.12: *^{31}P- and ^{15}N-NMR shifts[ppm] of **9** and **11–14**.*

	anionic ligand			neutral ligand		
Nucleus	^{31}P	^{15}N		^{31}P	^{15}N	
		N_{imino}	N_{Py}		N_{imino}	N_{Py}
9	-	-	-	-0.32	-343	-61
11	18.03	-331	-145	-	-	-
12	15.36	-334	-139	8.46	-339	-68
13	11.3	-345	-137	-0.60	-332	-63
14	26.4	-348	-182	-	-	-

Deprotonation at the C_α-atom in the iminophosphorane $Ph_2P(CH_2Py)(NSiMe_3)$, (**9**), results in downfield shifts for the phosphorus nuclei in the ^{31}P-NMR spectra compared to the resonance of the iminophosphorane **9** and the neutral ligands in **12** and **13**. The delocalized negative charge and metal coordination at the P bounded nitrogen atom decreases the electron density at the phosphorus centre. In the zinc complex **14**, the phosphorus nuclei have the lowest electron density, according to the two fold positive charge of the zinc cation in comparison to the alkali metal complexes.

In the starting material **9** and in both neutral ligands of **12** and **13**, the pyridyl nitrogen atoms resonate at similar frequencies (δ= -61 to -68). The observed small differences arise from metal coordination at the ring nitrogen atom. However, the ^{15}N-NMR resonances for

the pyridyl ring nitrogen atoms in the anionic ligands are considerably shifted to higher fields (δ= -137 to -182) with respect to **9** (δ= -61) and to the neutral ligands in **12** and **13**. Remarkably, they reflect the polarizing abilities of the metal, hence the upfield shift due to sodium coordination (in **13**) is less pronounced than the changes induced from the lithium cation (in **11**, **12**) or the zinc cation (in **14**). These NMR-spectroscopical shifts can be explained by a considerable charge transfer from the carbanionic atom C1 to the hetero-aromatic ring and accumulation at the pyridyl nitrogen atom.
Additionally, the almost invariant ^{15}N-NMR spectroscopical shift of the imino nitrogen atom in all compounds indicates, that the charge density at this nitrogen atom is less affected by the deprotonation.

The charge transfer in the anionic ligands of **11**–**14** to the pyridyl substituent is also evident from the ^{1}H- and ^{13}C-NMR spectroscopical experiments. In table 3.13 these chemical shifts are compared to those of the iminophosphorane **9** and the neutral ligands in **12** and **13**. The shifts are assigned according to the following scheme:

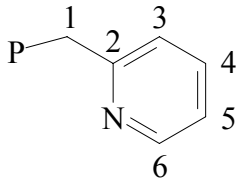

Table 3.13: *^{1}H- and ^{13}C-NMR shifts [ppm] of **9** and **11**–**14**.*

	^{1}H					^{13}C					
	1	3	4	5	6	1	2	3	4	5	6
9	3.56	7.18	7.07	6.55	8.28	43.2	152.3	125.6	129.5	121.6	149.6
11	3.58	6.42	6.71	5.77	7.12	55.8	167.8	118.9	134.8	106.9	147.5
a	4.11	6.60	7.00	5.95	7.33	59.0	166.3	118.4	134.2	103.6	148.0
12 b	3.78	6.85	7.00	6.42	8.46	39.7	150.7	126.6	128.3	121.5	152.2
a	3.39	6.18	6.64	5.51	7.15	58.2	168.0	117.9	133.5	103.9	147.8
13 b	3.85	7.15	7.44	6.98	8.31	42.5	155.3	125.8	131.1	122.1	149.8
14	3.32	6.28	6.56	5.53	7.12	59.2	166.6	120.2	134.8	106.5	146.9

a = anionic ligand, b = neutral ligand

Deprotonation at the C_{α}-atom in **9** results in an upfield shift for the pyridyl hydrogen atoms compared to the corresponding atoms in the neutral ligands of **12** and **13** and the parent iminophosphorane **9**. The charge density is accumulated in the pyridyl substituent. In the ^{13}C-NMR, the deprotonated C1 atoms in the anionic ligands resonate at lower fields compared to the neutral ligands. Additionally, the carbon atom atoms adjacent to the ring nitrogen atoms are shifted downfield.

4 Conclusion and Prospects

4.1 Diphenyl(-2-)picolylphosphane

The coordination behaviour of the $[Ph_2P(CHPy)]^-$-anion to metal cations of different *Lewis*-acidity was examined. The metal derivatives **2**–**5** and **7**–**8** were prepared by reaction of $Ph_2P(CH_2Py)$, (**1**), with lithiumorganics or the metal bistrimethylsilylamides. Transmetallation of the lithiated species **2** with $ZnCl_2$ in presence of ZnO gave the zinc complex **6** (Scheme 4.1).

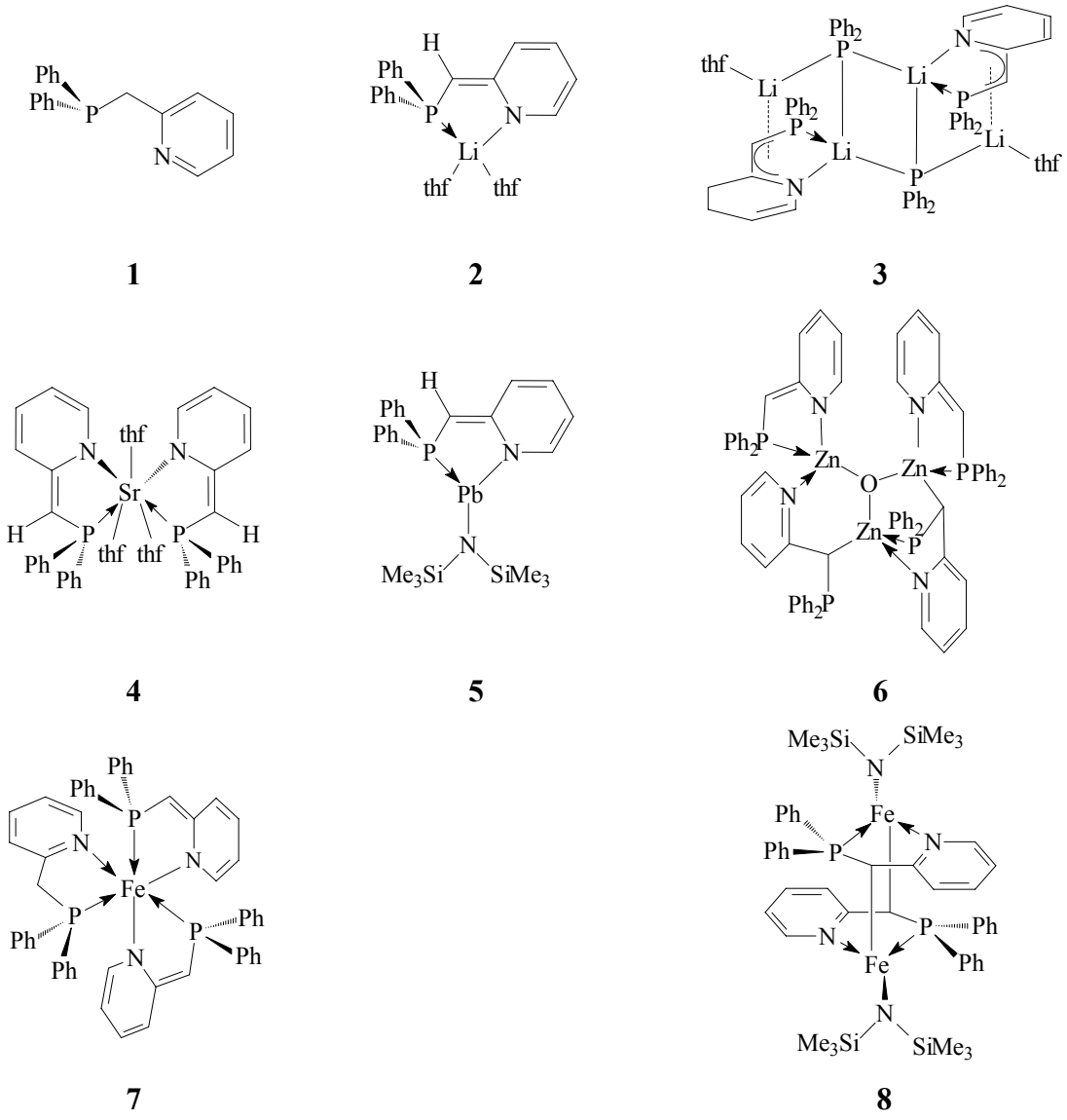

1 **2** **3**

4 **5** **6**

7 **8**

Scheme 4.1: *The parent phosphane **1** and its metalated derivatives **2**–**8**.*

In the characterized metal complexes, the $[Ph_2P(CHPy)]^-$-anion features three different coordination modes:

1) bidentate, (*P,N*)-chelating
2) tridentate, (*P,N*)-chelating, C-coordinating
3) (*C,N*)-coordinating

Which of these coordination modes is realized depends on various parameters. First, soft *Lewis*-acids like Sr^{2+} (**4**) and Pb^{2+} (**5**) are exclusively (*P,N*)-chelated by the $[Ph_2P(CHPy)]^-$-anions. With the harder *Lewis*-acids Li^+, (**2**, **3**), Zn^{2+} (**6**) and Fe^{2+} (**7**, **8**) different coordination modes are possible: In homoleptic complexes the $[Ph_2P(CHPy)]^-$-anion also prefers (*P,N*)-rather than [M]–C-coordination (**2**, **7**). However in heteroleptic complexes the $[Ph_2P(CHPy)]^-$-fragment can bind to a metal cation *via* the P- and N-atoms and additionally coordinate a second cation *via* the C_α-atom (**6**, **8**) or the [HC–C_{Py}]-moiety (**3**). In the zinc complex **6**, one anion coordinates only *via* the pyridyl N-and the C_α-atom to cations. Here, the phosphorus centre is not involved in coordination. C_α-metal coordination involves sp^3-hybridization of the carbon atom, in contrast to the sp^2-character found for the exclusively (*P,N*)-coordinating anion. This kind of coordination flexibility and switching of the hybridization at the deprotonated carbon centre is closely related to that found for the $[HC(Py)_2]^-$-anion. In $[(thf)_2Li\{HC(Py)_2\}]$ the deprotonated carbon atom has sp^2-character, but in $[MeZn\{HC(Py)_2\}]_2$ it is sp^3-hybridized.

The following scheme gives an overwiew about the different coordination modes, observed for the $[Ph_2P(CHPy)]^-$-anion:

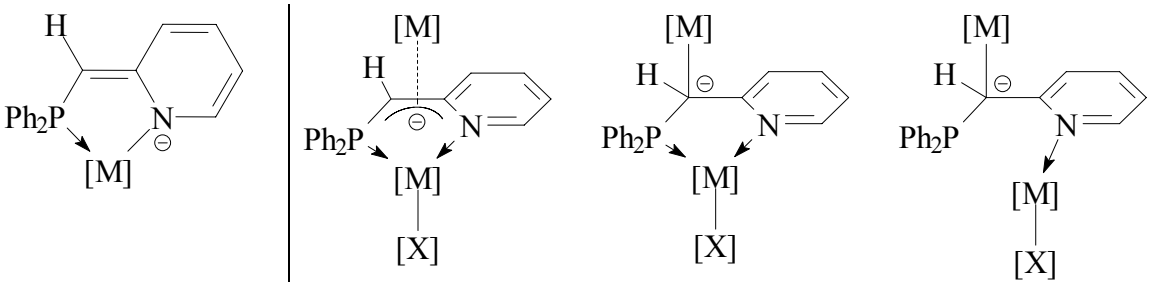

[M] = hard or soft *Lewis*-acid

[M] = hard *Lewis*-acid

[X] = anion with localized charge

amide	"carbanionic"	carbanion	carbanion
P-donor	(*P,N*)-donor	(*P,N*)-donor	N-donor

Scheme 4.2: *Coordination modes and classification of the $[Ph_2P(CHPy)]^-$-anion.*

In conclusion, the phosphane $Ph_2P(CH_2Py)$, (**1**), is a very versatile starting material for the preparation of highly flexible, hemilabile, ambident ligands. This *Janus head* responds very sensitive to the *Lewis*-acidity and the charge concentration of the coordinated metal and adapts the coordination mode to the electronic requirements of the cation (electronic differentiation).

Prospects

Thinking about the applications of phosphanes in catalysis, $Ph_2P(CH_2Py)$, (**1**), seems to be a promising starting material to synthesize mixed-metal coordination compounds in which soft transition metals together with the hard $[Me_2Al]^+$-fragment are coordinated. In these type of complexes, the $[Me_2Al]^+$-residue can be regarded as a MAO equivalent, which is omnipresent as co-catalyst in various catalytical cycles. The different bonding modes of the anionic ligand together with the activation properties of the MOA analogue $[Me_2Al]^+$-residue, should lead to a very versatile class of catalysts. The aluminium complex should be available *via* transmetallation of the lithiated phosphane $[(thf)_2Li\{Ph_2PC(H)Py\}]$, (**2**), with Me_2AlCl. Once isolated, this compound should be reacted with transition metal fragments of different *Lewis*-acidity (Scheme 4.3).

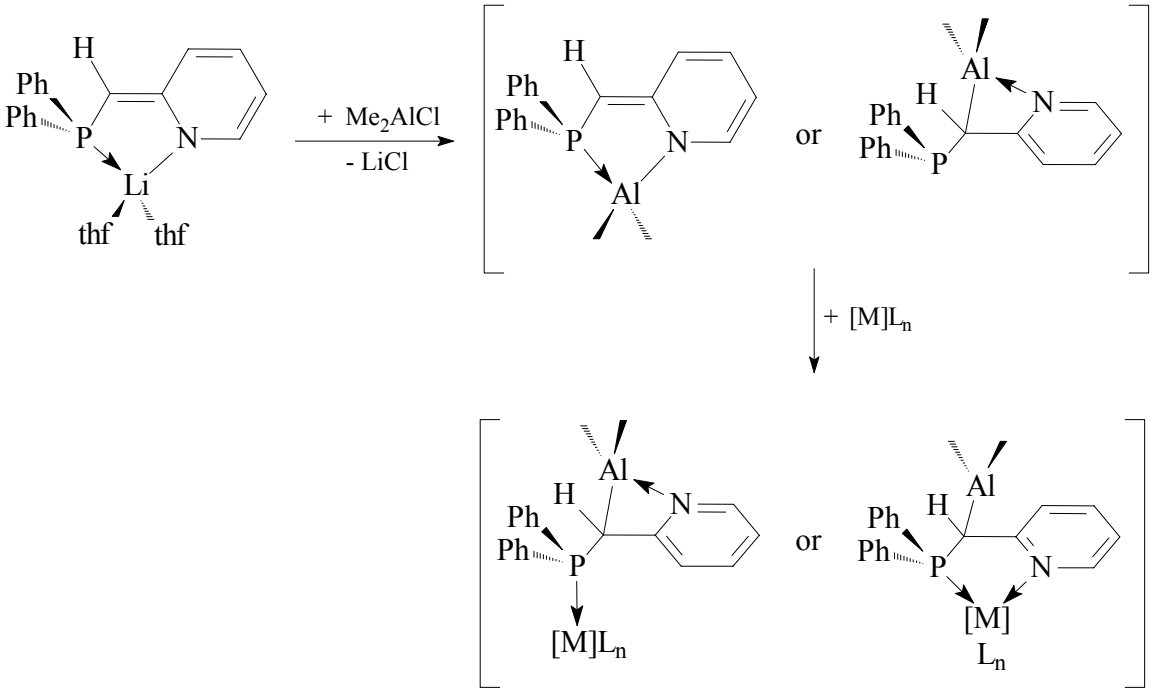

Scheme 4.3: *A heterobimetallic complex, synergetically combining hemilability and the activation properties of the MAO equivalent* $[Me_2Al]^+$.

Carbenes are widely used for the stereoselective formations of cyclopropanes. The introduction of good leaving groups, such as halides or alkoxides, at C_α-position in the phosphane **1**, leads to potential carbene precursors. Removal of the resting acidic hydrogen atom with strong bases, followed by intramolecular salt elimination, should give *Bertrand*-type phosphorus stabilized carbenes. (Scheme 4.4).[186]

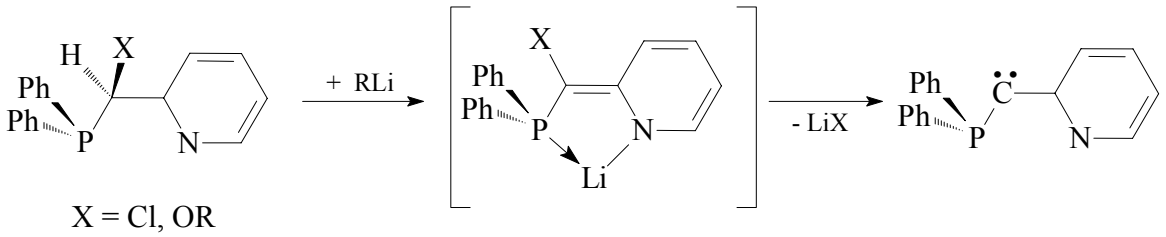

Scheme 4.4: *Proposed reaction sequence for the formation of carbenes.*

The two phosphanes $PhP(CH_2Py)_2$ and $P(CH_2Py)_3$ are already known for a long time.[187] The additional pyridyl nitrogen atoms and the acidic hydrogen atoms makes these phosphanes very interesting for the synthesis of highly charged systems. The isolation of $[(thf)_2Li_4(PPh_2)_2\{Ph_2PC(H)Py\}_2]$, (**3**), showed, that the P–CH_2 bond in **1** can easily be cleaved with lithiumorganics. Thus, cleavage of a P–CH_2 bond in the two abovementioned phosphanes should lead to *sec*. phosphanes, with a higher geometrical flexibility and even more reactive centres than in dipyridylphosphane Py_2PH, currently studied (Scheme 4.5).

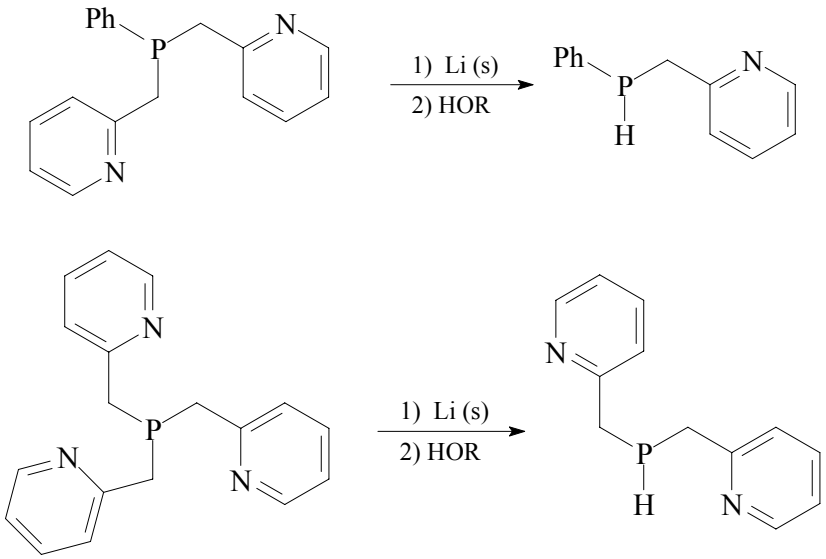

Scheme 4.5: *Synthesis of sec. phosphanes derived from $Ph_2P(CH_2Py)$,(**1**).*

4.2 Diphenyl(-2-)picolyliminophosphorane

In this work first results on the reactivity and coordination behaviour of the iminophosphorane $Ph_2P(CH_2Py)(NSiMe_3)$, (**9**), and its anion were presented. Several derivatives of **9** could be synthesized and completely characterized (Scheme 4.6).

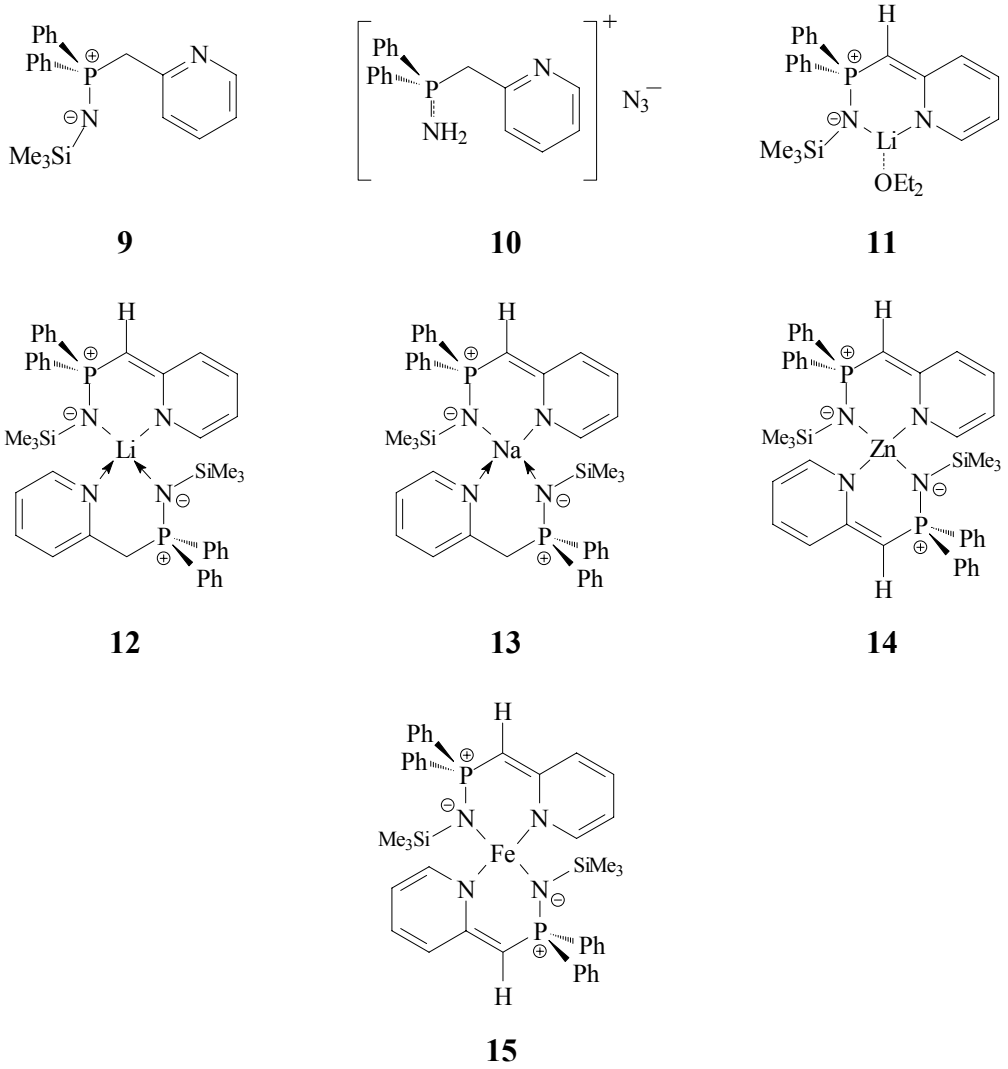

9 **10** **11**

12 **13** **14**

15

Scheme 4.6: *The iminophosphorane* ***9*** *and its derivatives* ***10–15****.*

In all metal complexes the C_α-deprotonated anion of $Ph_2P(CH_2Py)(NSiMe_3)$, (**9**), prefers (*N*,*N*')-side arm- rather than C-coordination. The electron deficient pyridyl substituent at the C_α-atom leads to charge delocalization in the anionic $[Ph_2P(CHPy)(NSiMe_3]^-$-moiety. The pronounced upfield shifted NMR-resonances of the pyridyl nitrogen atoms in the

anions illustrate the high negative charge at these atoms and prove their amidic character, reflected in the [M]–N_{Py} bond lengths.

The results of a topological analysis of **11**, performed by *Kocher* in our group, gave the first experimental prove for the nature of P–N bonds in iminophosphoranes. His results verified the theoretically predicted character of this bond as P^+–N^- single bond, contracted by high electrostatic interactions of the positive charged phosphorus with the negative charged nitrogen atom.

The structural parameters together with the NMR data of the derivatives **9**–**15**, discussed in this work, further substantiate these results and allow to derive some general trends of the bonding parameters in iminophosphoranes. The main tendencies can be summerized as follows:

1) The negative charge generated by deprotonation of the methylene bridge is delocalized over the exocyclic C–C bond and the connected pyridyl ring. The P–CH and HC–Py distances are remarkably contracted in comparison to the neutral molecule **9** or the neutral chelating ligands in **12** and **13**.
2) The P–C bonds in the anionic ligands show ylidic character.
3) The delocalization of the negative charge results in a more pronounced amidic character of the pyridyl nitrogen atom.
4) The description of the P–N interaction as a P^+–N^- single bond, contracted by electrostatic interactions, results in short N–Si contacts, due to strong interactions of the negative nitrogen atom with the electropositive silicon atom.
5) Metal coordination at the imino nitrogen atom of the neutral iminophosphorane gives slightly longer P–N bonds than in the uncomplexed free iminophosphorane and longer N–Si distances, because of the ionic character of the M–N interaction, reducing the electrostatic contributions to the N–Si-bonding.
6) Deprotonation of the C_α-position next to the positive charged phosphorus atom perturbs the P^+–N^- interaction, causing a remarkable elongation of the P–N and N–Si bonds, depending on the electronic requirements of the metal cations.
7) The bifurcated donation mode of the imino nitrogen atom, described by *Kocher* for **11**, together with the M–N_{imino} contacts in **11**–**15**, which are much shorter than expected for M←N donor bonds show, that the imino nitrogen atom cannot be

regarded as simple 2e-donor. The M–N_{imino} distances in all complexes reflect a high ionic contribution to the bonding. This leads to a description of the imino nitrogen atom between a monoanionic two and four electron donating centre.

8) The structural and NMR-parameters of **10** clearly shows that the salt must be described as a phosphoniumazide salt according to $[Ph_2(PyCH_2)P^+–NH_2][N_3]^-$, rather than as an iminiumphosphane. The negatively charged imino nitrogen atom of the zwitterionic $P^+–^-NR$ bond is protonated, leaving the positive charge at the phosphorus atom.

The bonding parameters of the iminophosphorane **9** and all its derivatives **10**–**15**, together with the almost fixed ^{15}N-NMR resonances for the imino nitrogen atoms in these compounds prove, that hypervalent central phosphorus is not required to describe the bonding situation in iminophosphoranes. It is much more appropriate to assign charges in the resonance formula even of the starting material $Ph_2P(CH_2Py)(NSiMe_3)$, (**9**) (Scheme 4.7).

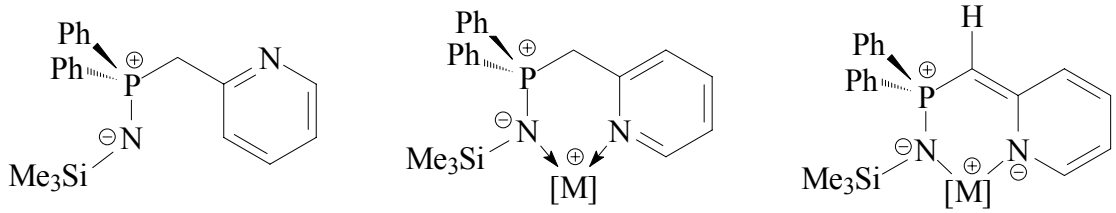

9 **12, 13** **11–15**

Scheme 4.7: *The iminophosphorane **9** and its anion.*

This polar single bond corresponds best with the reactivity of iminophosphoranes described in literature: metalorganics in polar solvents can easily cleave this bond rather than the wrongly assigned P=N double bond. Therefore, transimination or the *retro*-Staudinger reaction of iminophosphoranes seem unorthodox but suitable synthetic accesses to phosphanes.

Prospects

The application of the iminophosphorane **9** and its metalated derivatives in transimination reactions should be tested in future projects.

In all the currently isolated metal derivatives, the $[Ph_2P(CHPy)(NSiMe_3)]^-$-anion acts as bidentate (*N*,*N*')-chelating ligand. However, it seems sensible to envisage appropriate *Lewis*-acidity metal fragments coordinated to the C_α-position. Another interesting study in the context of the isolation of heterobimetallic complexes would be the coordination behaviour of the dianion of $Ph_2P(CH_2Py)(NSiMe_3)$, (**9**) (Scheme 4.8).

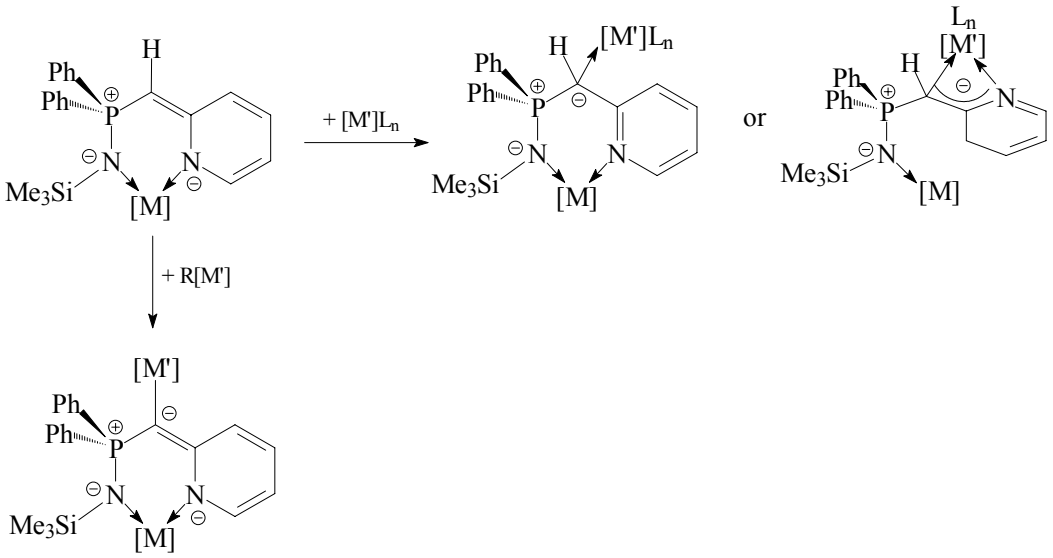

Scheme 4.8: *Synthesis of heterobimetallic complexes.*

The incorporation of additional $[H_2CPy]$-substituents at the phosphorus atom in iminophosphoranes, leads to even more flexible ligands, providing multiple reaction centres and side arm donating atoms. As monoanions or as multiple negatively charged species, these systems should be able to stabilize metal fragments in unusual coordination modes and should enable hemilabile behaviour by dissociation of e.g. one pyridyl side arm, giving a vacant coordination site for substrate binding in catalytic cycles. Furthermore, reduction of these iminophosphoranes to phosphane(III)amines seems feasible (Scheme 4.9).

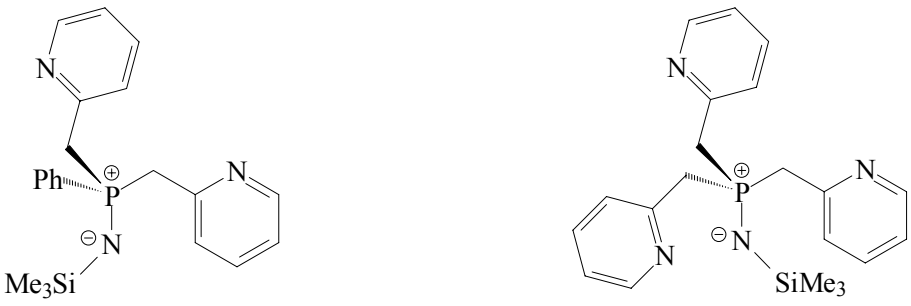

Scheme 4.9: *Methylene bridged pyridyliminophosphoranes.*

5 Zusammenfassung und Ausblick

5.1 Diphenyl(-2-)picolylphosphan

Es wurde das Koordinationsverhalten des $[Ph_2P(CHPy)]^-$-Anions gegenüber Metallkationen unterschiedlicher *Lewis*-Azidität untersucht. Die Metallderivate **2**–**5** und **7**–**8** wurden durch Reaktionen von $Ph_2P(CH_2Py)$, (**1**), mit Lithiumalkylen oder Metallbistrimethylsilylamiden dargestellt. Transmetallierung der lithiierten Verbindung **2** mit $ZnCl_2$ in Gegenwart von ZnO ergab den Zinkkomplex **6** (Schema 5.1).

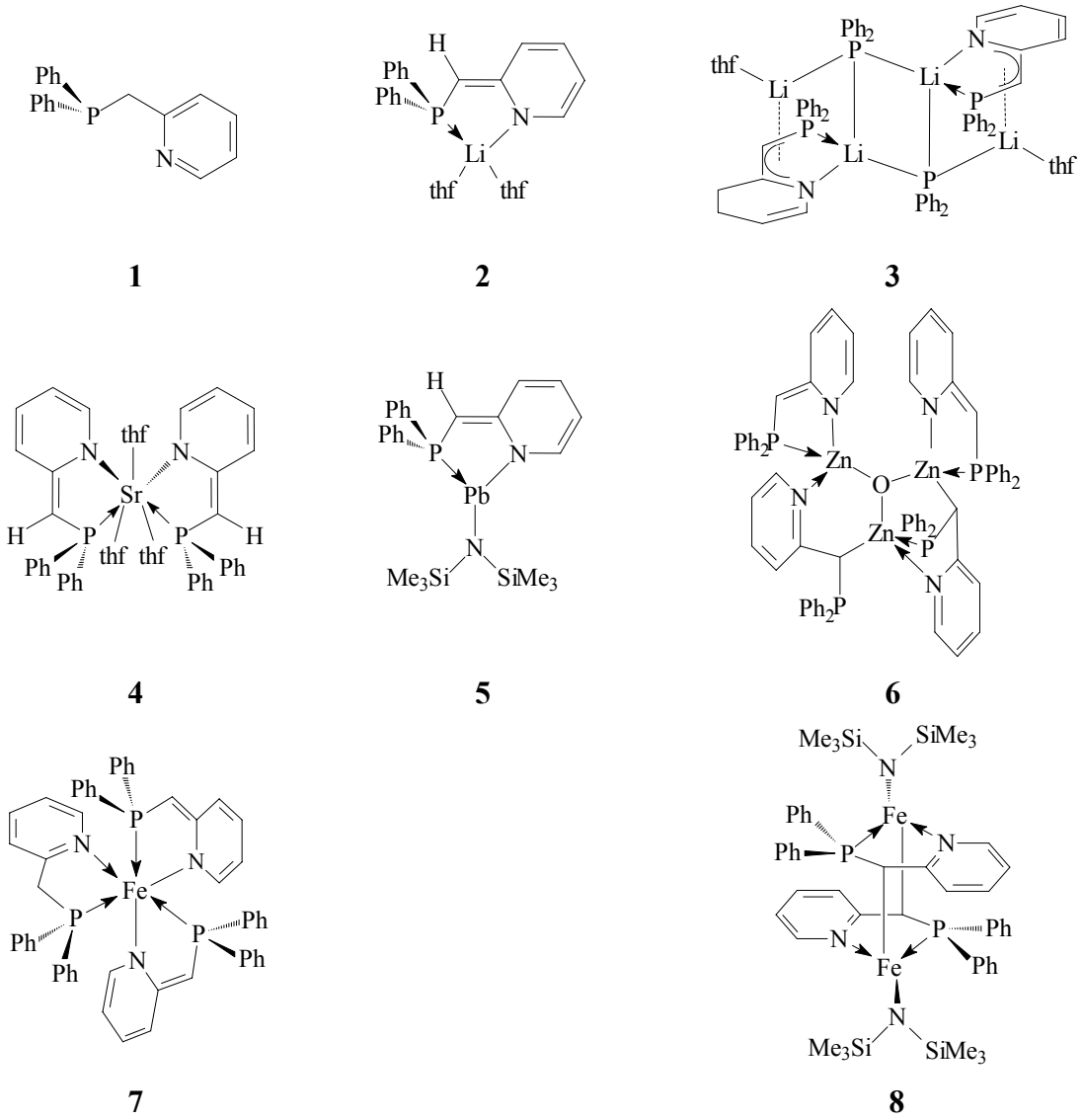

Schema 5.1: *Das Phosphan **1** und seine metallierten Derivate **2**–**8**.*

In den charakterisierten Metallkomplexen tritt das $[Ph_2P(CHPy]^-$-Anion in drei verschiedenen Koordinationsmodi auf:

1) bidentat, (*P,N*)-chelatisierend
2) tridentat, (*P,N*)-chelatisierend, C-koordinierend
3) (*C,N*)-koordinierend

Welcher dieser Koordinationsmodi tatsächlich realisiert wird hängt von mehreren Parametern ab. Erstens werden weiche *Lewis*-Säuren, wie Sr^{2+} (**4**) und $Blei^{2+}$ (**5**), ausschließlich (*P,N*)-chelatisiert. Mit den härteren *Lewis*-Säuren Li^+ (**2**, **3**), Zn^{2+} (**6**) und Fe^{2+} (**7**, **8**) sind auch andere Koordinationsarten möglich: In homoleptischen Komplexen, wird (*P,N*)-Chelatisierung gegenüber [M]–C-Koordination bevorzugt (**2**, **7**). Das $[Ph_2P(CHPy]^-$-Fragment kann jedoch in heteroleptischen Komplexen über die P- und N-Atome an das Metall binden und zusätzlich ein weiteres Metallkation über das C_α-Atom (**6**, **8**) oder die [HC–C_{Py}]-Einheit koordinieren (**3**). Im Zinkkomplex **6** koordiniert ein Anion nur über das Pyridyl-N- und das C_α-Atom. Das Phosphoratom ist nicht in die Koordination mit eingebunden. Bei C_α-Metallkoordination wird eine sp^3-Hybridisierung des Kohlenstoffatoms beobachtet, während in den ausschließlich (*P,N*)-koordinierenden Anionen sp^2-Charakter dominiert.

Diese Art von Koordinationsflexibilität und Änderung des Hybridisierungszustandes des deprotonierten Kohlenstoffzentrums wurde schon für das $[HC(Py)_2]^-$-Anion beobachtet. In $[(thf)_2Li\{HC(Py)_2\}]$ zeigt das zentrale C-Atom sp^2-Charakter, während in $[MeZn–\{HC(Py)_2\}]_2$ das Kohlenstoffatom sp^3-hybridisiert ist.

Das folgende Schema gibt einen Überblick über die verschiedenen Koordinationsmodi des $[Ph_2P(CHPy)]^-$-Anion :

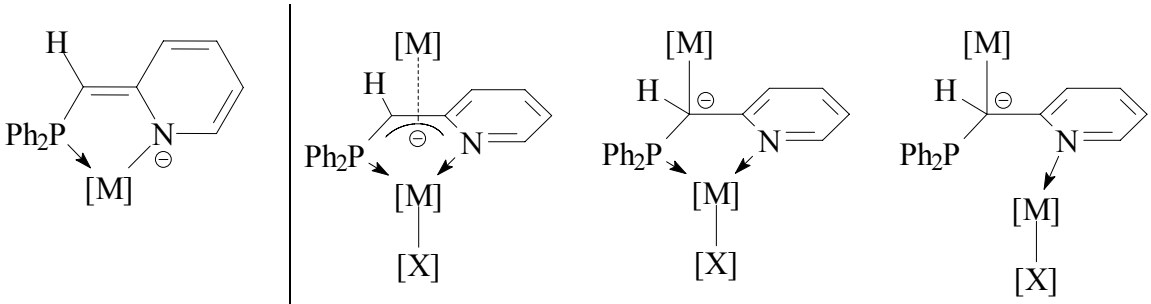

[M] = harte oder weiche *Lewis*-Säure	[M] = harte *Lewis*-Säure [X] = Anion mit lokalisierter Ladung		
Amid	"carbanionisch"	Carbanion	Carbanion
P-Donor	(*P,N*)-Donor	(*P,N*)-Donor	N-Donor

Schema 5.2: *Koordinationsmodi und Klassifiezierung des $[Ph_2P(CHPy)]^-$-Anions.*

Zusammenfassend läßt sich feststellen, dass das Phosphan $Ph_2P(CH_2Py)$, (**1**), ein vielseitiges Ausgangsmaterial zur Synthese hoch flexibler, hemilabiler, ambidenter Liganden ist. Dieser *Janus*-Kopf reagiert ausgesprochen sensitiv auf die Ladungs–dichtekonzentration des koordinierten Metalls und passt seinen Koordinationsmodus entsprechend den elektronischen Anforderungen des Kations an (elektronische Differenzierung).

Ausblick

Betrachtet man die Anwendung von Phosphanen in der Katalyse, scheint $Ph_2P(CH_2Py)$, (**1**), eine viel versprechende Startverbindung zur Synthese gemischt-metallischer Koordinationsverbindungen zu sein, in denen weiche Übergangsmetalle zusammen mit dem harten $[Me_2Al]^+$-Fragment koordiniert werden können. In diesem Typus von Komplexen kann die $[Me_2Al]^+$-Einheit als MAO-Äquivalent aufgefasst werden, das als Co-Katalysator in katalytischen Zyklen omnipräsent ist. Die unterschiedlichen Bindungsmodi des anionischen Liganden, zusammen mit den Aktivierungseigenschaften des MAO-analogen $[Me_2Al]^+$-Fragmentes, sollten zu einer viel versprechenden Katalysatorenklasse führen. Der Aluminiumkomplex könnte über eine Transmetallierung des lithiierten Phosphans (**2**) mit Me_2AlCl dargestellt werden. Dieser Komplex sollte anschließend mit Übergangsmetallfragmenten unterschiedlicher *Lewis*-Azidität umgesetzt werden (Schema 5.3).

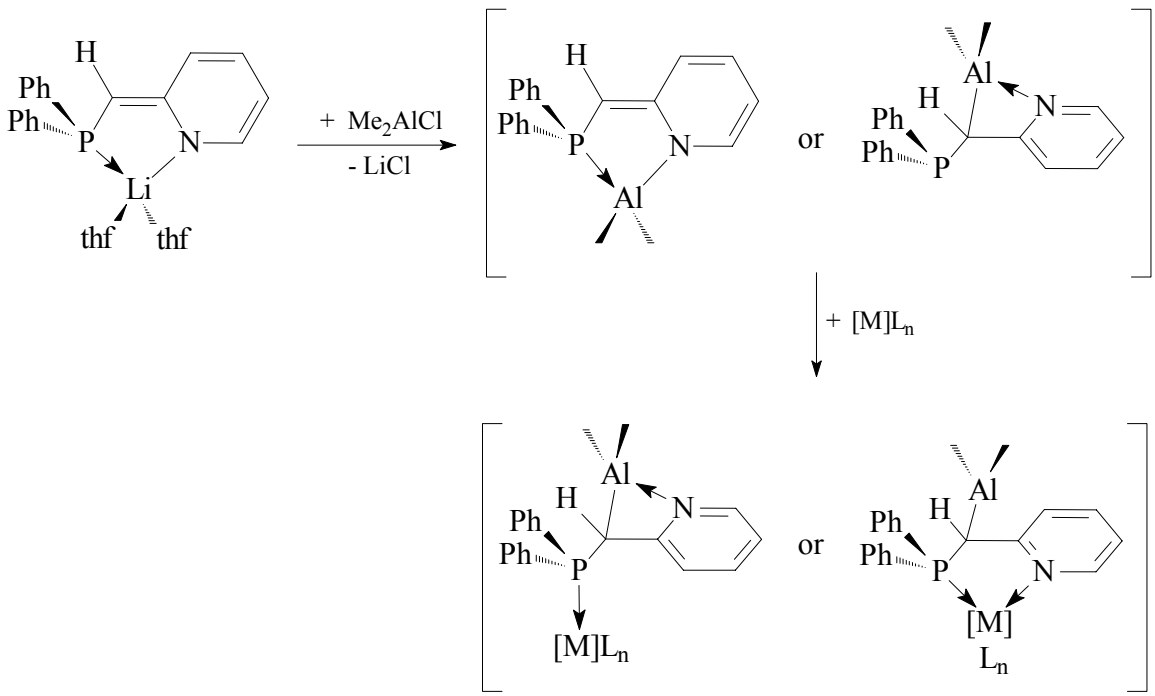

Schema 5.3: *Ein heterobimetallischer Komplex, der Hemilabilität mit den Aktivierungseigenschaften des MAO-Äquivalents $[Me_2Al]^+$ synergetisch verbindet.*

Carbene sind zur stereoselektiven Darstellung von Cyclopropanen weit verbreitet. Die Einführung von guten Abgangsgruppen, wie Halogeniden oder Alkoxiden, in C_α-Position des Phosphans **1**, führt zu potentiellen Carbenvorläufern. Entfernung des letzten aziden Wasserstoffatoms mit starken Basen, gefolgt von einer intramolekularen Salzeliminierung sollte *Bertrand*-artige phosphorstabilisierte Carbene ergeben (Schema 5.4).[186]

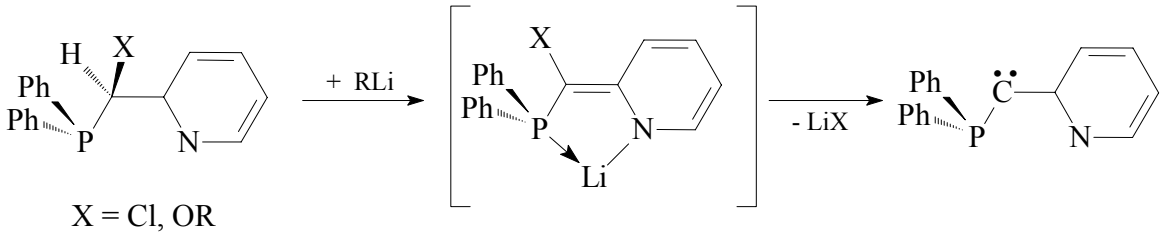

Schema 5.4: *Mögliche Reaktionssequenz zur Darstellung von Carbenen.*

Die beiden Phosphane $PhP(CH_2Py)_2$ und $P(CH_2Py)_3$ sind schon seit langer Zeit bekannt.[187] Durch die zusätzlichen Pyridyl-Stickstoff- und aziden Wasserstoffatome sind diese Phosphane im Hinblick auf die Darstellung hochgeladener Systeme sehr interessant.

Die Isolierung von $[(thf)_2Li_4(PPh_2)_2\{Ph_2PC(H)Py\}_2]$, (**3**), zeigte, dass die P–CH_2-Bindung in **1** leicht durch Lithiumorganyle gespalten werden kann. Daher sollte die Spaltung einer P–CH_2-Bindung in den zwei zuvor beschriebenen Systemen zu *sek.* Phoshanen führen, die weitaus höhere geometrische Flexibilität und mehr reaktive Zentren aufweisen als bei–spielsweise das Dipyridylphosphan Py_2PH, das zur Zeit noch untersucht wird (Schema 5.5).

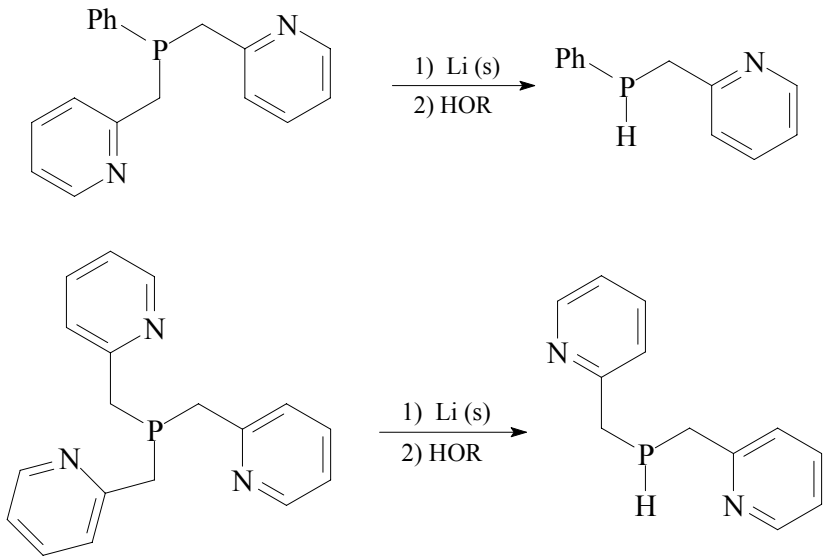

Schema 5.5: *Synthese von sek. Phosphanen, abgeleitet von $Ph_2P(CH_2Py)$,(**1**).*

5.2 Diphenyl(-2-)picolyliminophosphoran

In dieser Arbeit wurden erste Ergebnisse zur Reaktivität und zum Koordinationsverhalten des Iminophosphorans $Ph_2P(CH_2Py)(NSiMe_3)$, (**9**), und seines Anions vorgestellt. Mehrere Derivate von **9** wurden synthetisiert und vollständig charakterisiert (Schema 5.6).

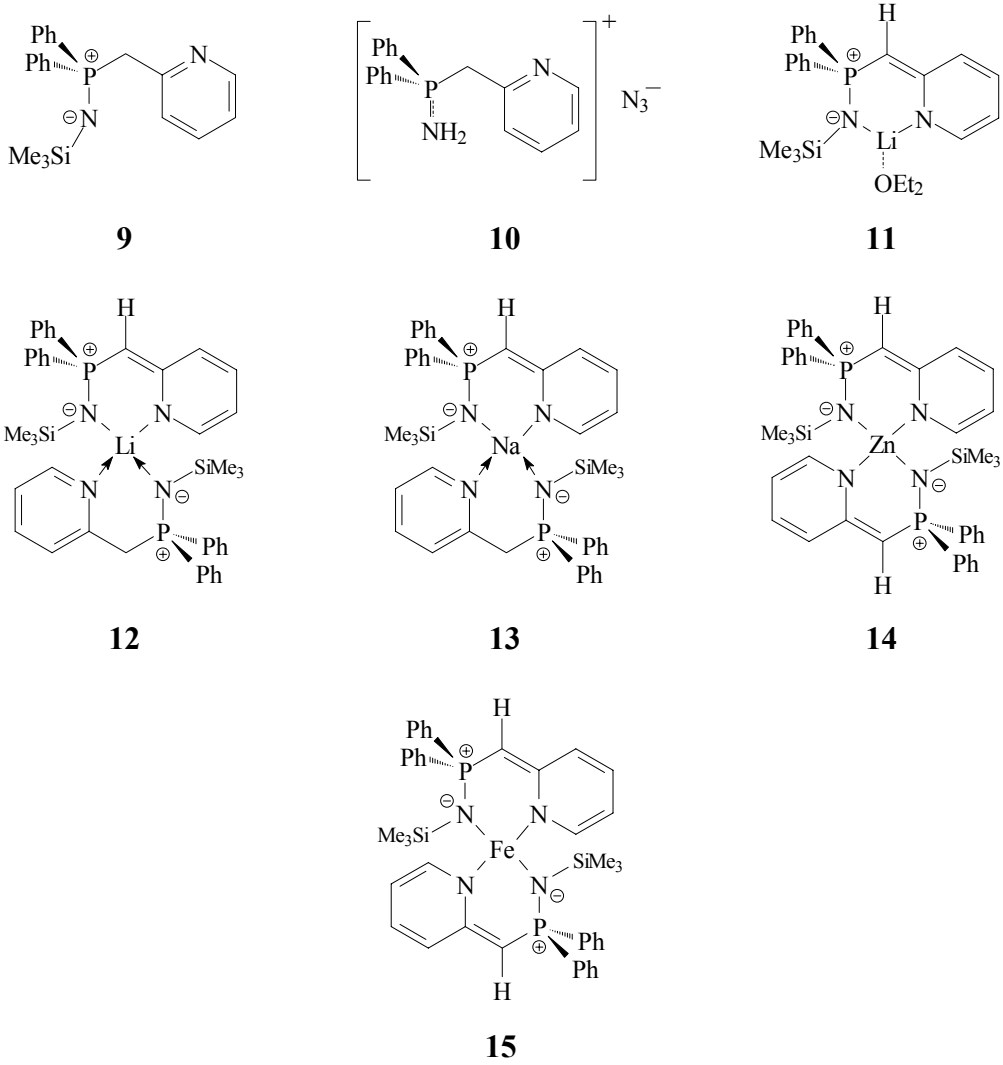

9 **10** **11**

12 **13** **14**

15

Schema 5.6: *Das Iminophosphoran* ***9*** *und seine Derivate* ***10–15****.*

In allen Metallkomplexen bevorzugt das C_α-deprotonierte Anion von $Ph_2P(CH_2Py)$–$(NSiMe_3)$, (**9**), (*N,N'*)-Seitenarm- gegenüber C-Koordination. Der elektronendefizitäre Pyridylsubstituent verursacht eine Delokalisation der Ladungsdichte innerhalb des $[Ph_2P(CHPy)(NSiMe_3)]^-$-Systems.

Die ausgeprägte Hochfeldverschiebung der NMR-Resonanzen der Pyridylstickstoffatome der Anionen belegt ihre hohe negative Ladungsdichte und beweist den amidischen Charakter der N_{Py}-Atome, der sich in den kurzen [M]–N_{Py} Bindungslängen widerspiegelt.

Die Ergebnisse einer topologischen Analyse von **11**, die von *Kocher* in unserer Arbeitsgruppe durchgeführt wurde, erbrachten den ersten experimentellen Beweis zur Bindungsnatur der P–N Bindung in Iminophosphoranen. Seine Ergebnisse bestätigten den theoretisch vorausgesagten Charakter dieser Bindung als P^+–N^- Einfachbindung, die durch starke elektrostatische Wechselwirkungen des positiv geladenen Phosphoratoms mit dem negativ geladenen Stickstoffatom verkürzt ist.

Die Strukturparameter und die NMR-Daten der Derivate **9**–**15**, die in dieser Arbeit diskutiert wurden, untermauern weiter diese Ergebnisse und erlauben, einige generelle Trends zu den Bindungsparametern in Iminophosphoranen abzuleiten. Die wichtigsten Tendenzen lassen sich wie folgt zusammenfassen:

1) Die negative Ladung, die durch Deprotonierung der Methylenbrücke generiert wird, ist über die exocyclische C–C Bindung und den daran gebunden Pyridylring delokalisiert. Die P–CH und HC–Py Abstände sind im Vergleich zum neutralen Molekül **9** oder den Neutralliganden in **12** und **13** deutlich verkürzt.
2) Die P–C Bindung der anionischen Liganden hat ylidischen Charakter.
3) Die Delokalisierung der negativen Ladung führt zu einem ausgeprägten amidischen Charakter des Pyridylstickstoffatoms.
4) Die Beschreibung der P–N Wechselwirkung als eine P^+–N^- Einfachbindung, verkürzt durch elektrostatische Beiträge, ergibt kurze N–Si Kontakte, aufgrund von starken Wechselwirkungen des negativ geladenen Stickstoffatoms mit dem elektropositiven Siliziumatom.
5) Metallkoordination am Iminostickstoffatom des Neutralliganden führt zu leicht längeren P–N Bindungen im Vergleich zu dem unkomplexierten freien Iminophosphoran und längeren N–Si Abständen, da der ionische Charakter der M–N Wechselwirkung die elektrostatischen Beiträge zur N–Si Bindung schwächt.

6) Deprotonierung in Nachbarschaft zum positiv geladenen Phosphoratom stört die $P^+–N^-$ Bindungssituation und verursacht eine bemerkenswerte Verlängerung sowohl der P–N- als auch der N–Si Bindungen. Der Grad des Einflusses ist abhängig von den elektronischen Anforderungen des Metallkations.
7) Das von *Kocher* als gegabelt donierend beschriebene Iminostickstoffatom in **11**, zusammen mit den $M–N_{imino}$ Kontakten in **11**–**15**, die sehr viel kürzer sind als für M←N Donorbindungen erwartet, zeigt, dass das Iminostickstoffatom nicht als einfacher zwei Elektronendonor aufzufassen ist. Dies führt zu einer Beschreibung des Iminostickstoffatoms zwischen einem monoanionischen zwei und vier Elektronendonor.
8) Die Struktur- und NMR-Parameter zeigen deutlich, dass das Salz **10** als Phosphoniumazidsalz, gemäß $[Ph_2(PyCH_2)P^+–NH_2][N_3]^-$ zu beschreiben ist und nicht als Iminiumphosphan. Das negativ geladene Iminostickstoffatom der zwitterionischen $P^+–^-NR$ Bindung ist protoniert und die positive Ladung verbleibt am Phosphoratom.

Die Bindungsparameter des Iminophosphorans und seiner Derivate **10**–**15**, zusammen mit den annähernd konstanten ^{15}NMR-Resonanzen der Iminostickstoffatome dieser Verbindungen beweisen, dass ein hypervalentes Phosphoratom zur Beschreibung der Bindungssituation in Iminophosphoranen nicht notwendig ist. Es ist vielmehr angebracht, sogar in der Ausgangsverbindung $Ph_2P(CH_2Py)(NSiMe_3)$, (**9**), den Atomen in den Resonanzformeln Ladungen zuzuweisen (Schema 5.7).

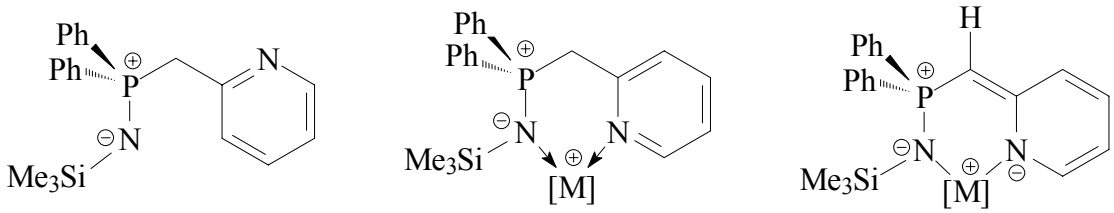

9 **12, 13** **11–15**

Schema 5.7: *Das Iminophosphoran* ***9*** *und sein Anion.*

Diese polare Einfachbindung entspricht am Besten der Reaktivität von Iminophos–phoranen, die in der Literatur beschrieben ist: in polaren Lösungsmitteln spalten metallorganische Reagenzien diese Bindung leichter, als die falsch zugewiesene P=N

Doppelbindung. Daher stellen Transiminierungen oder *Retro-Staudinger* Reaktionen zwar unorthodoxe, aber geeignete synthetische Zugänge zu Phosphanen dar.

Ausblick

Der Einsatz des Iminophosphorans **9** und der metallierten Derivate in Transiminierungen sollte in zukünftigen Projekten getestet werden.

In allen zurzeit isolierten Metallderivaten fungiert das $[Ph_2P(CHPy)(NSiMe_3)]^-$-Anion als (*N,N'*)-chelatisierender Ligand. Jedoch sollte man die Möglichkeit in Betracht ziehen, Metallfragmente geeigneter *Lewis*-Azidität an das C_α-Atom zu koordinieren. Eine andere interessante Studie im Zusammenhang mit der Isolierung heterobimetallischer Komplexe wäre das Koordinationsverhalten des Dianions von $Ph_2P(CH_2Py)(NSiMe_3)$, (**9**) (Schema 5.8)

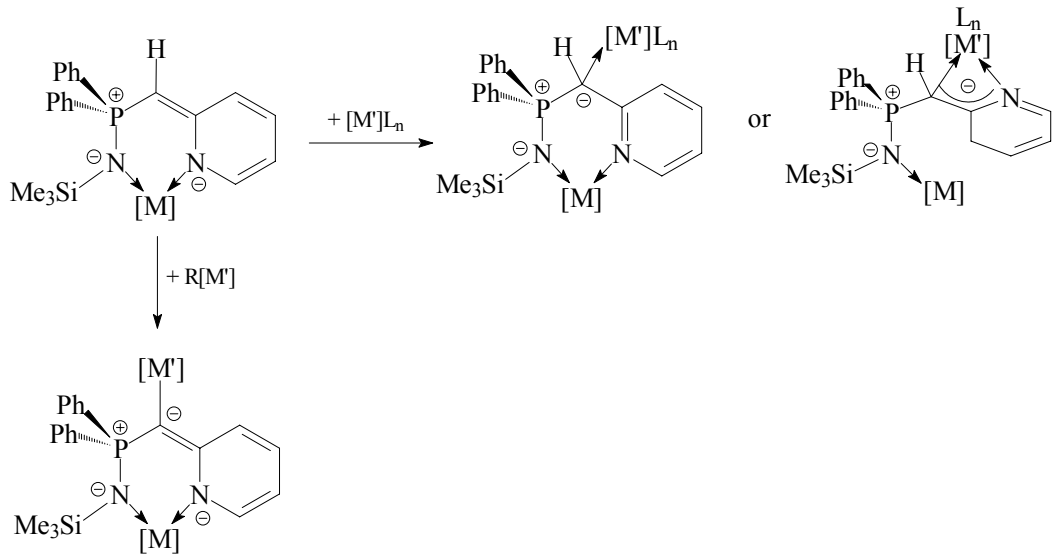

Schema 5.8: *Synthese von heterobimetallischen Komplexen.*

Der Einbau zusätzlicher $[H_2CPy]$-Substituenten am Phosphoratom in Iminophosphoranen führt zu viel flexibleren Liganden, die multiple Reaktionszentren und Donoratome zur Seitenarmkoordination bereitstellen. Als Monoanionen oder mehrfach negativ geladen, sollten diese Systeme in der Lage sein, Metallfragmente in unüblichen Koordinationsmodi zu stabilisieren und durch Dissoziation, beispielsweise eines Pyridyl-Seitenarms, hemilabiles Verhalten zeigen, was zu einer freien Koordinationsstelle zur Substratbindung in katalytischen Zyklen führen würde. Desweiteren scheint eine Reduktion dieser Iminophosphorane zu Phosphan(III)aminen praktikabel (Schema 5.9).

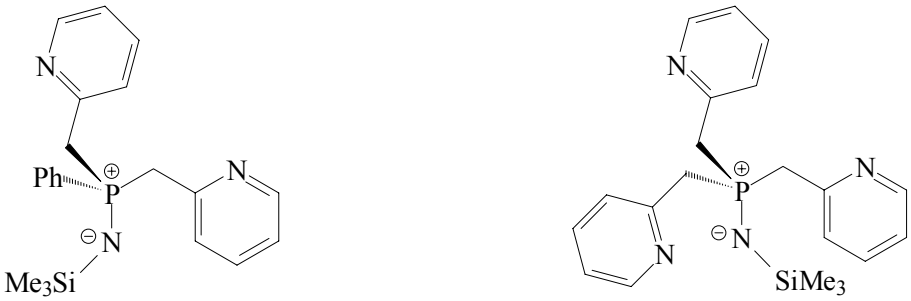

Schema 5.9: *Methylen-verbrückte Pyridyliminophosphorane.*

6 Experimental Section

6.1 General Techniques

All experiments were performed in an atmosphere of dry nitrogen either by using modified Schlenk techniques or in an argon drybox. Solvents were freshly distilled from sodium-potassium alloy prior to use. The reactants used were commercially available or synthesized according to published procedures.

$Ph_2P(CH_2Py)$[28]
$[(Et_2O)Li\{N(SiMe_3)_2\}]$[148]
$[(thf)_2Sr\{N(SiMe_3)_2\}_2]$[48]
$[(Et_2O)Li(H_2CPy)]_2$[29]
$[Pb\{N(SiMe_3)_2\}_2]$[58]
$[Fe\{N(SiMe_3)_2\}_2]_2$[79]
$[Zn\{N(SiMe_3)_2\}_2]$[174]

NMR spectra were recorded at r.t. on a Bruker DRX 300 spectrometer at 300.1 (^{1}H), 75.5 (^{13}C), 121.5 (^{31}P), 59.6 (^{29}Si), 155.5 (^{7}Li), 79.4 (^{23}Na) and 30.4 MHz (^{1}H, ^{15}N-HMBC). Chemical shifts are δ values relative to the solvent used for ^{1}H, ^{13}C and ^{1}H-^{15}N-HMBC-NMR, to H_3PO_4 (85%) for ^{31}P, to ext. sat. LiCl solution for ^{7}Li, to 0.1 M NaCl in D_2O for ^{23}Na, and to $SiMe_4$ for ^{29}Si-NMR, respectively.

The obtained NMR shifts were assigned according to the following schemes:

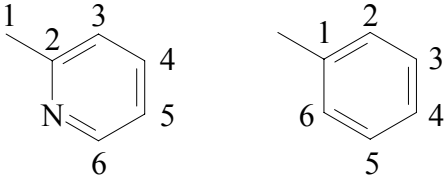

Multiplicities are abbreviated as follows:
s = singulet, d = doublet, t = triplet, q = quartet, m = multiplet, b = broad

Elemental analyses were performed by the micro-analytical laboratory of the Institut für Anorganische Chemie, Würzburg.

The melting and decomposition points were determined *via* differential thermo analysis (DTA) with a Du Pont, Thermal Analyzer 9000 and a DCS cell at the Institut für Anorganische Chemie, Würzburg.

6.2 Preparation of the compounds 1–15

6.2.1 Ph_2PCH_2Py, (1)

The procedure described in literature for the preparation of Ph_2PCH_2Py, (**1**), was modified: $[(Et_2O)Li(H_2CPy)]_2$ was freshly prepared by addition of 4.66 g (50.0 mmol) 2-methylpyridine to a solution of 34.4 ml (55.0 mmol) *n*-BuLi (1.6 M in hexane) in 100 ml Et_2O at 0°C and used *in situ*. This orange solution was added to a solution of 11.47 g (52.0 mmol) Ph_2PCl in 500 ml Et_2O over a period of 5 h at -78°C. The yellow reaction suspension was stirred for 30 min at -78°C, then the solvent was evaporated without allowing the reaction mixture to warm up. The resulting yellow solid was dried in vacuum and then distilled in vacuum. The obtained yellow viscous oil was cooled to -10°C. After the addition of 40 ml hexane and stirring for 15 min at -10°C a white precipitate is formed, which can be isolated by filtration. Drying in vacuum yields 11.79 g (42.5 mmol, 85%) of white, pure Ph_2PCH_2Py, (**1**). The reverse order, addition of Ph_2PCl to a solution of $[(Et_2O)Li(H_2CPy)]_2$ and not as described above, results in the formation of $(Ph_2P)_2CHPy$ as major product and not of **1**. It is important to mention that the use of thf as solvent, short reaction time and warming the reaction mixture to higher temperatures than -20°C leads to high amounts of $(Ph_2P)_2CHPy$. Dissolving the phosphane **1** in Et_2O, and storage of the clear solution at -24°C affords colourless needles.

Yield: 11.79 g (42.5 mmol, 85%)
Melting point: 54°C
^{31}P-NMR (benzene-d_6): δ = -11.4 (s)
^{1}H-NMR (benzene-d_6): δ =3.49 (s, 2H, H-1), 6.45 (dd, 1H, H-5), 6.71 (d, 1H, H-3), 6.87 (dddd, 1H, H-4), 8.29 (d, 1H, H-6), 6.79–7.02 (m, 6H, *m*-, *p*- PhH), 7.32-7.45 (m, 4H, *o*-PhH)
^{1}H, ^{15}N-HMBC-NMR (benzene-d_6): δ = -62

6.2.2 [(thf)$_2$Li{Ph$_2$PC(H)Py}], (2)

To 2.00 g (7.21 mmol) of Ph_2PCH_2Py, (**1**), in 30 ml Et_2O, 4.96 ml (7.93 mmol) of *n*-BuLi (1.6 M in hexane) were added dropwise at -78°C. After warming to r.t., and stirring for an additional hour, the solvent was evaporated. Recrystallization of the crude orange solid from hexane / thf and storage of the solution at 4°C for 48h gives 2.69 g (6.63 mmol, 92%) of [(thf)$_2$Li{Ph$_2$PC(H)Py}], (**2**), as orange needles, isolated by filtration and drying in vacuum.

Yield: 2.69 g (6.63 mmol, 92%)
Decomposition point: 82°C
^{31}P-NMR (toluene-d$_8$): δ = -23.5 (s)
^{7}Li-NMR (toluene-d$_8$): δ = 1.65 (s)
^{1}H, ^{15}N-HMBC-NMR (toluene-d$_8$): δ = -160 (PyN)
^{1}H-NMR (toluene-d$_8$): δ = 3.83 (d, $^{2}J_{P–H}$ = 7.1 Hz, 1H, H-1), 5.68 (dd, 1H, H-5), 6.43 (d, 1H, H-3), 6.70 (dd, 1H, H-4), 7.24 (d, 1H, H-6), 6.92–7.11 (m, 6H, *m*-, *p*- PhH), 7.62–7.67 (m, 4H, *o*-PhH), 1.16 (t, 4H, $OCH_2C\underline{H_2}$), 3.37 (t, 4H, OCH_2),
^{13}C-NMR (toluene-d$_8$): δ = 60.1 (d, C-1), 101.7 (s, C-5), 118.3 (d, C-3), 137.4 (d, C-4), 146.9 (s, C-6), 170.2 (d, C-2), 126.9 (*p*-PhC), 127.9 (*m*-PhC), 128.6 (*ipso*-PhC), 132.3 (*o*-PhC)
Elemental analysis:
CHN, found, (calcd.) [%]: C 72.86 (73.06), H 7.42 (7.31), N 3.15 (3.28)

6.2.3 [(thf)$_2$Li$_4$(PPh$_2$)$_2${Ph$_2$PC(H)Py}$_2$], (3)

To 1.00 g (3.61 mmol) of Ph_2PCH_2Py, (**1**), in 40 ml toluene 2.48 ml (3.97 mmol) of MeLi (1.6 M in Et_2O) were added at -78°C. After warming to r.t., and stirring for 7 d, thf was added dropwise to the orange suspension until a clear solution was obtained. Storage of this solution for four days at -16°C yields 2.29 g (2.09 mmol, 58%) of crystalline **3**. Compound **3** was isolated by filtration, washed several times with pentane and dried in vacuum.

Yield: 2.29 g (2.09 mmol, 58%)

Decomposition point: 60°C

^{31}P-NMR (benzene-d$_6$): δ = -24.5 (s, Ph_2P), -18.3 (s, Ph_2PCHPy)

^{7}Li-NMR (benzene-d$_6$): δ = 1.37 (s, $LiPPh_2$), 2.52 (sb, $Li(PPh_2)_2(Ph_2PCHPy)$).

^{1}H-NMR (benzene-d$_6$): δ = 3.60 (d, $^{2}J_{P-H}$ = 8.4 Hz, 2H, H-1), 5.88 (dd, 2H, H-5), 6.48(d, 2H, H-3), 6.74 (dd, 2H, H-4), 7.35 (sb, 2H, H-6), 7.01–7.04 (mb, 24H, *m*-, *p*- PhH), 7.57–7.62 (mb, 16H, *o*- PhH), 3.28 (t, 4H, OCH_2), 1.19 (t, 4H, $OCH_2C\underline{H_2}$).

^{13}C-NMR (benzene-d$_6$): δ = 51.5 (C-1), 105.9 (s, C-5), 116.8 (d, C-3), 135.5 (s, C-4), 148.1 (d, C-6), 169.7 (d, C-2), 122.5–122.7 (*p*-PhC), 127.2-127.4 (*ipso*-PhC), 127.6–127.8 (*m*-PhC), 132.0–132.8 (*o*-PhC), 23.7 ($OCH_2\underline{C}H_2$), 65.7 ($O\underline{C}H_2$).

Elemental analysis:

CHN, found, (calcd.) [%]: C 73.10 (74.59), H 6.21 (6.08), N 2.29 (2.56)

6.2.4 [(thf)$_3$Sr{Ph$_2$PC(H)Py}$_2$], (4)

To a solution of 1.00 g (3.61 mmol) of Ph_2PCH_2Py, (**1**), in 30 ml thf, a solution of 1.10 g (1.99 mmol) $[(thf)_2Sr\{N(SiMe_3)_2\}_2]$ in 10 ml thf was added dropwise at 0°C. After warming to r.t. the orange solution was stirred for 3 h. The volume of the solution was reduced to half and the clear orange solution stored at 4°C for several days, yielding 2.60 g (3.04 mmol, 72%) of $[(thf)_3Sr\{Ph_2PC(H)Py\}_2]$, (**4**) as orange blocks.

Yield: 2.60 g (3.04 mmol, 72%)

Melting point: 108°C

^{31}P-NMR (thf-d$_8$): δ = -21.1 (sb)

^{1}H-NMR (thf-d$_8$): δ = 3.41 (d, $^{2}J_{P-H}$ = 9.0 Hz, 2H, H-1), 5.32 (dd, 2H, H-5), 6.05 (d, 2H, H-3), 6.35 (dd, 2H, H-4), 7.21 (d, 2H, H-6),), 7.07–7.19 (m, 12H, *m*-, *p*- PhH), 7.42–7.53 (m, 8H, *o*- PhH), 3.55 (t, 6H, OCH_2), 1.72 (t, 6H, $OCH_2C\underline{H_2}$)

^{13}C-NMR (thf-d$_8$): δ = 60.5 (d, C-1), 101.5 (s, C-5), 120.9 (d, C-3), 132.9 (s, C-4), 149.4 (s, C-6), 158.9 (d, C-2), 127.7–127.9 (*ipso*-PhC),128.1–128.3 (*p*-PhC),128.4–128.6 (*m*-PhC), 131.9–132.2 (*o*-PhC), 25.8 ($O\underline{C}H_2$), 67.6 ($OCH_2\underline{C}H_2$)

Elemental analysis:

CHN, found, (calcd.) [%]: C 66.10 (67.31), H 6.28 (6.35), N 3.55 (3.27)

6.2.5 [Pb{$Ph_2PC(H)Py$}{$N(SiMe_3)$}$_2$], (5)

To 0.50 g (1.80 mmol) Ph_2PCH_2Py, (**1**), 0.95 g (1.80 mmol) [Pb{$N(SiMe_3)_2$}$_2$] were mixed in a drybox. To the resulting dark red suspension ca. 15 ml of hexane were added at -24°C. Storing of the clear solution at this temperature yields 1.10 g (1.71 mmol, 95%) [Pb{$Ph_2PC(H)Py$}{$N(SiMe_3)$}$_2$], (**5**) as red blocks. **5** is only stable in the solid state. In solution, slow decomposition is observed.

Yield: 1.10 g (1.71 mmol, 95%)
Melting point: 43°C
^{31}P-NMR (toluene-d$_8$): δ = 61.17 (t, $^1J_{P\text{-}Pb}$ = 2679.5 Hz)
^{1}H-NMR (toluene-d$_8$): δ = 0.22 (s, 18H, $SiMe_3$), 4.58 (d, $^2J_{P–H}$ = 6.4 Hz, 1H, H-1), 5.62 (dd, 1H, H-5), 6.53 (dd, 1H, H-4), 6.79 (d, 1H, H-3), 7.15 (d, 1H, H-6), 6.99–6.11 (*m*-, *p*-PhH), 7.33–7.47 (*o*-PhH)
^{13}C-NMR (toluene-d$_8$): δ = 6.2 (s, $SiMe_3$) 61.8 (d, C-1), 105.3 (s, C-5), 121.0 (d, C-3), 134.5 (s, C-4), 144.8 (d, C-6),172.9 (d, C-2), 128.1–130.0 (d, *m*-,*p*- PhH), 132.4 (d, *o*-PhH).
^{29}Si-NMR (toluene-d$_8$): δ = -1.72 (s)
^{1}H, ^{15}N-HMBC-NMR (toluene-d$_8$): δ = -268.0 ($N(SiMe_3)_2$), -71.5 (N_{Py})
Elemental analysis:
CHN, found, (calcd.) [%]: C 44.98 (44.77), H 5.13 (5.17), N 4.45 (4.35)

6.2.6 [Zn_3{$Ph_2PC(H)Py$}$_4$O], (6)

A solution of 1.00 g (2.34 mmol) [$(thf)_2$Li{$Ph_2PC(H)Py$}], (**2**), in 30 ml Et_2O was added to a suspension of 0.18 g (1.30 mmol) $ZnCl_2$, containing ZnO impurities, in 20 ml Et_2O at r.t. The suspension was stirred for 48h, then it was filtered to remove the white precipitate (LiCl). The volume of the orange solution was reduced by evaporation. Storage of the solution at r.t. affords [Zn_3{$Ph_2PC(H)Py$}$_4$O], (**6**) as yellow blocks. The elemental analysis showed, that the non coordinating ether molecule found in the solid state structure is removed during drying the complex in vacuum.

Yield: 1.03 g (0.80 mmol, 34%)

Decomposition point: 189°C

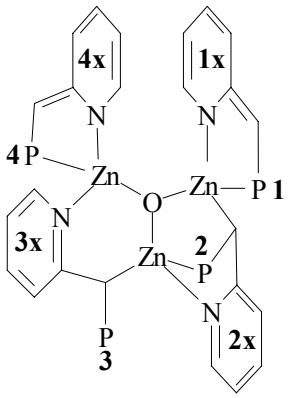

^{31}P-NMR (benzene-d$_6$): δ = -35.6 and -32.4 (s, P1,4), -29.8 (s, P-2), -27.5 (s, P-3)

In the ^{1}H-NMR only the pyridyl-H could be assigned *via* H-H-COSY-NMR.

^{1}H-^{1}H–COSY–NMR (benzene-d$_6$): δ = 3.12 (d, 1H, H-31), 3.70 and 3.90 (d, 2H, H-11,H-41), 3.98 (d, 1H, H-21), 5.15 (dd, 1H, H-35), 5.41 (dd, 1H, H-25), 5.80 and 5.90 (m, 2H, H-15, H-45), 6.10 and 6.14 (m, 2H, H-13, H-43), 6.35 (m, 1H, H-33), 6.45 (m, 1H, H-23), 6.51 (m, 1H, H-34), 6.55 (m, 1H, H-24), 6.60 and 6.62 (m, 2H, H-14, H-44), 6.60 (m, 1H, H-36) 6.83 (m, 1H, H-26), 7.15 and 7.4 (m, 2H, H-16, H-46)

Elemental analysis:

CHN, found, (calcd.) [%]: C 66.01 (65.26), H 4.42 (4.30), N 4. 19 (4.35)

6.2.7 *rac*-[*OC*-6-43]-[(Ph$_2$PCH$_2$Py)Fe{Ph$_2$PC(H)Py}$_2$], (7)

To 1.00 g (3.61 mmol) of solid Ph$_2$PCH$_2$Py, (**1**), 0.45 g (1.20 mmol) pure, liquid [Fe{N(SiMe$_3$)$_2$}$_2$] were added *via* a syringe in a drybox. The suspension turned immediately dark red. It was stirred for 3 hours at r.t., then Et$_2$O was added until a clear solution was obtained. After five days, dark red crystals of [(Ph$_2$PCH$_2$Py)Fe{Ph$_2$PC(H)Py}$_2$], (**7**), were obtained. The iron complex was isolated by filtration and dried in vacuum. The elemental analysis showed, that the non coordinating ether molecule found in the crystal structure was removed during drying in vacuum.

Yield: 2.62 g (2.96mmol, 82%)

Melting point: 212°C

The NMR-shifts were assigned according to the following scheme:

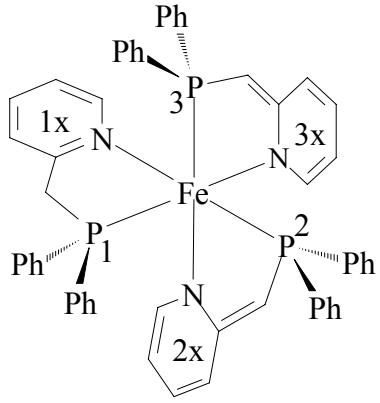

^{31}P-NMR (thf-d$_8$): δ = 36.01 (dd, $^2J_{P2\text{-}P3}$ = 44.2 Hz, $^2J_{P2\text{-}P1}$ = 41.7 Hz P-2), 39.77 (dd, $^2J_{P2\text{-}P3}$ = 44.2 Hz, $^2J_{P1\text{-}P3}$ = 32.2 Hz, P-3), 54.03 (dd, $^2J_{P1\text{-}P2}$ = 41.7 Hz, $^2J_{P1\text{-}P3}$ = 32.2 Hz, P-1)

^{1}H-NMR (thf-d$_8$): δ = 3.56 (d, 2H, H-11), 3.62 (d, 1H, H-21), 3.70 (d, 1H, H-31), 4.84 (dd, 1H, H-25), 5.05 (dd, 1H, H-35), 5.96 (d, 1H, H-24), 6.05 (d, 1H, H-34), 6.25 (dd, 1H, H-15), 6.62 (dd, 2H, H-23, H-33), 6.83 (dd, 1H, H-14), 6.99 (1H, H-13), 7.43 (d, 2H, H-26, H-36), 7.98 (d, 1H, H-16), 7.04–7.39 (m, 30H, hH).

Elemental analysis:

CHN, found, (calcd.) [%]: C 73.25 (73.23), H 5.37 (5.23), N 4.73 (4.74)

6.2.8 [Fe{Ph$_2$PC(H)Py}{N(SiMe$_3$)}$_2$]$_2$, (8)

To 0.5 g (1.80 mmol) of solid Ph_2PCH_2Py, (**1**), 0.68 g (1.80 mmol) pure, liquid [Fe{N(SiMe$_3$)$_2$}$_2$] were added *via* a syringe in a drybox. The suspension turned immediately red. It was stirred for 2 hours at r.t., then 10 ml hexane were added. The red suspension was stirred for an additional hour. The solvent and formed $HN(SiMe_3)_2$ were evaporated in vacuum. The resulting red solid was dissolved in 10 ml hexane and 5 ml Et_2O. Storage of the solution at r.t. for seven days affords red crystals of [Fe{Ph$_2$PC(H)Py}{N(SiMe$_3$)}$_2$]$_2$, (**8**). Filtration and drying the solid in vacuum yields 1.47 g (1.49 mmol, 83%).

Due to paramagnetic parts in the NMR samples no NMR data could be obtained.

Yield: 1.47 g (1.49 mmol, 83%)
Decomposition point: 98°C
Elemental analysis:
CHN, found, (calcd.) [%]: C 59.01 (58.53), H 6.64 (6.75), N 5.57 (5.69)

6.2.9 $Ph_2P(CH_2Py)(NSiMe_3)$, (9)

To 1.00 g (3.61 mmol) Ph_2PCH_2Py, (**1**), 0.46 g (3.97 mmol) N_3SiMe_3 were added. The reaction mixture was refluxed for 3 h. Evaporation of the excess of N_3SiMe_3 and distillation of the crude product under vacuum gives 1.29 g (3.53 mmol, 98%) of pure $Ph_2P(CH_2Py)(NSiMe_3)$ (**9**) as a colourless oil. Storage of the oil at r.t. affords $[Ph_2P(CH_2Py)(NSiMe_3)]_2$, (**9b**), as colourless plates. Addition of hexane to the oil and storage of the solution at -16°C gives the second polymorph $Ph_2P(CH_2Py)(NSiMe_3)$, (**9a**), as colourless plates.

Yield: 1.29g (3.53 mmol, 98%)
Melting point: 44 °C; **decomposition point:** 257°C
^{31}P NMR (toluene-d$_8$): δ =-0.32 (s)
^{29}Si NMR (toluene-d$_8$): δ =-10.61 (s)
^{1}H, ^{15}N HMBC (toluene-d$_8$): δ =-343 (s, $NSiMe_3$), -61 (s, pyN)
^{1}H NMR (toluene-d$_8$): δ = 0.23 (s, 18H, $SiMe_3$), 3.56 (d, $^{2}J_{P\text{-}H}$ = 14.1 Hz, 2H, H-1), 6.55 (dddd, 1H, H-5), 7.07 (m, 1H, H-4), 7.18 (d, 1H, H-3), 8.28 (d, 1H, H-6), 7.00–7.05 (m, 6H, *m-,p*-PhH), 7.65–7.81 (m, 4H, *o*-PhH)
^{13}C NMR (toluene-d$_8$): δ = 4.8 (d, $^{3}J_{Si\text{-}C}$ = 3.0 Hz $SiMe_3$), 43.2 (d, C-1), 121.6 (d, C-5), 125.6 (d, C-3), 129.5 (d, C-4), 149.6 (d, C-6), 152.3 (d, C-2), 129.2 (*m*-PhC), , 131.0 (*p*-PhC), 131.8 (*o*-PhC), 134.9 (*ipso*-PhC)
Elemental analysis:
CHN, found, (calcd.) [%]: C 69.24 (69.44), H 7.72 (7.68), 7.43 (7.36)

6.2.10 $[Ph_2P(CH_2Py)NH_2][N_3]$, (10)

0.41 g (1.48 mmol) $Ph_2P(CH_2Py)$, (**1**), were solved in 30 ml thf. To this solution first 0.5 ml H_2O, then 1.8 ml N_3SiMe_3 were added. After stirring for 1 h at r.t. the solution was refluxed for 2 h. Evaporation of the solvent, and distillation under vacuum resulted in 0.23 g (0.69 mmol, 46%) of pure **10**. Dissolving the white solid in thf / hexane (1:4) and storage of the clear solution at -16°C affords colourless needles of **10**.

Yield: 0.23 g (0.69 mmol, 46%)
Melting ponit: 86°C
^{31}P-NMR (thf-d_8): δ = 22.03
^{1}H, ^{15}N HMBC-NMR (thf-d_8): δ = -335 (s, $NSiMe_3$), -60 (s, pyN)
^{1}H-NMR (thf-d_8): δ = 2.85 (sb, 2H, NH_2), 3.89 (d, 2H., H-1), 7.10 (dd, 1H, H-5), 7.24 (d, 1H, H-3), 7.52 (dd, 1H, H-4), 8.45 (d, 1H, H-6), 7.39–7.42 (m, 6H, *m-,p*-PhH), 7.69–7.73 (m, 4H, *o*-PhH)
Elemental Analysis:
CHN, found, (calcd.) [%]: C 64.79 (64.47), H 5.52 (5.41) 21.04 (20.88)

6.2.11 $[(Et_2O)Li\{Ph_2P(CHPy)(NSiMe_3)\}]$, (11)

a) 0.50 g (1.37 mmol) $Ph_2P(CH_2Py)(NSiMe_3)$, (**9**), were solved in 10 ml Et_2O and cooled to -78°C. To this solution 0.94 ml (1.51 mmol) MeLi (1.6 M in Et_2O) were added dropwise. After warming up to r.t. and stirring the yellow solution for 2h the volume of the solvent was reduced. After 48 h 0.48 g (1.08 mmol, 79%) of crystalline **11** were isolated.
b) 0.50 g (1.37 mmol) $Ph_2P(CH_2Py)(NSiMe_3)$, (**9**), were solved in 10 ml Et_2O and cooled to -78°C. To this solution a solution of 0.94 ml (1.51 mmol) *n*-BuLi (1.6 M in Et_2O) were added dropwise. After warming up to r.t. and stirring the yellow solution for 2h the volume of the solvent was reduced. After 3 days 0.35 g (0.95 mmol, 69%) of crystalline **11** were isolated.
c) 0.50 g (1.37 mmol) $Ph_2P(CH_2Py)(NSiMe_3)$, (**9**), were solved in 10 ml Et_2O and cooled to -78°C. A solution of 0.36 g (1.51 mmol) $[(Et_2O)Li\{N(SiMe_3)_2\}]$ in 10 ml Et_2O was added dropwise. After warming to r.t. and stirring the yellow solution for 2h the

volume of the solvent was reduced. After 5 days 0.83 g (1.14 mmol, 83%) of crystalline **11** were isolated.

Yield: a) 0.48 g (1.08 mmol, 79%), b) 0.35 g (0.95 mmol, 69%), c) 0.83 g (1.14 mmol, 83%)
Melting point: 104 °C
^{31}P NMR (toluene-d$_8$): δ = 18.03 (s)
^{7}Li NMR (toluene-d$_8$): δ = 1.50 (s)
^{29}Si NMR (toluene-d$_8$): δ = -8.63 (s)
^{1}H, ^{15}N HMBC-NMR (toluene-d$_8$): δ = -331 ($NSiMe_3$), -145 (pyN)
^{1}H NMR (toluene-d$_8$): δ = 0.11 (s, 9H, $SiMe_3$), 3.58 (d, $^{2}J_{P\text{-}H}$ = 18.2 Hz, 1H, H-1), 5.77 (dd, 1H, H-5), 6.42 (d, 1H, H-3), 6.71 (dd, 1H, H-4), 7.12 (d, 1H, H-6), 7.01–7.06 (m, 6H, *m-,p*-PhH), 7.79–7.82 (m, 4H, *o*-PhH), 3.08 (q, 4H, OCH_2CH_3), 0.93 (t, 6H, OCH_2CH_3)
^{13}C NMR (toluene-d$_8$): δ = 4.9 (d, $^{3}J_{Si\text{-}C}$ = 3.8 Hz, $SiMe_3$), 55.8 (d, C-1), 106.9 (s, C-5), 118.9 (d, C-3), 134.8 (d, C-4), 147.5 (s, C-6), 167.8 (d, C-2), 128.8 (*m*-Ph-C), 130.3 (*p*-PhC), 132.5 (*o*-PhC), 137.4 (*ipso*-PhC)
Elemental analysis:
CHN, found, (calcd.) [%]: C 66.63 (67.54), H 7.60 (7.71), 6.50 (6.30)

6.2.12 [{Ph$_2$P(CH$_2$Py)NSiMe$_3$}Li{Ph$_2$P(CHPy)NSiMe$_3$}], (12)

0.50 g (1.37 mmol) $Ph_2P(CH_2Py)(NSiMe_3)$, (**9**), were solved in 30 ml Et_2O and cooled to -78°C. To this solution 0.43 ml (0.69 mmol) MeLi (1.6 M in Et_2O) were added dropwise. After warming to r.t. and stirring for additional 8 h the yellow clear solution was allowed to stand at r.t. for three days, yielding 0.80 g (1.08 mmol, 79%) [{$Ph_2P(CH_2Py)NSiMe_3$}Li{$Ph_2P(CHPy)NSiMe_3$}], (**12**) as yellow blocks.

Yield: 0.80 g (1.08 mmol, 79%)
Decomposition point: 77°C

The NMR shifts were assigned according to the following scheme:

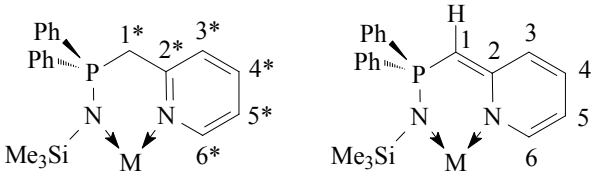

The hetero nuclei are given an asterisk in the neutral ligand.

^{31}P NMR (benzene-d$_6$): δ = 8.46 (sb, P*), 15.36 (s, P)

^{7}Li NMR (benzene-d$_6$): δ = 1.70 (s)

^{1}H, ^{29}Si-HMBC-NMR (benzene-d$_6$): δ = -9.5 (s, Si), -1.82 (s, Si*)

^{1}H, ^{15}N HMBC-NMR (benzene-d$_6$): δ = -339 (Me_3SiN*), -334 (Me_3SiN), -139 (PyN), -68 (PyN*)

^{1}H NMR (benzene-d$_6$): δ = 0.39 (s, 9h, $SiMe_3$*), 0.50 (s, 9H, $SiMe_3$), 3.78 (d, $^{2}J_{P\text{-}H}$ = 13.9 Hz, 2H, H-1*), 4.11 (d, $^{2}J_{P\text{-}H}$ = 23.6 Hz, 1H, H-1), 5.95 (dd, 1H, H-5), 6.42 (dd, 1H, H-5*), 6.60 (d, 1H, H-3), 6.85 (d, 2H, H-3*), 7.00 (m, 2H, H-4, H-4*), 7.33 (d, 1H, H-6), 8.46 (d, 1H, H-6*), 7.25–7.30 (m, 6H, *m*-, *p*-PhH), 7.21–7.24 (m, 6H, *m*-, *p*-PhH*), 7.52–7.70 (m, 4H, *o*-PhH*), 8.08–8.25 (m, 4H, *o*-PhH)

^{13}C NMR (benzene-d$_6$): δ = 2.9 (d, $^{3}J_{Si\text{-}C}$ = 4.5 Hz, $SiMe_3$*), 3.8 (d, $^{3}J_{Si\text{-}C}$ = 4.5 Hz, $SiMe_3$), 39.7 (d, C-1*), 59.0 (d, C-1), 103.6 (s, C-5), 118.4 (d, C-3), 121.5 (d, C-5*), 126.6 (s, C-3*), 128.3 (d, C-4*), 134.2 (d, C-4), 148.0 (s, C-6), 150.7 (s, *ipso*-PyC*), 152.2 (s, C-6*), 166.3 (s, *ipso*-PyC), 128.3 (*m*-PhC), 128.5 (*m*-Ph-C*), 129.8 (*p*-PhC), 130.7 (*p*-PhC*), 131.4 (*o*-PhC*), 132.8 (*o*-PhC), 137.7 (*ipso*-PhC), 138.5 (*ipso*-PhC*)

Elemental analysis:

CHN, found, (calcd.) [%]: C 69.01 (68.64), H 6.52 (6.72) 7.73 (7.62)

6.2.13 [{$Ph_2P(CH_2Py)NSiMe_3$}Na{$Ph_2P(CHPy)NSiMe_3$}], (13)

To a solution of 2.00 g (5.49 mmol) $Ph_2P(CH_2Py)(NSiMe_3)$, (**9**), in 40 ml thf a suspension of 0.11 g (2.75 mmol) $NaNH_2$ in 5 ml thf was added at r.t. After three days, the yellow reaction mixture was filtered and the volume of the sovent was reduced by evaporation. Storage of the clear yellow solution at r.t. for several days, gives 3.05 g (4.06 mmol, 74%) [{$Ph_2P(CH_2Py)NSiMe_3$}Na{$Ph_2P(CHPy)NSiMe_3$}], (**13**), as yellow blocks.

Yield: 3.05 g (4.06 mmol, 74%)

Decomposition point: 33°C

The NMR shifts were assigned according to the following scheme:

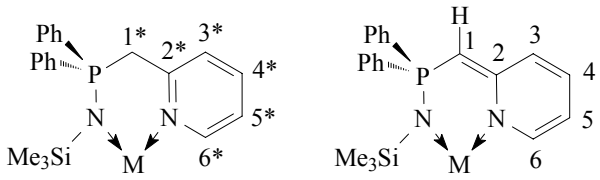

The hetero nuclei are given an asterisk in the neutral ligand.

^{31}P NMR (thf-d$_8$): δ = -0.6 (sb, P*), 11.3 (sb, P)

^{23}Na NMR (thf-d$_8$): δ = 5.02 sb

^{29}Si NMR (thf-d$_8$): δ = -13.9 (d, $^2J_{Si\text{-}P}$ = 8.3 Hz, Si), -12.8 (d, , $^2J_{Si\text{-}P}$ = 23.3 Hz, Si*)

^{1}H, ^{15}N HMBC-NMR (thf-d$_8$): δ = -345 (Me_3SiN*), -332 (Me_3SiN), -137 (PyN), -63 (PyN*)

^{1}H NMR (thf-d$_8$): δ = -0.14 (s, 9H, $SiMe_3$*), -0.20 (s, 9H, $SiMe_3$), 3.39 (d, $^2J_{P\text{-}H}$ = 22.3 Hz, 1H, H-1), 3.85 (d, $^2J_{P\text{-}H}$ = 14.1 Hz, 2H, H-1*), 5.51 (dd, 1H, H-5), 6.18 (d, 1H, H-3), 6.64 (dd, 1H, H-4), 6.98 (dd, 1H, H-5*), 7.14–7.17 (m, 2H, H-6, H-3*), 7.44 (dd, 1H, H-4*), 8.31 (d, 1H, H-6*), 7.18–7.25 (m, 8H, *m*-, *p*-PhH, *p*-PhH*), 7.69–7.77 (m, 8H, *o*-PhH, *o*-PhH*), 7.31–7.38 (m, 4H, *m*-PhH*)

^{13}C NMR (thf-d$_8$): δ = 3.87 (d, $^3J_{Si\text{-}C}$ = 4.5 Hz, $SiMe_3$), 3.69 (d, $^3J_{Si\text{-}C}$ = 3.0 Hz, $SiMe_3$*), 42.5 (d, C-1*), 58.2 (d, C-1), 103.9 (s, C-5), 117.9 (d, C-3), 122.1 (d, C-5*), 125.8 (d, C-3*), 131.1 (d, C-4*), 133.5 (d, C-4), 147.8 (s, C-6), 149.8 (d, C-6*), 155.3 (d, *ipso*-PyC*),168.0 (d, *ipso*-PyC), 128.2 (*m*-, *p*-PhC), 128.8 (*m*-PhC*), 129.5 (*p*-PhC*), 132.0 and 132.8 (*o*-PhC, *o*-PhC*), 137.3 (*ipso*-PhC*), 141.3 (*ipso*-PhC)

Elemental analysis:

CHN, found, (calcd.) [%]: C 66.36 (67.17), H 6.70 (6.58), N 7.21 (7.46)

6.2.14 [Zn{$Ph_2P(CHPy)NSiMe_3$}$_2$], (14)

0.29 g (0.75 mmol) [Zn{$N(SiMe_3)_2$}$_2$] were solved in 10 ml Et_2O and added slowly to a solution of 0.50 g (1.37 mmol) $Ph_2P(CH_2Py)(NSiMe_3)$, (**9**), in 25 ml Et_2O at r.t. After stirring the yellow solution for 2 h, the volume of the solvent was reduced. Storage of the

solution at 4°C over night, yields 0.54 g (0.68 mmol, 91%) of [Zn{$Ph_2P(CHPy)NSiMe_3$}$_2$], (**14**), as yellow plates.

Yield: 0.54 g (0.68 mmol, 91%)

Decomposition point: 176°C

^{31}P-NMR (toluene-d$_8$): δ = 26.4 (s)

^{29}Si-NMR (toluene-d$_8$): δ = 1.32 (d, $^2J_{Si-P}$ = 1.8 Hz)

^{1}H, ^{15}N-HMBC-NMR (toluene-d$_8$): δ = -348 ($NSiMe_3$), -182 (PyN)

^{1}H-NMR (toluene-d$_8$): δ = 0.17 (s, 18H, $SiMe_3$), 3.32 (d, $^2J_{P-H}$ = 20.9 Hz, 2H, H-1), 5.53 (dd, 2H, H-5), 6.28 (d, 2H, H-3), 6.56 (dd, 2H, H-4), 7.12 (d, 2H, H-6), 7.01–7.06 (m, 12H, *m*-,*p*-PhH), 7.73–7.91 (m, 8H, *o*-PhH)

^{13}C-NMR (toluene-d$_8$): δ = 4.7 (d, $^3J_{Si-C}$ = 3.8 Hz, $SiMe_3$), 59.2 (d, C-1), 106.5 (s, C-5), 120.2 (d, C-3), 134.8 (d, C-4), 146.9 (s, C-6), 166.6 (s, C-2), 128.5 (*m*-PhC), 131.0 (*p*-PhC), 133.1 and 133.4 (*o*-PhC), 138.2 (*ipso*-PhC)

Elemental analysis:

CHN, found, (calcd.) [%]: C 63.85 (63.67), H 6.67 (6.11), N 6.71 (7.07)

6.2.15 [Fe{$Ph_2P(CHPy)NSiMe_3$}$_2$], (15)

To 0.50 g (1.37 mmol) of solid $Ph_2P(CH_2Py)(NSiMe_3)$, (**9**), 0.26 g (0.69 mmol) pure, liquid [Fe{$N(SiMe_3)_2$}$_2$] were added *via* a syringe in a drybox. The suspension turned immediately red. It was stirred for 1 h at r.t., then 10 ml hexane and 5 ml Et_2O were added, giving a clear red solution. Storage of the solution for three days affords red crystals of [Fe{$Ph_2P(CHPy)NSiMe_3$}$_2$], (**15**), as red blocks. Filtration and drying in vacuum yields 0.99 g (1.27 mmol, 93%).

Due to paramagnetic parts in the NMR samples no NMR data could be obtained.

Yield: 0.99 g (1.27 mmol, 93%)

Melting point: 258°C

Elemental analysis:

CHN, found, (calcd.) [%]: C 63.78 (64.44) H 6.23 (6.18), N 6.99 (7.16)

7 Crystallographic Section

7.1 Crystal application

A sample of the crystalline material was taken from the mother liquor, using standard Schlenk techniques and covered with an inert oil.[188] The crystals were prepared in the inert oil (separation from satellites or checking for twinning under a microscope fitted with a polarizer). A suitable crystal was mounted on the top of a glass fibre in a drop of inert oil and shock cooled on the diffractometer. Data of compounds **1**–**7** and **9**–**15** were collected at low temperature.[189] The data for compound **8** were collected at room temperature.

7.2 Data collection

All data were measured using graphite monochromated MoK_α radiation (λ = 71.073 pm) on a Bruker D8 goniometer platform, equipped with a Smart Apex CCD camera.

After mounting the crystal and centreing with a camera a rotation frame was taken to aligne the beam centre relative to the CCD camera. A single run (usually 50 frames in the ω-scan mode with steps of 0.3°) was performed to check the crystals quality and the unit cell. Data collection was performed in the ω-scan mode with steps usually between 0.1° - 0.3°. For every single run an exact orientation matrix was determined and refined using the tools of SMART V 5.6.[190] The program SAINT-NT[191] was employed to integrate the frames.

7.3 Absorption correction

The obtained data were absorption corrected applying SADABS2.[192] The program uses an empirical model, in which a model function is refined by fitting reflexes of equal symmetry. With the obtained hkl-file structure solution and refinement was processed.

7.4 Structure solution and refinement

General: All structures were solved by direct methods with SHELXTL-NT V5.1.[193] They were refined by full-matrix least-squares procedures on F^2, using SHELXTL-NT V5.1. The values g_1 and g_2 of the weighting scheme are given in the crystallographic tables. The denoted *R*-values are defined as follows:

$$wR2 = \sqrt{\frac{\sum w(F_0^2 - F_C^2)^2}{\sum wF_0^4}} \qquad w^{-1} = \sigma^2 \cdot F_0^2 + (g1 \cdot P)^2 + g2 \cdot P \qquad P = \frac{(F_0^2 + 2 \cdot F_C^2)}{3} \qquad R1 = \frac{\sum \| F_0 | - | F_C \|}{\sum | F_0 |}$$

If not mentioned otherwise the hydrogen atoms of the molecules were refined using a riding model. The U_{iso} values for the hydrogen atoms of a CH_3 group were set to be 1.5, those of all other hydrogen atoms to be 1.2 of the U_{eq} values of the corresponding C atoms.

The anisotropic replacement parameters (ADP) were drawn at 50% probability level.

Disorder: Structures containing disordered fragments were refined using *constraints* and *restraints*. A *constraint* is a mathematical operation, fixing structural parameters on exact values. *Restraints* contain additional chemical or crystallographical informations and include standard deviations. The *restraints* add to the data of the refinement.
In structures featuring chemically identical, but crystallographic independent fragments, distance *restraints* are useful. The SAME instruction fits 1,2 and 1,3 distances of chemically equal groups with an effective standard deviation. The SADI instruction fits 1,2 distances with an effective standard deviation. The *rigid bond restraint* (DELU) fits components of the anisotropic displacement parameters in the direction of the bond to be equal with an effective standard deviation. *Simularity restraints* (SIMU) are weak *restraints*, which adjust the ADPs of neighbouring atoms in a determined radius. *ISOR restraints* force the ADPs in more spherical, isotrop behaviour, allowing anisotropic refinement of disordered positions with minor occupation factors.

Non coordinating solvent molecules on special positions can be refined using DFIX and DANG *restraints*. With DFIX, 1,2 distances are refined to a given value with an given standard deviation; the DANG instruction is applied in an analogous way on 1,3 distances.

7.5 Structure refinement of compounds 1–15

7.5.1 $Ph_2P(CH_2Py)$, (1)

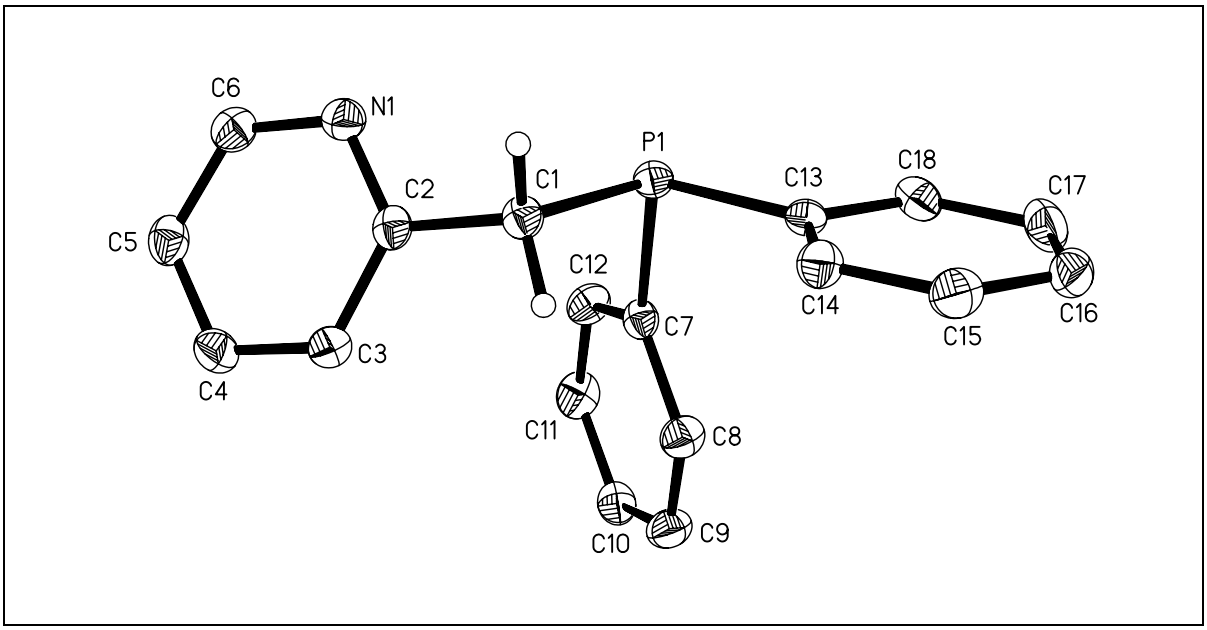

Figure 5.1: *Solid state structure of $Ph_2P(CH_2Py)$, **(1)**.*

Compound **1** crystallizes as colourless plates in the centrosymmetrical monoclinic space group $P2_1/n$. The asymmetric unit contains the complete molecule.

7.5.2 [(thf)$_2$Li{Ph$_2$P(CHPy)}], (2)

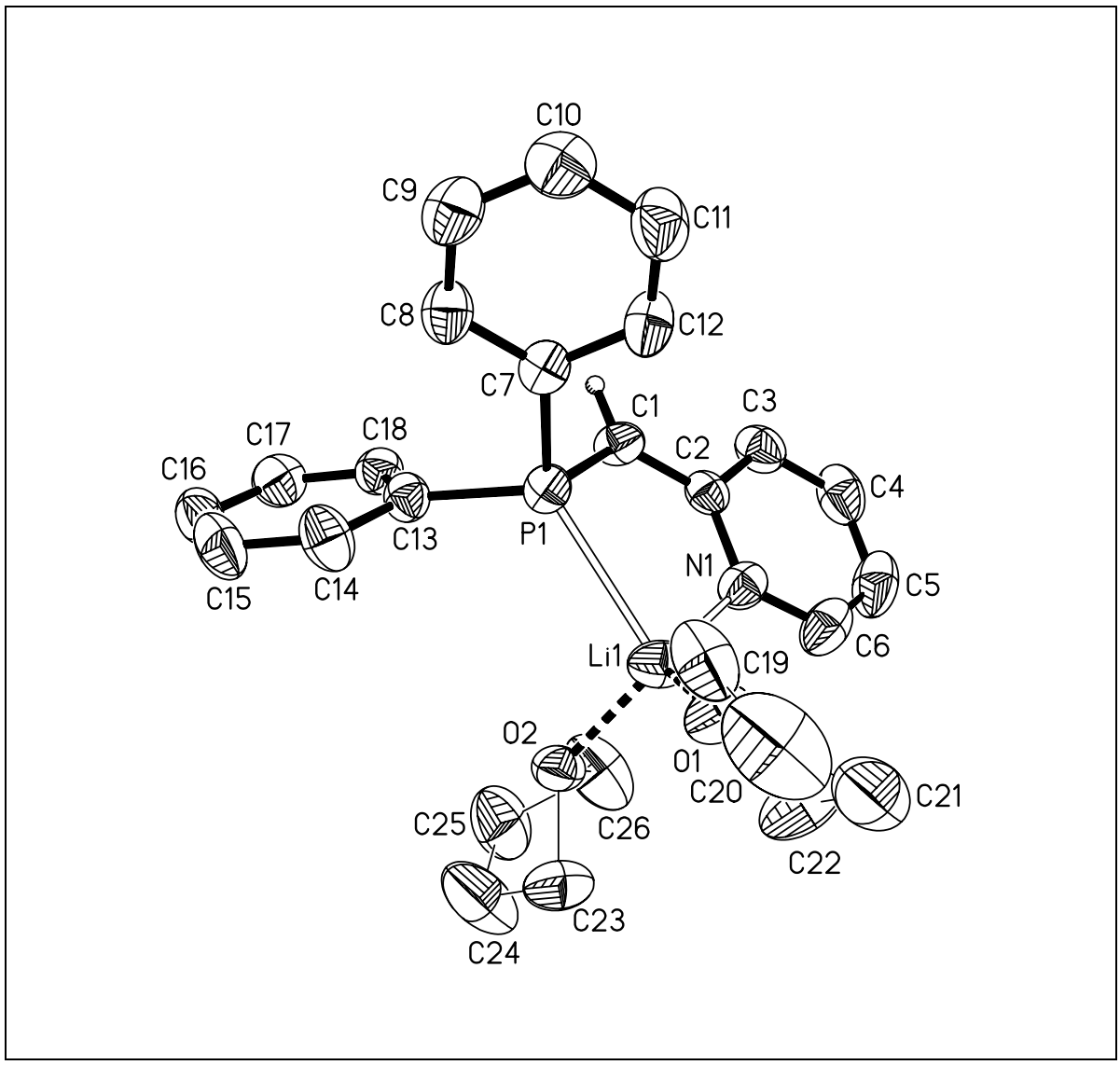

Figure 5.2: *Solid state structure [(thf)$_2$Li{Ph$_2$P(CHPy)}], (**2**).*

Compound **2** crystallizes as orange needles, in the chiral monoclinic space group Cc. The asymmetric unit contains the complete molecule. The flack-x parameter[194] refined to 0.01(10). The coordinated disordered thf molecule O2 to C26 was refined using distance and ADP *restraints* (SAME, SADI, SIMU, DELU). The site occupation factors refined to 0.53 and 0.47, respectively.

7.5.3 [(thf)Li{$Ph_2P(CHPy)$}(Ph_2P)}]$_2$, (3)

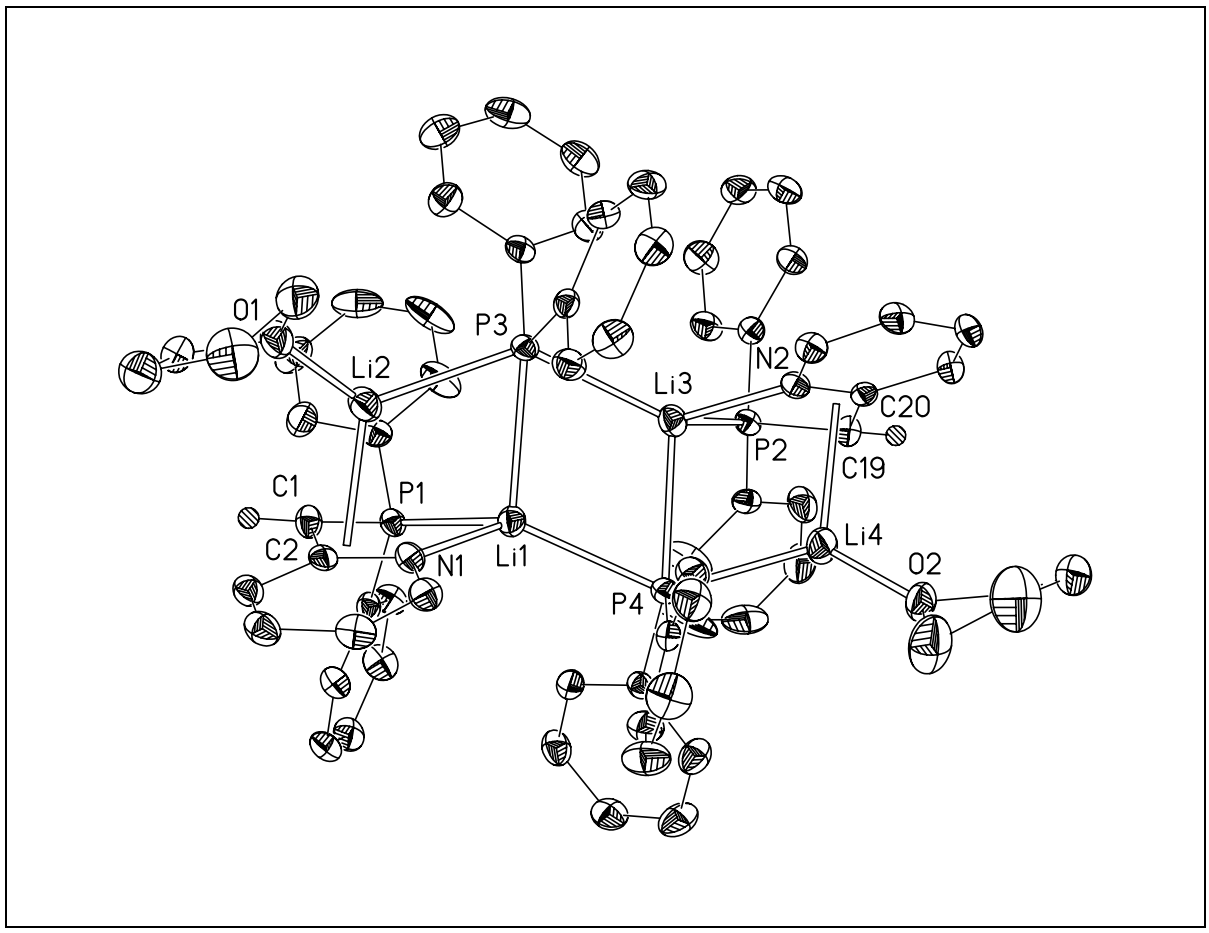

Figure 5.3: *Solid state structure of [(thf)Li{$Ph_2P(CHPy)$}(Ph_2P)}]$_2$, **(3)**.*

Compound **3** crystallizes at -16°C as orange plates, in the centrosymmetrical triclinic space group $P\bar{1}$. The asymmetric unit contains the complete molecule. The two thf molecules (O1, O2) coordinated to Li3 and Li4 respectively, point at the same direction.

7.5.4 $[(thf)_3Sr\{Ph_2P(CHPy)\}_2]$, (4)

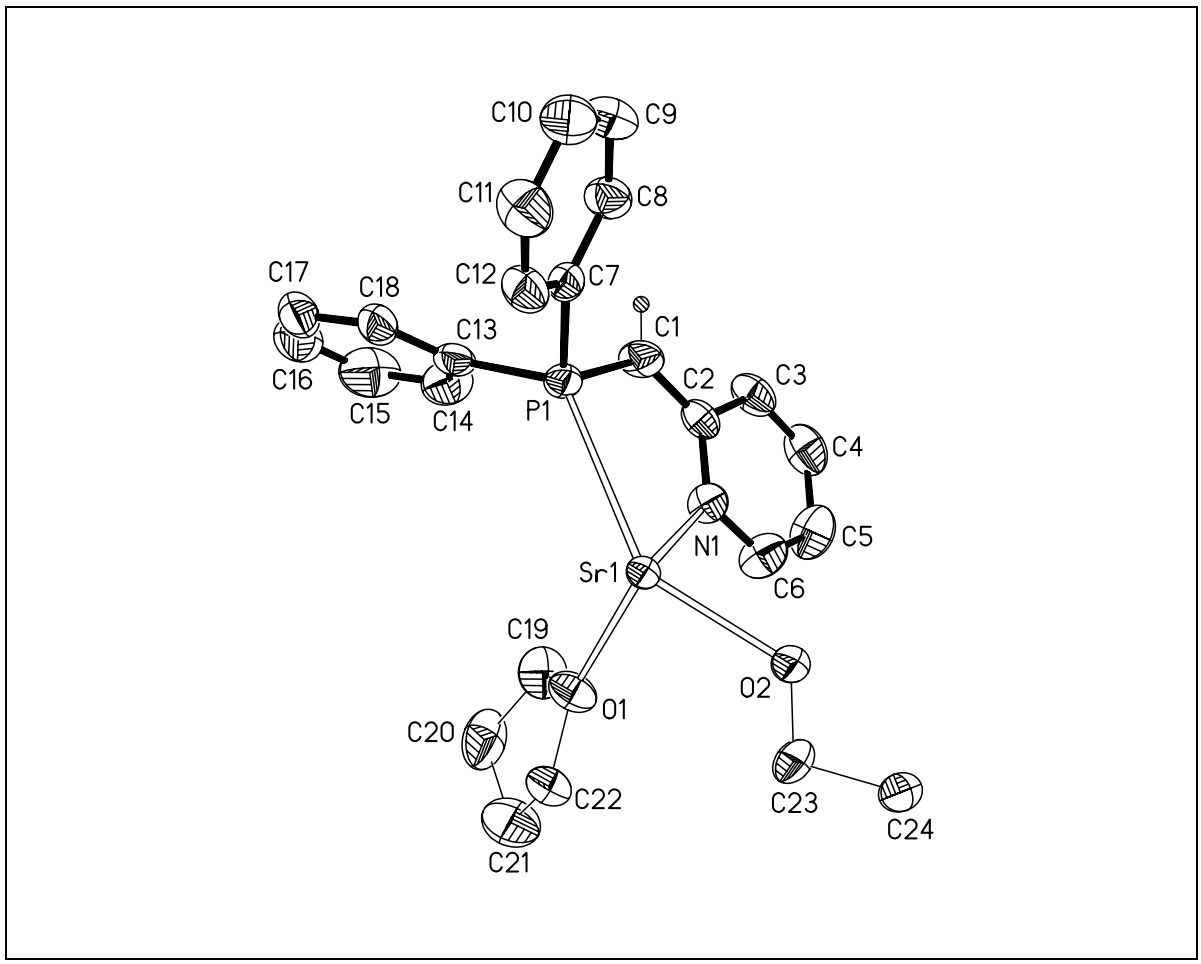

Figure 5.4: *Solid state structure of $[(thf)_3Sr\{Ph_2P(CHPy)\}_2]$, (**4**).*

Compound **4** crystallizes at 4 °C as orange blocks from a thf/hexane solution. Structure solution and refinement was performed in the centrosymmetrical monoclinic space group C2/c. Solution and refinement in the chiral space group Cc was also possible. However, the refinement of the flack-x parameter[194] resulted in 0.5. Thus, the centrosymmetrical space group was chosen. The asymmetric unit contains half of the molecule. The complete molecule is obtained by the 2 fold axis in (½, y, ¾), on which the Sr atom is located and translation by (0, 1, 1). The coordinated thf molecules (O1 to C22 and O2 to C24A) are disordered and were refined using distance and ADP *restraints* (SADI, SAME, SIMU, DELU). The site occupation factors refined to 0.55 / 0.45 and 0.63 / 0.37, respectively. The position of the hydrogen atom H1 at the C1 atom was taken from the difference Fourier map and refined freely.

7.5.5 [Pb{Ph$_2$P(CHPy)}{N(SiMe$_3$)$_2$}]$_2$, (5)

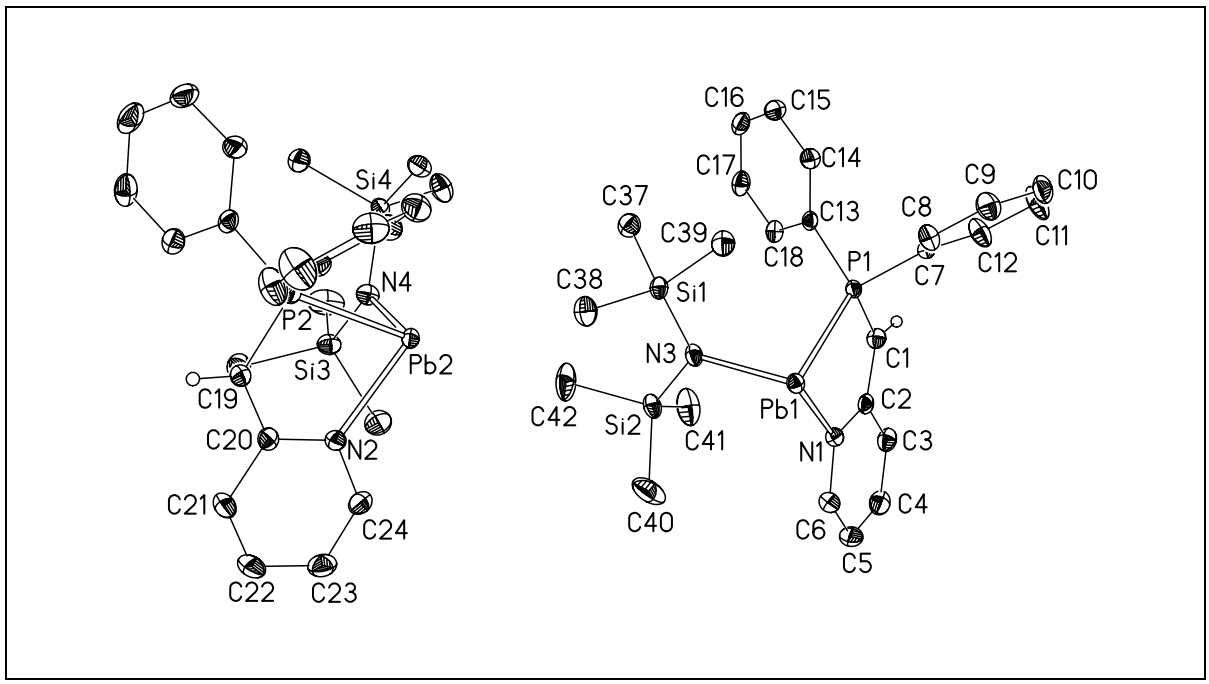

Figure 5.5: *Solid state structure of [Pb{Ph$_2$P(CHPy)}{N(SiMe$_3$)$_2$}]$_2$, **(5)**.*

Compound **5** crystallizes at -24°C as dark red blocks in the centrosymmetrical triclinic space group $P\bar{1}$. The asymmetric unit contains two independent molecules of **5**. The positions of the hydrogen atoms H1 and H19 at C1 and C19, respectively, were taken from the difference Fourier map and refined freely.

7.5.6 $[Zn_3O\{Ph_2P(CHPy)\}_4]+0.5(Et_2O)$, (6)

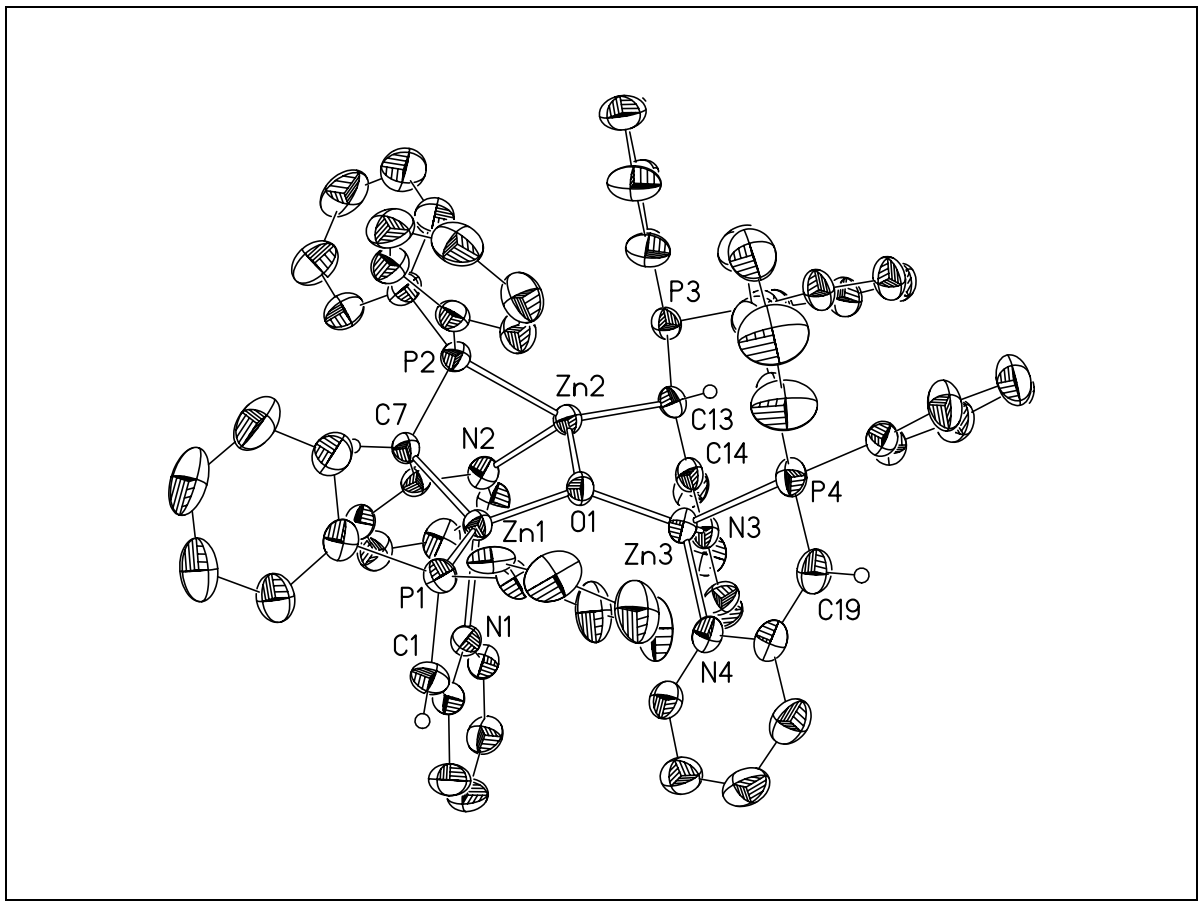

Figure 5.6: *Solid state structure of $[Zn_3O\{Ph_2P(CHPy)\}_4]+0.5(Et_2O)$, (**6**). The non coordinated ether molecule at a special position is omitted for clarity.*

Compound **6** crystallizes at r.t. in the centrosymmetrical triclinic space group $P\bar{1}$, as yellow blocks. The phenyl groups C31–C36 at P1 and C67–C72 at P4 are disorderd, They were refined using the SAME *restraint*. The site occupation factors refined to 0.54 and 0.46 for C31–C36 and 0.58 and 0.42 for C67–C72. The $[Ph_2P]$-residue at C13 and C13 is also disorder. The two positions were refined using the SAME, SADI, SIMU, DELU *restraints*. The phenyl groups were refined as ideal hexagons with the AFIX 66 *constraint*. The site occupation factors for this fragment refined to 0.82 and 0.18, respectively. The non coordination ether molecule was removed from the special position using the PART-1/PART 0 instruction. The site occupation factor was set to 0.50. The 1,2-distances of the solvent molecule were *restraint* (DFIX, DANG). Anisotopic refinement of the solvent molecule was possible with ADP-*restraints* in addition to the ISOR instruction for one carbon atom. The hydrogen atoms H1, H7 and H19 were taken from the Fourier map and refined freely.

7.5.7 [{$Ph_2P(CH_2Py)$}Fe{$Ph_2P(CHPy)$}$_2$]+(Et_2O), (7)

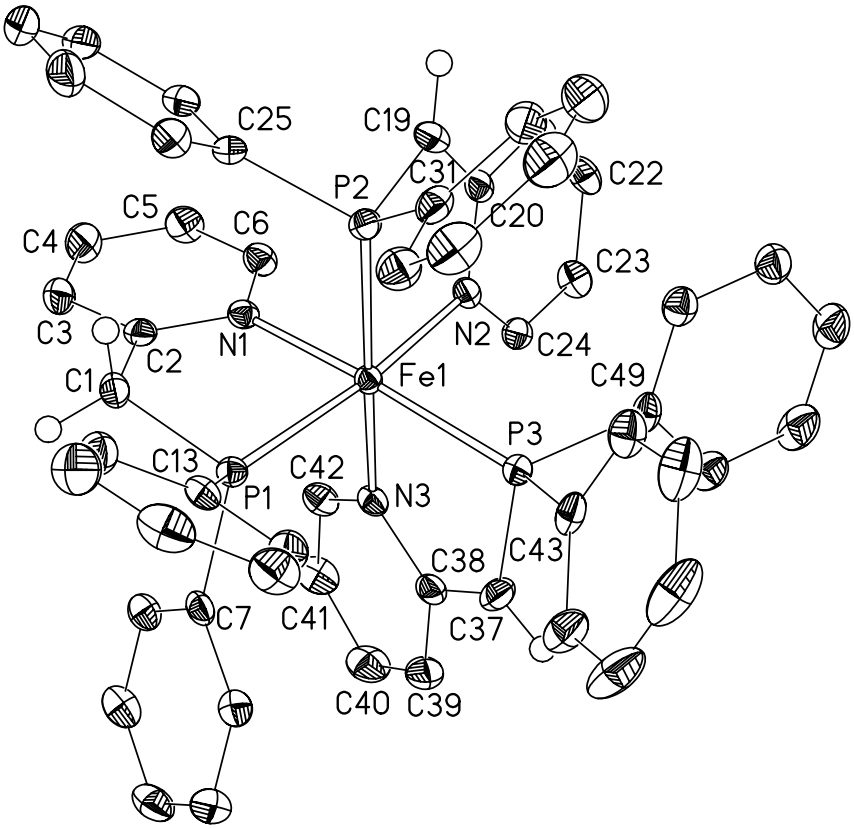

Figure 5.7: *Solid state structure of [{$Ph_2P(CH_2Py)$}Fe{$Ph_2P(CHPy)$}$_2$]+(Et_2O), (7). The non coordinating ether molecule omitted for clarity.*

Compound **7** crystallizes at r.t in the centrosymmetrical monoclinic space group $P2_1/n$ as dark red blocks. The positions of the hydrogen atoms H1A, H1B, H19 and H37 at the methylene bridges C1, C19 and C37, respectively were taken from the difference Fourier map and refined freely. The non coordinating ether molecule is disordered. The two positions were refined using ADP-*restraints* (SIMU, DELU) and DFIX. The site occupation factors refined to 0.57 and 0.43.

7.5.8 $[Fe\{Ph_2P(CHPy)\}\{N(SiMe_3)_2\}]_2$, (8)

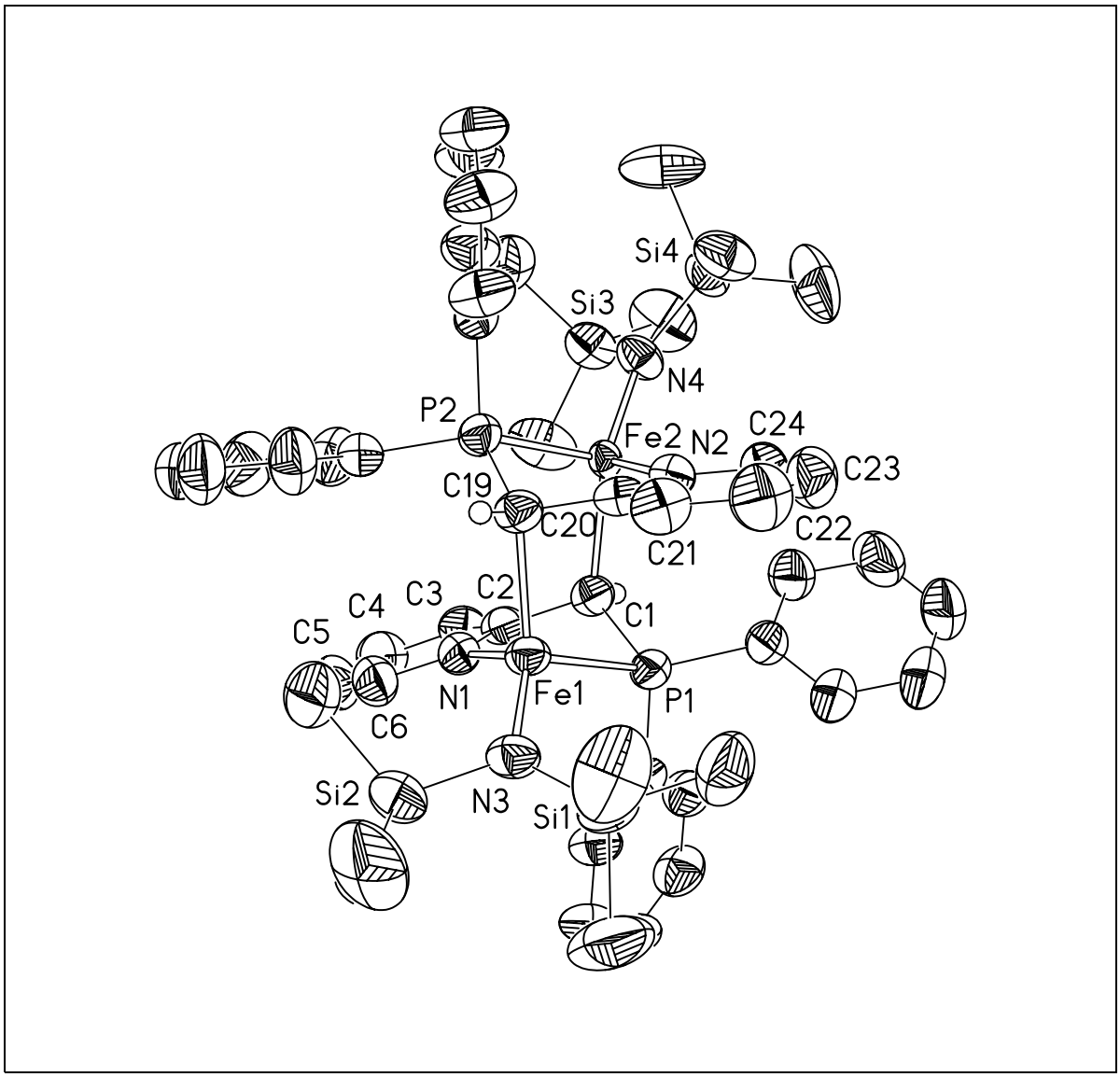

Figure 5.8: *Solid state structure of* $[Fe\{Ph_2P(CHPy)\}\{N(SiMe_3)_2\}]_2$, (***8***).

Compound **8** crystallizes at r.t. in the centrosymmetrical triclinic space group $P\bar{1}$ as red needles. The positions of the hydrogen atoms H1 and H19 at C1 and C19, respectively were taken from the difference Fourier map and refined freely. The fragment containing Fe2, N4 and the $SiMe_3$ groups at Si3 and Si4 is disordered. The three positions were refined using the SADI and ADP-*restraints* (SIMU, DELU). The site occupation factors were refined four cycles freely, then fixed to 0.53, 0.35 and 0.12.

7.5.9 $Ph_2P(CH_2Py)NSiMe_3$, (9a)

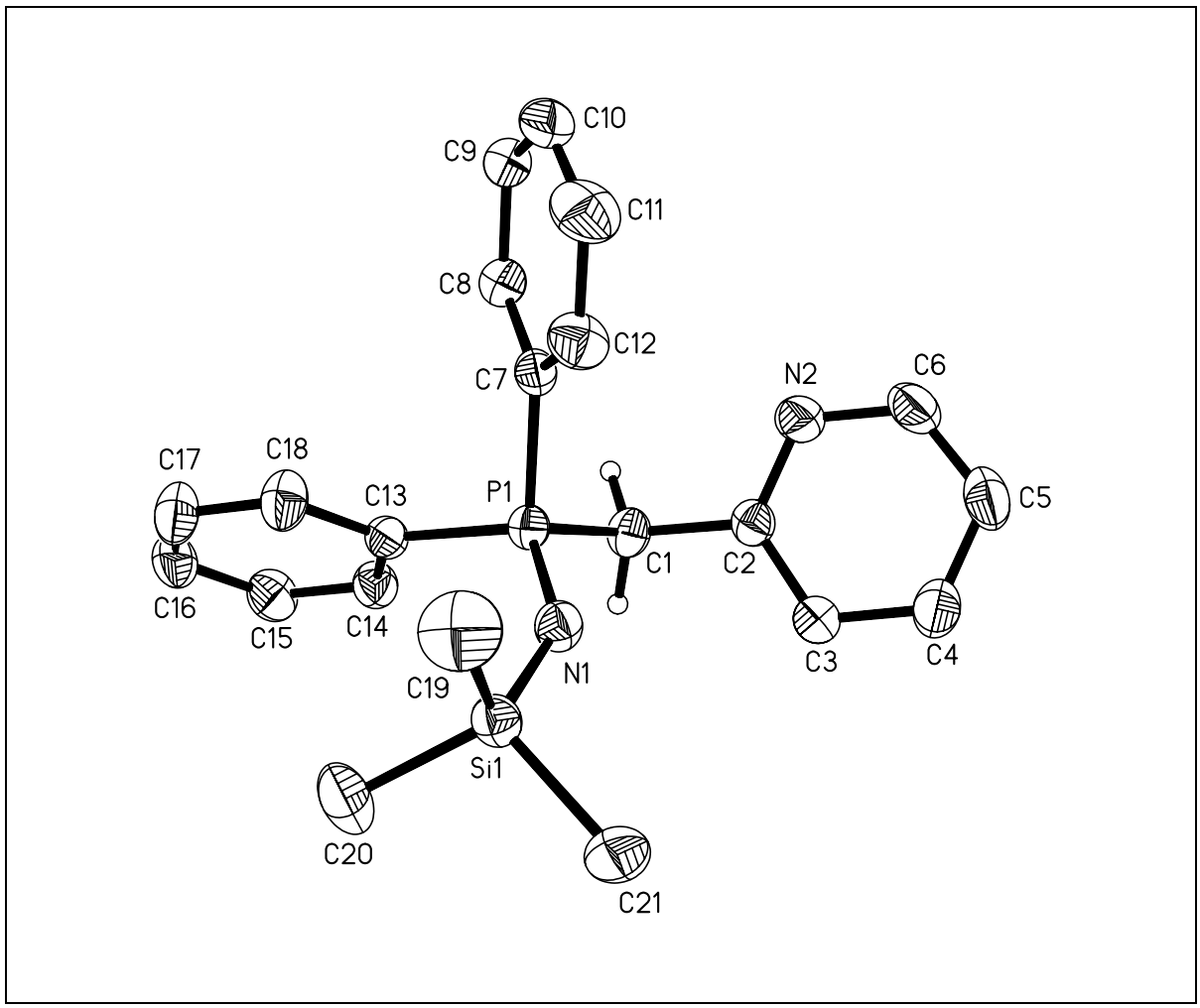

Figure 5.9: *Solid state structure of $Ph_2P(CH_2Py)NSiMe_3$, (**9a**).*

Compound **9a** crystallizes from a hexane solution at -16°C after three days in the centrosymmetrical triclinic space group $P\bar{1}$ as colourless plates.

7.5.10 $[Ph_2P(CH_2Py)NSiMe_3]_2$, (9b)

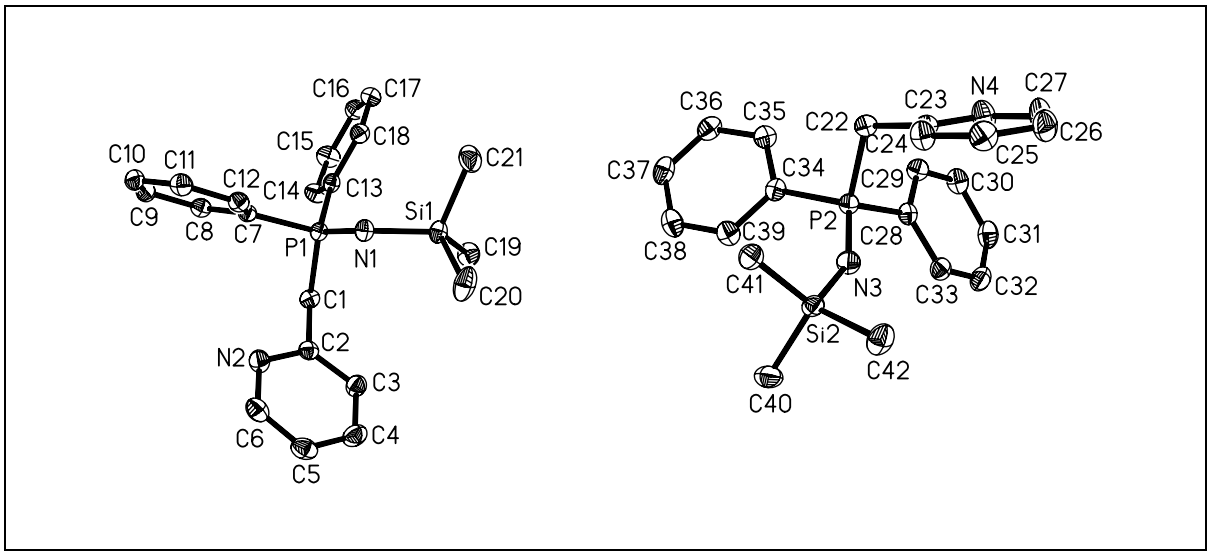

Figure 5.10: *Solid state structure of* $[Ph_2P(CH_2Py)NSiMe_3]_2$, ***(9b)***.

Compound **9b** crystallizes from the oil, obtained after distillation, in the centrosymmetrical triclinic space group $P\bar{1}$ as colourless plates. The positions of the hydrogen atoms H1A, H1B and H22A, H22B were taken from the difference Fourier map and refined freely.

7.5.11 $[Ph_2P(CH_2Py)NH_2][N_3]$, (10)

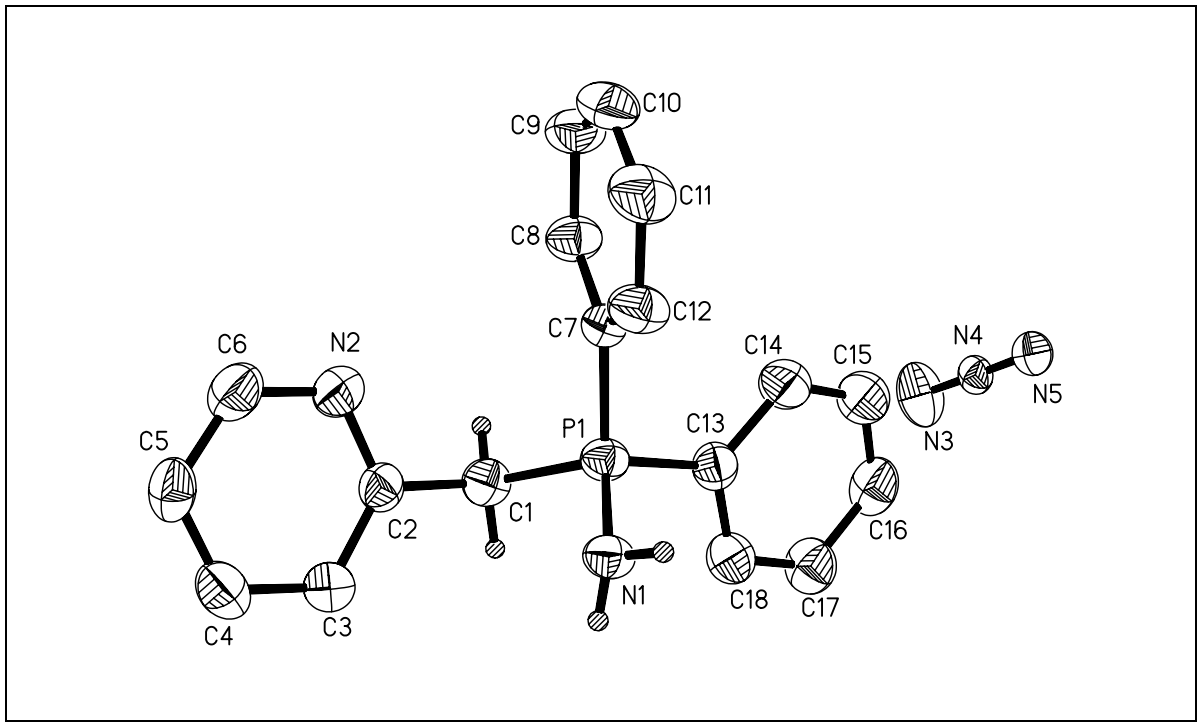

Figure 5.11: *Solid state structure of,* ***(10)****.*

Compound **10** crystallizes from a thf/hexane solution at -16°C after three days in the centrosymmetrical monoclinic space group $P2_1/n$ as colourless needles. The positions of the hydrogen atoms H98 and H99 at N1 were taken from the difference Fourier map and refined freely.

7.5.12 [(Et$_2$O)Li{Ph$_2$P(CHPy)NSiMe$_3$}], (11)

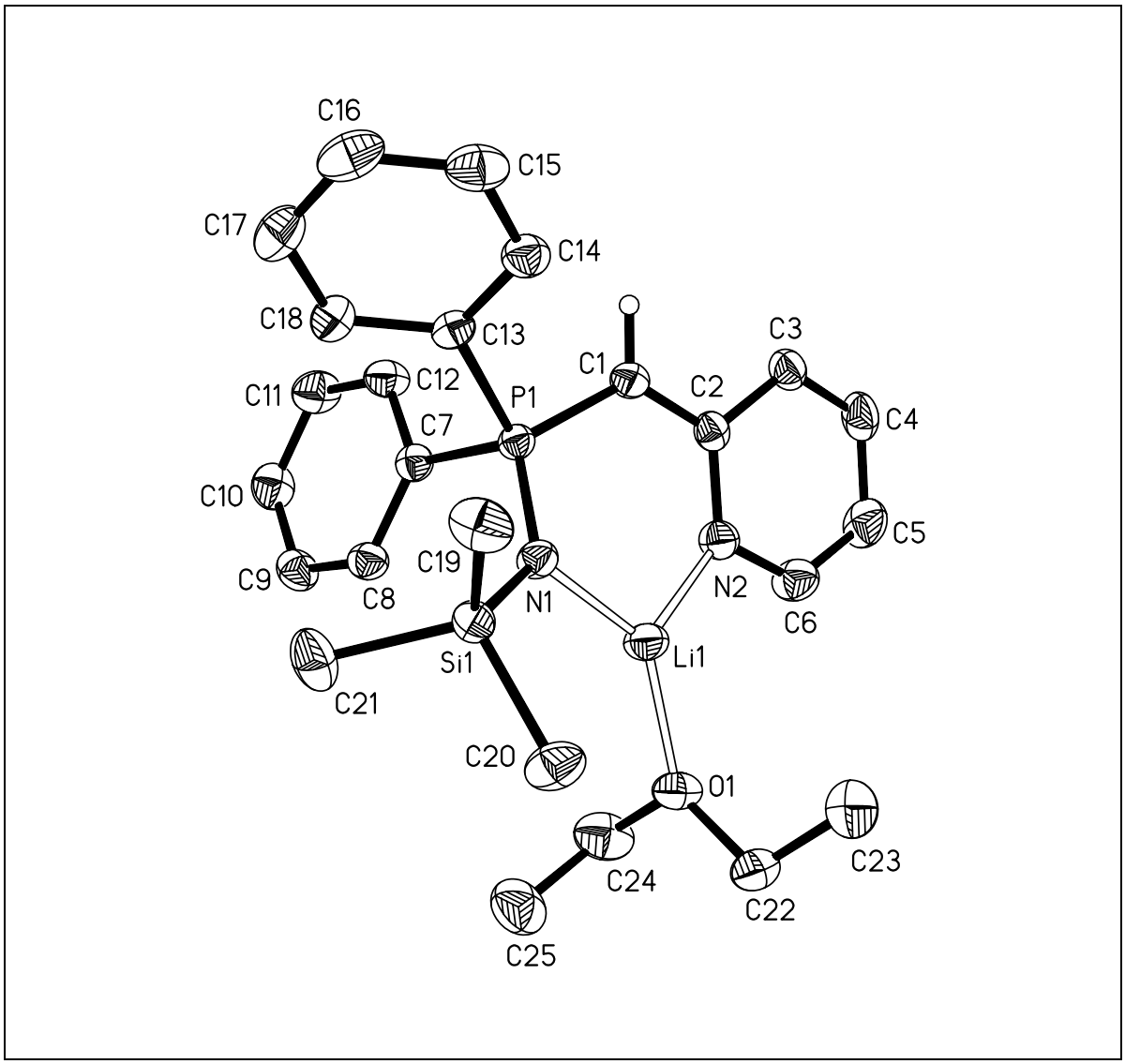

Figure 5.12: *Solid state structure of [(Et$_2$O)Li{Ph$_2$P(CHPy)NSiMe$_3$}], (**11**).*

Compound **11** crystallizes at r.t. in the centrosymmetrical triclinic space group $P\bar{1}$ as yellow blocks. The positions of the hydrogen atom H1 at the C1 atom was taken from the difference Fourier map and refined freely.

7.5.13 [{$Ph_2P(CH_2Py)NSiMe_3$}Li{$Ph_2P(CHPy)NSiMe_3$}], (12)

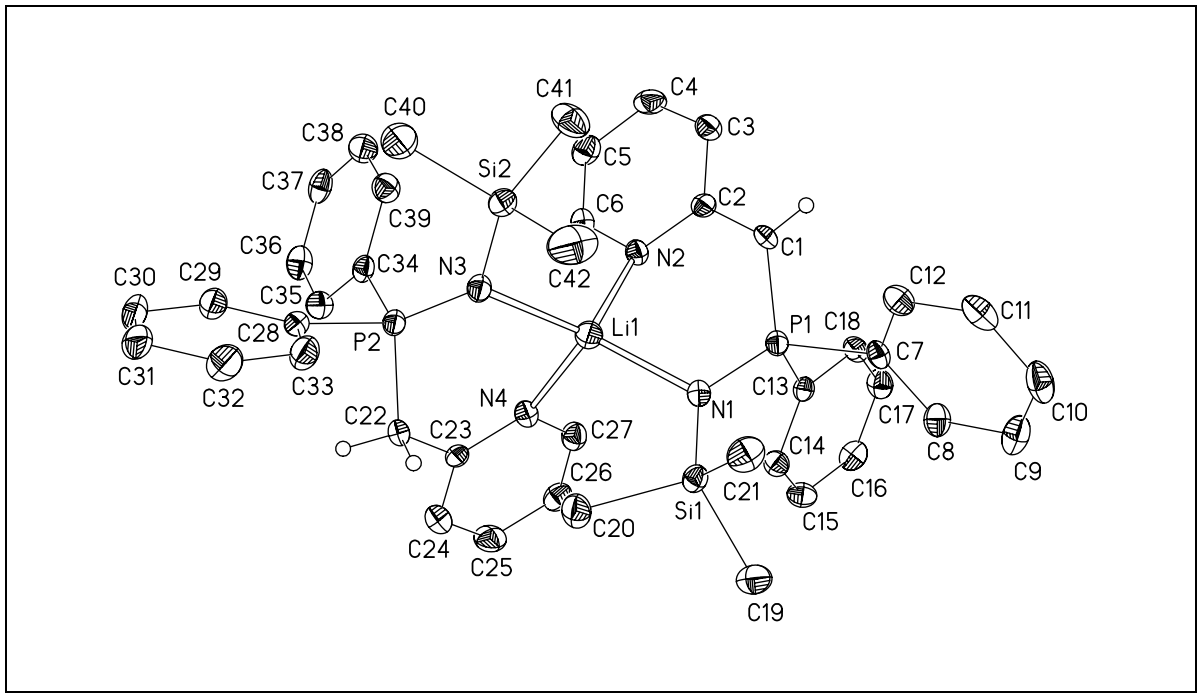

Figure 5.13: *Solid state structure of [{$Ph_2P(CH_2Py)NSiMe_3$}Li{$Ph_2P(CHPy)NSiMe_3$}], (**11**).*

Compound **12** crystallizes at r.t. in the centrosymmetrical triclinic space group $P\bar{1}$ as yellow blocks. The positions of the hydrogen atoms H1 at C1 and H22A, H22B at C22 were taken from the difference Fourier map and refined freely.

7.5.14 [{$Ph_2P(CH_2Py)NSiMe_3$}Na{$Ph_2P(CHPy)NSiMe_3$}], (13)

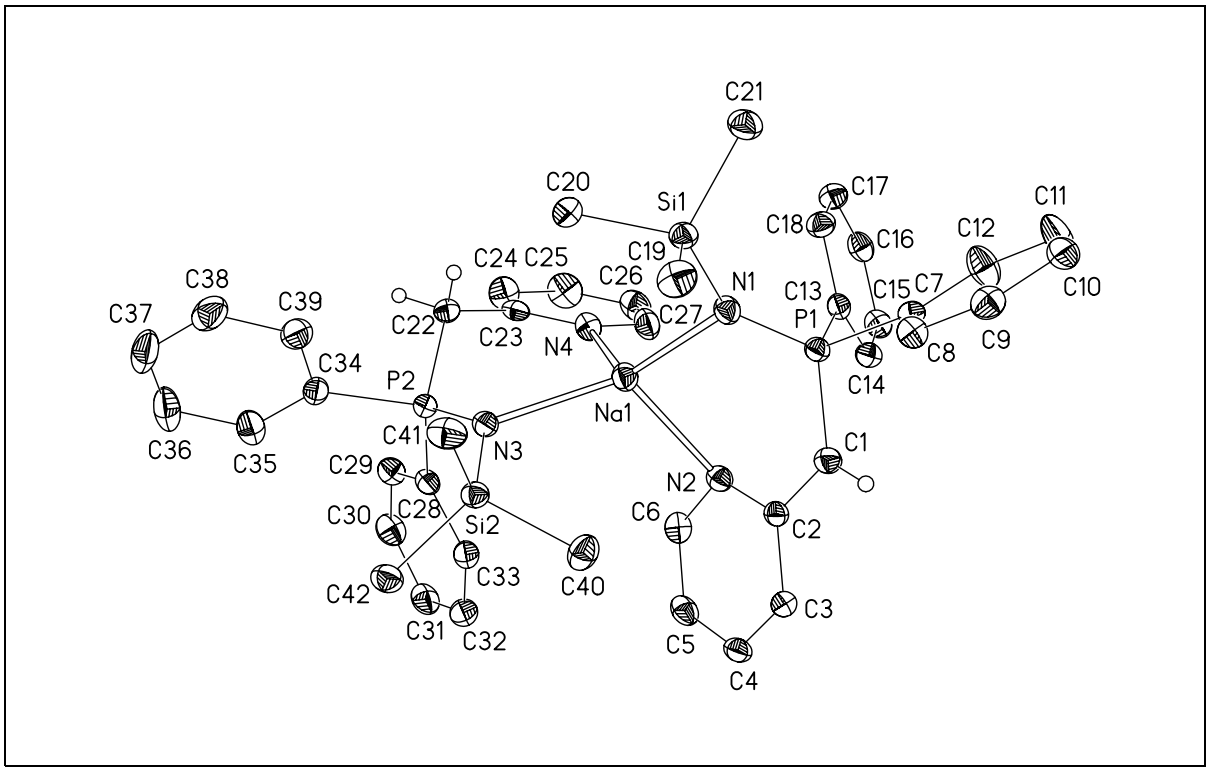

Figure 5.14: *Solid state structure of [{$Ph_2P(CH_2Py)NSiMe_3$}Na{$Ph_2P(CHPy)NSiMe_3$}],* ***(13)****.*

Compound **13** crystallizes at r.t. in the centrosymmetrical monoclinic space group $P2_1/n$ as yellow blocks. The positions of the hydrogen atoms H1 at C1 and H22A, H22B at C22 were taken from the difference Fourier map and refined freely.

7.5.15 [Zn{Ph$_2$P(CHPy)NSiMe$_3$}$_2$], (14)

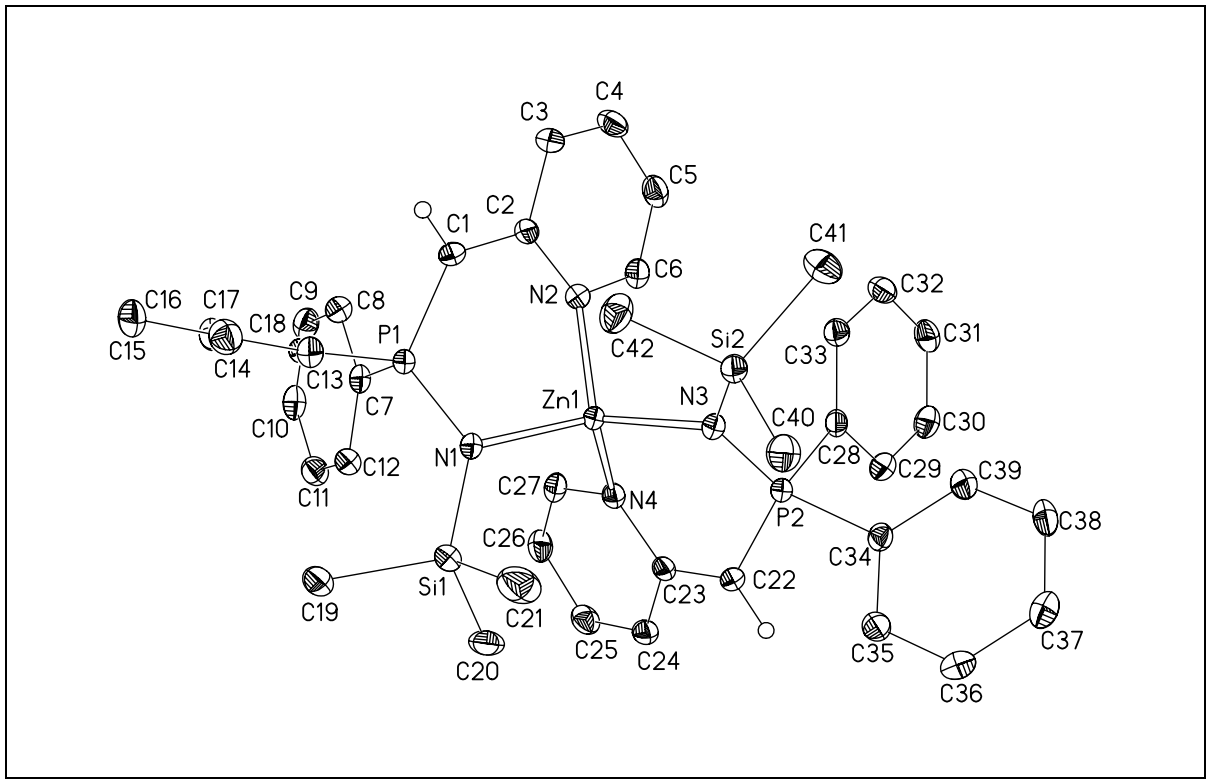

Figure 5.15: *Solid state structure of [Zn{Ph$_2$P(CHPy)NSiMe$_3$}$_2$], (**14**).*

Compound **14** crystallizes at 4°C in the centrosymmetrical triclinic space group $P\bar{1}$ as yellow plates. The positions of the hydrogen atoms H1 at C1 and H22 at C22 were taken from the difference Fourier map and refined freely.

7.5.16 [Fe{$Ph_2P(CHPy)NSiMe_3$}$_2$], (15)

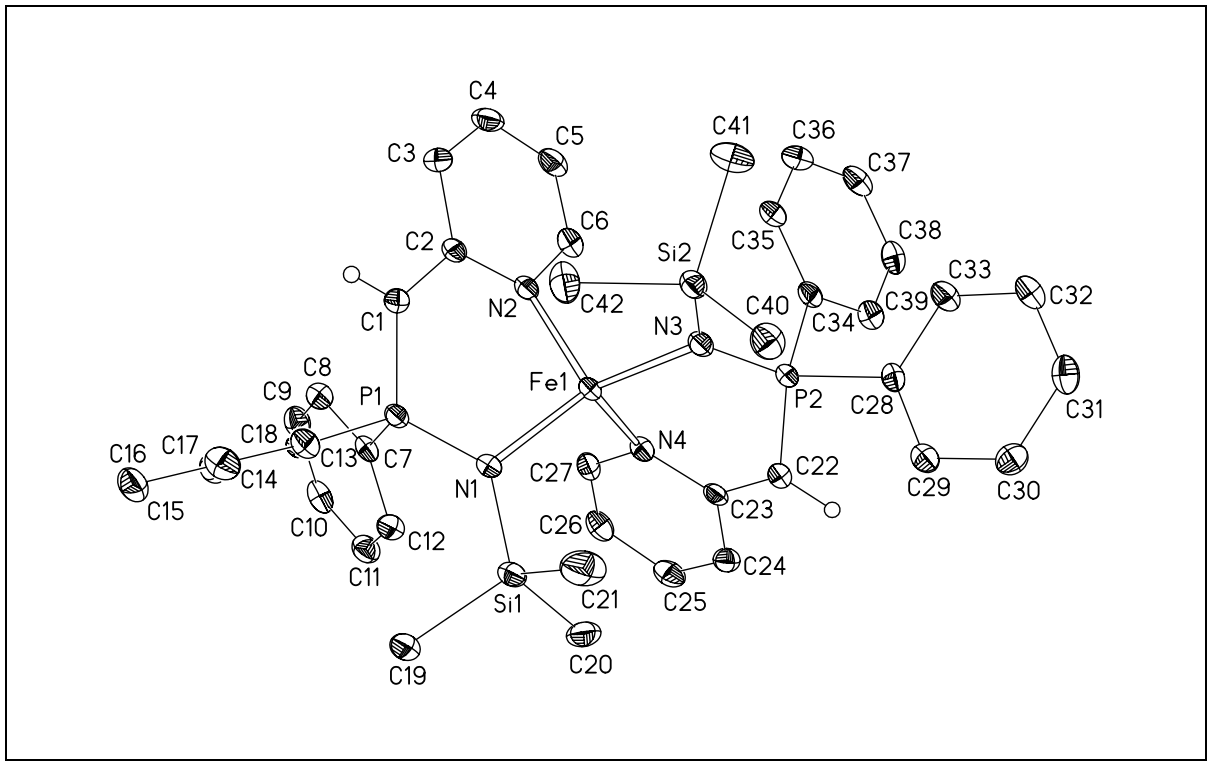

Figure 5.16: *Solid state structure of [Fe{$Ph_2P(CHPy)NSiMe_3$}$_2$], (**15**).*

Compound **15** crystallizes at r.t. in the centrosymmetrical triclinic space group $P\bar{1}$ as red blocks. The positions of the hydrogen atoms H1 at the C1 atom and H22 at C22 were taken from the difference Fourier map and refined freely.

Table 5.1: *Crystal data and structure refinement for compound **1** to **3**.*

Compound	**1**	**2**	**3**
Identification code	ENGLAND	ITALIEN	GRIECHE
Formula	$C_{18}H_{16}NP$	$C_{26}H_{31}LiNO_2P$	$C_{68}H_{66}Li_4N_2O_2P_4$
CCDC no.	-	-	-
M_r [gmol^{-1}]	277.29	427.43	1094.87
T [K]	100(2)	173(2)	173(2)
Crystal system	monoclinic	monoclinic	triclinic
Space group	$P2_1/n$	Cc	$P\bar{1}$
a [pm]	1562.04(9)	1008.08(11)	1154.71(7)
b [pm]	578.72(4)	1523.59(16)	1187.09(7)
c [pm]	1602.16(10)	1573.02(17)	2261.87(13)
α [°]			97.5480(10)
β [°]	96.7670(10)°	93.108(2)°	92.8930(10)
γ [°]			102.5320(10)°
V [nm^{-3}], *Z*	1.43824(16), 4	2.4124(4), 4	2.9903(3), 2
ρ_{calcd} [Mgm^{-3}]	1.281	1.177	1.216
μ [mm^{-1}]	0.180	0.135	0.172
F(000)	584	912	1152
Crystal size [mm]	0.4 x 0.4 x 0.05	0.4 x 0.1 x 0.1	0.4 x 0.2 x 0.1
θ range [°]	1.72 to 26.43	2.43 to 26.37	1.78 to 25.35
Reflections collected	14074	19578	36725
Unique reflections	3262	4886	10887
R(int)	0.0272	0.0124	0.0468
Absorption correction	empirical	empirical	empirical
Max. and min. transmission	1.000000 and 0.862628	1.000000 and 0.857803	1.000000 and 0.878178
Data / restraints / parameters	2945 / 0 / 181	4886 / 184 / 327	10886 / 0 / 721
Goodness-of-fit on F^2	1.060	1.104	1.020
Final R indices [I>2σ(I)]	R1 = 0.0358 wR2 = 0.0902	R1 = 0.0427 wR2 = 0.1082	R1 = 0.0470 wR2 = 0.1057
R indices (all data)	R1 = 0.0398 wR2 = 0.0933	R1 = 0.0431 wR2 = 0.1086	R1 = 0.0682 wR2 = 0.1151
Largest diff. peak and hole [e nm^{-3}]	419 and -182	280 and -196	537 and -272
Flack x parameter[194]	-	0.01(10)	-
g1 / g2	0.0478 / 0.6755	0.0594 / 1.0218	0.0501 / 1.9476

Table 5.2: *Crystal data and structure refinement for compounds **4** to **6**.*

Compound	**4**	**5**	**6**
Identification code	LUPIAC	ZWEIGELT	VATIKAN
Formula	$C_{48}H_{54}N_2O_3P_2Sr$	$C_{24}H_{33}N_2PPbSi_2$	$C_{72}H_{60}N_4OP_4Zn_3$+0.5Et_2O
CCDC no.	-	-	-
M_r [gmol^{-1}]	856.49	643.86	1354.29
T [K]	173(2)	100(2)	173(2)
Crystal system	monoclinic	triclinic	triclinic
Space group	C2/c	P $\bar{1}$	P $\bar{1}$
a [pm]	1103.25(8)	859.44(15)	1266.88(6)
b [pm]	2159.88(15)	1748.2(3)	1355.52(7)
c [pm]	1910.53(13)	1841.1(3)	2206.51(11)
α [°]		102.425(3)	102.5850(10)
β [°]	100.6420(10)	96.536(3)	92.7750(10)
γ [°]		95.131(3)	116.3710(10)
V [nm^{-3}], *Z*	4.4743(5), 4	2.6652(8), 4	3.2673(3), 2
ρ_{calcd} [Mgm^{-3}]	1.271	1.605	1.377
μ [mm^{-1}]	1.318	6.493	1.239
F(000)	1792	1264	1398
Crystal size [mm]	0.3 x 0.3 x 0.3	0.15 x 0.15 x 0.1	0.3 x 0.2 x 0.2
θ range [°]	3.26 to 26.37	2.29 to 28.28	2.15 to 25.05
Reflections collected	35381	73736	52698
Unique reflections	4696	13243	11554
R(int)	0.0223	0.0266	0.0226
Absorption correction	empirical	empirical	empirical
Max. and min. transmission	1.000000 and 0.871707	1.000000 and 0.648136	1.000000 and 0.878264
Data / restraints / parameters	4562 / 261 / 331	13238 / 0 / 561	11549 / 1240 / 862
Goodness-of-fit on F^2	1.031	1.085	1.045
Final R indices [I>2σ(I)]	R1 = 0.0244	R1 = 0.0179	R1 = 0.0288
	wR2 = 0.0658	wR2 = 0.0405	wR2 = 0.0735
R indices (all data)	R1 = 0.0256	R1 = 0.0206	R1 = 0.0324
	wR2 = 0.0666	wR2 = 0.0412	wR2 = 0.0755
Largest diff. Peak and hole [e nm^{-3}]	294 and –167	1226 and –362	387 and –228
g1 / g2	0.0430 / 2.3526	0.0185 / 2.1865	0.0426 / 1.3861

Table 5.3: *Crystal data and structure refinement for compounds 7 to* ***9a****.*

Compound	**7**	**8**	**9a**
Identification code	UNGARN	NEPAL	CHILE
Formula	$C_{54}H_{46}FeN_3P_3$+Et_2O	$C_{48}H_{66}Fe_2N_4P_2Si_4$	$C_{21}H_{25}N_2PSi$
M_r [gmol^{-1}]	959.82	985.05	364.49
CCDC no.	-	-	231738
T [K]	100(2)	293(2)	173(2)
Crystal system	monoclinic	triclinic	triclinic
Space group	$P2_1/n$	$P\bar{1}$	$P\bar{1}$
a [pm]	1223.28(4)	1240.1(7)	905.67(5)
b [pm]	3424.87(12)	1288.9(7)	1064.73(6)
c [pm]	1233.96(4)	1805.3(10)	1145.95(6)
α [°]		83.784(10)	97.0510(10)
β [°]	115.3450(10)	82.791(11)	99.3490(10)
γ [°]		71.046(10)	107.1020(10)
V [nm^{-3}], *Z*	4.6722(3), 4	2.70(1), 2	1.02496(10), 2
ρ_{calcd} [Mgm^{-3}]	1.365	1.211	1.181
μ [mm^{-1}]	0.472	0.719	0.198
F(000)	2016	1040	388
Crystal size [mm]	0.3 x 0.2 x 0.2	0.3 x 0.1 x 0.06	0.4 x 0.4 x 0.05
θ range [°]	1.92 to 26.40	3.00 to 25.35	1.83 to 26.37
Reflections collected	69564	45059	13417
Unique reflections	9566	9884	4165
R(int)	0.0302	0.0233	0.0189
Absorption correction	empirical	empirical	empirical
Max. and min. transmission	1.000000 and 0.927267	1.000000 and 0.845611	1.000000 and 0.913874
Data / restraints / parameters	9566 / 121 / 662	9865 / 535 / 757	4165 / 0 / 229
Goodness-of-fit on F^2	1.131	1.024	1.051
Final R indices [I>2σ(I)]	R1 = 0.0400	R1 = 0.0385	R1 = 0.0343
	wR2 = 0.0934	wR2 = 0.1013	wR2 = 0.0940
R indices (all data)	R1 = 0.0427	R1 = 0.0471	R1 = 0.0389
	wR2 = 0.0948	wR2 = 0.1074	wR2 = 0.0973
Largest diff. Peak and hole [e nm^{-3}]	628 and –246	1130 and –306	336 and –196
g1 / g2	0.0375 / 4.6727	0.0565 / 1.4306	0.0573 / 0.2635

Table 5.4: *Crystal data and structure refinement for compounds* ***9b*** *to* ***11****.*

Compound	**9b**	**10**	**11**
Identification code	HMM	PATAG	FEUERL
Formula	$C_{21}H_{25}N_2Psi$	$C_{18}H_{18}N_5P$	$C_{25}H_{34}LiN_2OPSi$
M_r [gmol^{-1}]	364.49	335.34	444.54
CCDC no.	233365	233366	-
T [K]	100(2)	173(2)	100(2)
Crystal system	triclinic	monoclinic	triclinic
Space group	$P\bar{1}$	$P2_1/n$	$P\bar{1}$
a [pm]	905.44(4)	1262.67(19)	1041.06(5)
b [pm]	1207.01(5)	936.31(15)	1052.92(5)
c [pm]	1933.88(9)	1456.6(2)	1294.69(7)
α [°]	72.4170(10)		73.1340(10)
β [°]	81.4120(10)	90.943(4)	81.1260(10)
γ [°]	89.5070(10)		67.6820(10)°
V [nm^{-3}], *Z*	1.99066(15), 4	1.7218(5), 4	1.25484(11), 2
ρ_{calcd} [Mgm^{-3}]	1.216	1.294	1.177
μ [mm^{-1}]	0.204	0.169	0.176
F(000)	776	704	476
Crystal size [mm]	0.4 x 0.2 x 0.05	0.4 x 0.1 x 0.07	0.4 x 0.4 x 0.4
θ range [°]	1.77 to 26.37	2.12 to 25.39	1.65 to 26.40
Reflections collected	54152	8959	26398
Unique reflections	8151	3355	5143
R(int)	0.0299	0.0459	0.0246
Absorption correction	empirical	empirical	empirical
Max. and min. transmission	1.000000 and 0.831522	1.000000 and 0.600715	1.000000 and 0.861417
Data / restraints / parameters	8150 / 0 / 473	3136 / 0 / 225	5143 / 0 / 289
Goodness-of-fit on F^2	1.054	1.031	1.024
Final R indices [I>2σ(I)]	R1 = 0.0396	R1 = 0.0608	R1 = 0.0330
	wR2 = 0.0989	wR2 = 0.1538	wR2 = 0.0909
R indices (all data)	R1 = 0.0454	R1 = 0.0892	R1 = 0.0344
	wR2 = 0.1030	wR2 = 0.1701	wR2 = 0.0921
Largest diff. peak and hole [e nm^{-3}]	584 and –219	802 and –304	365 and –296
g1 / g2	0.0564 / 1.0395	0.1049 /0.1271	0.0551 / 0.4120

Table 5.5: *Crystal data and structure refinement for compounds **12** to **14**.*

Compound	**12**	**13**	**14**
Identification code	NEUSEE	LEMBERG	PORTUGAL
Formula	$C_{42}H_{49}LiN_4P_2Si_2$	$C_{42}H_{49}N_4NaP_2Si_2$	$C_{42}H_{48}N_4P_2Si_2Zn$
M_r [gmol^{-1}]	734.91	750.96	792.33
CCDC no.	231740	231741	232888
T [K]	100(2)	173(2)	100(2)
Crystal system	triclinic	monoclinic	triclinic
Space group	$P\bar{1}$	$P2_{1/}n$	$P\bar{1}$
a [pm]	1011.46(6)	1124.06(18)	1026.46(5)
b [pm]	1104.73(7)	1488.1(2)	1077.28(5)
c [pm]	1825.93(11)	2478.7(4)	1830.69(9)
α [°]	93.3760(10)		85.8180(10)
β [°]	93.6010(10)	101.283(3)	80.9470(10)
γ [°]	98.7470(10)		79.7270(10)
V [nm^{-3}], *Z*	2.0077(2), 2	4.0661(11), 4	1.96499(16), 2
ρ_{calcd} [Mgm^{-3}]	1.216	1.227	1.339
μ [mm^{-1}]	0.203	0.211	0.803
F(000)	780	1592	832
Crystal size [mm]	0.4 x 0.4 x 0.35	0.4 x 0.4 x 0.4	0.4 x 0.2 x 0.08
θ range [°]	2.11 to 26.41	3.05 to 26.37	2.04 to 26.44°.
Reflections collected	22724	87301	42026
Unique reflections	8174	8675	8072
R(int)	0.0400	0.0950	0.0310
Absorption correction	none	none	empirical
Max. and min. transmission			1.000000 and 0.854799
Data / restraints / parameters	8170 / 0 / 478	8300 / 0 / 478	8067 / 0 / 474
Goodness-of-fit on F^2	0.922	1.086	1.067
Final R indices [I>2σ(I)]	R1 = 0.0410	R1 = 0.0414	R1 = 0.0347
	wR2 = 0.0859	wR2 = 0.1150	wR2 = 0.0905
R indices (all data)	R1 = 0.0581	R1 = 0.0482	R1 = 0.0377
	wR2 = 0.0890	wR2 = 0.1188	wR2 = 0.0920
Largest diff. Peak and hole [e nm^{-3}]	479 and –360	813 and –276	1389 and –248
g1 / g2	0.0480 / 0.0000	0.0809 / 0.0000	0.0510 / 1.5386

Table 5.6: *Crystal data and structure refinement for compound* ***15****.*

Compound	**15**
Identification code	BULGAR
Formula	$C_{42}H_{48}FeN_4P_2Si_2$
M_r [gmol^{-1}]	782.81
CCDC no.	232887
T [K]	100(2)
Crystal system	triclinic
Space group	$P\bar{1}$
a [pm]	1028.83(6)
b [pm]	1081.12(6)
c [pm]	1836.20(11)
α [°]	85.8120(10)
β [°]	81.1290(10)
γ [°]	79.9010(10)
V [nm^{-3}], *Z*	1.9845(2), 2
ρ_{calcd} [Mgm^{-3}]	1.310
μ [mm^{-1}]	0.556
F(000)	824
Crystal size [mm]	0.2 x 0.2 x 0.15
θ range [°]	2.03 to 25.35°.
Reflections collected	30624
Unique reflections	7251
R(int)	0.0295
Absorption correction	empirical
Max. and min. transmission	1.000000 and 0.863101
Data / restraints / parameters	7243 / 0 / 474
Goodness-of-fit on F^2	1.089
Final R indices [I>2σ(I)]	R1 = 0.0414
	wR2 = 0.1162
R indices (all data)	R1 = 0.0443
	wR2 = 0.1181
Largest diff. peak and hole [e nm^{-3}]	992 and –487
g1 / g2	0.065 / 2.550

8 References

[1] a) L. H. Gade*, J. Organomet. Chem*. **2002**, *661*, 85; b) W. E. Piers, D. J. H. Emslie, *Coord. Chem. Rev.* **2002**, *233-234*, 131; b) C. J. Elsevier, J. Reedijk, P. H. Walton, M. D. Ward, *J. Chem. Soc. Dalton Trans.* **2003**, 1869.

[2] a) D. W. Bruce, D. O'Hare*, Inorganic Materials*, Wiley, **1992**; b) O. Kahn, *Molecular Magnetism*, VCH, **1993**; c) J. A. McCleverty, M. D. Ward, *Acc. Chem. Res.* **1998**, *31*, 842.

[3] a) R. Robson, *J. Chem. Soc. Dalton Trans*. **2000**, 3735; b) B. Moulton, M. J. Zaworotko, *Chem. Rev.* **2001**, *101*, 1629.

[4] a) J. Heck, S. Dabek, T. Meyer-Friedrichsen, H. Wong, *Coord. Chem. Rev.* **1999**, *192*, 1217; b) B. J. Coe, *Chem. Eur. J.* **1999**, *5*, 2464; c) H. Le Bozec, T. Renouard, *Eur. J. Inorg. Chem.* **2000**, 229; d) H. Le Bozec, T. Le Bouder, O. Maury, A. Bondon, I. Ledoux, S. Deveau, J. Zyss, *Adv. Mater.* **2001**, *13*, 1677; e) Z. Fei, N. Kocher, C. J. Mohrschlodt, H. Ihmles, D. Stalke, *Angew. Chem.* **2003**, *115*, 807; *Angew. Chem. Int. Ed.* **2003**, *42*, 783; f) B. J. Coe, L. A. Jones, J. A. Harris, B. S. Brunschwig, I. Asselberghs, K. Clays, A. Persoons, *J. Am. Chem. Soc*. **2003**, *125*, 862; g) A. P. de Silva, B. McCaughan, O. F. McKinney, M. Querol, *J. Chem. Soc. Dalton Trans.* **2003**, 1902.

[5] a) J. P. Collman, L. Fu, *Acc. Chem. Res.* **1999**, *32*, 455; b) C. E. MacBeth, A. P. Golombek, V. G. Young, C. Yang, K. Kuzera, M. P. Hendrich, A. S. Borovik, *Science* **2000**, *289*, 938; c) E. Kimura, *Acc. Chem. Res.* **2001**, *34*, 171; d) R. Gupta, C. E. MacBeth, V. G. Young, A. S. Borovik*, J. Am. Chem. Soc.* **2002**, *124*, 1136; e) D. K. Garner, S. B. Fitch, L. H. McAlexander, L. M. Bezold, A. M. Arif, L. M. Berreau, *J. Am. Chem. Soc.* **2002**, *124*, 9970; f) T. D. P. Stack, *J. Chem. Soc. Dalton Trans.* **2003**, 1881; g) M. K. Zart, T. N. Sorrell, D. Powell, A. S. Borovik, *J. Chem. Soc. Dalton Trans*. **2003**, 1986.

[6] a) T. Ziegler, *Chem. Rev.* **1991**, *91*, 651; b) N. Koga, K. Morokuma, *Chem. Rev.* **1991**, *91*, 823; c) J. W. J. Knapen, A. W. van der Made, J. C. de Wilde, P. W. N. M. van Leeuwen, P. Wijkens, D. M. Grove, G. van Koten, *Nature* **1994**, *372*, 659; d) E. Drent, P. H. M. Budzelaar, *Chem. Rev.* **1996**, *96*, 663; e) S. D. Ittel, L. K. Johnson, M. Brookhart, *Chem. Rev.* **2000**, *100*, 1169; f) G. W. Coates, *Chem. Rev*. **2000**, *100*, 1223; g) T. M. Trnka, R. H. Grupps, *Acc. Chem. Res*. **2001**, *34*, 18; h) R. Kreiter, A. W. Kleij, R. J. M. Klein Gebbink, G. van Koten, *Top. Curr. Chem.* **2001**, *217*, 163; i) N. A. Cooley, S. M. Green, D. F. Wass, K. Heslop, A. G. Orpen, P. G. Pringle, *Organometallics* **2001**, *20*, 4769; j) I. T. Horvath, *Appl. Homogeneous Catal. Organomet. Compd.* **2002**, *2*, 634; k) W. Leitner, *Appl. Homogeneous Catal. Organomet. Compd.* **2002**, *2*, 852; l) Z. Freixa, P. W. N. M. van Leeuwen, *J. Chem. Soc. Dalton Trans.* **2003**, 1890; m) J. Okuda, *J. Chem. Soc. Dalton Trans.* **2003**, 2367.

[7] a) E. Uhlig, M. Schäfer, *Z. Anorg. Allg. Chem.* **1968**, *359*, 67; b) W. J. Knebel, R. J. Angelici, *Inorg. Chim. Acta* **1973**, *7*, 713; c) W. J. Knebel, R. J. Angelici, *Inorg. Chem.* **1974**, *13*, 632; d) B. Åkermark, B. Krakenberger, S. Hansson, A. Vitagliano, *Organometallics* **1987**, *6*, 620; e) H. T. Dieck, G. Hahn, *Z. Anorg. Allg. Chem.* **1989**, *577*, 74.

[8] a) H. Yang, M. Alvarez, N. Lugan, R. Mathieu, *J. Chem. Soc. Chem. Commun.* **1995**, 1721; b) H. Yang, M. Alvarez-Gressier, N. Lugan, R. Mathieu, *Organometallics* **1997**, *16*, 1401; c) H. Yang, H. Gao, R. J. Angelici, *Organometallics* **2000**, *19*, 622.

[9] J. C. Jeffrey, T. B. Rauchfuss, *Inorg. Chem.* **1979**, *18*, 2658.

[10] a) J. A. Davies, F. R. Hartley, *Chem. Rev.* **181**, *81*, 79; b) E. Lindner, M. Haustein, H. A. Mayer, K. Gierling, R. Fawzi, M. Steinman, *Organometallics*, **1995**, *14*, 2246; c) P. Braunstein, F. Naud, *Angew. Chem.* **2001**, *113*, 702; *Angew. Chem. Int. Ed.* **2001**, *40*, 680; d) P. Braunstein, N. M. Boag, *Angew. Chem.* **2001**, *113*, 2493; *Angew. Chem. Int. Ed.* **2001**, *40*, 2427.

[11] a) P. R. Sharp, *Comprehensive Organometallic Chemistry II*, W. W. Abel, F. G. A. Stone, G. Wilkinson, Elsevier Science Inc., New York, **1995**, Vol. 8, 152; b) T. Kottke, D. Stalke, *Chem. Ber. /Recl.* **1997**, *130*, 1365; c) H. Werner, *J. Chem. Soc. Dalton Trans*. **2003**, 3829.

[12] a) A. Bader, E. Lindner, *Coord. Chem. Rev*. **1991**, *108*, 27; b) C. S. Slone, D. A. Weinberger, C. A. Mirkin, *Prog. Inorg. Chem*. **1999**, *48*, 233.

[13] a) E. B. Springman, E. L. Angleton, H. Birkedal-Hansen, H. E. van Wart, *Proc. Natl. Acad. Sci. USA* **1990**, *87*, 364; b) H. E. van Wart, H. Birkedal-Hansen, *Proc. Natl. Acad. Sci. USA* **1990**, *87*, 5578.

[14] T. G. Traylor, C. K. Chang, J. Geibel, A. Berzinis, T. Mincey, J. Cannon, *J. Am. Chem. Soc*. **1979**, *101*, 6716.

[15] a) G. R. Newkome, *Chem. Rev.* **1993**, *93*, 2067; b) P. R. Sharp In *Comprehensive Coordination Chemistry*, E. W. Abel, F. G. A. Stone, G. Wilkinson, Pergamon Press, Oxford, **1995**, Vol. 8, Chapter 2, 152; c) Z. Z. Zhang, H. Cheng, *Coord. Chem. Rev.* **1996**, *147*, 1; d) P. Espinet, K. Soulantica, *Coord. Chem. Rev*. **1999**, *193-195*, 499.

[16] a) P. v. Matt, A. Pfaltz, *Angew. Chem.* **1993**, *105*, 614; *Angew. Chem. Int. Ed. Engl.* **1993**, *32*, 566; b) A. Togni, U. Burckhardt, V. Gramlich, P. S. Pregosin, R. Salzmann, *J. Am. Chem. Soc.* **1996**, *118*, 1031; c) W. -P. Deng, X. -L. Hou, L. -X. Dai, Y. -H. Yu, W. Xia, *Chem. Commun.* **2000**, 285.

[17] a) T. Hayashi, C. Hayashi, Y. Uozumi, *Tetrahedron Asymmetry* **1995**, *6*, 2503; b) Y. Nishibayashi, K. Segawa, K. Ohe, S. Uemura, *Organometallics* **1995**, *14*, 5486.

[18] a) J. M. Valk, G. A. Whitlock, T. P. Layzell, J. M. Brown, *Tetrahedron Asymmetry* **1995**, *6*, 2593; b) H. Doucet, E. Fernandez, T. P. Layzell, J. M. Brown, *Chem. Eur. J.* **1999**, *5*, 1320.

[19] a) Q. Jiang, D. van Plew, S. Murtuza, X. Zhang, *Tetrahedron Lett.* **1996**, *37*, 797; b) T. Langer, G. Helmchen, *Tetrahedron Lett.* **1996**, *37*, 1381; c) J. X. Gao, T. Ikariya, R. Noyori, *Organometallics* **1996**, *15*, 1087.

[20] P. Braunstein, M. Knorr, C. Stern, *Coord. Chem. Rev*. **1998**, *178-180*, 903.

[21] F. Baier, Z. Fei, H. Gornitzka, A. Murso, S. Neufeld, M. Pfeiffer, I. Rüdenauer, A. Steiner, T. Stey, D. Stalke, *J. Organomet. Chem*. **2002**, *661*, 111.

[22] L. Mahalakshmi, D. Stalke In *Structure and Bonding–Group 13 Elements*; Eds. D. A. Atwood, H. W. Roesky, Springer Verlag, Heidelberg, **2002**, *103*, 85.

[23] a) E. C. Constable, P. J. Steel, *Coord. Chem. Rev.* **1989**, *93*, 205; b) P. J. Steel, *Coord. Chem. Rev.* **1990**, *106*, 227; c) C. E. Kriley, P. E. Fanwick, I. P. Rothwell, *J. Am. Chem. Soc.* **1994**, *116*, 5225; d) D. T. Davies, *Aromatische Heterocyclen*, VCH, Weinheim, **1995**; e) T. Eicher, S. Hauptmann, *Chemie der Heterocyclen*, VCH, Weinheim, **1995**.

[24] A. Steiner, D. Stalke, *J. Chem. Soc. Chem. Comm.* **1993**, 444.

[25] A. Steiner, D. Stalke, *Organometallics* **1995**, *14*, 2422.

[26] M. Pfeiffer, T. Stey, H. Jehle, B. Klüpfel, W. Malisch, V. Chandrasekhar, D. Stalke, *Chem. Commun.* **2001**, 337.

[27] M. Pfeiffer, F. Baier, T. Stey, D. Leusser, D. Stalke, B. Engels, D. Moigno, W. Kiefer, *J. Mol. Model.* **2000**, *6*, 299.

[28] M. Alvarez, N. Lugan, R. Mathieu, *J. Chem. Soc. Dalton Trans.* **1994**, 2755.

[29] U. Pieper, *π-Wechselwirkungen in Alkalimetallorganischen Systemen*, PhD thesis, Universität Göttingen, **1993**.

[30] P. Rademacher, *Strukturen organischer Moleküle*, VCH, Weinheim, **1987**.

[31] T. Stey, D. Stalke, *Lead structures in lithium organic chemistry*, In *The chemistry of organolithium compounds*, Eds. Z. Rappoport, I. Marek, Wiley, **2003**.

[32] a) G. Fraenkel, W. R. Winchester, P. G. Williard, *Organometallics* **1989**, *8*, 2308; b) S. Blaurock, O. Kühl, E. Hey-Hawkins, *Organometallics* **1997**, *16*, 807.

[33] L. T. Byrne, L. M. Engelhardt, G. E. Jacobson, W. -P. Leung, R. I. Papasergio, C. L. Raston, B. W. Skelton, P. Twiss, A. H. White, *J. Chem. Soc. Dalton Trans.* **1989**, 105.

[34] a) H. H. Karsch, A. Appelt, B. Deubelly, G. Müller, *J. Chem. Soc. Chem. Commun.* **1987**, 1033; b) M. Winkler, M. Lutz, G. Müller, *Angew. Chem.* **1994**, *106*, 2372; *Angew. Chem. Int. Ed. Engl.* **1994**, *33*, 2279; c) M. D. Fryzuk, J. B. Love, S. J. Rettig, *Chem. Commun.* **1996**, 2783; d) A. Feustel, G. Müller, *Chem. Commun.* **2001**, 1024; e) S. Ekici, D. Gudat, M. Nieger, L. Nyulaszi, E. Niecke*, Angew. Chem.* **2002**, *114*, 3515; *Angew. Chem. Int. Ed.* **2002**, *41*, 3367.

[35] H. H. Karsch, G. Grauvogel. P. Mikulcik, P. Bissinger, G. Müller, *J. Organomet. Chem.* **1994**, *465*, 65.

[36] D. J. Brauer, S. Hietkamp, O. Stelzer, *J. Organomet. Chem.* **1986**, *299*, 137.

[37] a) L. M. Engelhardt, G. E. Jacobson, P. C. Junk, L. Raston, B. W. Skelton, A. H. White, *J. Chem. Soc. Dalton Trans.* **1988**, 1011; b) U. Pieper, D. Stalke, *Organometallics* **1993**, *12*, 1201.

[38] M. D. Fryzuk, S. A. Johnson, B. O. Patrick, A. Albinati, S. A. Mason, T. F. Koetzle, *J. Am. Chem. Soc.* **2001**, *123*, 3960.

[39] a) G. Wittig, A. Maercker, *J. Organomet. Chem.* **1967**, *8*, 491. b) E. P. Kyba*, J. Am. Chem. Soc.* **1976**, *98*, 4805. c) S. Oae, *Croat. Chim. Acta* **1986**, *59*, 129. d) Y. Uchida, M. Kawai, H. Masauji, S. Oae, *Heteroatom. Chem.* **1993**, *4*, 421.

[40] a) Y. Uchida, K. Onoue, N. Tada, F. Nagao, S. Oae, *Tetrahedron Lett.* **1989**, *30*, 567. b) S. Oae, Y. Uchida, *Acc. Chem. Res.* **1991**, *24*, 202.
[41] P. H. Budzelaar, *J. Org. Chem.* **1998**, *63*, 1131.
[42] E. Drent, P. H. M. Budzelaar, *Eur. Pat. Appl.* EP. -A386834, **1990**.
[43] R. E. Mulvey, K. Wade, D. R. Armstrong, G. T. Walker, R. Snaith, W. Clegg, D. Reed, *Polyhedron* **1987**, *6*, 987.
[44] R. A. Jones, A. L. Stuart, T. C. Wright, *J. Am. Chem. Soc.* **1983**, *105*, 7459.
[45] P. B. Hitchcock, M. F. Lappert, W. -P. Leung, D. -S. Liu, T. C. W. Mak, Z. -X. Wang, *J. Chem. Soc. Dalton Trans.* **1999**, 1257.
[46] P. B. Hitchcock, M. F. Lappert, D. -S. Liu, *J. Chem. Soc. Chem. Commun*. **1994**, 2637.
[47] M. Said, M. Thornton-Pett, M. Bochmann, *Organometallics* **2001**, *20*, 5629.
[48] a) M. Westerhausen, *Inorg. Chem*. **1991**, *30*, 96; b) M. Westerhausen, W. Schwarz, *Z. Anorg. Allg. Chem.* **1991**, *606*, 177.
[49] M. Westerhausen, M. H. Digeser, W. Schwarz, *Inorg. Chem.* **1997**, *36*, 521.
[50] R. Fleischer, D. Stalke, *Inorg. Chem.* **1997**, *36*, 2413.
[51] M. Westerhausen, W. Schwarz, *Z. Anorg. Allg. Chem.* **1991**, *606*, 177.
[52] A. F. Waters, A. H. White, *Aust. J. Chem.* **1996**, *49*, 35.
[53] a) F. H. Allen and O. Kennard, *Chem. Des. Automat. News* **1993**, **8**, 131; b) Cambridge Structural Database, release 5. 25, January 2004.
[54] M. D. Francis, P. B. Hitchcock, J. F. Nixon, *Chem. Commun*. **2000**, 2027.
[55] M. Westerhausen, C. Birg, M. Krofta, P. Mayer, T. Seifert, H. Nöth, A. Pfitzner, T. Nilges, H. -J. Deiseroth, *Z. Anorg. Allg. Chem.* **2000**, *626*, 1073.
[56] a) M. Westerhausen, *J. Organomet. Chem.* **1994**, *479*, 141; b) M. Westerhausen, M. H. Digeser, H. Nöth, J. Knizek, *Z. Anorg. Allg. Chem.* **1998**, *624*, 215; c) M. Westerhausen, M. H. Digeser, H. Nöth, W. Ponikwar, T. Seifert, K. Polborn, *Inorg. Chem.* **1999**, *38*, 3207; d) S. Blair, K. Izod, W. Clegg, *Inorg. Chem.* **2002**, *41*, 3886; e) M. Westerhausen, S. Weinrich, G. Kramer, H. Piotrowski, *Inorg. Chem.* **2002**, *41*, 7072.
[57] J. Emsley, *The Elements*, 2nd Ed., Clarendon Press, Oxford, **1991**.
[58] M. J. S. Gynane, D. H. Harris, M. F. Lappert, P. P. Power, P. Rivière, M. Rivière-Baudet, *J. Chem. Soc. Dalton Trans*. **1977**, 2004.
[59] T. Fjeldberg, H. Hope, M. F. Lappert, P. P. Power, A. J. Thorne, *J. Chem. Soc. Chem. Commun.* **1983**, 639.
[60] L. Pu, B. Twamley, P. P. Power, *Organometallics* **2000**, *19*, 2874.
[61] K. Wieghardt, K. Kleine-Boymann, B. Nuber, J. Weiss, L. Zsolnai, G. Huttner, *Inorg. Chem*. **1986**, *24*, 1647.
[62] S. S. Al-Juaid, A. G. Avent, C. Eaborn, M. S. Hill, P. B. Hitchcock, D. J. Patel, J. D. Smith, *Organometallics* **2001**, *20*, 1223.
[63] A. H. Cowley, D. M. Giolando, R. A. Jones, C. M. Nunn, J. M. Power, *Polyhedron* **1988**, *7,* 1909.
[64] S. C. Goel, M. Y. Chiang, D. J. Rauscher, W. E. Buhro, *J. Am. Chem. Soc*. **1993**, *115*, 160.

[65] A. Winkler, W. Bauer, F. W. Heinemann, V. Garcia-Montalvo, M. Moll, J. Ellermann, *Eur. J. Inorg. Chem.* **1998**, 437.
[66] a) A. L. Balch, D. E. Oram, *Organometallics* **1986**, *5*, 2159; b) A. L. Balch, D. E. Oram, *Inorg. Chem.* **1987**, *26*, 1906.
[67] H. Gornitzka, C. Hemmert, G. Bertrand, M. Pfeiffer, D. Stalke, *Organometallics* **2000**, *19*, 112.
[68] S. Wingerter, M. Pfeiffer, F. Baier, T. Stey, D. Stalke, *Z. Anorg. Allg. Chem.* **2000**, *656*, 1121.
[69] S. M. Godfrey, C. A. McAuliffe, R. G. Pritchard, J. M. Sheffield, *Inorg. Chim. Acta* **1999**, *292*, 213.
[70] P. Pérez-Lourido, J. Romero, J. A. García-Vázquez, A. Sousa, K. Maresca, J. Zubieta, *Inorg. Chem.* **1999**, *38*, 3709.
[71] W. A. Herrmann, W. R. Thiel, J. G. Kuchler, J. Behm, E. Herdtweck, *Chem. Ber.* **1990**, 123, 1963.
[72] M. Westerhausen, T. Bollwein, M. Warchhold, H. Nöth, *Z. Anorg. Allg. Chem.* **2001**, *627*, 1141.
[73] M. J. Henderson, R. I. Papasergio, C. L. Raston, A. H. White, M. F. Lappert, *J. Chem. Soc. Chem. Commun.* **1986**, 672.
[74] a) A. J. de Koning, J. Boersma, G. J. M. van der Kerk, *J. Organomet. Chem.* **1980**, *186*, 159; b) A. L. Spek, *Cryst. Struct. Commun.* **1982**, *11*, 1621.
[75] a) J. Dekker, J. W. Munninghoff, J. Boersma, A. L. Spek, *Organometallics* **1987**, *6*, 1236; b) D. M. Knotter, M. D. Janssen, D. M. Grove, W. J. J. Smeets, E. Horn, A. L. Spek, G. v. Koten, *Inorg. Chem.* **1991**, *30*, 4361; c) A. J. Edwards, M. A. Paver, P. R. Raithby, C. A. Russell, D. S. Wright, *Organometallics* **1993**, *12*, 4687; d) M. Steiner, H. Grützmacher, H. Prtizkow, L. Zsolnai, *Chem. Commun*. **1998**, 285; e) A. B. Charette, J. -F. Marcoux, C. Molinaro, A. Beauchemin, C. Brochu, E. Isabel, *J. Am. Chem. Soc*. **2000**, *122*, 4508.
[76] P. C. Andrews, C. L. Raston, B. W. Skelton, A. H. White, *Organometallics* **1998**, *17*, 779.
[77] a) J. Kim, B. Chen, T. M. Reinecke, H. Li, M. Eddaoudi, D. B. Moler, M. O'Keeffe, O. M. Yaghi, *J. Am. Chem. Soc.* **2001**, *123*, 8239; b) G. Zhu, J. M. Tanski, G. Parkin, *J. Chem. Cryst.* **2002**, *32*, 469.
[78] a) S. C. Abrahams, J. L. Bernstein, *Acta Crystallogr.* **1969**, *B25*, 1233; b) T. M. Sabine, S. Hogg, *Acta Crystallogr.* **1969**, *B25*, 2254.
[79] a) R. A. Andersen, K. Faegri, J. C. Green, A. Haaland, M. F. Lappert, W. -P. Leung, K. Rypdal, *Inorg. Chem.* **1988**, *27*, 1782; b) M. M. Olmstead, P. P. Power, S. C. Shoner, *Inorg. Chem.* **1991**, *30*, 2547.
[80] M. di Vaira, S. Midollini, L. Sacconi, *Inorg. Chem.* **1981**, *20*, 3430.
[81] A. J. Blake, A. J. Atkins, R. O. Gould, M. Schröder, *Z. Kristallogr*. **1992**, *198*, 287.
[82] J. T. Mague, J. L. Krinsky, *Inorg. Chem*. **2001**, *40*, 1962.

[83] a) B. A. Katz, C. E. Strouse*, J. Am. Chem. Soc.* **1979**, *101*, 6214; b) L. Wiehl, G. Kiel, C. P. Köhler, H. Spiering, P. Gütlich, *Inorg. Chem.* **1986**, *25*, 1565; c) M. -H. Yang, T. -W. Lin, C. -C. Chou, H. -C. Lee, H. -C. Chang, G. -H. Lee, M. -K. Leung, S. -M. Peng, *Chem. Commun.* **1997**, 2279; d) Y. Zang, J. Kim, Y. Dong, E. C. Wilkinison, E. H. Appelman, L. Que Jr. *J. Am. Chem. Soc.* **1997**, *119*, 4197; e) B. Singh, J. R. Long, F. F. de Biani, D. Gatteschi, P. Stavropoulos, *J. Am. Chem. Soc.* **1997**, *119*, 7030; f) P. A. Anderson, T. Astley, M. A. Hitchman, F. R. Keene, B. Moubaraki, K. S. Murray, B. W. Skelton, E. R. T. Tiekink, H. Toftlund, A. H. White, *J. Chem. Soc. Dalton Trans.* **2000**, 3505.

[84] W. -P. Leung, H. K. Lee, L. -H. Weng, B. -S. Luo, Z. -Y. Zhou, T. C. W. Mak, *Organometallics* **1996**, *15*, 1785.

[85] W. Lau, J. C. Huffmann, J. K. Kochi, *Organometallics* **1982**, *1*, 155.

[86] A. Klose, E. Solari, C. Floriani, A. Chiesi-Villa, C. Rizzoli, N. Re, *J. Am. Chem. Soc.* **1994**, *116*, 9123.

[87] B. S. Snyder, R. H. Holm, *Inorg. Chem.* **1988**, *27*, 2339.

[88] A. R. Hermes, G. S. Girolami, *Organometallics* **1987**, *6*, 763.

[89] F. Cecconi, M. Di Vaira, S. Midollini, A. Orlandini, L. Sacconi, *Inorg. Chem.* **1981**, *20*, 3423.

[90] a) H. Müller, W. Seidel, H. Görls, *J. Organomet. Chem*. **1993**, *445*, 133; b) A. Klose, E. Solari, R. Ferguson, C. Floriani, A. Chiesi-Villa, C. Rizzoli, *Organometallics* **1993**, *12*, 2414; c) D. H. Hill, M. A. Parvez, A. Sen, *J. Am. Chem. Soc.* **1994**, *116*, 2889; d) H. Müller, W. Seidel, H. Görls, *Angew. Chem.* **1995**, *107*, 386; *Angew. Chem. Int. Ed. Engl.* **1995**, *34*, 325; e) R. J. Wehmschulte, P. P. Power, *Organometallics* **1995**, *14*, 3264.

[91] D. Auer, C. Strohmann, A. V. Arbuznikov, M. Kaupp, *Organometallics* **2003**, *22*, 2442.

[92] M. Kaupp, Privat Communication.

[93] H. Staudinger, J. Meyer, *Helv. Chim. Acta* **1919**, *2*, 635.

[94] a) A. W. Johnson, *Ylides and Imines of Phosphorus*, Wiley, New York, **1993**; b) G. Singh, H. Zimmer, *Organomet. Chem. Rev*. **1967**, *2*, 279; c) Y. G. Gololobov, I. N. Zhmurova, L. F. Kasukhin, *Tetrahedron* **1981**, *37*, 437; d) Y. G. Gololobov, L. F. Kasukhin, *Tetrahedron* **1992**, *48*, 1353.

[95] E. F. V. Scriven, K. Turnbull *Chem. Rev*. **1988**, *88*, 297.

[96] a) H. G. Khorana, *Chem. Rev.* **1953**, *53*, 145; b) F. Kurzer, K. Douraghi-Zadeh, *Chem. Rev.* **1967**, *67*, 107; c) G. K. Cantrell, T. Y. Meyer, *Organometallics*, **1997**, *16*, 5381; d) G. K. Cantrell, T. Y. Meyer *J. Am. Chem. Soc.* **1998**, *120*, 8035.

[97] a) H. Zimmer, G. Singh, *J. Org. Chem*. **1963**, *28*, 483; b) H. Zimmer, M. Jayawant, *Tetrahedron Lett*. **1966**, 5061; c) H. Zimmer, M. Jayawant, P. Gutsch, *J. Org. Chem*. **1970**, *35*, 2826.

[98] a) S. A. Foster, L. Y Leyshon, D. G. Saunders, *J. Chem. Soc. Chem. Commun.* **1973**, 29; b) P. Molina, P. M. Fresneda, P. Alarcon, *Tetrahedron Lett.* **1988**, *29*, 379; c) N. I. Gusnar, *Russ. Chem. Rev*. **1991**, *60*, 146.

[99] a) S. A. Bell, S. J. Geib, T. Y. Meyer, *Chem. Commun.* **2000**, 1375; b) S. A. Bell, T. Y. Meyer, S. J. Geib, *J. Am. Chem. Soc.* **2002**, *124*, 10698; c) M. C. Burland, T. Y Meyer, *Inorg. Chem*. **2003**, *42*, 3438.

[100] F. F Stewart, C. J. Orme, M. K. Harrup, R. P. Lash, D. H. Welnkauf, J. D. McCoy, *Polym. Mater. Sci. Eng*. **2001**, *85*, 577.

[101] J. Crommen, J. Vandorpe, E. Schacht, *J. Controlled Release* **1993**, *24*, 167.

[102] a) P. Molina, M. Alajarin, A. Vidal, *Tetrahedron Lett.* **1988**, *29*, 3849; b) P. Molina, A. Arques, M. V. Vinader, *Synthesis* **1990**, 469; c) P. Molina, M. Alajarin, C. Lopez-Leonardo, *Tetrahedron Lett.* **1991**, *32*, 4041.

[103] a) A. V. Kirsanov, *Isv. Akad. Nauk SSSR* **1950**, 426; b) A. V. Kirsanov, *Zh. Obshch. Khim*. **1952**, *22*, 269.

[104] A. Steiner, S. Zacchini, P. I. Richards, *Coord. Chem. Rev.* **2002**, *227*, 193.

[105] I. A. Koppel, R. Schwesinger, T. Breuer, P. Burk, K. Herodes, I. Koppel, I. Leito, M. Mishima, *J. Phys. Chem. A* **2001**, *105*, 9575.

[106] A. Steiner, D. Stalke, *Angew. Chem.* **1995**, *107*, 1908; *Angew. Chem. Int. Ed. Engl.* **1995**, *34*, 1752.

[107] S. Wingerter, M. Pfeiffer, A. Murso, C. Lustig, T. Stey, V. Chandrasekhar, D. Stalke, *J. Am. Chem. Soc*. **2001**, *123*, 1381.

[108] a) M. T. Ashby, Z. Li, *Inorg. Chem.* **1992**, *31*, 1321; b) G. Trinquier and M. T. Ashby, *Inorg. Chem.* **1994**, *33*, 1306.

[109] D. G. Gilheany, *Chem. Rev*. **1994**, *94*, 1339.

[110] a) W. Kutzelnigg, *Angew. Chem.* **1984**, *96*, 262; *Angew. Chem. Int. Ed. Engl.* **1984**, *23*, 272; b) E. A. Reed, P. v. R. Schleyer, *J. Am. Chem. Soc.* **1990**, *112*, 1434; c) E. Magnusson, *J. Am. Chem. Soc.* **1993**, *115*, 1051; d) A. Dobado, H. Martínez-García, J. M. Molina, M. R. Sundberg, *J. Am. Chem. Soc.* **1998**, *120*, 8461; e) D. B. Chesnut, *J. Phys. Chem. A* **2003**, *107*, 4307.

[111] a) T. Naito, S. Nagase, H. Yamataka, *J. Am. Chem. Soc.* **1994**, *116*, 10080; b) A. A. Restrepo-Cossio, C. A. Gonzalez, F. Marí, *J. Phys. Chem. A* **1998**, *102*, 6993; c) H. Yamataka, S. Nagase, *J. Am. Chem. Soc.* **1998**, *120*, 7530; d) J. A. Doblado, H. Martínez-Garcia, J. M. Molina, M. R. Sundberg, *J. Am. Chem. Soc.* **2000**, *122*, 1144.

[112] a) J. Koketsu, Y. Ninomiya, Y. Suzuki, N. Koga, *Inorg. Chem.* **1997**, *36*, 694; b) W. C. Lu, C. C. Sun, Q. J. Zang, C. B. Liu, *Chem. Phys. Lett.* **1999**, *311*, 491; c) W. C. Lu, C. B. Liu, C. C. Sun, *J. Phys. Chem. A* **1999**, *103*, 1078.

[113] D. S. Yufit, J. A. K. Howard, M. G. Davidson, *J. Chem. Soc. Perkin Trans. 2* **2000**, 249.

[114] a) J. S. Millar, M. O. Visscher, K. G. Caulton, *Inorg. Chem.* **1974**, *13*, 1632; b) E. W. Abel, S. A. Mucklejohn, *Phosphorus, Sulfur Relat. Elem.* **1981**, *9*, 235; c) J. Vincente, A. Arcas, D. Bautista, M. C. Ramírez de Arellano, *Organometallics* **1998**, *17*, 4544.

[115] a) M. Fukui, K. Itoh, Y. Ishii, *Bull. Chem. Soc. Jpn.* **1975**, *48*, 2044; b) E. W. Abel, S. A. Mucklejohn, *Inorg. Chim. Acta.* **1979**, *37*, 107; c) H. F. Sleiman, S. Mercer, L. McElwee-White, *J. Am. Chem. Soc.* **1989**, *111*, 8007; d) P. Imhoff, C. J. Elsevier, C. H. Stam, *Inorg. Chim. Acta* **1990**, *175*, 209.

[116] K. Dehnicke, F. Weller, *Coord. Chem. Rev.* **1997**, *158*, 103.
[117] K. Dehnicke, M. Krieger, W. Massa, *Coord. Chem. Rev.* **1999**, *82*, 19.
[118] K. Dehnicke, F. Weller, J. Strähle, *Chem. Soc. Rev.* **2001**, *30*, 125.
[119] a) T. V. Lubben, P. T. Wolczanski, G. D. van Duyne, *Organometallics* **1984**, *3*, 977; b) D. W. Stephan, J. C. Stewart, F. Guérin, R. E. v. H. Spence, W. Xu, D. G. Harrison, *Organometallics* **1999**, *17*, 1116; c) D. W. Stephan, F. Guérin, R. E. v. H. Spence, L. Koch, X. Gao, S. J. Brown, J. W. Swabey, Q. Wang, W. Xu, P. Zoricak, D. G. Harrison, *Organometallics* **1999**, *17*, 2046.
[120] a) R. E. v. H. Spence, S. J. Brown, R. P. Wurz, D. Jeremic, D. W. Stephan, *PCT Int. Appl.* **2001**, WO 2000-CA978 20000824; CA 99-2282070; b) D. W. Stephan, J. C. Stewart, F. Guérin, S. Courtenay, J. Kickham, E. Hollink, C. Beddie, A. Hoskin, T. Graham, P. Wie, R. E. v. H. Spence, W. Xu, L. Koch, X. Gao, D. G. Harrison, *Organometallics* **2003**, *22*, 1937.
[121] G. Boche, *Angew. Chem.* **1989**, *101*, 286; *Angew. Chem. Int. Ed. Engl.* **1989**, *28*, 277.
[122] J. F. Bickley, M. C. Copsey, J. C. Jeffery, A. P. Leedham, C. A. Russell, D. Stalke, A. Steiner, T. Stey, S. Zacchini, *J. Chem. Soc. Dalton Trans.* **2004**, in press.
[123] a) F. Lopéz-Ortiz, E. Peláez-Arango, B. Tejerina, E. Pérez-Carreno, S. Garcia-Granda, *J. Am. Chem. Soc.* **1995**, *117*, 9972; b) A. Müller, B. Neumüller, K. Dehnicke, *Chem. Ber.* **1996**, *129*, 253; c) A. Müller, B. Neumüller, K. Dehnicke, *Angew. Chem.* **1997**, *109*, 2447; *Angew. Chem. Int. Ed. Engl.* **1997**, *36*, 2350; d) P. B. Hitchcock, M. F. Lappert, P. G. H. Uiterweerd, Z. -X. Wang, *J. Chem. Soc. Dalton Trans.* **1999**, 3413, e) I. Fernandez, G. Alvarez, M. Julia, N. Kocher, D. Leusser, D. Stalke, J. Gonzalez, F. Lopéz-Ortiz, *J. Am. Chem. Soc.* **2002**, *124*, 15184.
[124] a) E. Hey, C. Ergezinger, K. Dehnicke, *Z. Naturforsch. B* **1988**, *44*, 205; b) D. Fenske, E. Hartmann, K. Dehnicke, *Z. Naturforsch. B* **1988**, *43*, 1611; c) C. Ergezinger, F. Weller, K. Dehnicke, *Z. Naturforsch. B* **1988**, *43*, 1621; d) S. Maier, W. Hiller, J. Strähle, C. Ergezinger, K. Dehnicke, *Z. Naturforsch. B* **1988**, *43*, 1628; e) D. Stalke, M. Wedler, F. T. Edelmann, *J. Organomet. Chem.* **1992**, *431*, C1.
[125] a) M. Veith, J. Böhnlein, *Chem. Ber.* **1989**, *122*, 603; b) M. Veith, J. Böhnlein, V. Huch, *Chem. Ber.* **1989**, *122*, 841.
[126] a) F. Pauer, D. Stalke, *J. Organomet. Chem.* **1991**, *418*, 127; b) F. T. Edelmann, F. Knösel, F. Pauer, D. Stalke, W. Bauer, *J. Organomet. Chem.* **1992**, *438*, 1; c) R. Fleischer, D. Stalke, *J. Organomet. Chem.* **1998**, *550*, 173; d) R. Fleischer, D. Stalke, *Coord. Chem. Rev.* **1998**, *176*, 431.
[127] a) H. Schmidbaur, K. Schwirten, H. Pickel, *Chem. Ber.* **1969**, *102*, 564; b) W. Wolfsberger, W. Hager, *Z. Anorg. Allg. Chem.* **1976**, *425*, 169; c) W. Wolfsberger, W. Hager, *Z. Anorg. Allg. Chem.* **1977**, *433*, 247; d) H. W. Roesky In *The Chemistry of Inorganic Ring Systems. Studies in Inorganic Chemistry*, R. Steudel, Elsevier, Amsterdam **1989**; e) A. Steiner, D. Stalke, *Inorg. Chem.* **1993**, *32*, 1977; f) M. Witt, H. W. Roesky, *Chem. Rev.* **1994**, *94*, 1163.
[128] K. L. Paciorek, R. H. Kratzer, *J. Org. Chem*. **1966**, *31*, 2426.

[129] G. Fries, J. Wolf, M. Pfeiffer, D. Stalke, H. Werner, *Angew. Chem.* **2000**, *112*, 575; *Angew. Chem. Int. Ed.* **2000**, *39*, 564.
[130] J. T. B. H Jastrzebski, G. van Koten, M. Konijn, C. H. Stam, *J. Am. Chem. Soc.* **1982**, *104*, 5490.
[131] S. Harder, J. Boersma, L. Brandsma, A. van Heteren, J. A. Kanters, W. Bauer, P. v. R. Schleyer *J. Am. Chem. Soc.* **1988**, *110*, 7802.
[132] H. J. Reich, W. S. Goldenberg, B. Ö. Gudmundson, A. W. Sanders, K. J. Kulicke, K. Simon, I. A. Guzei, *J. Am. Chem. Soc.* **2001**, *123*, 8067.
[133] A. Steiner, *Aromatische N–Heterocyclen als verbrückende Substituenten zwischen höheren Hauptgruppenhomologen*, PhD thesis, Universität Göttingen, **1994**.
[134] S. Wingerter, *Iminophosphorane und Aminoiminophosphorane - Reaktivität und Koordinationsverhalten*, PhD thesis, Universität Würzburg, **1999**.
[135] M. Pfeiffer, *Reaktivität und Koordinationsverhalten ambidenter Ligandsysteme*, PhD thesis, Universität Würzburg, **2000**.
[136] W. -P. Leung, Z. -X. Wang, H. -W Li, Q. -C. Yang, T. C. W. Mak, *J. Am. Chem. Soc.* **2001**, *123*, 8123.
[137] N. Kocher, D. Leusser; A. Murso, D. Stalke, *Chem. Eur. J.* **2004**, in press.
[138] a) A. F. Cameron, N. S. Hair, D. G. Norris, *Acta Crystallogr. B* **1974**, *30*, 221; b) E. Niecke, D. Gudat, *Angew. Chem.* **1991**, *103*, 251; *Angew. Chem. Int. Ed. Engl.* **1991**, *30*, 217.
[139] A. Murso, D. Stalke, *Z. Anorg. Allg. Chem.*, submitted.
[140] a) G. R. Desiraju, *Crystal Engineering-The Design of Organic Solids*, Elsevier, Amsterdam, 1989; b) J. Wouters and F. Ooms, *Curr. Pharm. Des*. **2001**, 7, 529; c) J. Starbuck, R. Docherty, M. H. Charlton and D. Buttar, *J. Chem. Soc. Perkin Trans. 2,* **1999**, 677.
[141] S. Chitsaz, H. Folkerts, J. Grebe, T. Gröb, K. Harms, W. Hiller, M. Krieger, W. Massa, J. Merle, M. Möhlen, B. Neumüller, K. Dehnicke, *Z. Anorg. Allg. Chem.* **2000**, *626*, 775.
[142] F. Weller, D. Nuszhär, F. Gingl, J. Strähle, K. Dehnicke, *Z. Anorg. Allg. Chem.* **1991**, *602*, 7.
[143] G. A. Jeffrey, *An Introduction to Hydrogen Bonding*, Oxford University Press, Oxford **1997**.
[144] a) G. R. Desiraju, *Angew. Chem.* **1995**, *107*, 2541; *Angew. Chem. Int. Ed. Engl.* **1995**, *34*, 2328; b) G. R. Desiraju, T. Steiner, *The Weak Hydrogen Bond in Structural Chemistry and Biology*, Oxford University Press, Oxford **1999**; c) T. Steiner, *Angew. Chem.* **2002**, *114*, 50; *Angew. Chem. Int. Ed.* **2002**, *41*, 48.
[145] A. Dietrich, B. Neumüller, K. Dehnicke, *Z. Anorg. Allg. Chem.* **2000**, *626*, 1837.
[146] a) H. Schmidbaur, *Fortschr. Chem. Forsch.* **1969**, *13*, 167; b) H. Schmidbaur, *Adv. Orgonomet. Chem.* **1970**, *9*, 259.
[147] H. Vogt, A. Fischer, P. G. Jones, *Z. Naturforsch B* **1996**, 865.
[148] L. M. Engelhard, B. S. Jolly, P. C. Junk, C. L. Raston, B. W. Skelton, A. H. White, *Aust. J. Chem.* **1986**, *39*, 1337.
[149] H. Gornitzka, D. Stalke, *Angew. Chem.* **1994**, *106*, 695; *Angew. Chem. Int. Ed. Engl.* **1994**, *33*, 693.

[150] R. P. K. Babu, K. Aparna, R. McDonald, R. G. Cavell, *Organometallics* **2001**, *20*, 1451.
[151] M. T. Gamer, P. W. Roesky, *Z. Anorg. Allg. Chem.* **2001**, *627*, 877.
[152] R. P. K. Babu, K. Aparna, R. McDonald, R. G. Cavell, *Inorg Chem.* **2000**, *39*, 4981.
[153] a) K. Gregory, P. v. R. Schleyer, R. Snaith, *Adv. Inorg. Chem*. **1991**, *37*, 47; b) R. E. Mulvey, *Chem. Soc. Rev.* **1991**, *20*, 167; c) R. E. Mulvey, *Chem. Soc. Rev*. **1998**, *27*, 339.
[154] M. F. Lappert, M. J. Slade, A. Singh, J. L. Atwood, R. D. Rogers, R. Shakir*, J. Am. Chem. Soc.* **1983**, *105*, 302.
[155] a) P. B. Hitchcock, M. F. Lappert, Z. -X. Wang, *J. Chem. Soc. Chem. Commun.* **1997**, 1113; b) A. Müller, B. Neumüller, K. Dehnicke, *Angew. Chem.* **1997**, *109*, 2447; *Angew. Chem. Int. Ed.* **1997**, *36*, 2350.
[156] T. Chivers, A. Downard, Y. P. A. Glenn, *J. Chem. Soc. Dalton Trans.* **1998**, *16*, 2603.
[157] T. Chivers, A. Downard, M. Parvez, *Inorg. Chem.* **1999**, *38*, 4347.
[158] a) R. Appel, *Pure Appl. Chem.* **1987**, *59*, 977; b) D. G. Gilheany, In *The Chemistry of Organophosphorus Compounds*, F. R. Hartley, Wiley-Interscience, Chichester, **1990**, Vol. 1, Chapter 2, 9.
[159] a) J. C. J. Bart, *J. Chem. Soc. B*. **1969**, 350; b) H. Schmidbaur, A. Schier, C. M. F. Frazao, G. Müller, *J. Am. Chem. Soc.* **1986**, *108*, 976; c) H. Schmidbaur, J. Jeong, A. Schier, W. Graf, D. L. Wilkinson, G. Müller, *New J. Chem.* **1989**, *13*, 341.
[160] A. Müller, M. Möhlen, B. Neumüller, N. Faza, W. Massa, K. Dehnicke, *Z. Anorg. Allg. Chem.* **1999**, *625*, 1748.
[161] N. Kocher, *Experimental Charge Density Studies of Highly Polar Bonds***,** PhD thesis, Würzburg, **2003**.
[162] a) N. K.Hansen, P.Coppens *Acta Cryst.* **1978**, *A34*, 909; b) T. Koritsanszky, S. Howard, T. Richter, Z. W. Su, P. R. Mallinson, N. K. Hansen, *XD – A Computer Program Package for Multipole Refinement and Analysis of Electron Densities from Diffraction Data*. *User Manual*; Freie Universität Berlin **1995**.
[163] R. F. W. Bader, *Atoms in Molecules – A Quantum Theory*; Clarendon Press, Oxford **1990**.
[164] Y. A. Abramov, L. Brammer, W. T. Klooster, R. M. Bullock, *Inorg. Chem.* **1998**, *37*, 6317.
[165] A. Volkov, C. Gatti, Y. A. Abramov, *Acta Crystrystallogr. Sect A*. **2000**, *56*, 252.
[166] W. Scherer, P. Sirsch, D. Shorokhov, G. McGrady, S. A. Mason, M. G. Gardiner *Chem. Eur. J.* **2002**, *8*, 2324.
[167] D. Leusser, B. Walfort, D. Stalke, *Angew. Chem*. **2002**, *114*, 2183; *Angew. Chem. Int. Ed*. **2002**, *41*, 2079.
[168] A. Müller, M. Marsch, K. Harms, J. C. W. Lorenz, G. Boche, *Angew. Chem.* **1996**, *108*, 1639; *Angew. Chem. Int. Ed. Engl.* **1996**, *35*, 1518.
[169] R. I. Papasergio, B. W. Skelton, P. Twiss, A. H. White, C. L. Raston, *J. Chem. Soc. Dalton Trans.* **1990**, 1161.

[170] a) W. N. Setzer, P. v. R. Schleyer, *Adv. Organomet. Chem.* **1985**, *24*, 353; b) C. Schade, P. v. R. Schleyer, *Adv. Organomet. Chem.* **1987**, *27*, 169; c) K. Gregory, P. v. R. Schleyer, *Adv. Organomet. Chem.* **1991**, *37*, 47; d) D. Hoffmann, W. Bauer, F. Hampel, N. J. R. v. E. Hommes, P. v. R. Schleyer, P. Otto, U. Pieper, D. Stalke, D. S. Wright, R. Snaith, *J. Am. Chem. Soc.* **1994**, *116*, 528.

[171] D. Hoffmann, W. Bauer, P. v. R. Schleyer, U. Pieper, D. Stalke, *Organometallics* **1993**, *12*, 1193.

[172] U. Schümann, U. Behrens, E. Weiss, *Angew. Chem.* **1989**, *101*, 481; *Angew. Chem. Int. Ed. Engl.* **1989**, *28*, 476.

[173] G. Rabe, H. W. Roesky, D. Stalke, F. Pauer, G. M. Sheldrick, *J. Organomet. Chem.* **1991**, *403*, 11.

[174] H. Bürger, W. Sawodny, U. Wannagat, *J. Organomet. Chem.* **1965**, *3*, 113.

[175] A. Murso, D. Stalke, *Inorg. Chem.*, submitted.

[176] A. Haaland, K. Hedberg, P. P. Power, *Inorg. Chem.* **1984**, *23*, 1972.

[177] J. Dekker, J. Boersma, L. Fernholt, A. Haaland, A. L. Spek, *Organometallics* **1987**, *6*, 1202.

[178] a) A. Kasani, R. McDonald, R. G. Cavell, *Organometallics* **1999**, *18*, 3775; b) M. S. Hill, P. B. Hitchcock, *J. Chem. Soc. Dalton Trans*. **2002**, 4694.

[179] M. Krieger, R. O. Gould, K. Harms, S. Parsons, K. Dehnicke, *Chem. Ber.* **1996**, *129*, 1621.

[180] S. Wingerter, H. Gornitzka, G. Bertrand, D. Stalke, *Eur. J. Inorg. Chem.* **1999**, 173.

[181] N. A. Bell, P. T. Moseley, H. M. M. Shearer, C. B. Spencer, *J. Chem. Soc. Chem. Commun.* **1980**, 359.

[182] S. Wingerter, M. Pfeiffer, T. Stey, M. Bolboacá, W. Kiefer, V. Chandrasekhar, D. Stalke, *Organometallics* **2001**, *20*, 2730.

[183] U. Riese, K. Harms, J. Pebler, K. Dehnicke, *Z. Anorg. Allg. Chem.* **1999**, *625*, 746.

[184] T. J. J. Sciarone, A. Meetsma, B. Hessen, J. H. Teuben, *Chem. Commun.* **2002**, 1580.

[185] S. Al-Benna, M. J. Sarsfield, M. Thomton-Pett, D. L. Omsby, P. J. Maddox, P. Brès, M. Bochmann, *J. Chem. Soc. Dalton Trans.* **2000**, 4247.

[186] a) W. A. Herrmann, C. Köcher, *Angew. Chem.* **1997**, *109*, 2256; *Angew. Chem. Int. Ed. Engl.* **1997**, *36*, 2162; b) D. Bourissou, G. Bertrand, *Adv. Organomet. Chem.* **1999**, *44*, 175; c) D. Bourissou, O. Guerret, F. P. Gabai, G. Bertrand, *Chem. Rev.* **2000**, *100*, 39, d) S. Goumri-Magnet, T. Kato, H. Gornitzka, A. Baceiredo, G. Bertrand, *J. Am. Chem. Soc.* **2000**, *122*, 4464; e) N. Merceron, K. Miqueu, A Baceiredo, G. Bertrand, *J. Am. Chem. Soc*. **2002**, *124*, 6806.

[187] a) B. Chiswell, *Aust. J. Chem.* **1967**, *20*, 2533; b) E. Lindner, H. Rauleder, W. Hiller, *Z. Naturforsch B* **1983**, *38*, 417; c) E. Lindner, H. Rauleder, P. Wegner, *Z. Naturforsch B* **1984**, *39*, 1224.

[188] D. Stalke, *Chem. Soc. Rev.* **1998**, *27*, 171.

[189] a) H. Hope, *Acta Crystallogr*. **1988**, *B 44*, 22; b) T. Kottke, D. Stalke, *J. Appl. Crystallogr*. **1993**, *26*, 615; c) T. Kottke, R. J. Lagow, D. Stalke, *J. Appl. Crystallogr*. **1996**, *29*, 465.

[190] Bruker, SMART-NT, Data Collection Software, Version 5. 6, Bruker Analytical X-ray Instruments Inc., Madison, Wisconsin (USA), **2000**.
[191] Bruker, SAINT-NT, Data Reduction Software, Version 6, Bruker Analytical X-ray Instruments Inc., Madison, Wisconsin (USA), 1999.
[192] G. M. Sheldrick, SADABS 2, Empirical Absorption Correction Program, University of Göttingen (Germany), **2001**.
[193] Bruker, SHELX-TL; Version 6, Bruker Analytical X-ray Instruments Inc., Madison, Wisconsin (USA), **2000**.
[194] a) H. D. Flack, *Acta Crystallogr.* **1983**, *A39*, 876. b) G. Bernadinelli, H. D. Flack, *Acta Crystallogr.* **1985**, *A41*, 500.

Publikationen

1. S. Wingerter, M. Pfeiffer, A. Murso, C. Lustig, T. Stey, V. Chandrasekhar, D. Stalke, „Phosphorus-Based Ambidentate Chelating Ligands: Pyridyl-N- and Imido-N-Metal Coordination in the $Py_2P(NSiMe_3)_2^-$ Anion“, *J. Am. Chem. Soc.* **2001**, *123*, 1381.
2. J. Heinicke, A. Surana, N. Peulecke, R. K. Bansal, A. Murso, D. Stalke, „Metalated 1,3-azaphospholes: 1H-1,3-benzazaphosphole and 1,3-benzaza-phospholide tungsten(0) and tungsten(II) complexes“, *Eur. J. Inorg. Chem.* **2001**, 2563.
3. M. Pfeiffer, A. Murso, L. Mahalakshmi, D. Moigno, W. Kiefer, D. Stalke, „Experimental and computational study on a variety of structural motifs and coordination modes in aluminum complexes of Di(2-pyridyl)amides and –phosphanides“, *Eur. J. Inorg. Chem.* **2002**, 3222.
4. F. Baier, Z. Fei, H. Gornitzka, A. Murso, S. Neufeld, M. Pfeiffer, I. Rüdenauer, A. Steiner, T. Stey, D. Stalke, „Phosphane- and phosphorane Janus Head ligands in metal coordination“, *J. Organomet. Chem*. **2002**, *661*, 111.
5. M. Kaupp,T. Kopf, A. Murso, D. Stalke, C. Strohmann, J. R. Hanks, F. G. N. Cloke, P. B. Hitchcock, „Trigonal Prismatic Structure of Tris(butadiene)molybdenum and Related Complexes Revisited: Diolefin or Metallacyclopentene Coordination?“, *Organometallics* **2002**, *21*, 5021.
6. H. Glaser, R. Puchta, N. J. R. van Eikema Hommes, D. Leusser, A. Murso, D. Stalke, W. Bauer, R. W. Saalfrank, „A domino aldol addition/hemiketal formation/hemiketal formation/epimerization route to a heteroadamantane. A crystal-structure, NMR, and computational study“, *Helv. Chim. Acta* **2002**, *85*, 3828.
7. J. Hartung, S. Drees, M. Greb, P. Schmidt, I. Svoboda, H. Fuess, A. Murso, D. Stalke, „(Schiff-base)vanadium(V) complex-catalyzed oxidations of substituted bis(homo-allylic) alcohols - stereoselective synthesis of functionalized tetrahydrofurans“, *Eur. J. Org. Chem.* **2003**, *13*, 2388.
8. M. Bolboaca, T. Stey, A. Murso, D. Stalke, W. Kiefer, „P-N bond length alterations monitored by infrared absorption and Fourier transform Raman spectroscopy in combination with density functional theory calculations“, *Appl. Spectrosc.* **2003**, *57*, 970.
9. N. Kocher, D. Leusser, A. Murso, D. Stalke, „Metal Coordination to the Formal P=N Bond and Charge Density Evidence against Hypervalent Phosphorus(V)”, *Chem. Eur. J.* **2004**, in press.

10. A. Murso, D. Stalke, „The C_α-deprotonated Iminophosphorane $Ph_2P(CH_2Py)(NSiMe_3)$ as a (N,N)-Chelating Ligand to Iron and Zinc", *Inorg. Chem.*, submitted.
11. A. Murso, D. Stalke, „Polymorphism of $Ph_2P(CH_2Py)(NSiMe_3)$ and its Staudinger Reaction with Hydrogenazide", *Z. Anorg. Allg. Chem.*, submitted.

Posterpräsentationen

„Reactivity of Iminophosphoranes and Phosphanamines"
ICCC 35, Heidelberg, **2002**.

„Reactivity and Coordination Behaviour of Janus Head Type Iminophosphoranes and Phosphanamines"
1st Conference on Electron Density, Würzburg, **2002**.

„Alkyllithium-mediated P–C Bond Cleavage Reactions"
ALKCHEM-3, Würzburg. **2003**.

„Experimental charge density and topological analysis of highly polar bonds in a semistabilized phosphorus compound"
ALKCHEM-3, Würzburg, **2003**.

Lebenslauf

Persönliche Angaben

Name:	Alexander Murso
Geburtsdatum:	17.05.1974
Geburtsort:	Heilbronn
Familienstand:	ledig

Schulbildung

1980 – 1984	Manfred-Kyber Grundschule in Löwenstein
06.1984 – 05.1993	Justinus-Kerner-Gymnasiums in Weinsberg
19.05.1993	Abschluss der Allgemeinen Hochschulreife

Grundwehrdienst

07.1993 – 06.1994	Wehrdienstzeit in der Deutsch-Französischen Brigade
11.05.1994	Verleihung der Ehrenmedaille der Bundeswehr

Studium

10.1994 – 02.2001	Studium der Chemie (Diplom) an der Bayerischen Julius-Maximilians Universität Würzburg
31.10.1997	Diplom-Vorprüfung
06.2000 – 02.2001	Diplomarbeit im Arbeitskreis von Prof. Dr. D. Stalke am Institut für Anorganische Chemie der Universität Würzburg zum Thema: *„Phosphan- und Phosphoran Januskopfliganden – Synthese, Reaktivität und Koordinationsverhalten“*
27.02.2001	Abschluss des Studiums der Chemie als Dipl.-Chem. Univ. Gesamtnote: „sehr gut“
seit 04.2001	Promotionsstudium im Arbeitskreis von Prof. Dr. D. Stalke am Institut für Anorganische Chemie der Universität Würzburg zum Thema *„ELECTRONIC RESPONSE OF PHOSPHORUS AND NITROGEN BASED LIGANDS ON METAL COORDINATION“*
01.04.2001	Verleihung eines Promotionsstipendiums der DFG im Rahmen des Graduiertenkollegs 690 *„Elektronendichte – Theorie und Experiment“*

Erklärung

Hiermit erkläre ich an Eides statt, dass ich die Dissertation “ELECTRONIC RESPONSE OF PHOSPHORUS AND NITROGEN BASED LIGANDS ON METAL COORDINATION” selbständig angefertigt habe und keine anderen als die von mir angegebenen Quellen und Hilfsmittel benutzt habe.

Ich erkläre außerdem, dass diese Dissertation weder in gleicher oder anderer Form bereits in einem anderen Prüfungsverfahren vorgelegen hat.

Ich habe früher außer den mit dem Zulassungsgesuch urkundlich vorgelegten Graden keine weiteren akademischen Grade erworben oder zu erwerben versucht.

Würzburg, den 25.03.2004

Unterschrift

(Vor- und Zuname)